Wrocław University of Science and Technology

Faculty of Chemistry

Metabolomics analysis of time and oxygen effect of Fibrosarcoma cell line (HT1080)

Submitted by

Badr Saif Mohsen Qasem

at

The Department of Biochemistry, Molecular Biology and Biotechnology

Supervisor:

Prof. dr hab. Piotr Młynarz,

Faculty of Chemistry,

Wroclaw University of Science and Technology.

Wrocław, 2023

Foreword

This thesis dissertation is the result of more than four years of research at the Department of Biochemistry, Molecular Biology and Biotechnology, Faculty of Chemistry, Wroclaw University of Science and Technology under the supervision of prof. Piotr Młynarz.

This thesis aims at contributing new metabolic phenotype analysis-based approaches to improve the investigation of fibrosarcoma cell line metabolism *in vitro*, with particular emphasis on metabolic responses to pathological results of various oxygen concentrations. Moreover, this thesis also contributes to a novel *in vitro* model, to investigate intracellular and extracellular reoxygenation and deoxygenation metabolome by 1D ^{1}H NMR.

Preface

This thesis is the product of a long scientific journey with Department of Biochemistry, Molecular Biology, and Biotechnology, Faculty of Chemistry, Wroclaw University of Science and Technology. It was challenging, full of obstacles, individual thinking, and scientific and personal growth. Doing my Ph.D. wasn't easy. However, the experiences that I gained, enthusiasm, motivation, persistence, and hard work, until I finally achieved my goals, wouldn't happen without the help of extraordinary people whom I wish to acknowledge.

I am grateful to my supervisor, Prof. Piotr Mlynarz, for his valuable knowledge, bringing me to the exciting field of biochemistry and chemistry, for his guidance, support, trust, encouragement, energy, and for being a demanding boss when necessary. Dr. Wojciech Wojtowicz, for your help and inspiration regarding spectroscopy data processing and multivariate analysis and all kinds of support during this process, and for always keeping his door open for a fruitful and exciting scientific discussion. I would like to thank my colleagues on Professor Mlynarz's team for a very pleasant, humorous, and professional working environment. Special thanks to Paweł Dąbrowski for introducing me to NMR analysis. Most importantly, I feel grateful for the support of my family and friends during this process.

Badr Qasem

Wroclaw, May 2022

Abstract

Oxygen molecular effect on cancer cells metabolism has been a concern for decades, at the beginning with Louis Pasteur's and his understanding of glucose fermentation. In the 1930s, Otto Warburg came with his new understanding of cancer biology by introducing the alteration of cancer cells' metabolism in the presence or absence of oxygen molecules by increasing glucose uptake and producing lactate through aerobic glycolysis (Warburg Effect). For more than 100 years scientists published different studies trying to fully understand of Warburg effect and hypoxia-metabolic reprogramming effect on cancer cell progression. However, still is a lot of questions unanswered so far. For instance, why do cells choose the less sufficient way to produce ATP and lose carbon in form of lactate which is required for the biosynthetic process. What are the exact proportions of activity of cancer cells between glycolytic and the TCA cycle? And the most curious question, what is the role of stromal components in the microenvironment ?. Is there any most advanced technology to answer all these questions?. By using a metabolomics platform including mass spectrometry (MS), nuclear magnetic resonance (NMR) spectroscopy, and chemometric methods to analyse a large number of metabolites present in cancer cell line samples the brighter light can be shed on identifying pathological biochemical pathways.

Chapter 1

Starts by introducing the state of the art in cancer biology, cancer metabolism, and the progression process and explores "Warburg effect" last consideration on metabolism reprogramming and cancer progression. Moreover, highlights the role of some essential and nonessential amino acids in cancer cell metabolism during different stress exposure to understand the metabolism alterations. In addition, the importance of oxygen molecules to cancer cell metabolism and its concentrations *in vitro* and *in vivo* terminology were described. A brief introduction also includes the contributions of NMR-based *in vitro* metabolomics and chemometric analysis as powerful and advantageous technology to investigate cultured cell line metabolome.

Chapter 2

In this chapter, focused on the NMR-based *in vitro* metabolomics studies on HT1080 cell line at selected oxygen concentrations as hypoxia 1%, normoxia 6%, and hyperoxia 21% by using 1D ^{1}H NMR spectroscopy based on cells extracts (intracellular) and post cultured medium (extracellular), including sampling during incubation in the time intervals. Latest studies suggested that across many types of tumors after assessment of their degree of hypoxia using a set of genetic hypoxia markers revealed a great variation among tumours type in terms of potential hypoxia influence. Moreover, the normoxia term very often used 21% of oxygen concentration in *in vitro* studies, which is much higher than physiological oxygen concentration. Therefore, there is a need to develop a novel methodology to mimic the oxygen pressure on body tissues, that could distinguish the differences between oxygen environment saturation (hypoxia ≤ 1 and normoxia 6% and hyperoxia 21%). Hence, the metabolic profile information was collected by using 1D ^{1}H NMR spectra from each interval of incubation time (12h, 24, and 36h with respect to the control samples) of fibrosarcoma cell line including intra and extracellular metabolites analysis. The chemometric analyses were applied to determine the potential of metabolites for discrimination purposes between interval incubation time. Besides, increasing the oxygen content and the possibilities of metabolite changes could be performed, namely at hypoxia at 1%, normoxia at 6%, and hyperoxia at 21% condition.

Chapter 3

In this chapter of the doctoral dissertation, uses novel terms and methodology for inducing hypoxic-reoxygenation and normoxic-deoxygenation *in vitro* models to screen HT1080 cell line by looking at extracellular and intracellular metabolome. Behind this concept, tumor hypoxia arises from the rapid and uncontrolled proliferation of cancer cells, leading to increased acquisition of nutrients and oxygen to meet the energy demands. However, a quick depletion of oxygen and nutrient supply developed in parts of the tumour. Means, there is a transition of cells from sufficient oxygen and nutrients supply to hypoxic conditions with insufficient oxygen and nutrients supply normoxic-deoxygenation. In another hand, the hypoxic region within tumours generates different strategies to acquire an adequate quantity of oxygen and nutrients for cancer progression. For instance, induce the production of angiogenic proteins to build new vessels for blood flow and cancer cell mobility through

epithelial-mesenchymal transition (EMT) and metastasis. Thereby, cancer cells become normoxic cells with a sufficient supply of oxygen and nutrients (hypoxic-reoxygenation). Both these terms develop different metabolic phenotypes of cancer cells, so the combination of the analyses for intracellular and extracellular metabolites including normoxic vs. deoxygenized normoxic cells (DNCs) and hypoxic vs. reoxygenized hypoxic cells (RHCs) through incubation time experiments were conducted.

Streszczenie

Wpływ tlenu molekularnego na metabolizm komórek nowotworowych jest przedmiotem zainteresowania od kilku dziesięcioleci, począwszy od eksperymentów Louisaa Pasteura i jego rozumienia fermentacji glukozy. W latach 30 XX wieku Otto Warburg przyszedł z nowym zrozumieniem biologii nowotworów, wprowadzając zmiany metabolizmu komórek nowotworowych w obecności lub braku cząsteczek tlenu, poprzez zwiększenie przyswajania glukozy i produkcję mleczanu na drodze glikolizy aerobowej (efekt Warburga). Od ponad 100 lat naukowcy publikują różne badania, próbując pełniej zrozumieć efekt Warburga i efekt reprogramowania metabolicznego hipoksji na postępowanie komórek nowotworowych. Jednak do tej pory wiele pytań pozostaje bez odpowiedzi. Na przykład, dlaczego komórki wybierają mniej wydajny sposób produkcji ATP i tracą atomy węgiela w postaci mleczanu, który jest potrzebny do procesów biosyntetycznych. Jakie są dokładne proporcje działalności komórek nowotworowych między glikolizą a cyklem TCA?

A najciekawsze pytania brzmią jaka jest rola składników stromalnych w mikrośrodowisku. Czy istnieją najnowocześniej technologie, aby odpowiedzieć na te wszystkie pytania? Dzięki platformie metabolomika, w tym spektrometrii masowej (MS), spektroskopii magnetycznego rezonansu jądrowego (NMR) i metodom chemometrii, analizując dużą liczbę metabolitów obecnych w próbkach linii komórek nowotworowych, można uzyskać więcej informacji dotyczących identyfikacji patologicznych ścieżek biochemicznych.

Rozdział 1

Rozpoczyna się od przedstawienia aktualnego stanu wiedzy o biologii nowotworów, metabolizmie oraz procesie progresji nowotworów, najnowszych rozważań na temat efektu Warburga związanych z reprogramowaniem metabolizmu i progresją nowotworów. Ponadto podkreśla rolę niektórych aminokwasów niezbędnych w metabolizmie komórek nowotworowych. Dodatkowo opisano ważność cząsteczek tlenu dla metabolizmu komórek nowotworowych oraz ich stężenia w terminologii *in vitro* i *in vivo*. Krótki wstęp obejmuje również wkład spektroskopii NMR w analizę metabolomu *in vitro* wraz z analizą chemometryczną jako nieocenioną technologią badania metabolomu linii komórek hodowanych *in vitro*.

Rozdział 2

W tym fragmencie pracy skupiono się na badaniach z wykorzystaniem metody 1D ^{1}HNMR w badaniach metabolomu *in vitro* linii komórek HT1080, przy wybranych stężeniach tlenu jako hipoksja 1%, normoksja 6% i hiperoksja 21% na podstawie ekstraktów komórek (metabolomu wewnątrzkomórkowego) oraz płynów pohodowlanych (metabolomu zewnątrzkomórkowego), włącznie z próbkowaniem w czasie inkubacji w odstępach czasowych. Ostatnie doniesienia literaturowe sugerują, że w różnych typach nowotworów po ocenie ich stopnia hipoksji za pomocą zestawu genetycznych markerów hipoksji stwierdzono dużą różnorodność między nimi. Ponadto termin normoksja jest używany względem 21% stężenia tlenu w badaniach *in vitro*. Stężenie to jest znacznie wyższe niż fizjologiczne stężenie tlenu. Z tego względu istnieje potrzeba opracowania nowej metodologii do symulowania fizjologicznego ciśnienia tlenu w tkankach, które mogłoby wskazać różnice między nasyceniem środowiska tlenem (hipoksja ≤ 1 i normoksja 6% i hiperoksja 21%). Dlatego też, przeprowadzono badania profilu metabolicznego linii komórek fibrosarcomy za pomocą spektroskopii 1D ^{1}H NMR z uwzględnieniem interwałów czasowych inkubacji (12h, 24, i 36h w odniesieniu do próbek kontrolnych), włącznie z analizą metabolitów wewnątrzkomórkowych i zewnątrzkomórkowych. Zastosowano analizy chemometryczne, aby określić „potencjał metabolitów" do celów dyskryminacji między interwałami inkubacji. Poza tym, zwiększając zawartość tlenu, a przez to możliwości zmian w szlakach

biochemicznych można było przeprowadzić badania metabolomiczne w warunkach hipoksji przy 1% O_2, normoksji przy 6% O_2 i hiperoksji przy 21% O_2.

Rozdział 3

To zastosowanie nowego podejścia do indukcji *in vitro* modeli typu hipoksja-reoksygenacja i normoksja-deoksygenacja, z zastosowaniem linii komórek HT1080 oraz analizą metabolomu ekstracellularnego i intracellularnego. Zgodnie z obowiązującą koncepcją, hipoksja nowotworu wynika z szybkiej i niekontrolowanej proliferacji komórek nowotworowych, prowadząc do zwiększonego pozyskiwania składników odżywczych i tlenu w celu wypełnienia wymagań energetycznych procesów kancerogenzy. Jednak szybka proliferację komórek nowotworowych powoduje utrudniony dostęp do zaopatrzenia w tlen i składniki odżywcze. Oznacza to, że dochodzi do przejścia komórek z dostatecznym dostarczaniem tlenu i składników odżywczych do warunków hipoksji z niedostatecznym dostarczaniem tlenu i składników odżywczych (normoksja-deoksygenacja). Z drugiej strony, region hipoksyczny wewnątrz guzów generuje różne strategie pozyskiwania odpowiedniej ilości tlenu i składników odżywczych dla progresji nowotworu. Na przykład, indukuje produkcję białek angiogennych, aby budować nowe naczynia dla przepływu krwi i ruchu komórek nowotworowych poprzez przejście epitelialno-mezenchymalne (EMT) i metastazę. W ten sposób komórki nowotworu stają się komórkami normoksycznymi z dostatecznym dostarczaniem tlenu i składników odżywczych (hipoksja-reoksygenacja). Oba te pojęcia rozwijają różne fenotypy metaboliczne komórek nowotworu. W związku z tym zostało przeprowadzone połączenie analiz metabolitów wewnątrzkomórkowych i zewnątrzkomórkowych, w tym komórek normoksycznych i denormoksycznych (DNC) oraz komórek hipoksycznych i reoksygenowanych hipoksycznych (RHC) przez przeprowadzenie eksperymenty w czasie.

List of abbreviations

Abbreviation	FULL FORM
2D	Two-dimensional
Ac-CoA	Acetyl Coenzyme A
HMDB	Human Metabolome Data Base
LDL	Low-density lipoprotein
LDL-R	Low-density lipoprotein cholesterol receptor
VLDL	Very low-density lipoprotein
NMR	Nuclear magnetic resonance
MS	Mass-spectrometry
PCA	Principal component analysis
PLS	Partial least square
PLS-R	Partial least square regression
PCA	Principal component analysis
TSP	3-Trimethylsilylpropionic acid
NAD+	Nicotinamide adenine nucleotide (oxidized)
DNCs	Deoxygenized Normoxic Cells
DNC	Normoxia-deoxygenation Condition
RHCs	Reoxygenized Hypoxic Cells
RHC	Hypoxia- reoxygenation Condition
NADH	Nicotinamide adenine nucleotide (reduced)
RMSECV	Root-Mean-Square Error of Cross-Validation
ATP	Adenosine-3-phosphate
PBS	Phosphate buffered saline
PC	Pyruvate carboxylase
PDH	Pyruvate dehydrogenase
pO2	The partial pressure of oxygen
PPP	Pentose phosphate pathway
TCA	Tricarboxylic acid
MCT	Monocarboxylate transporter
BCAAs	Branched-chain amino acids
MEM	Minimum Essential Media
FBS	Fetal bovine serum
HIF-1	Hypoxia inducible factor- 1
LAT1	Large amino acid transporter 1
ASCT2	Alanine, serine, cysteine transporter 2
GBM	Human glioblastoma
BCAT1	Branched chain amino acid transaminase 1
BCKD	Branched-chain alpha-ketoacid dehydrogenase
mTORC1	Mammalian target of rapamycin complex 1

IDH1	Dehydrogenase-1
αKG	α-ketoglutarate
SLC1A5	Solute carrier family 1 (neutral amino acid transporter_member 5)
NAD	Nicotinamide adenine dinucleotide
Nampt	Nicotinamide phosphoribosyltransferase
Nmnat	Mononucleotide adenylyltransferase
NMN/NAMN	Nicotinamide mononucleotide
Naprt	Nicotinate phosphoribosyltransferase
GAPDH	Glyceraldehyde-3-phosphate dehydrogenase
PRPP	Poly ADP-ribose polymerase
CD38/157	Cluster of Differentiation 38/157
LDH	Lactate dehydrogenase
ALAT	Alanine aminotransferase
PDH	Pyruvate dehydrogenase
PDAC	Pancreatic ductal adenocarcinoma
OGD	Oxygen-glucose deprivation
CRC	Colorectal cancer
PUMA	p53 upregulated modulator of apoptosis
Bax/Bcl-2	Bcl-2-associated X protein/ B-cell lymphoma 2
tCho	Choline-containing compounds
PCho	Phosphocholine
GPC	Glycerophosphocholine
CHKα	Choline kinase-α
CTL1	Choline transporter-like protein 1
TNBC	Triple-negative breast cancer
NF-κB	Nuclear factor kappa-light-chain-enhancer of activated B cells
AKT-ERK	Protein kinase B-Extracellular signal-regulated kinase
3PG	3-phosphoglycerate
pPYR	3-phosphohydroxypyruvate
PHGDH	Phosphoglycerate dehydrogenase
PSAT	Phosphoserine aminotransferase
pSER	Phosphoserine
PSPH	Phosphoserine phosphatase
SHMT1/2	Serine hydroxymethyltransferases 1/2
GCS	Glycine cleavage system
THF	Tetrahydrofolate
IMP	Inosine monophosphate
HPRT	Hypoxanthine-guanine phosphoribosyltransferase
APRT	Adenine phosphoribosyltransferase
PPP	Pentose phosphate pathway

PFKFB	6-phospho-2-kinase/fructose-2,6-biphosphatase
PFK-1	Phosphofructokinase-1
METTL9	Methyltransferase 9
FH	Fumarate hydratase
Keap1	Kelch-like ECH-associated protein 1
Nrf2	Nuclear factor (erythroid-derived 2)-like 2
SDH	Succinate dehydrogenase
ROS	Reactive oxygen species
ACSS1/2	Acetyl-CoA synthetase 1/2
KRAS	Kirsten rat sarcoma viral oncogene
ATF4	Activating transcription factor 4
ASNS	Asparagine synthetase
GOT	Glutamic oxaloacetic transaminase
OTC	Ornithine transcarbomylase
OAT	Ornithine aminotransferase
ODC	Ornithine decarboxylase
PI3K/AKT	Phosphatidylinositol 3-kinase and protein kinase B
SSAT	Spermidine/spermine N(1)-acetyltransferase
GSK3β	Glycogen synthase kinase-3 beta
PCC	Propionyl-CoA carboxylase
OCFA	Odd-chain fatty acid
UDP-GlcNAc	Uridine diphosphate N-acetylglucosamine
HBP	Hexosamine biosynthetic pathway
TGF-β	Transforming growth factor-β
OSSC	Oral squamous cell carcinoma
SAM	Methyl-donor S-adenosylmethionine
1-MNA	1-methylnicotinamide
PAAD	Pancreatic Adenocarcinoma
SHh	Sonic Hedgehog
NNMT	N-methyltransferase
LDHA	Lactate dehydrogenase A
MCTs	Monocarboxylic acid solute transporters
AATs	Amino acid transporters
GCN2	General control of nonderepressible protein kinase 2
FADH2	Flavin adenine dinucleotide
CAT-1	Cationic amino acid transporter-1
CLL	Chronic lymphocytic leukemia
GLUT 1/3/4/5	Glucose transporter type-1/3/4/5
TME	Tumor microenvironment
ABC	ATP-binding cassette
PANX1	Cconnexin hemichannels, pannexin 1
CALHM1	Calcium homeostasis modulator 1

VRACs	Volume-regulated anion channels
MACs	Maxi-anion channels
GFAT	Glutamine fructose-6-phosphate amidotransferase
HK2	Hexokinase 2
PGI	Phosphoglucose isomerase
PGK	Phosphoglycerate kinase
PGM	Phosphoglycerate mutase
PDK1/MXI1	3-phosphoinositide-dependent protein kinase 1/MAX interactor 1
COX4I2	Cytochrome c oxidase subunit 4 isoform 2
CK	Choline kinase
PC-PLC/D	Phosphatidylcholine-specific phospholipase C/D
BCKDH	Branched-chain α-keto acid dehydrogenase complex
KIC	2-keto-isocaproate/4-methyl-2-oxopentanoic acid
KMV	α-keto-β-methylvaleric acid/3-methyl-2-oxopentanoate
KIV	2-keto-isovalerate/3-methyl-2-oxobutanoic acid
AA	Acetoacetate
HDACs	3-hydroxybutyrate on class I histone deacetylases
Kbhb	Histone lysine β-hydroxybutyrylation
CPT-1	Carnitine palmitoyltransferase-1
DEGs	Differentially expressed genes
ER	Endoplasmic reticulum
CHOP	CCAAT-enhancer-binding protein homologous protein
NAA	N-acetylasparate
Met	Methionine
HCY	Homocysteine
SAH	Adenosylhomocysteine
SAM	S-adenosylmethionine
tHcy	Total homocysteine
SAHH	S-adenosylhomocysteine hydrolase
CAFs	Cancer-associated fibroblasts
MDSCs	Myeloid-derived suppressor cells
ECM	Extracellular matrix
F6P	Fructose-6- phosphate
F1,6 bP	Fructose-1,6-biphosphate
GA-3P	Glyceraldehyde 3-phosphate
1,3BPG	1,3-biphosphoglycerate
PEP	Phosphoenolpyruvate
FASN	Fatty acid synthase
ACLY	ATP-citrate lyase
ETC	Electron transport chain

AMPK	Adenosine monophosphate-activated protein kinase
OXPHOS	Oxidative phosphorylation
EAAs	Essential amino acids
NEAAs	Nonessential amino acids
IDH 1/2/3	Isocitrate dehydrogenase 1/2/3
XCT	Cystine transporter
ME 1	NADP-dependent malic enzyme 1
GLS1	Glutaminase 1
MFN1/2	Mitofusin 1/2
OPA1	Optic atrophy 1
PHGDH	Phosphoglycerate dehydrogenase
PSAT1	Phosphoserine aminotransferase
PSPH	Phosphoserine phosphatase
GOT	Glutamate-oxaloacetate transaminase

Main Chapters

Chapter -1 Introduction……..... 15

Chapter -2 Quantitative ^{1}H NMR analysis of intracellular and extracellular metabolome of HT1080 cell line under hypoxia, normoxia, and hyperoxia…….. 40

Chapter -3 The effect of hypoxia-reoxygenation and normoxia-deoxygenation in HT1080 cell line metabolome by ^{1}H NMR analysis…… 118

CHAPTER 1

Introduction

Contents

1 Introduction 19

1.1. The malignant properties of human tumorigenesis 19

1.2. The transformation of normal human cells into cancer cells 19

1.3. The multistage of carcinogenesis 20

1.4. Tumor microenvironment and cancer progression 20

1.5. The Warburg Effect past and present 25

1.6. Cancer cells metabolism 26

1.6.1. Glycolysis/TCA cycle intermediates for biosynthesis and NADPH production 26

1.6.2. Glutamine metabolism 27

1.6.3. Non-Essential Amino Acids metabolism 28

1.6.4. Branched-Chain Amino Acid (BCAA) Metabolism 28

2 *In vitro* models for metabolomics research 29

3 1D ^{1}H NMR as Tool to Investigate cancer cells metabolome - in vitro researches 29

4 The terminology of hypoxia, normoxia, and hyperoxia - Cell Biology Perspective 31

5 References 34

1. Introduction

1.1. The malignant properties of human tumorigenesis

The definition of cancer has been established for centuries as a diversity of neoplastic diseases with various explanations about its origin. Despite many efforts, cancerous diseases still are the leading cause of worldwide death [1,2]. In 2018 there were about 18.1 million new cases and 9.5 million of them were related to deaths. The prediction estimate by 2040 the number per year will be 29.5 million, and 16.4 million cases of cancer-related deaths [3]. Therefore the understanding of cancer and its causes should allow us to prevent and reduce this disease from happening.

Epidemiological studies suggest that 90%–95% of cancers are correlated to environmental factors such as infections, lifestyle, chemical exposure, and sunlight overexposure, while the rest 5%–10% due to DNA mutation and modification in gene expression leading the normal cells to be transformed into cancer cells [4]. The concept of cancer in the modern term has been defined as carcinogenesis or tumorigenesis, which seems to be more convenient to define tumor cell transformation and describe the tumor development processes [5].

Different risk factors lead to the disturbance of the cellular homeostasis related to dysplastic, hyperplastic, or regenerative changes, which can be classified into three main groups carcinogenic factors. The primary factors include pathological agents such as viruses or bacteria, chemical materials, and physical agents that interfere with genetic materials. The secondary factors are more explicit being related to specific gene effects for a single type of cancer and represent the hereditary factors such as gastric cancer and melanoma of the Lipizzaner horse breed. There are multiple stages for carcinogenesis recognized in different studies at least four stages are required to define the concept of carcinogenesis, initiation, promotion, malignant conversion, and progression [6,7].

1.2. The transformation of normal human cells into cancer cells

Many theories have explained how the normal cells transformed to become cancerous and develop tumors (also called neoplasm) but it is still a debatable matter today. The neoplasm essentially came as a consequence of abnormal growth of tissue

with uncoordinated characteristics that differ from the normal tissue, which can include benign tumors and malignant (invasive) cancers.

Determine the differences between benign and malignant tumors required to run several lab diagnosis methods such as imaging tests, endoscopic exams, genetic tests, and tumor biopsies by the pathologist to disclose the structure and morphology of the tissue borders, speed of growth, invasion properties, and recurrences. For instance, benign tumors can't invade other organs in most cases and are characterized by slow growth and almost no medical complications. However, the malignant tumors spread from "'their primary location", become more metastasized, uncontrollable, fast growth with irregular borders, and cause medical complications that require intensive and various medical treatments [8,9].

Cancer is defined as a genetic disease with unique characteristics acquired by the accumulation of various and multiple mutations within cells undergoing cancer cell transformation. These alterations could be genetic and epigenetic both of them represent an essential part of tumorigenesis. The induction of genetic aberration could be by mutagenic chemicals, UV light, aging, and oxygen radicals, resulting in genomic instability which is described in human cancers as gene amplifications, deletions, insertions, rearrangements, and point mutations. However, epigenetic alterations (epimutations) usually develop from aging and chronic inflammation, bacterial and viral infections, cigarette smoking, and estrogen (*in vitro* culture) as a consequence of various environmental stimuli [10].

1.3. The multistage of carcinogenesis

The tumorigenesis initiation is an early stage of somatic mutations occurring in single or multiple cells within normal tissue. These mutated cells pass the changes to their daughter cells to develop cancer cells and then start to intensive proliferate rate to form selective clonal expansion of these selective mutated cells, as part of the second stage of tumor promotion.

At the malignant stage, the selective mutated cells start to express another mutation to form another malignant phenotype with the maintenance and development of its malignancy (**Figure** 1) [7,11–14].

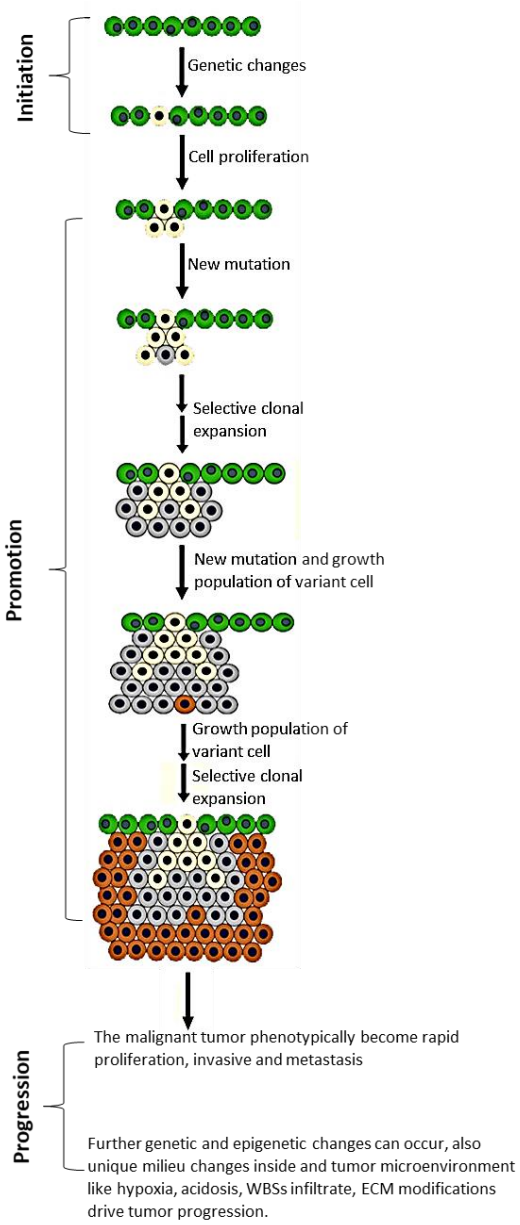

Figure 1. Schematic representation of the multistage process of carcinogenesis

1.4. Tumor microenvironment and cancer progression

Understating the multiple stages of tumorigenesis at the cellular level as consequences of molecular change accumulation, contribute to developing unique features by allowing cancer cells to manifest autonomous proliferation, apoptosis resistance, invasiveness, immune system evasiveness, immortality, and metastasis. In addition, the impact of stromal components on the tumor microenvironment (TME) including their interactions with tumor cells shapes the most suitable environment for cancer development [15].

The harbors components of the tumor microenvironment (TME) mainly from various stromal cells such as cancer-associated fibroblasts (CAFs), myeloid-derived suppressor cells (MDSCs), myofibroblasts, endothelial cells, neutrophils, macrophages, and other innate and adaptive immune cells, and adipocytes, Beside the extracellular matrix (ECM).

The interaction between intratumoral and stromal cells plays a major role in tumorigenesis regulations of aggressiveness. However, the normal tissues surrounding this complex structure the of tumor also act as an essential part by supporting the cancer cells with nutrients, gas exchange, and metabolites regulations for growth to maintain the tissue homeostasis. In another hand, the extracellular matrix (ECM) is mainly created by cancer-associated fibroblasts (CAFs) to support the structure of the tumor and facilitate other biological properties such as proliferation, invasion, and metastasis. But regarding the EMC composition is usually built from various macromolecules, mostly structural proteins working as scaffolds such as collagens, glycoproteins, proteoglycans, and polysaccharides. Studies suggested the importance of TME components to overcome the acidic environment, and lack of oxygen supply, and organize these complex elements to induce angiogenesis and increase the oxygen and nutrient supply, in addition, to metabolic waste removal [15–19].

1.5.The Warburg Effect past and present

Otto Warburg in 1924 found in the contrast to the most normal tissues. There are three metabolic properties in the culture tumor tissues accompanied by an increase in the consumption of glucose rate in harmony with a high rate of lactate secretion. This phenomenon occurs even with oxygen present (aerobic glycolysis), which most cancer cells depend on this phenomenon is called “the Warburg effect”. Unlike normal cells essentially rely on mitochondrial oxidative phosphorylation to generate the demand energy for cellular processes. Knowing that hypoxia does the same elsewhere not just in tumors. However, Warburg’s analysis is still unclear to determine the exact proportion between glycolysis and oxidative phosphorylation (OXPHOS) in cancer cells [20,21]. Otto Warburg defined aerobic glycolysis as an inefficient way to produce energy or as unconventional metabolism presented by tumor cells [22]. But this raises many questions first why cancer cells do proliferate in a less efficient

way for ATP production. From the 1920s until today was extensive study about Warburg Effect, and scientists proposed different hypotheses to understand the functions of the Warburg effect related to ATP, biosynthesis process, ROS (Reactive Oxygen Species), acidification, and recently acetylation [23,24].

All these metabolic pathways are responsible for the activation of oncogenic signals. But the high glucose uptake, which is converted to lactate doesn't provide a sufficient amount of carbon for these pathways because carbon is secreted as waste to extracellular space. Thus if aerobic glycolysis on the Warburg effect concept supports anabolic processes it should be done indirectly. Meaning all these biosynthetic pathways that branch from the glycolysis pathway builds a large pool of intermediates metabolites. However, the study suggested on over 80 non-small cell lung cancer (NSCLC) - cell lines that, the rate of nutrient consumption/secretion varied greatly, with glucose consumption being six to seven fold higher and lactate secretion being fifteen fold higher, which was concluded as a non-related Warburgian form of metabolism [25]. Other evidence proved the importance of mitochondrial activity for cancer cell proliferation in lung and brain tumors *in vivo* studies by using a ^{13}C stable isotope, which suggested the activity of both glycolysis and TCA cycle in the tumor tissues to promote cell proliferation [26,27].

In conclusion, it can't be said that occurs of aerobic glycolysis as Otto Warburg's concept as symptoms of oxidative metabolism impairment [28]. Because it does not predict the impairment of oxidative metabolism. Hence, extrapolating this conclusion, even in tumors where pyruvate oxidation is suppressed and lactate is produced, the cells can still rewire their mitochondrial metabolism to produce other metabolic byproducts and intermediates that are important for biosynthesis [20].

1.6. Cancer cells metabolism

Cancer cell metabolism plays a hallmark of tumorigenesis and is a direct outcome of genetic mutations followed by metabolic enzyme changes to promote malignant transformation [29–31].

1.6.1. The Glycolysis/TCA cycle intermediates for biosynthesis and NADPH production

Both glucose and amino acids are essential nutrients for cancer cells and are abundant in the extracellular fluids that supply mammalian organisms or in cell culture media for *in vitro* studies. This allows cells to obtain the necessary nutrients that support the survival and biosynthetic demands for cell proliferation [21,32]. In the past several decade's clinicians and scientists became interested in the connection between cellular glucose metabolism and tumor progression, showing that in normal cells and tissues, glucose is catabolized to generate pyruvate and ATP through the glycolysis pathway. However, pyruvate in oxygenated cells involves three relevant processes via the TCA cycle, glycolysis, and electrons transfer phosphorylation to generate 36 molecules of ATP from each glucose molecule [21,33,34]. Whereas, the Warburg effect, characterized by the preferential use of aerobic glycolysis in cancer cells, is capable of providing sufficient energy for cell proliferation. This is despite the fact that the metabolism of glucose to lactate through aerobic glycolysis generates only 2 ATPs per molecule of glucose [21] (**Figure** 1).

Thus helping to capture the glucose and use a significant fraction of it to facilitate other pathways and NADPH production such as the pentose phosphate pathway for ribonucleotide synthesis and serine biosynthesis from glycolysis and glutaminolysis pathways via 3-phosphoglycerate (3-PG). Followed by a one-carbon metabolism cycle to engage in purine and glutathione biosynthesis and glycine synthesis, phospho-glycerol synthesis for glycerolipids, hexosamine pathway for protein glycosylation and generates glycogen as glucose storage [35–37]. However, most cancer cells use the majority of glucose and converted it to pyruvate, which most of it is converted to lactate via lactate dehydrogenase and achieves a maximum rate of glycolysis and releasing NAD+ from NADH [23,38] (**Figure** 1).

Under nutrients deprivation a stress condition for the cells as a consequence of upregulation of glucose metabolism via glycolysis and induce vulnerability to ROS - induced cell death [39,40]. But if the cancer cells suffer hypoglycemia would increase energetic stress, thus resulting in selective cytotoxicity [41]. On the other side, the cancer cell undergoes a complex metabolic mode, which is more frequently changeable depending on how severe the stress conditions are, to find another strategy

for survival. Interestingly, under these circumstances oxidative stress, decreased ATP production [42]. The decline of NADPH, and induce intracellular ROS, cancer cells start to activate adenosine monophosphate-activated protein kinase (AMPK) which works as a metabolite-sensor for ATP levels, which leads to inhibit fatty acid synthesis (FAS) and NADPH consumption will decrease by AMPK, whilst induce fatty acid oxidation (FAO) will increases the flux from malate to pyruvate by AMPK and generating NADPH. Besides, another way to generate NADPH by activation of isocitrate transformation to alpha-ketoglutarate (α-KG) via isocitrate dehydrogenase 1 (IDH1). All these processes lead to minimizing intracellular ROS activity and cell death due to glucose starvation [35] (**Figure** 1).

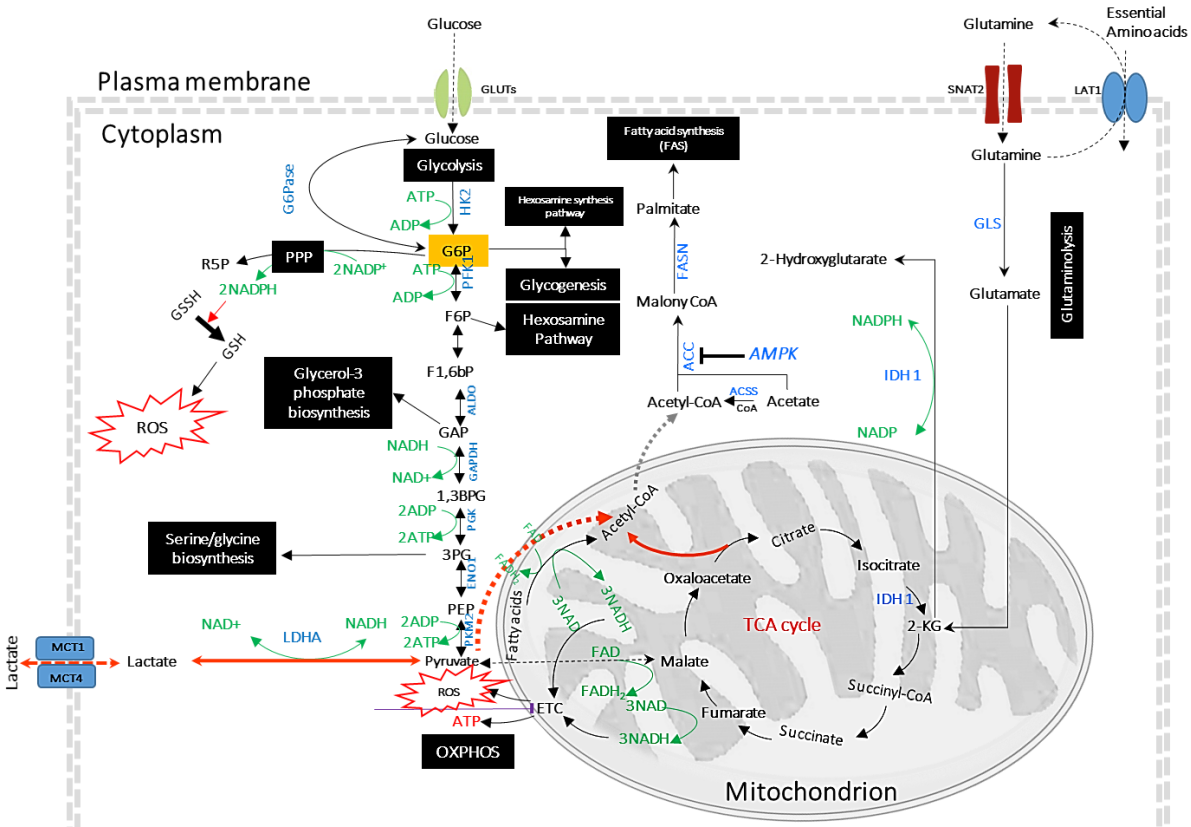

Figure 2. Glycolysis/TCA connection as intermediates for biosynthesis and NADH production from glucose on cancer cells metabolism; GLUT1, glucose transporter 1; SNAT2, glutamine transporter; G6P, glucose-6-phosphate; F6P, fructose-6- phosphate; F1,6 bP, fructose-1,6-biphosphate; GA-3P, glyceraldehyde 3-phosphate; 1,3BPG, 1,3-biphosphoglycerate; 3PG, 3-phosphoglycerate; PEP, phosphoenolpyruvate; PPP, pentose phosphate pathway; R5P, ribose 5-phosphate; GSSH, glutathione persulfide; GSH, glutathione; ROS, reactive oxygen species; GLS, glutaminase; HK2, Hexokinase 2; PFK1, Phosphofructokinase-1; G6Pase, Glucose 6-phosphatase; Aldo, aldolase; GAPDH, glyceraldehyde 3-phosphate dehydrogenase; PGK, phosphoglycerate kinase; Eno1, enolase-1; PKM2, pyruvate kinase M2; LDH-A, lactate dehydrogenase A; PDH, pyruvate

dehydrogenase; IDH 1, isocitrate dehydrogenase 1; ACC, acetyl-CoA carboxylases; ACSS2, cytoplasmic acetyl-CoA synthetase; FASN, fatty acid synthase; ACSS2, acetyl-CoA synthetase 2; PDH, pyruvate dehydrogenase; PDK1, pyruvate dehydrogenase kinase 1; ACLY, ATP-citrate lyase; MCT1, monocarboxylate transporter 1; ATP, adenosine tri-phosphate; ADP, adenosine di-phosphate; NADP/NADPH, nicotinamide adenine dinucleotide phosphate; NAD, nicotinamide adenine dinucleotide; FAD/$FADH_2$, flavin adenine dinucleotide; ETC, electron transport chain; AMPK, adenosine monophosphate-activated protein kinase; OXPHOS, oxidative phosphorylation; MCT2/4, monocarboxylate transporter 2/4; LAT1, L-type amino acid transporter 1.

1.6.2. Glutamine metabolism

Over the past six decades, researchers used culture cell lines as a robust tool for cancer biology studies, and the importance of supplying exogenous nutrients in culture media for cell lines proliferation such as glucose and other amino acids. There are two main groups of amino acids: essential amino acids (EAAs) and nonessential amino acids (NEAAs), EAAs are 9 amino acids and cannot be synthesized by human cells such as histidine, threonine, valine, methionine, lysine, leucine, tryptophan, phenylalanine and isoleucine. However, NEAAs are 11 amino acids that cells can synthesize by *de novo* biosynthesis such as aspartate, glycine, alanine, proline, arginine, glutamate, asparagine, cysteine, glutamine, tyrosine, and serine. Six of them are conditionally essential including glutamine, glycine, arginine, cysteine, proline and tyrosine, because of the pathological or physiological conditions, besides, the organismal level or cell types [43]. Several recent reviews and studies focus on the roles of NEAAs on cancer progression for potential therapy, and one of the important NEAAs is glutamine, which is defined as a second nutrient and fuel for cancer cells. It is abundant in extracellular fluids, plasma, and skeletal muscle and is classified as a conditional amino acid. The glutamine plays a major role in reprogramming cancer cells' metabolism to sustain cell biosynthetic processes, maintain energy demands, and redox homeostasis. The fundamental roles of glutamine are involved by serving as the source of carbon and nitrogen to support the TCA cycle anaplerosis, glutathione production, and lipids and nucleotides synthesis [44].

Glutamine is connected with the TCA cycle through α-ketoglutarate for generating NADH and FADH2 leading to ATP production via the electron transport chain (ETC). In addition, building blocks of intermediates macromolecules support *de novo* biosynthesis and gluconeogenesis. However, under stress conditions such as hypoxia and mitochondria defectiveness, the glutamine-derived α-ketoglutarate is converted to isocitrate by activation of isocitrate dehydrogenase via reductive carboxylation and then converted to malate which generates NADPH and lipid biosynthesis to support cells proliferation and survival [45–47]. Also, glutamine-derived glutamate contributes to glutathione in a secondary way, which starts by importing cystine from extracellular space coupled with an efflux of glutamate via cystine transporter (XCT) (gene name SLC7A11) into the cell, then cystine is converted into cysteine, and both glycine and cysteine support to generate glutathione [48] (**Figure** 2).

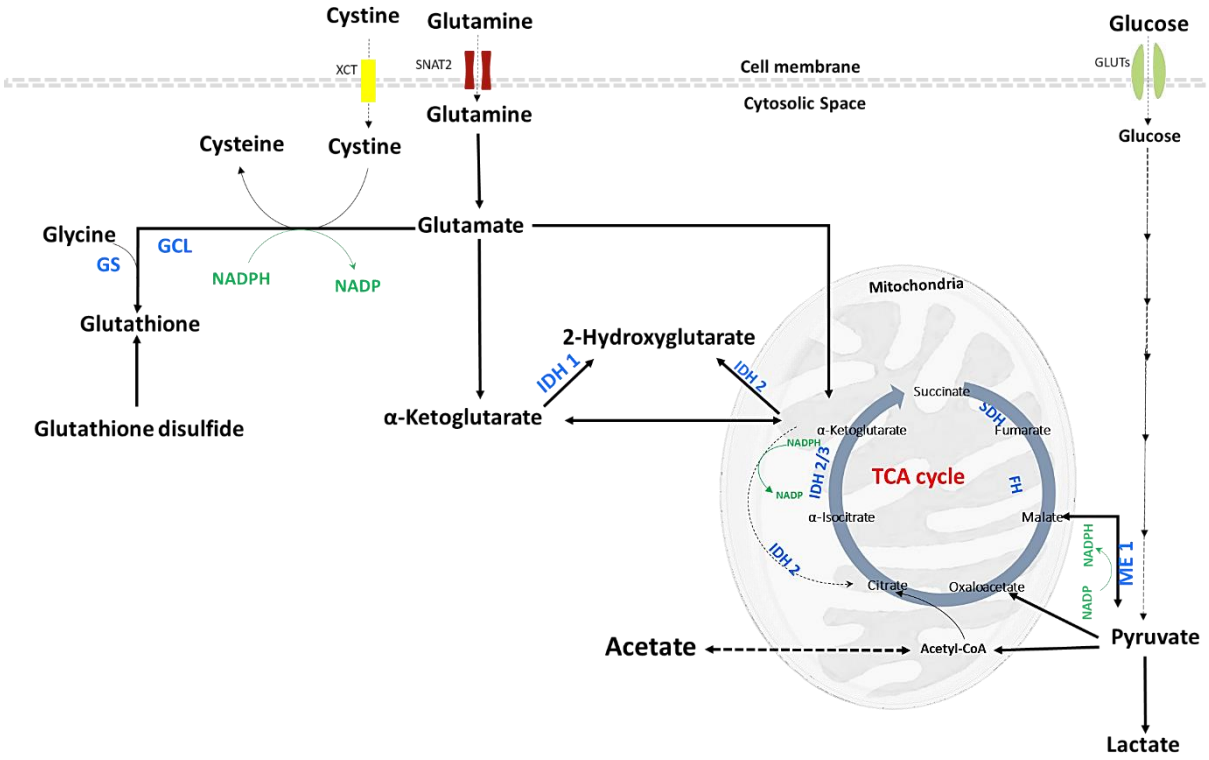

Figure 3. Glutamine metabolism as intermediates for biosynthesis and NADH production on cancer cells; GLUT1, glucose transporter 1; SNAT2, glutamine transporter; IDH 1/2/3, isocitrate dehydrogenase 1/2/3; ME 1, NADP-dependent malic enzyme 1; SDH, Succinate dehydrogenase; FH, fumarate hydratase; XCT, cystine transporter; GS, glutathione synthetase; GCL, glutamate-cysteine ligase.

Another aspect of glutamine metabolism in cancer cells has an effect on cell mitochondrial morphology and glutaminase 1 (GLS1), whereas GLS 1 is working as a metabolite-sensor of glutamine availability. As a result glutamine derivative in cancer cells, leads to a significant increase in reactive oxygen species (ROS) which subsequently damages the structure and function of mitochondria. To counteract this, mitochondria undergo fusion as a strategy to maximize efficiency by diluting damaged mitochondrial proteins and repair damage to preserve the integrity of mitochondrial DNA. Three GTPases, mitofusin 1 (MFN1), mitofusin 2 (MFN2), and optic atrophy 1 (OPA1) have been identified as being involved in this process. However, the molecular mechanisms by which the signal of glutamine shortage is sensed and transmitted to maintain the quality of mitochondria remains to be fully understood [49].

1.6.3. Non-Essential Amino Acids metabolism

Another NEAA, that takes researchers' attention in cancer cells' metabolism is serine, which is classified as the center hub of building blocks of cellular macromolecules through specific metabolic reprogramming and anabolic pathways to maintain redox balance, amino acids synthesis (glycine and cysteine), phospholipids production (phosphatidylserine), the donation to one-carbon units via folate pathway to accelerate cell proliferation and growth. Therefore many tumors rely on serine availability in extracellular space. The serine deprivation *in vitro* and *in vivo* studies showed inhibition of cancer cell proliferation and tumor growth [50–52].

De novo serine biosynthesis takes part from glycolysis, especially from 3-phosphoglycerate and converted to 3-phosphohydroxypyruvate via phosphoglycerate dehydrogenase (PHGDH) [53], the phosphoserine aminotransferase (PSAT1) and phosphoserine phosphatase (PSPH) enzymes convert 3-phosphohydroxypyruvate to serine than to glycine via serine hydroxymethyltransferase 1 and 2 (SHMT 1,2).

This provides a relevant relation of serine, and glycine to one-carbon metabolism to tumor metabolism [54,55]. In hypoxia, the *de novo* serine biosynthesis will induce all activity of enzymes mentioned above and overexpress phosphoglycerate dehydrogenase (PHGDH) for some cancers. For instance, a recent

study on breast cancers suggested that the main factor for inducing phosphoglycerate dehydrogenase (PHGDH) expression is hypoxia and there was a positive correlation of expression between HIF target genes and phosphoglycerate dehydrogenase (PHGDH) [56]. Interestingly, when apoptosis occurs, the PHGDH transcription is inhibited by p53 and minimizes the serine synthesis reactions [57].

The intracellular aspartate is critical for biosynthetic reactions and maintains redox statue, despite poor uptake of aspartate from extracellular space, most of the aspartate is driven by glutamine catabolism through mitochondria. It is required to generate aspartate by glutamine entering the TCA cycle as α-ketoglutarate (α-KG) two critical enzymes including glutaminases (GLSs) [58]. Another study revealed mitochondrial glutamine transporter encodes by the SLC1A5 gene allow glutamine enters the mitochondria for mitochondrial glutaminolysis. However, both ways that generate α-ketoglutarate (α-KG) generate amine groups from NH4+ via glutamate dehydrogenase or aspartate, aspartate biosynthesis from glutamine in cancer cells is known to occur through the action of the enzyme glutaminase (GA), which converts glutamine into α-ketoglutarate (α-KG). The conversion of glutamate to α-KG is then catalyzed by either glutamate dehydrogenase (GDH) or glutamate-oxaloacetate transaminase (GOT). This metabolic pathway is frequently elevated in cancer cells, which have a heightened dependence on glutamine as an energy source [59,60]. Mitochondrial impairment is a common feature in cancer cells and the inhibition of the electron transport chain (ETC) is correlated to aspartate level as a limiting metabolite for cancer cell proliferation under hypoxia [61]. Meaning, from the recent study, that under low concentration of oxygen leads to ETC inhibition and regulates the cellular aspartate level by inducing aspartate/glutamate transporter SLC1A3, therefore the limitation of aspartate at hypoxia leads to limit tumor growth [62].

1.6.4. Branched-Chain Amino Acid (BCAA) Metabolism

The branched-chain amino acids (BCAAs) are essential amino acids and play an important role in cell proliferation and survival mechanisms but the mechanism is still unclear. BCAAs cannot be synthesized by organisms, which are obtained via exogenous sources [63]. BCAAs enter the cells via sodium ion and pH-independent

L-type amino acid transporters SLC7. The LAT1 (SLC7A5) has a high affinity for importing BCAAs and other EAAs such as, phenylalanine, tryptophan, tyrosine, and histidine and efflux of intracellular components (e.g. tyrosine, histidine, and glutamine). However, LAT1 (SLC7A5) is pH-dependent, meaning the activity of BCAAs transporter depends on the environment pH, inducing its activity at neutralpH and becoming lower in an acidic environment [64,65]. Intracellular catabolism of branched-chain amino acids (BCAAs) involves their conversion to branched-chain α-keto acids (BCKAs) such as α-ketoisocaproate (KIC), α-keto-β-methylvalerate (KMV), and α-ketoisovalerate (KIV). This process is catalyzed by branched-chain amino acid transaminases (BCATs), which facilitate the transfer of the amino group from BCAAs to α-ketoglutarate (α-KG) and the concomitant production of glutamate. Then the BCKAs are metabolized by the branched-chain α-ketoacid dehydrogenase complex (BCKDC or BCKDH complex) into isobutyryl-CoA, α-methylbutyryl-CoA and isovaleryl-CoA via multiple enzymatic reactions to achieve final products acetoacetate, acetyl-CoA and succinyl-CoA [66].

In humans, there are two groups of BCAA transaminases, one located in the cytoplasm called BCAT1 and another called BCAT2, which are located in mitochondria, however, both of them have the same role to generate α-ketoglutarate (α-KG) and synthesize glutamate [67].

A recent study suggested that PDAC and HPDE cell lines are required a carbon source from BCAAs for lipid biosynthesis via branched-chain aminotransferases 2 (BCAT2) or branched-chain keto acid dehydrogenase E1 subunit alpha (BCKDHA). After the knockdown of these enzymes, the proliferation of the PDAC cell line was suppressed. However, the HPDE cell line was induced showing no effect on pancreatic cancer and making the role of BCAA more ambiguous [68]. In addition, a recent study revealed that under hypoxia the BCAAs transporter LAT1 (SLC7A5) was upregulated by both HIF-1 and HIF-2 in glioblastoma cells and induced BCAT1 expression and therefore induce cells proliferation [69].

2. *In vitro* models for metabolomics research

Metabolomics is an emerging powerful tool and analytical profiling technology used in biomedical research, for providing information

about the characterization of the biological system of different biological samples (e.g. serum, urine, cells, and tissues), for biomarker discovery, altered metabolic pathways identification, diagnosis, and toxicity assay. Metabolomics presents a window on metabolic regulations by both high-throughput analytical chemistry and multivariate data analysis combination [70,71]. *In vitro* cell culture metabolomics studies of both 2D and 3D types face many challenges to their quality, for that required accuracy design for experiments processes, starting from cell culture normalization to metabolome extraction [72,73].

In addition, 2D monolayer cell culture is easy for data normalization than the 3D cell spheroid technique because of the number, size, and morphology of the cells. However, 3D has an advantage by mimicking the tumor complexity *in vivo* [73]. Nevertheless, both provide precise information about the changes in metabolic pathways.

3. 1D ^{1}H NMR as Tool to Investigate *in vitro* research

NMR-based metabolomics using high-resolution NMR spectroscopy and chemometric methods which has been proven to be an important technology giving highly reproducible results through time and laboratories. In addition, this method is providing structural and quantitative information [74]. Its application to the cell culture has been confirmed as an efficient technique to understand the effect of different chemical and physical factors, gene function, and medical diagnosis.

The NMR signals are directly proportional to the molecule concentration and each metabolite manifests several spectroscopic handles and gives us the ability to measure these signals for each metabolite [74], followed by data preprocessing applying wide range of statistical tools, and multivariate analysis. Moreover, for intracellular metabolome acquisition by 1H NMR, it require for cells count to obtain a reasonable and quantifiable signal should be several million as recommended [75].

4. The terminology of hypoxia, normoxia, and hyperoxia - in cell biology

In the fifties, the term tumor hypoxia was hardly known, as the rareness of publications devoted to hypoxia. Start by an influencing article published by Gray et al, in 1953 and 1955 revealed the importance of oxygen tension on radiotherapy treatment, which more effective under well-oxygenated cancer cells. Meaning,

from the periphery and the center of each tumor, there is a falling oxygen tension gradient, which is measured by the degree of anoxia of the cells, not by the degree of hypoxia. Thereby this phenomenon got the attention of radiobiologist and radiotherapist communities to the importance of oxygen concentration [76,77].

In 1981 Dorland's Medical Dictionary defined "hypoxia" as a reduction of oxygen levels, which is much lower than physiological levels, even with sufficient supply from blood circulation to the tissues [78]. Because of that, in arise the problem to recognize the difficulties of *in vitro* model and oxygen tension to mimic the exact oxygen tensions that occur *in vivo* [79–82].

Furthermore, Peter Ebbesen and colleagues proposed a method to address technical challenges in measuring oxygen flow to cells. They recommended using metabolic state measurements, particularly glycolysis, which is directly influenced by oxygen concentration [83].

Moreover, the anaerobic metabolism in pathological and healthy situations isn't identical. Hence to that evidence, from the medical point of view, by making *in vivo* a standard for oxygen concentration should be measured and found in normal body tissue during the pathological and non-pathological state as normoxia term. The hyperoxia term usually doesn't exist *in vivo* studies because of the lack of atmospheric oxygen concentration of 21% within human tissues, except for some areas of the human body exposed to this concentration such as the middle ear site and skin upper layer (dermis).

However, *in vitro* studies always carry out the experiments in hyperoxia. Therefore, using hypoxia, normoxia, and hyperoxia terminology for *in vitro* research should be classified as discriminatory factors in the medium. Besides all, *in vitro* cell, and cultivation studies should take attention to the most relevant tension oxygen in the culture medium since the culture medium has no perfusion of blood, which imitated the *in vivo* condition [84].

In, the 1990s, the beginning identification of tumor hypoxia markers for cancer therapy on excised rodent tissue [85], and showed a positive correlation between the severity of human tumors and tumor cells' malignancy to hypoxia [86,87]. Many studies have been published since then on tumor hypoxia, but arguments still arise on using the term normoxia as the normal oxygen level in laboratories, it's about 20–21% oxygen (160 mmHg). In addition, the 20-21% oxygen concentration is a normal

atmospheric pressure, which is much higher in comparison to peripheral tissue oxygenation. For instance, the oxygen concentration at lung alveoli is about 14.5%, when it reaches the arterial blood is approximately 9.5%, and on arrival to the venous end of circulation is approx. 6.5%. Thus, the median of peripheral tissues oxygen levels is between (3.4% - 6.1%) [88,89].

In addition, the term hypoxia should be observed, because there are differences between physiological and pathological hypoxia. For instance, a study of the expression of HIF1α and HIF1β from 0% to 20% oxygen revealed that 0.5% oxygen was the highest level of expression and 1.5–2% oxygen was the lowest, and significantly low above 4% oxygen (91). Thereby, the effective response to maintain homeostatic mechanisms by reversing to the preferred oxygen level is called physiological hypoxia, and its oxygen concentration range is varied depending on tissue type [89].

However, pathological hypoxia is the opposite of physiological hypoxia, because the homeostatic mechanisms required for oxygen deprivation aren't effective and can't be reversed, that's why pathological hypoxia positively correlated with tumor progression by inducing the angiogenesis mechanisms to increase the oxygen supply to the tumor.

There is no absolute level of oxygen for defining pathological hypoxia depending on the tissue of origin. This argument allowed multiple studies for almost 12 human tumor types carried out on 2257 patients, in comparison to their normal tissue measurement suggesting that the median range of oxygen concentration in human tumors was from 0.3% to 4.2% (2–32 mmHg), and mostly below 2%. Whereas were almost certain that, pathological hypoxia occurs at lower than 1% (7.5 mmHg). Besides, the median range of oxygen concentration in normal tissues was from 3.4% to 6.8% and the average was 6% [87,90,91].

Regarding the term hyperoxia, several studies refer to hyperoxia *in vitro* models as an anti-cancer effect and as a reversible effect of hypoxia-induced radioresistance (RR) and therefore inhibit tumor growth and recover homeostasis in the tumor microenvironment to normoxia [92] at 85% O_2 [93], some used 90% O_2 [92] and others 60% O_2 [92,94–96] on various cell lines. Other studies determined the term hyperoxia at 95% O_2 [97,98]. Despite the anti-cancer effect of hyperoxia and different oxygen concentrations for this term showing, no particular laboratory standards.

However, since already defined terms hypoxia and normoxia by scientists and physiopathologist (also clinicians). Based on this, the 21% O_2 for *in vitro* studies is much higher than human peripheral tissue oxygenation. Due to this fact, using 21% O_2 as normoxia as standard *in vitr*o research models is misrepresented, and should be referred to as hyperoxia [99].

5. References

1. Cao, Y. Tumorigenesis as a Process of Gradual Loss of Original Cell Identity and Gain of Properties of Neural Precursor/Progenitor Cells. *Cell & Bioscience* **2017**, *7*, 61, doi:10.1186/s13578-017-0188-9.
2. Hanahan, D.; Weinberg, R.A. Hallmarks of Cancer: The Next Generation. *Cell* **2011**, *144*, 646–674, doi:10.1016/j.cell.2011.02.013.
3. Cancer Statistics - NCI Available online: https://www.cancer.gov/about-cancer/understanding/statistics (accessed on 13 December 2022).
4. Chang-Lin, J.-E.; Burke, J.A.; Peng, Q.; Lin, T.; Orilla, W.C.; Ghosn, C.R.; Zhang, K.-M.; Kuppermann, B.D.; Robinson, M.R.; Whitcup, S.M.; et al. Pharmacokinetics of a Sustained-Release Dexamethasone Intravitreal Implant in Vitrectomized and Nonvitrectomized Eyes. *Investigative Ophthalmology & Visual Science* **2011**, *52*, 4605–4609, doi:10.1167/iovs.10-6387.
5. Baba, A.I.; Câtoi, C. Chapter 2 - Carcinogenesis. In *CARCINOGENESIS*; The Publishing House of the Romanian Academy, 2007.
6. Das, S.; Kundu, M.; Jena, B.C.; Mandal, M. Chapter 25 - Causes of Cancer: Physical, Chemical, Biological Carcinogens, and Viruses. In *Biomaterials for 3D Tumor Modeling*; Kundu, S.C., Reis, R.L., Eds.; Materials Today; Elsevier, 2020; pp. 607–641 ISBN 978-0-12-818128-7.
7. Weston, A.; Harris, C.C. Multistage Carcinogenesis. *Holland-Frei Cancer Medicine. 6th edition* **2003**.
8. Patel, A. Benign vs Malignant Tumors. *JAMA Oncology* **2020**, *6*, 1488, doi:10.1001/jamaoncol.2020.2592.
9. Hahn, W.C.; Counter, C.M.; Lundberg, A.S.; Beijersbergen, R.L.; Brooks, M.W.; Weinberg, R.A. Creation of Human Tumour Cells with Defined Genetic Elements. *Nature* **1999**, *400*, 464–468, doi:10.1038/22780.
10. Takeshima, H.; Ushijima, T. Accumulation of Genetic and Epigenetic Alterations in Normal Cells and Cancer Risk. *npj Precis. Onc.* **2019**, *3*, 1–8, doi:10.1038/s41698-019-0079-0.
11. Watson, A.Y.; Bates, R.R.; Kennedy, D. *Assessment of Carcinogenicity: Generic Issues and Their Application to Diesel Exhaust*; National Academies Press (US), 1988;
12. Weiss, R.A. Multistage Carcinogenesis. *Br J Cancer* **2004**, *91*, 1981–1982, doi:10.1038/sj.bjc.6602318.

13. Thompson, T.C.; Southgate, J.; Kitchener, G.; Land, H. Multistage Carcinogenesis Induced by Ras and Myc Oncogenes in a Reconstituted Organ. *Cell* **1989**, *56*, 917–930, doi:10.1016/0092-8674(89)90625-9.
14. Kulesz-Martin, M.; Ouyang, X.; Barling, A.; Gallegos, J.R.; Liu, Y.; Medler, T. Multistage Carcinogenesis: Cell and Animal Models. In *Carcinogenesis*; Elsevier Inc., 2018; Vol. 7–15, pp. 11–35 ISBN 978-0-08-100601-6.
15. Ribeiro Franco, P.I.; Rodrigues, A.P.; de Menezes, L.B.; Pacheco Miguel, M. Tumor Microenvironment Components: Allies of Cancer Progression. *Pathol Res Pract* **2020**, *216*, 152729, doi:10.1016/j.prp.2019.152729.
16. Kwon, Y.; Kim, M.; Kim, Y.; Jung, H.S.; Jeoung, D. Exosomal MicroRNAs as Mediators of Cellular Interactions Between Cancer Cells and Macrophages. *Frontiers in Immunology* **2020**, *11*.
17. Neophytou, C.M.; Panagi, M.; Stylianopoulos, T.; Papageorgis, P. The Role of Tumor Microenvironment in Cancer Metastasis: Molecular Mechanisms and Therapeutic Opportunities. *Cancers* **2021**, *13*, 2053, doi:10.3390/cancers13092053.
18. Tsai, M.-J.; Chang, W.-A.; Huang, M.-S.; Kuo, P.-L. Tumor Microenvironment: A New Treatment Target for Cancer. *ISRN Biochem* **2014**, *2014*, 351959, doi:10.1155/2014/351959.
19. Brassart-Pasco, S.; Brézillon, S.; Brassart, B.; Ramont, L.; Oudart, J.-B.; Monboisse, J.C. Tumor Microenvironment: Extracellular Matrix Alterations Influence Tumor Progression. *Frontiers in Oncology* **2020**, *10*.
20. DeBerardinis, R.J.; Chandel, N.S. We Need to Talk about the Warburg Effect. *Nat Metab* **2020**, *2*, 127–129, doi:10.1038/s42255-020-0172-2.
21. Vander Heiden, M.G.; Cantley, L.C.; Thompson, C.B. Understanding the Warburg Effect: The Metabolic Requirements of Cell Proliferation. *Science* **2009**, *324*, 1029–1033, doi:10.1126/science.1160809.
22. Jones, W.; Bianchi, K. Aerobic Glycolysis: Beyond Proliferation. *Frontiers in Immunology* **2015**, *6*.
23. Liberti, M.V.; Locasale, J.W. The Warburg Effect: How Does It Benefit Cancer Cells? *Trends Biochem Sci* **2016**, *41*, 211–218, doi:10.1016/j.tibs.2015.12.001.
24. Patra, K.C.; Wang, Q.; Bhaskar, P.T.; Miller, L.; Wang, Z.; Wheaton, W.; Chandel, N.; Laakso, M.; Muller, W.J.; Allen, E.L.; et al. Hexokinase 2 Is Required for Tumor Initiation and Maintenance and Its Systemic Deletion Is Therapeutic in Mouse Models of Cancer. *Cancer Cell* **2013**, *24*, 213–228, doi:10.1016/j.ccr.2013.06.014.
25. Chen, P.-H.; Cai, L.; Huffman, K.; Yang, C.; Kim, J.; Faubert, B.; Boroughs, L.; Ko, B.; Sudderth, J.; McMillan, E.A.; et al. Metabolic Diversity in Human Non-Small Cell Lung Cancer Cells. *Mol Cell* **2019**, *76*, 838-851.e5, doi:10.1016/j.molcel.2019.08.028.
26. Fan, T.W.; Lane, A.N.; Higashi, R.M.; Farag, M.A.; Gao, H.; Bousamra, M.; Miller, D.M. Altered Regulation of Metabolic Pathways in Human Lung Cancer Discerned by 13C Stable Isotope-Resolved Metabolomics (SIRM). *Molecular Cancer* **2009**, *8*, 41, doi:10.1186/1476-4598-8-41.
27. Maher, E.A.; Marin-Valencia, I.; Bachoo, R.M.; Mashimo, T.; Raisanen, J.; Hatanpaa, K.J.; Jindal, A.; Jeffrey, F.M.; Choi, C.; Madden, C.; et al. Metabolism of [U-13C]Glucose in

Human Brain Tumors in Vivo. *NMR in Biomedicine* **2012**, *25*, 1234–1244, doi:10.1002/nbm.2794.

28. Warburg, O. On the Origin of Cancer Cells. *Science* **1956**, *123*, 309–314, doi:10.1126/science.123.3191.309.
29. Pavlova, N.N.; Thompson, C.B. The Emerging Hallmarks of Cancer Metabolism. *Cell Metab* **2016**, *23*, 27–47, doi:10.1016/j.cmet.2015.12.006.
30. Oliveira, G.L.; Coelho, A.R.; Marques, R.; Oliveira, P.J. Cancer Cell Metabolism: Rewiring the Mitochondrial Hub. *Biochimica et Biophysica Acta (BBA) - Molecular Basis of Disease* **2021**, *1867*, 166016, doi:10.1016/j.bbadis.2020.166016.
31. Jang, M.; Kim, S.S.; Lee, J. Cancer Cell Metabolism: Implications for Therapeutic Targets. *Exp Mol Med* **2013**, *45*, e45–e45, doi:10.1038/emm.2013.85.
32. Ackermann, T.; Tardito, S. Cell Culture Medium Formulation and Its Implications in Cancer Metabolism. *Trends Cancer* **2019**, *5*, 329–332, doi:10.1016/j.trecan.2019.05.004.
33. Xia, L.; Oyang, L.; Lin, J.; Tan, S.; Han, Y.; Wu, N.; Yi, P.; Tang, L.; Pan, Q.; Rao, S.; et al. The Cancer Metabolic Reprogramming and Immune Response. *Molecular Cancer* **2021**, *20*, 28, doi:10.1186/s12943-021-01316-8.
34. Navale, A.M.; Paranjape, A.N. Glucose Transporters: Physiological and Pathological Roles. *Biophys Rev* **2016**, *8*, 5–9, doi:10.1007/s12551-015-0186-2.
35. Hay, N. Reprogramming Glucose Metabolism in Cancer: Can It Be Exploited for Cancer Therapy? *Nat Rev Cancer* **2016**, *16*, 635–649, doi:10.1038/nrc.2016.77.
36. Pan, S.; Fan, M.; Liu, Z.; Li, X.; Wang, H. Serine, Glycine and One-carbon Metabolism in Cancer (Review). *International Journal of Oncology* **2021**, *58*, 158–170, doi:10.3892/ijo.2020.5158.
37. Possik, E.; Al-Mass, A.; Peyot, M.-L.; Ahmad, R.; Al-Mulla, F.; Madiraju, S.R.M.; Prentki, M. New Mammalian Glycerol-3-Phosphate Phosphatase: Role in β-Cell, Liver and Adipocyte Metabolism. *Front Endocrinol (Lausanne)* **2021**, *12*, 706607, doi:10.3389/fendo.2021.706607.
38. DeNicola, G.M.; Cantley, L.C. Cancer's Fuel Choice: New Flavors for a Picky Eater. *Mol Cell* **2015**, *60*, 514–523, doi:10.1016/j.molcel.2015.10.018.
39. Spitz, D.R.; Sim, J.E.; Ridnour, L.A.; Galoforo, S.S.; Lee, Y.J. Glucose Deprivation-Induced Oxidative Stress in Human Tumor Cells. A Fundamental Defect in Metabolism? *Ann N Y Acad Sci* **2000**, *899*, 349–362, doi:10.1111/j.1749-6632.2000.tb06199.x.
40. Aykin-Burns, N.; Ahmad, I.M.; Zhu, Y.; Oberley, L.W.; Spitz, D.R. INCREASED LEVELS OF SUPEROXIDE AND HYDROGEN PEROXIDE MEDIATE THE DIFFERENTIAL SUSCEPTIBILITY OF CANCER CELLS VS. NORMAL CELLS TO GLUCOSE DEPRIVATION. *Biochem J* **2009**, *418*, 29–37, doi:10.1042/BJ20081258.
41. Simons, A.L.; Mattson, D.M.; Dornfeld, K.; Spitz, D.R. Glucose Deprivation-Induced Metabolic Oxidative Stress and Cancer Therapy. *J Cancer Res Ther* **2009**, *5 Suppl 1*, S2-6, doi:10.4103/0973-1482.55133.
42. Schafer, Z.T.; Grassian, A.R.; Song, L.; Jiang, Z.; Gerhart-Hines, Z.; Irie, H.Y.; Gao, S.; Puigserver, P.; Brugge, J.S. Antioxidant and Oncogene Rescue of Metabolic Defects Caused by Loss of Matrix Attachment. *Nature* **2009**, *461*, 109–113, doi:10.1038/nature08268.

43. Choi, B.-H.; Coloff, J.L. The Diverse Functions of Non-Essential Amino Acids in Cancer. *Cancers* **2019**, *11*, 675, doi:10.3390/cancers11050675.
44. Alam, M.M.; Lal, S.; FitzGerald, K.E.; Zhang, L. A Holistic View of Cancer Bioenergetics: Mitochondrial Function and Respiration Play Fundamental Roles in the Development and Progression of Diverse Tumors. *Clinical and Translational Medicine* **2016**, *5*, e3, doi:10.1186/s40169-016-0082-9.
45. Wise, D.R.; Ward, P.S.; Shay, J.E.S.; Cross, J.R.; Gruber, J.J.; Sachdeva, U.M.; Platt, J.M.; DeMatteo, R.G.; Simon, M.C.; Thompson, C.B. Hypoxia Promotes Isocitrate Dehydrogenase-Dependent Carboxylation of α-Ketoglutarate to Citrate to Support Cell Growth and Viability. *Proceedings of the National Academy of Sciences* **2011**, *108*, 19611–19616, doi:10.1073/pnas.1117773108.
46. Mullen, A.R.; Wheaton, W.W.; Jin, E.S.; Chen, P.-H.; Sullivan, L.B.; Cheng, T.; Yang, Y.; Linehan, W.M.; Chandel, N.S.; DeBerardinis, R.J. Reductive Carboxylation Supports Growth in Tumour Cells with Defective Mitochondria. *Nature* **2012**, *481*, 385–388, doi:10.1038/nature10642.
47. Metallo, C.M.; Gameiro, P.A.; Bell, E.L.; Mattaini, K.R.; Yang, J.; Hiller, K.; Jewell, C.M.; Johnson, Z.R.; Irvine, D.J.; Guarente, L.; et al. Reductive Glutamine Metabolism by IDH1 Mediates Lipogenesis under Hypoxia. *Nature* **2012**, *481*, 380–384, doi:10.1038/nature10602.
48. Jiang, J.; Srivastava, S.; Zhang, J. Starve Cancer Cells of Glutamine: Break the Spell or Make a Hungry Monster? *Cancers* **2019**, *11*, 804, doi:10.3390/cancers11060804.
49. Cai, W.-F.; Zhang, C.; Wu, Y.-Q.; Zhuang, G.; Ye, Z.; Zhang, C.-S.; Lin, S.-C. Glutaminase GLS1 Senses Glutamine Availability in a Non-Enzymatic Manner Triggering Mitochondrial Fusion. *Cell Res* **2018**, *28*, 865–867, doi:10.1038/s41422-018-0057-z.
50. Labuschagne, C.F.; van den Broek, N.J.F.; Mackay, G.M.; Vousden, K.H.; Maddocks, O.D.K. Serine, but Not Glycine, Supports One-Carbon Metabolism and Proliferation of Cancer Cells. *Cell Rep* **2014**, *7*, 1248–1258, doi:10.1016/j.celrep.2014.04.045.
51. Maddocks, O.D.K.; Labuschagne, C.F.; Adams, P.D.; Vousden, K.H. Serine Metabolism Supports the Methionine Cycle and DNA/RNA Methylation through De Novo ATP Synthesis in Cancer Cells. *Mol Cell* **2016**, *61*, 210–221, doi:10.1016/j.molcel.2015.12.014.
52. Maddocks, O.D.K.; Berkers, C.R.; Mason, S.M.; Zheng, L.; Blyth, K.; Gottlieb, E.; Vousden, K.H. Serine Starvation Induces Stress and P53-Dependent Metabolic Remodelling in Cancer Cells. *Nature* **2013**, *493*, 542–546, doi:10.1038/nature11743.
53. DeBerardinis, R.J. Serine Metabolism: Some Tumors Take the Road Less Traveled. *Cell Metabolism* **2011**, *14*, 285–286, doi:10.1016/j.cmet.2011.08.004.
54. Possemato, R.; Marks, K.M.; Shaul, Y.D.; Pacold, M.E.; Kim, D.; Birsoy, K.; Sethumadhavan, S.; Woo, H.-K.; Jang, H.G.; Jha, A.K.; et al. Functional Genomics Reveal That the Serine Synthesis Pathway Is Essential in Breast Cancer. *Nature* **2011**, *476*, 346–350, doi:10.1038/nature10350.
55. Amelio, I.; Cutruzzolá, F.; Antonov, A.; Agostini, M.; Melino, G. Serine and Glycine Metabolism in Cancer. *Trends Biochem Sci* **2014**, *39*, 191–198, doi:10.1016/j.tibs.2014.02.004.
56. Samanta, D.; Park, Y.; Andrabi, S.A.; Shelton, L.M.; Gilkes, D.M.; Semenza, G.L. PHGDH Expression Is Required for Mitochondrial Redox Homeostasis, Breast Cancer Stem Cell

Maintenance, and Lung Metastasis. *Cancer Research* **2016**, *76*, 4430–4442, doi:10.1158/0008-5472.CAN-16-0530.

57. Ou, Y.; Wang, S.-J.; Jiang, L.; Zheng, B.; Gu, W. P53 Protein-Mediated Regulation of Phosphoglycerate Dehydrogenase (PHGDH) Is Crucial for the Apoptotic Response upon Serine Starvation. *J Biol Chem* **2015**, *290*, 457–466, doi:10.1074/jbc.M114.616359.
58. Yoo, H.C.; Yu, Y.C.; Sung, Y.; Han, J.M. Glutamine Reliance in Cell Metabolism. *Exp Mol Med* **2020**, *52*, 1496–1516, doi:10.1038/s12276-020-00504-8.
59. Yoo, H.C.; Park, S.J.; Nam, M.; Kang, J.; Kim, K.; Yeo, J.H.; Kim, J.-K.; Heo, Y.; Lee, H.S.; Lee, M.Y.; et al. A Variant of SLC1A5 Is a Mitochondrial Glutamine Transporter for Metabolic Reprogramming in Cancer Cells. *Cell Metab* **2020**, *31*, 267-283.e12, doi:10.1016/j.cmet.2019.11.020.
60. Gorgoglione, R.; Impedovo, V.; Riley, C.L.; Fratantonio, D.; Tiziani, S.; Palmieri, L.; Dolce, V.; Fiermonte, G. Glutamine-Derived Aspartate Biosynthesis in Cancer Cells: Role of Mitochondrial Transporters and New Therapeutic Perspectives. *Cancers* **2022**, *14*, 245, doi:10.3390/cancers14010245.
61. Garcia-Bermudez, J.; Baudrier, L.; La, K.; Zhu, X.G.; Fidelin, J.; Sviderskiy, V.O.; Papagiannakopoulos, T.; Molina, H.; Snuderl, M.; Lewis, C.A.; et al. Aspartate Is a Limiting Metabolite for Cancer Cell Proliferation under Hypoxia and in Tumours. *Nat Cell Biol* **2018**, *20*, 775–781, doi:10.1038/s41556-018-0118-z.
62. Sullivan, L.B.; Luengo, A.; Danai, L.V.; Bush, L.N.; Diehl, F.F.; Hosios, A.M.; Lau, A.N.; Elmiligy, S.; Malstrom, S.; Lewis, C.A.; et al. Aspartate Is an Endogenous Metabolic Limitation for Tumour Growth. *Nat Cell Biol* **2018**, *20*, 782–788, doi:10.1038/s41556-018-0125-0.
63. Neinast, M.D.; Jang, C.; Hui, S.; Murashige, D.S.; Chu, Q.; Morscher, R.J.; Li, X.; Zhan, L.; White, E.; Anthony, T.G.; et al. Quantitative Analysis of the Whole-Body Metabolic Fate of Branched-Chain Amino Acids. *Cell Metab* **2019**, *29*, 417-429.e4, doi:10.1016/j.cmet.2018.10.013.
64. Puris, E.; Gynther, M.; Auriola, S.; Huttunen, K.M. L-Type Amino Acid Transporter 1 as a Target for Drug Delivery. *Pharm Res* **2020**, *37*, 88, doi:10.1007/s11095-020-02826-8.
65. Cosco, J.; Scalise, M.; Colas, C.; Galluccio, M.; Martini, R.; Rovella, F.; Mazza, T.; Ecker, G.F.; Indiveri, C. ATP Modulates SLC7A5 (LAT1) Synergistically with Cholesterol. *Sci Rep* **2020**, *10*, 16738, doi:10.1038/s41598-020-73757-y.
66. Yudkoff, M. Brain Metabolism of Branched-Chain Amino Acids. *Glia* **1997**, *21*, 92–98, doi:10.1002/(SICI)1098-1136(199709)21:1<92::AID-GLIA10>3.0.CO;2-W.
67. Raffel, S.; Falcone, M.; Kneisel, N.; Hansson, J.; Wang, W.; Lutz, C.; Bullinger, L.; Poschet, G.; Nonnenmacher, Y.; Barnert, A.; et al. BCAT1 Restricts AKG Levels in AML Stem Cells Leading to IDHmut-like DNA Hypermethylation. *Nature* **2017**, *551*, 384–388, doi:10.1038/nature24294.
68. Lee, J.H.; Cho, Y.; Kim, J.H.; Kim, J.; Nam, H.Y.; Kim, S.W.; Son, J. Branched-Chain Amino Acids Sustain Pancreatic Cancer Growth by Regulating Lipid Metabolism. *Exp Mol Med* **2019**, *51*, 1–11, doi:10.1038/s12276-019-0350-z.

69. Zhang, B.; Chen, Y.; Shi, X.; Zhou, M.; Bao, L.; Hatanpaa, K.J.; Patel, T.; DeBerardinis, R.J.; Wang, Y.; Luo, W. Regulation of Branched-Chain Amino Acid Metabolism by Hypoxia-Inducible Factor in Glioblastoma. *Cell. Mol. Life Sci.* **2021**, *78*, 195–206, doi:10.1007/s00018-020-03483-1.
70. Manchester, M.; Anand, A. Chapter Two - Metabolomics: Strategies to Define the Role of Metabolism in Virus Infection and Pathogenesis. In *Advances in Virus Research*; Kielian, M., Mettenleiter, T.C., Roossinck, M.J., Eds.; Academic Press, 2017; Vol. 98, pp. 57–81.
71. Moreno-Torres, M.; García-Llorens, G.; Moro, E.; Méndez, R.; Quintás, G.; Castell, J.V. Factors That Influence the Quality of Metabolomics Data in in Vitro Cell Toxicity Studies: A Systematic Survey. *Sci Rep* **2021**, *11*, 22119, doi:10.1038/s41598-021-01652-1.
72. Cuperlović-Culf, M.; Barnett, D.A.; Culf, A.S.; Chute, I. Cell Culture Metabolomics: Applications and Future Directions. *Drug Discov Today* **2010**, *15*, 610–621, doi:10.1016/j.drudis.2010.06.012.
73. Jaroch, K.; Modrakowska, P.; Bojko, B. Glioblastoma Metabolomics—In Vitro Studies. *Metabolites* **2021**, *11*, 315, doi:10.3390/metabo11050315.
74. Keun, H.C.; Ebbels, T.M.D.; Antti, H.; Bollard, M.E.; Beckonert, O.; Schlotterbeck, G.; Senn, H.; Niederhauser, U.; Holmes, E.; Lindon, J.C.; et al. Analytical Reproducibility in 1H NMR-Based Metabonomic Urinalysis. *Chem. Res. Toxicol.* **2002**, *15*, 1380–1386, doi:10.1021/tx0255774.
75. Aranibar, N.; Reily, M.D. NMR Methods for Metabolomics of Mammalian Cell Culture Bioreactors. In *Animal Cell Biotechnology: Methods and Protocols*; Pörtner, R., Ed.; Methods in Molecular Biology; Humana Press: Totowa, NJ, **2014**; pp. 223–236 ISBN 978-1-62703-733-4.
76. Gray, L.H.; Conger, A.D.; Ebert, M.; Hornsey, S.; Scott, O.C. The Concentration of Oxygen Dissolved in Tissues at the Time of Irradiation as a Factor in Radiotherapy. *Br J Radiol* **1953**, *26*, 638–648, doi:10.1259/0007-1285-26-312-638.
77. Thomlinson, R.H.; Gray, L.H. The Histological Structure of Some Human Lung Cancers and the Possible Implications for Radiotherapy. *Br J Cancer* **1955**, *9*, 539–549, doi:10.1038/bjc.1955.55.
78. Friel, J.P. *Dorland's Illustrated Medical Dictionary (26th Edition)*; 26th edition.; Saunders, W B Co, **1974**;
79. Amellem, O.; Sandvik, J.A.; Stokke, T.; Pettersen, E.O. The Retinoblastoma Protein-Associated Cell Cycle Arrest in S-Phase under Moderate Hypoxia Is Disrupted in Cells Expressing HPV18 E7 Oncoprotein. *Br J Cancer* **1998**, *77*, 862–872, doi:10.1038/bjc.1998.143.
80. Froese, G. The Respiration of Ascites Tumour Cells at Low Oxygen Concentrations. *Biochim Biophys Acta* **1962**, *57*, 509–519, doi:10.1016/0006-3002(62)91158-7.
81. Enholm, B.; Paavonen, K.; Ristimäki, A.; Kumar, V.; Gunji, Y.; Klefstrom, J.; Kivinen, L.; Laiho, M.; Olofsson, B.; Joukov, V.; et al. Comparison of VEGF, VEGF-B, VEGF-C and Ang-1 MRNA Regulation by Serum, Growth Factors, Oncoproteins and Hypoxia. *Oncogene* **1997**, *14*, 2475–2483, doi:10.1038/sj.onc.1201090.

82. Sonnewald, U.; Wang, A.Y.; Schousboe, A.; Erikson, R.; Skottner, A. New Aspects of Lactate Metabolism: IGF-I and Insulin Regulate Mitochondrial Function in Cultured Brain Cells during Normoxia and Hypoxia. *Dev Neurosci* **1996**, *18*, 443–448, doi:10.1159/000111439.
83. Ebbesen, P.; Toth, F.D.; Villadsen, J.A.; Nørskov-Lauritsen, N. In Vitro Interferon and Virus Production at in Vivo Physiologic Oxygen Tensions. *In Vivo* **1991**, *5*, 355–358.
84. Ebbesen, E.O.P., Juliana Denekamp, Bo Littbrand, Jorma Keski-Oja, Arne Schousboe, Ursula Sonnewald, Øystein Åmellem, Vladimir Zachar, Peter Hypoxia, Normoxia and Hyperoxia: Terminology for Medical In Vitro Cell Biology. *Acta Oncologica* **2000**, *39*, 247–248, doi:10.1080/028418600430888.
85. Tatum, J.L. Hypoxia: Importance in Tumor Biology, Noninvasive Measurement by Imaging, and Value of Its Measurement in the Management of Cancer Therapy. *International Journal of Radiation Biology* **2006**, *82*, 699–757, doi:10.1080/09553000601002324.
86. Jiang, J.; Tang, Y.; Liang, X. EMT: A New Vision of Hypoxia Promoting Cancer Progression. *Cancer Biology & Therapy* **2011**, *11*, 714–723, doi:10.4161/cbt.11.8.15274.
87. Vaupel, P.; Höckel, M.; Mayer, A. Detection and Characterization of Tumor Hypoxia Using PO2 Histography. *Antioxidants & Redox Signaling* **2007**, *9*, 1221–1236, doi:10.1089/ars.2007.1628.
88. Carreau, A.; El Hafny-Rahbi, B.; Matejuk, A.; Grillon, C.; Kieda, C. Why Is the Partial Oxygen Pressure of Human Tissues a Crucial Parameter? Small Molecules and Hypoxia. *J Cell Mol Med* **2011**, *15*, 1239–1253, doi:10.1111/j.1582-4934.2011.01258.x.
89. Höckel, M.; Vaupel, P. Tumor Hypoxia: Definitions and Current Clinical, Biologic, and Molecular Aspects. *J Natl Cancer Inst* **2001**, *93*, 266–276, doi:10.1093/jnci/93.4.266.
90. Jiang, B.H.; Semenza, G.L.; Bauer, C.; Marti, H.H. Hypoxia-Inducible Factor 1 Levels Vary Exponentially over a Physiologically Relevant Range of O2 Tension. *American Journal of Physiology-Cell Physiology* **1996**, *271*, C1172–C1180, doi:10.1152/ajpcell.1996.271.4.C1172.
91. McKeown, S.R. Defining Normoxia, Physoxia and Hypoxia in Tumours—Implications for Treatment Response. *BJR* **2014**, *87*, 20130676, doi:10.1259/bjr.20130676.
92. Joo, H.; Mo, J.Y.; Kim, I.K.; Kang, H.H.; Lee, S.H. P3.01-041 Anti-Cancer Effect of Hyperoxia on Human Lung Cancer Cells through Oxidative Stress Mediated ERK Signaling: Topic: Functional Biology in Lung Cancer. *Journal of Thoracic Oncology* **2017**, *12*, S1144–S1145, doi:10.1016/j.jtho.2016.11.1607.
93. Kim, S.W.; Kim, I.K.; Ha, J.H.; Yeo, C.D.; Kang, H.H.; Kim, J.W.; Lee, S.H. Normobaric Hyperoxia Inhibits the Progression of Lung Cancer by Inducing Apoptosis. *Exp Biol Med (Maywood)* **2018**, *243*, 739–748, doi:10.1177/1535370218774737.
94. Sun, S.; Lee, D.; Lee, N.P.; Pu, J.K.S.; Wong, S.T.S.; Lui, W.M.; Fung, C.F.; Leung, G.K.K. Hyperoxia Resensitizes Chemoresistant Human Glioblastoma Cells to Temozolomide. *J Neurooncol* **2012**, *109*, 467–475, doi:10.1007/s11060-012-0923-3.
95. Kim, S.W.; Kim, I.K.; Lee, S.H. Role of Hyperoxic Treatment in Cancer. *Exp Biol Med (Maywood)* **2020**, *245*, 851–860, doi:10.1177/1535370220921547.
96. Hatfield, S.M.; Kjaergaard, J.; Lukashev, D.; Belikoff, B.; Schreiber, T.H.; Sethumadhavan, S.; Abbott, R.; Philbrook, P.; Thayer, M.; Shujia, D.; et al. Systemic Oxygenation Weakens the Hypoxia and Hypoxia Inducible Factor 1α-Dependent and Extracellular Adenosine-

Mediated Tumor Protection. *J Mol Med (Berl)* **2014**, *92*, 1283–1292, doi:10.1007/s00109-014-1189-3.

97. Dong, D.; Fu, Y.; Chen, F.; Zhang, J.; Jia, H.; Li, J.; Wang, H.; Wen, J. Hyperoxia Sensitizes Hypoxic HeLa Cells to Ionizing Radiation by Downregulating HIF-1α and VEGF Expression. *Molecular Medicine Reports* **2021**, *23*, 1–1, doi:10.3892/mmr.2020.11700.
98. Wang, Y.; Yin, K.; Tian, J.; Xia, X.; Ma, J.; Tang, X.; Xu, H.; Wang, S. Granulocytic Myeloid-Derived Suppressor Cells Promote the Stemness of Colorectal Cancer Cells through Exosomal S100A9. *Adv Sci (Weinh)* **2019**, *6*, 1901278, doi:10.1002/advs.201901278.
99. Osrodek, M.; Hartman, M.L.; Czyz, M. Physiologically Relevant Oxygen Concentration (6% O2) as an Important Component of the Microenvironment Impacting Melanoma Phenotype and Melanoma Response to Targeted Therapeutics In Vitro. *International Journal of Molecular Sciences* **2019**, *20*, 4203, doi:10.3390/ijms20174203.

CHAPTER 2

Quantitative ^{1}H NMR analysis of intracellular and extracellular metabolome of HT1080 cell line under hypoxia, normoxia and hyperoxia

Contents

1 Introduction 42

2 Materials and Methods 43

2.1. Evaluation cell culturing process and experimental design 43

2.2. Cell Culturing medium (MEM) preparation 43

2.3. Culture media extraction 44

2.4. Cells extraction 44

2.5. Cell growth measurement 45

2.6. NMR data acquisition 46

2.7. Metabolites identification 46

2.8. Processing for data analysis 46

2.9. Statistical Analysis 47

2.9.1. Univariate Analysis 47

2.9.2. Multivariate Data Analysis (MVA) 47

3 Results 48

3.1. The experimental methodology evaluation 48

3.2. Effect of oxygen concentration on cells growth 48

3.3. Time-dependent effect on HT1080 cell line metabolome at various oxygen concentrations 49

3.3.1. Intracellular results 49

3.3.1.1. The intracellular metabolic profile changes at hypoxia, normoxia and hyperoxia in function of oxygen concentrations 49

3.3.1.2. The sensitivity of intracellular metabolome to hypoxia, normoxia and hyperoxia in function of time intervals 63

3.3.2. Extracellular results 74

3.3.2.1. The extracellular metabolic profile changes at hypoxia 1%, normoxia 6% and hyperoxia 21% in function of oxygen concentrations 76

3.3.2.2. The metabolic sensitivity of the extracellular metabolome to various oxygen concentrations in the time intervals function 87

4 Discussion 99

4.1. The metabolic changes of intracellular and extracellular metabolome at hypoxia, normoxia and hyperoxia through cultivation time 99

4.2 The sensitivity of the HT1080 cell's metabolome to hypoxia, normoxia and hyperoxia at each interval time point 106

5 Conclusion 110

5 References 111

1. Introduction

The role of oxygen molecule (O_2) is critical for all living organisms and plays a key in maintaining the bioenergetics system of the cells. Besides, and integrates with different inorganic and organic reactions for aerobic metabolism in cancer cells and has been massively explained by many studies. An extreme level of oxygen well known as hyperoxia (higher than normoxia) and hypoxia (lower than normoxia) both are stress promoters within the biological system. Thereby, the tumor has heterogeneous tissues and is divided into three types of tissue regions due to oxygen concentration exposure: normoxic, hypoxic, and necrotic regions. In the hypoxic region, cells reprogram their metabolism to preserve cell sustainability and diverge other regions within tumor tissue and, off course significantly from normal tissues [1].

Concluding that the hypoxic cells are randomly distributed even within the hypoxic region due to tumor vasculature [2–4]. It had been considered by many studies that oxygen concentration is essential and correlates to the final phenotype of cultivated cancer cells. In in vitro culture there is a range of settings that attempt to mimic tumor microenvironments such as 3D-culture and co-cultures. However, without considering the importance of overall incubator oxygen concentration and its impact on oxygen distribution within the tumor. Most recent study showed the variation of studies results depends on oxygen concentration.

Highlighting that 20.9% O_2 is atmospheric oxygen concentration which was for decades usually used for in vitro studies, is much higher than in human tissue and should be referred to as hyperoxia [5]. Shows that the physiological oxygen concentration corresponding to human peripheral tissue 6% O_2 should be defined as normoxia and the level of oxygen in normal tissue and tumor at pathological hypoxia (partial pressure of less than 8 mmHg 1% O_2) [6]. Thereby the metabolic perturbations of hypoxic cells have been studied and suggested the ability to identify hypoxia-related metabolites and their specific pathways by using ^{1}H NMR –based metabolomics method [7] as a precious tool due to its robustness, reproducibility, non-destructive sample measurements, and the possibility to quantify concentration [8].

In this study, we conducted an in vitro culture of HT1080 (Fibrosarcoma) cell line at different oxygen concentrations at 1% (hypoxia), 6% (normoxia), and 20.9% (hyperoxia) [6,9] to monitor metabolic profiles of intracellular and extracellular and compare the different oxygen concentrations during time intervals (12h, 24h, and 36h) by ^{1}H NMR spectroscopy to verify metabolome alterations according to conditions.

2. Materials and Methods

2.1.Evaluation cell culturing process and experimental design

To evaluate the number of cells number, media volume and incubation time. We have cultivated HT1080 cells line in T 75 cm^2 tissue culture flasks with at a density of 1 $x10^7$ cells per flask with 10-12 mL of MEM media for 48h and change media each 24h. We evaluate the cells confluence by inverted microscope (Leica DMi1, Wetzlar, Germany) and for cell growth, we counted the cells by a hemocytometer (Brand, Wertheim, Germany). The next step was to evaluate the optimal cells density for ^{1}H NMR reasonable detection, therefore, we used range of cells number with 4 x 10^6, 5 x 10^6, 7 x 10^6 and 1 x 10^7 respectively.

2.2.Cell Culturing medium (MEM) preparation

The HT1080 (human fibrosarcoma cell line) was purchased from American Type Culture ((ATCC® CCL-121™). Cells were kept for 72 h in T 75 cm^2 tissue culture flasks, in particular MEM culture medium. All the cells were used within the first 10 passages from unfreezing. The experiments start first by harvesting the number of cells required for all experiments. The cells were cultivated in Minimum Essential Medium Eagle (MEM) culture medium (Sigma Life Science, Sigma-Aldrich, Gillingham, UK) with 10% fetal bovine serum (FBS) (Biowest, origin South America, Riverside, MO, USA), 1% penicillin/streptomycin solution (HyClone, GE Healthcare Life Sciences, Wien, Austria), 1% L-glutamine solution (Trypsin-EDTA solution, Sigma-Aldrich, SL, USA), 1% MEM Non-essential Amino Acid Solution (100x) (Sigma-Aldrich, SL, USA). The cells were seeded in 75 cm^2 flasks at a density of 1 $x10^7$ cells per plate. For each plate, 10 mL of media was used. The cell culture was incubated in different O_2 concentrations, For hypoxia 1% and normoxia 6% O_2 in CO_2 –incubator with O_2 control

(Binder, Tuttlingen, Germany) 5% CO_2 conditions at 37 °C, and the time interval was 12h, 24h and 36h in triplicate and in separate plates. For hyperoxia 20.9% was with CO_2 –incubator (Binder, Tuttlingen, Germany) under 5% CO_2 conditions at 37 °C and 80% humidity. All experiment was conducted without any change of medium during 36h of incubation.

2.3.Culture medium extraction

Each time interval point was collected as 1 mL from each culturing flask and immediately stored at −80 °C. At the beginning of the analysis the medium was thawed out at room temperature and vortexed. Transfer 400 μL medium from each sample to a new Eppendorf tube with methanol 1.2 mL (LC-MS grade, Merck, Darmstadt, Germany). The mixture of medium-methanol was shaken for 10 min at 30 Hz (Tissiulyzer LT, Qiagen, Germantown, MD, USA), then incubated at −20 °C for 20 min and centrifuged for 30 min at 4 °C, 12000 rpm. Supernatant in 1 mL was transferred to a new Eppendorf tube and evaporated to dryness under a vacuum centrifuge (JWElectronic WP-03, Warsaw, Poland) at 40 °C, 1405 rpm. After evaporation, the samples were resuspended in 600 μL PBS buffer (pH, 7.3, 20% D_2O, 3mM TSP). Finally, 550 μL was transferred to an NMR cuvette (5 mm, SP type, ARMAR Chemicals, Döttingen, Switzerland). Prepared samples were stored at 4 °C until NMR spectra acquisition.

2.4.Cells extraction

After we reached 85-90% confluence, the medium was removed and the cells were washed with PBS (Phosphate Buffered Saline, Sigma-Aldrich, SL, USA). After that, the cells were deattached by adding 5 mL of trypsin-EDTA (Trypsin-EDTA solution, Sigma-Aldrich, SL, USA), and incubated for 5 min at 5% CO_2 conditions at 37 °C. Cells suspension was centrifuged for 5 min at 21 °C, 1940 rpm. The supernatant was discarded and the cell pellet was washed with PB (Phosphate buffered saline, Sigma-Aldrich, SL, USA), and centrifuged once again. Finally, the supernatant was removed and the cells were kept at −80 °C before extraction. The cell pellet was thawed at room temperature 25 °C and, the pallet was mixed with 1.5 mL of cold methanol (LC-MS grade, Merck, Darmstadt, Germany) together with 7mm stainless

steel beads (Qiagen GmbH, Hilden, Germany), and was homogenized for 10 min at 30 Hz (Tissiulyzer LT, Qiagen, Germantown, MD, USA) than incubated at −20 °C for 20 min, then the samples were centrifuged for 30 min at 4 °C, 12000 rpm. 1mL of Supernatant was transferred to a new Eppendorf tube and evaporated the samples to dryness under vacuum centrifuge (JWElectronic WP-03, Warsaw, Poland) at 40 °C, 1500 rpm. After evaporation the samples were kept at -80 °C until NMR analysis. Evaporated samples were thawed at room temperature 25 °C, and re-suspended in 600 µL PBS buffer (pH, 7.4, 20% D_2O, 0.33 mM of TSP). Finally, 550 µL was transferred to an NMR tube (5 mm, SP type, ARMAR Chemicals, Döttingen, Switzerland). The prepared samples were stored at 4 °C until NMR spectra acquisition.

2.5.Cells growth measurement

The proliferation was conducted separately, HT1080 cell line were plated into a 6-wells plate at a cell density of 1 x 10^6 cells per well. The plates were cultivated in 1% hypoxia, 6% normoxia and 20.9% hyperoxia, for 12h, 24h, and 36h in CO2 – incubator (Binder, Tuttlingen, Germany) under 5% CO_2 conditions at 37 °C and 80% humidity., For cell viability, the cells were first trypsinized and then stained with 0.4% Trypan Blue (Sigma, USA) in PBS for ~ 3 min at room temperature then counted by a hemocytometer (Brand, Wertheim, Germany). The growth curve was plotted. The population doubling time and growth rate were calculated during the exponential growth phase of the cells using the equations:

1. Cell doubling time (h):

$$T_d = (T2 - T1) \cdot \frac{\ln(2)}{\ln(\frac{q2}{q1})}$$

2. Growth rate cells (h):

$$gr = \frac{\ln\left(\frac{q2}{q1}\right)}{\Delta t}$$

T_d = Doubling period (time it takes for object to double in number)
gr = Growth rate
$(T_2\text{-}T_1)$ or Δt = Duration time at the exponential growth.
q_2 = the number of cells at time T_2.
q_1 = the number of cells at time T_1.

2.6. NMR data acquisition

The ^{1}H NMR spectra of cells and post-cultured media samples were recorded at 300 K using the Avance II spectrometer (Bruker, GmBH, Bremen, Germany). The proton operation frequency was set at 600.58 MHz. The 1D ^{1}H NMR spectra were recorded using a CPMG pulse sequence with water presaturation (cpmgpr1d in Bruker notation). For each sample, the spectra parameters were set respectively, width,20.01 ppm; 128 scans; spin-echo delay of 400 μs; 80 loops; time domain of 64k, the acquisition time of 2.73 s, and a relaxation delay of 3.5s.

2.7. Metabolites Identification NMR

The identification of resonance signals was obtained by assignments published in the literature, Chenomx software (v 8.5 Chenomx Inc., Edmonton, Canada), and online database Biological Magnetic Resonance Data Bank [10], and Human Metabolome Database [11]. For the intracellular metabolome 36 metabolites were identified. Fig. S1 and for extracellular metabolome 40 metabolites.

2.8. Processing for Data Analysis

The spectra were manually phased, then baseline-corrected with MestReNova software (Mestrelab Research v 14.1.1), and referenced to the TSP signal group (δ = 0.000 ppm) for both types of samples. The spectra prior were normalized to the constant sum of the TSP resonance signal. The signals of water were removed from the analysis. The icoshift algorithm and correlation optimized warping algorithm (COW) (if needed) were used for the alignment of resonance signals both implemented in MATLAB (v R2014a, MathWorks Inc., Natick, MA, USA) [12,13]. The sum of data points of the overlapping and non-overlapping resonances was obtained for calculation of the relative intensity of identified metabolites resonance signals for intracellular, however, for extracellular, the data matrix was calculated individually for each spectra to obtain the relative intensity of NMR measured metabolites. Before statistical analysis the relative intensity values of identified metabolites were normalized to the respective cells number that was determined by each incubation time point after 12h, 24h, and 36h at each oxygen concentration hypoxia 1%, normoxia 6% and hyperoxia 20.9%. Finally, quantified relative intensity

of post-culture media extracts and cells extracts for further analysis were prepared as separate data matrices.

2.9. Statistical Analysis

2.9.1 Univariate Analysis

The univariate analysis was calculated by using Statistica Software v.13 on relative intensity values of assigned intracellular and extracellular metabolites datasets with respect to the interval time points (12h, 24h and 36h) at (hypoxia 1%, normoxia 6%, and hyperoxia 21%). Multiple comparisons based on incubation time and conditions were tested by one-way ANOVA, Tukey's multiple-comparison posttest and multiplicity adjusted *p*-value was calculated to account for multiple comparisons with family-wise significance and confidence level at α = 0.05 (95% confidence interval). The boxplots were obtained by Rstudio (Rstudio Ver.R 3.0.1,Inc., Boston, NA, USA) based on triplicates for each condition (1% hypoxia, 6% normoxia, and 21% hyperoxia) during interval incubation time (12h, 24h, and 36h) with and without control samples.

2.9.2 Multivariate Data Analysis (MVA)

The multivariate data analysis was performed using SIMCA software (Ver. 17.0, Sartorius, Göttingen, Germany). The relative intensity values of assigned intracellular and extracellular metabolites were prepared as separate data matrices. A priori multivariate analysis variables were UV scaled and sample order was randomized. The MVA was divided into two parts unsupervised exploratory analysis and supervised regression analysis. The Principal Component Analysis (PCA) was used to show the overall clustering of data and determine potential outliers. The partial least squares regression model (PLS-R) with X block containing metabolites relative intensity and Y -block as incubation time (12h, 24h and 36h) at hypoxia 1%, normoxia 6% and hyperoxia 21% to construct a linear model and predict the model's parameters, such as the goodness-of-fit parameter R^2 which, used to evaluate the quality of the model together with the predictive validation parameter Q^2.

The most important metabolites identified by the PLS-R model were selected based on variable importance in projection (VIP) score above 1.00. The analysis of variance of cross-validated residuals (CV-ANOVA) for the partial least squares

regression model (PLS-R) used a significance level at alpha= 0.05 to assess model fit quality.

3. Results

3.1. The experimental methodology evaluation

The results showed that, the cells were growing healthy with maximum confluence up to 95% and viability higher than 97% with all conditions after 48h with change the media each 24h. We obtained between 1.6 x 10^7 - 1.8 x 10^7 cells/flask and allowed use to harvest all cells number required for whole experiments. Thereafter, we established the cultivation cells number start from 1 x 10^7 and volume of the medium up to 10 mL. Moreover, the cultivation time points was evaluated after 48h with changing the media every 24h. However, we have decided to cultivate the cells for period of time until 36h since will not change the medium during experiments to describe the starvation process and the mechanisms of metabolic reprogramming in HT1080 cells under conditions (hypoxia 1%, normoxia 6% and hyperoxia 21%) and incubation time points (12h, 24h and 36h) and minimizing the variations this analysis.

Furthermore, after we used range of cells number to determine NMR sensitivity, the results showed that, the most optimal cells number that deliver reasonable spectrum for quantification was 1 x 10^7 cells. This evaluation was established for all my thesis experiments.

3.2. Effect of Oxygen Concentration on Cells growth

Our direct counting assay revealed variations in the growth of HT1080 cells under different oxygen conditions: hypoxia, normoxia, and hyperoxia. These growth differences are illustrated in Figure 1. We observed that under hypoxia (1% O_2) during a 12h incubation, the cells entered an exponential growth phase, with a population-doubling time (PDT) of 36.37h and a growth rate of 0.019 cell per hour. In contrast, under normoxia (6% O_2) for 24h, the PDT was 38 hours and the growth rate was 0.018 cell per hour. Lastly, under hyperoxia (21% O_2) for 24 hours, the PDT was 27.39 hours and the growth rate was 0.025 cell per hour.

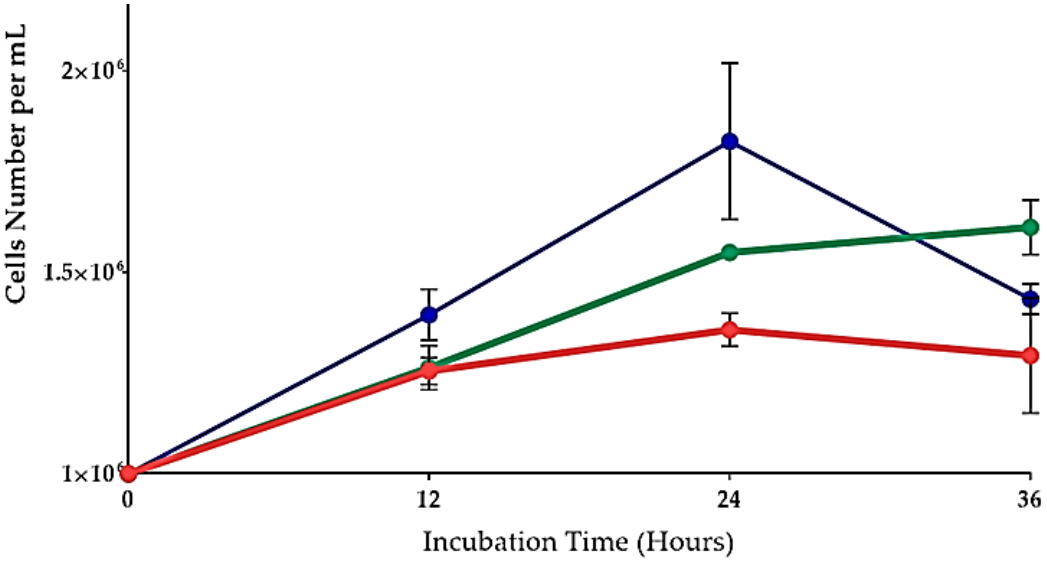

Figure 1. The HT1080 cells proliferation results for studied time intervals (12h, 24h and 36h) for different oxygen concentration (hypoxia 1%, normoxia 6% and hyperoxia 20.9%) The line points error bars was obtained from standard error of the mean (SEM). Red line— hypoxia 1%; Green line — normoxia 6%; Blue line—hyperoxia 21%.

3.3.Time-dependent effect on HT1080 cell line metabolome at various oxygen concentrations

3.3.1. Intracellular results

3.3.1.1.The intracellular metabolic profile changes at hypoxia, normoxia and hyperoxia in function of oxygen concentrations

For a sample set of a total 9 samples from cells extraction, for each condition (1%, 6% and 21%), we conducted ^{1}H NMR-based metabolome analysis and 35 metabolites were successfully assigned in cells extraction respectively (Figure 2, Table 1).

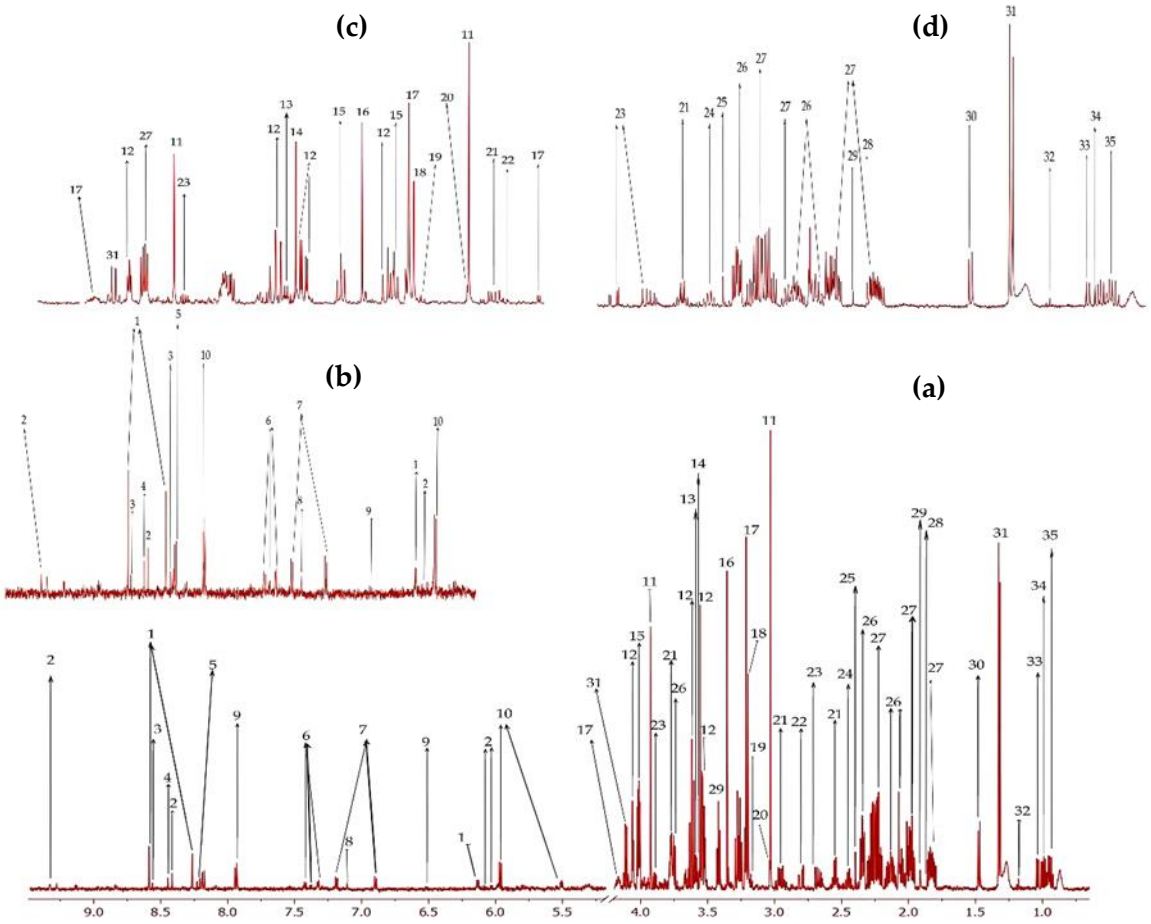

Figure 2. The representative ^{1}H NMR spectrum obtained from cells extracts of HT1080. (a) Full ^{1}H-NMR spectrum from δ 5.0 to δ 9.5; (b) Enlarged spectrum from δ 9.5 to δ 6.5; (c) Enlarged spectrum from δ 5.0 to δ 2.7; (d) Enlarged spectrum from δ 2.7 to δ 0.5. The metabolites were identified from 1- 35 as mentioned from Table 1 respectively.

Table 1. The chemical shifts and signal multiplicity of HT1080 cells extract metabolome identified by ^{1}H NMR spectroscopy.

No	Metabolites	Peak Assignments	Peak Centers (ppm)	HMDB ID
1	AMP	s	8.581, s (8.258)	HMDB0000045
2	NAD+	s	8.49, d(9.127), d(8.827), s (9.321), m(8.167)	HMDB0000902
3	IMP	s	8.555, s (8.222)	HMDB0000175
4	Formate	s	8.44	HMDB0000142
5	Hypoxanthine	s	8.201, s (8.182)	HMDB0000157
6	Phenylalanine	m	m (7.419), m(7.367), 7.320	HMDB0000159
7	Tyrosine	m	7.182, m (6.890)	HMDB0000158

8	Histidine	s	7.102	HMDB0000177
9	Fumarate	s	6.505	HMDB0000134
10	UDP-N-Acetylglucosamine	d	d(7.932), 5.967, dd(5.502), dd(4.350), m(4.274),s (2.066)	HMDB0000290
11	Creatine	s	3.919, s (3.024)	HMDB0000064
12	*myo*-Inositol	t	dd (4.055), 3.612, dd(3,525)	HMDB0000211
13	Threonine	d	3.580, m (4.237), d(1.317)	HMDB0000167
14	Glycine	s	3.55	HMDB0000123
15	Taurine	t	3.413, t (4.252)	HMDB0000251
16	Methanol (residual of extraction)	s	3.348	HMDB0001875
17	O-Phosphocholine	s	3.207	HMDB0001565
18	Choline	s	3.192	HMDB0000097
19	β-alanine	t	3.170, t(2.543)	HMDB0000056
20	Creatinine	s	3.029, s (4.050)	HMDB0000562
21	Glutathione	d	2.972	HMDB0000125
22	Asparagine	t	2.851	HMDB0000168
23	Aspartate	dd	2.798, t(3.888), dd(2.668)	HMDB0000191
24	Glutamine	m	2.436	HMDB0000641
25	Succinate	s	2.39	HMDB0000254
26	Glutamate	m	t (3.748), 2.322, m (2.117), m (2.040)	HMDB0060475
27	2-Hydroxyglutarate	m	2.274, t(2.218), m(1.980), m (1.821), t(4.010)	HMDB0059655
28	N-Acetylaspartate	s	2.008, dd (2.484), dd (2.678)	HMDB0000812
29	Acetate	s	1.906	HMDB0000042
30	Alanine	d	1.467	HMDB0000161
31	Lactate	t	q (4.102), 1.315	HMDB0000190
32	Ethanol	t	1.172	HMDB0000108
33	Valine	d	1.030, d (0.977)	HMDB0000883
34	Isoleucine	d	0.998	HMDB0000172
35	Leucine	t	0.955	HMDB0000687

***s**, singlet; **d**, doublet; **t**, triplet; **q**, quartet; **m**, multiplet; **dd**, doublet of doublet; **ppm value underline**, the quantitative peak.*

For exploring the changes in intracellular metabolome, we built PCA score loading plots of the ^{1}H NMR dataset and PLS regression model to predict the total scores either in each incubation time point (12h, 24h and 36h) or in each oxygen concentration (hypoxia 1%, normoxia 6% and hyperoxia 21%). Furthermore, the models were correctly evaluated and obtained the R^2X (cum), the total sum of variation in Y explained by the model R^2Y (cum) and goodness of prediction calculated by full cross validation Q^2(cum) scores and CV-ANOVA *p*-values for intracellular cell extracts in comparisons between oxygen concentrations groups or between incubation time groups.

Table 2. The multivariate analysis model summary of cell extract (intracellular) NMR-based metabolome in comparisons between 12h, 24h and 36h at 1%, 6% and 21% oxygen concentrations.

O_2 %	Incubation Time Comparison	Model Type	PC/LV	N =	R^2X (cum)	R^2Y (cum)	Q^2 (cum)	CV-ANOVA *p* value
1%	12h vs. 24h vs. 36h	PCA	2	9	0.797	–	–	–
	12h vs. 24h vs. 36h	PLS	3	9	0.85	0.989	0.916	$\mathbf{5.33 \times 10^{-2}}$
6%	12h vs. 24h vs. 36h	PCA	3	9	0.858	–	–	–
	12h vs. 24h vs. 36h	PLS	1	9	0.495	0.891	0.816	$\mathbf{6.25 \times 10^{-3}}$
21%	12h vs. 24h vs. 36h	PCA	2	9	0.861	–	–	–
	12h vs. 24h vs. 36h	PLS	2	9	0.86	0.982	0.971	$\mathbf{2.4 \times 10^{-3}}$

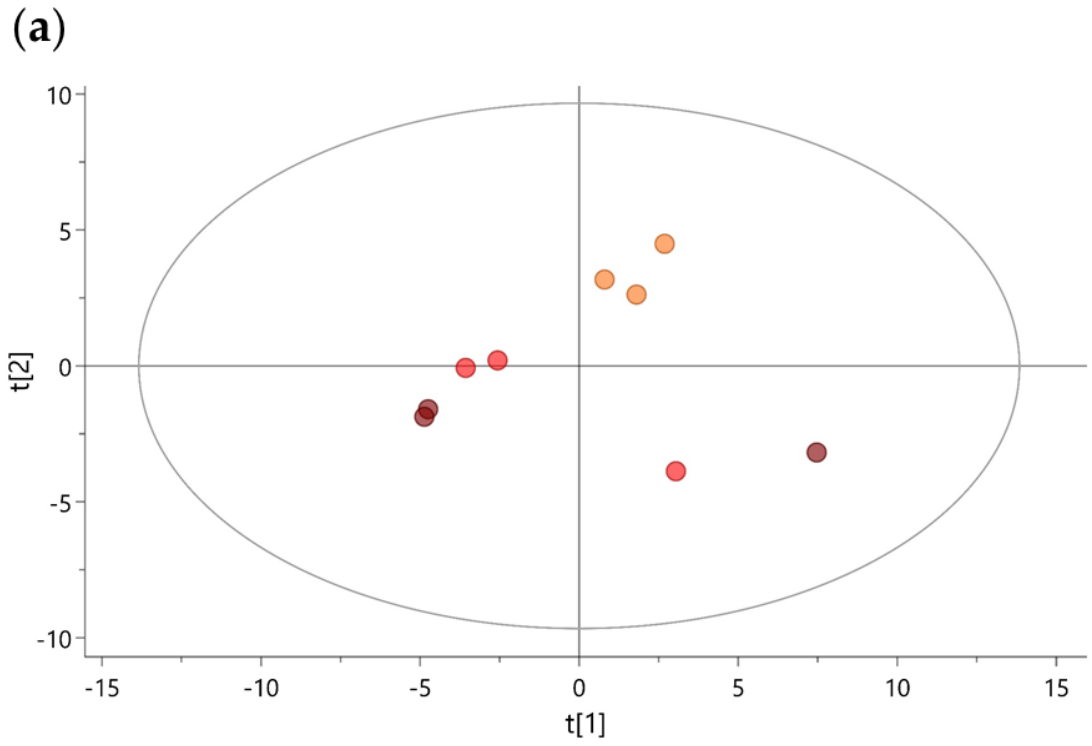

(b)

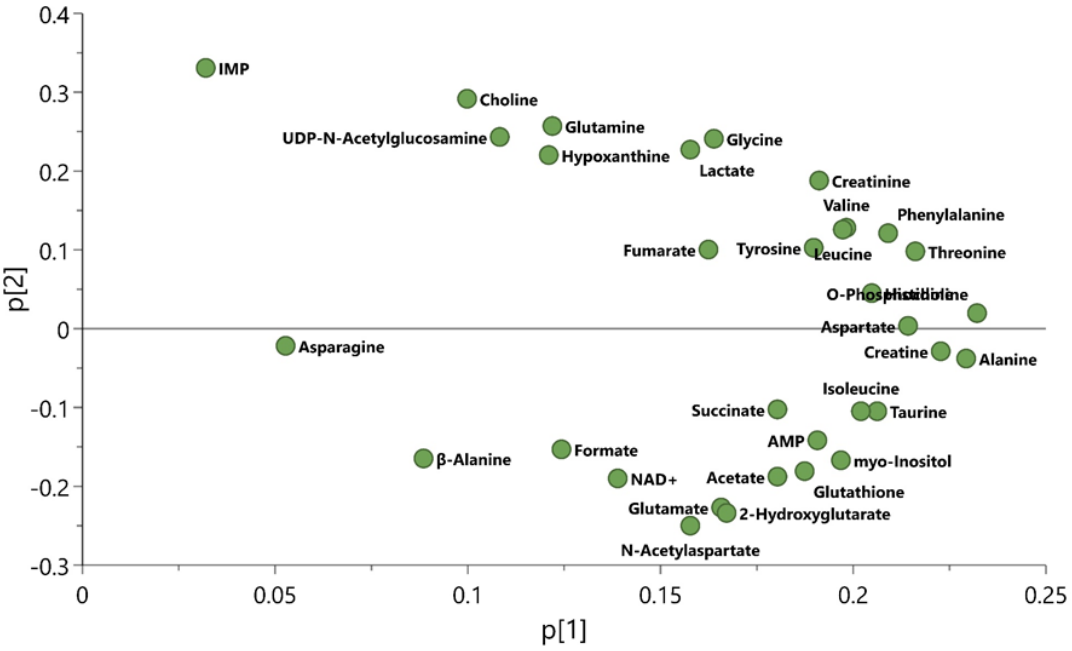
IMP
Choline
Glutamine
UDP-N-Acetylglucosamine
Glycine
Hypoxanthine
Lactate
Creatinine
Valine
Phenylalanine
Fumarate
Tyrosine
Leucine
Threonine
Aspartate
Asparagine
Creatine
Alanine
Isoleucine
Succinate
Taurine
AMP
β-Alanine
Formate
myo-Inositol
NAD+
Acetate
Glutathione
Glutamate
2-Hydroxyglutarate
N-Acetylaspartate
p[1]
p[2]

(c)

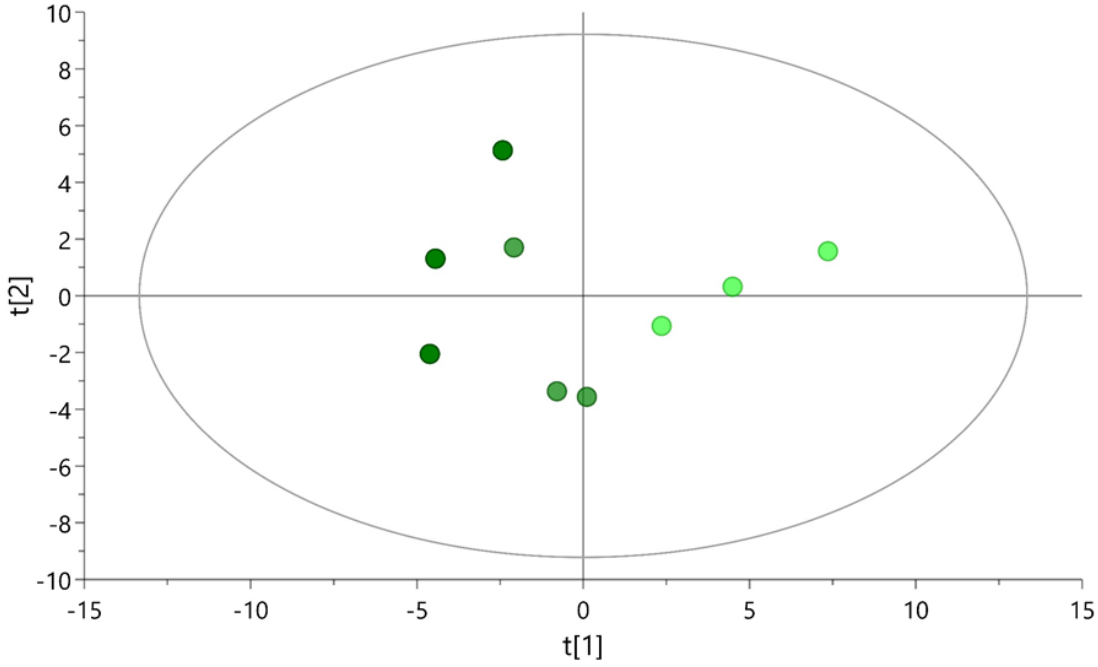
t[1]
t[2]

(**d**)

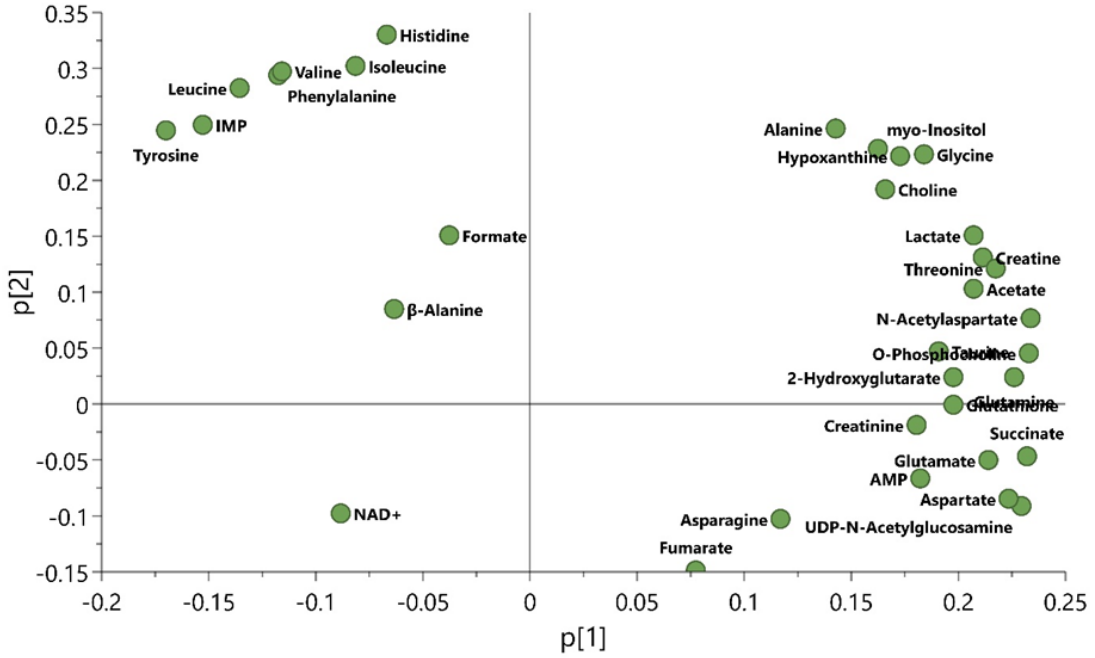
Histidine
Valine
Isoleucine
Leucine
Phenylalanine
IMP
Tyrosine
Formate
β-Alanine
NAD+
Alanine
myo-Inositol
Hypoxanthine
Glycine
Choline
Lactate
Creatine
Threonine
Acetate
N-Acetylaspartate
2-Hydroxyglutarate
Creatinine
Succinate
Glutamate
AMP
Aspartate
Asparagine
UDP-N-Acetylglucosamine
Fumarate
p[1]
p[2]

(**e**)

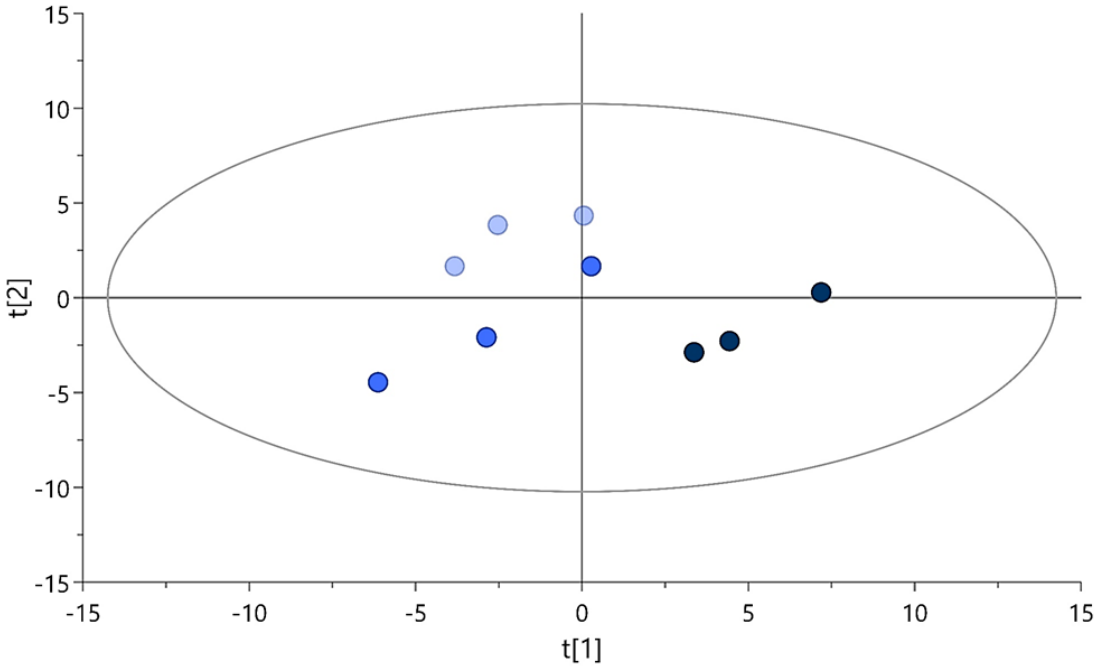
t[1]
t[2]

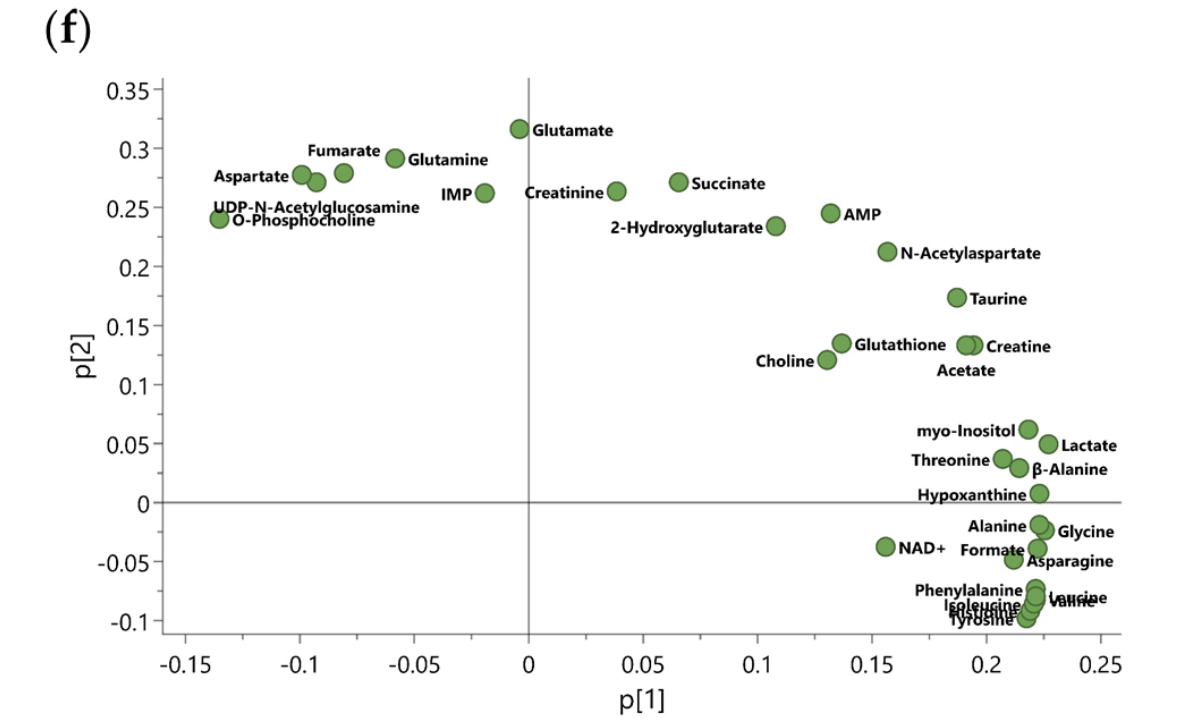

Figure 3. The Principal Component Analysis (PCA) scores plot and loadings plots for PCA model for 1H-NMR relative intensity data driven models for HT1080 cells extracts (intercellular) during incubation time at hypoxia 1%, normoxia 6% and hyperoxia 21% conditions. (a,b) at hypoxia 1%; (c, d) at normoxia 6%; (e, f) at hyperoxia 21%. Light red, hypoxia 1% after 12h; red, hypoxia 1% after 24h; dark red, hypoxia 1% after 36h; Light green, normoxia 6% after 12h; green, normoxia 6% after 24h; dark green, normoxia 6% after 36h; Light blue, hyperoxia 21% after 12h; blue, hyperoxia 21% after 24h; dark blue, hyperoxia 21% after 36h.

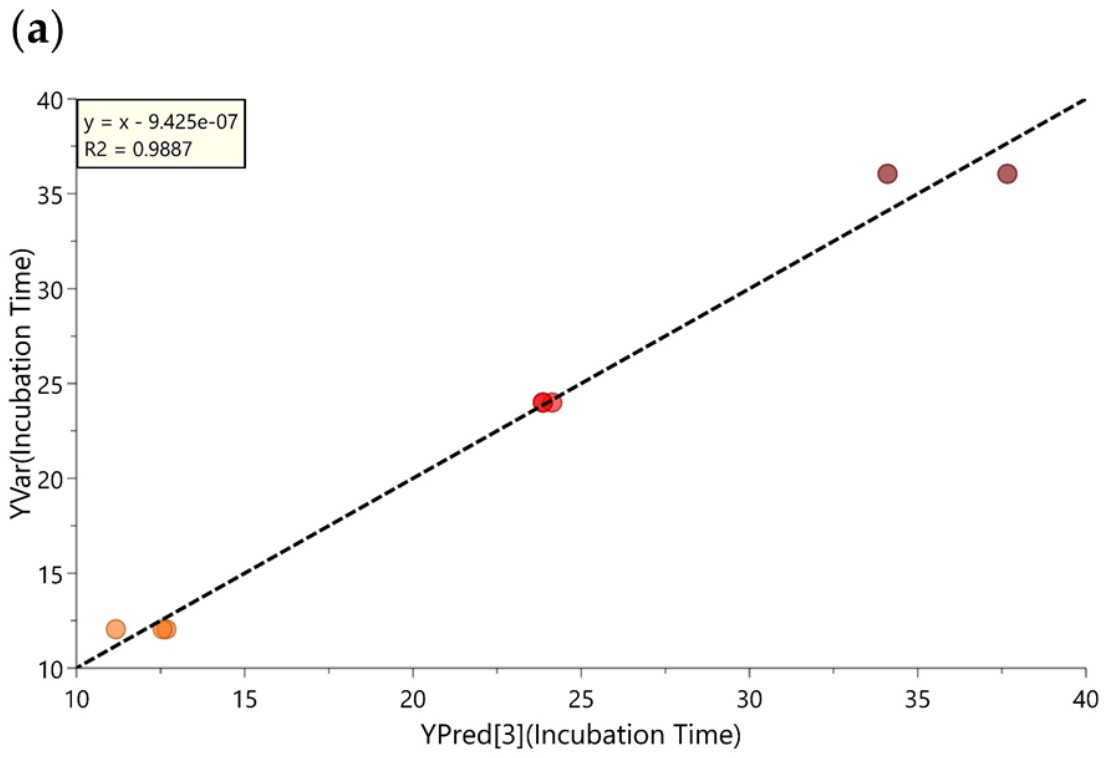

(b)

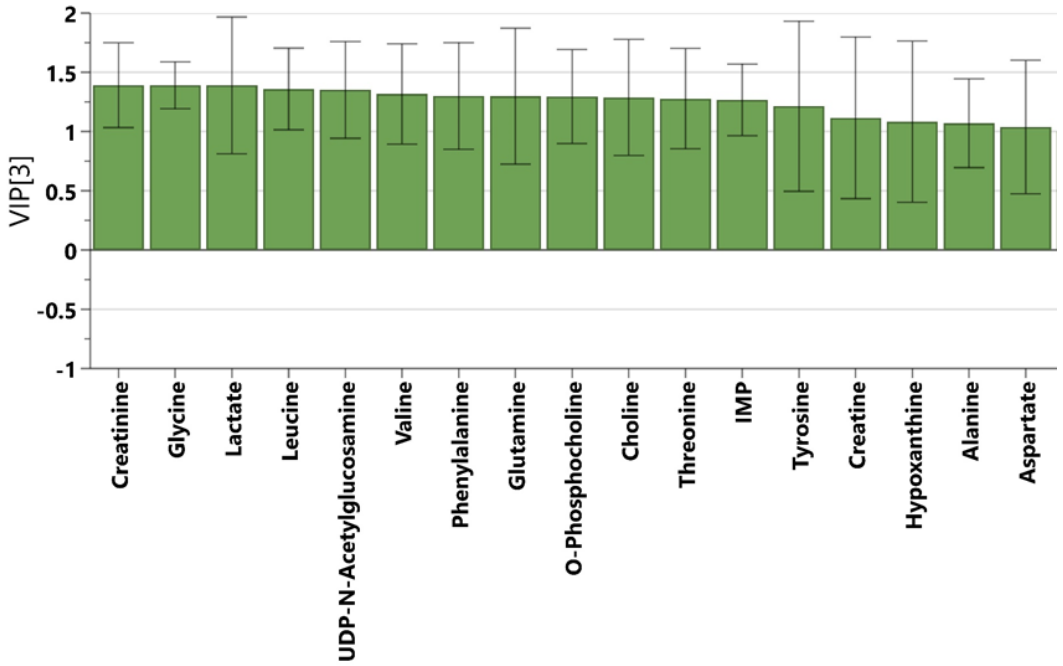
VIP[3]
2
1.5
1
0.5
0
-0.5
-1
Creatinine
Glycine
Lactate
Leucine
UDP-N-Acetylglucosamine
Valine
Phenylalanine
Glutamine
O-Phosphocholine
Choline
Threonine
IMP
Tyrosine
Creatine
Hypoxanthine
Alanine
Aspartate

(c)

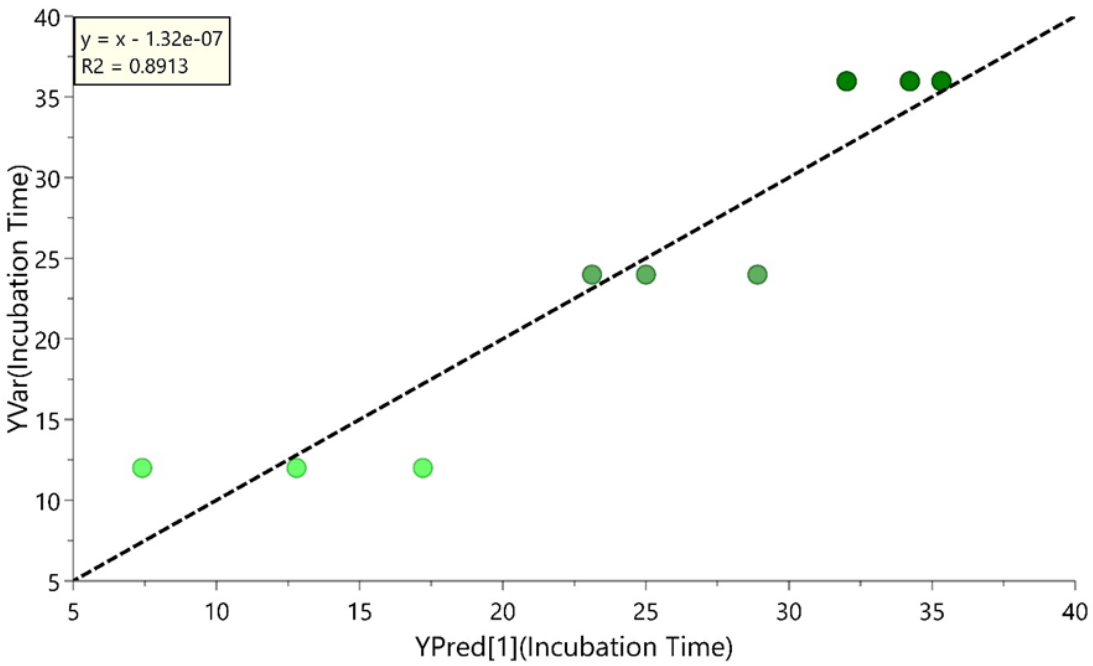
y = x - 1.32e-07
R2 = 0.8913
YVar(Incubation Time)
YPred[1](Incubation Time)
5
10
15
20
25
30
35
40

(**d**)

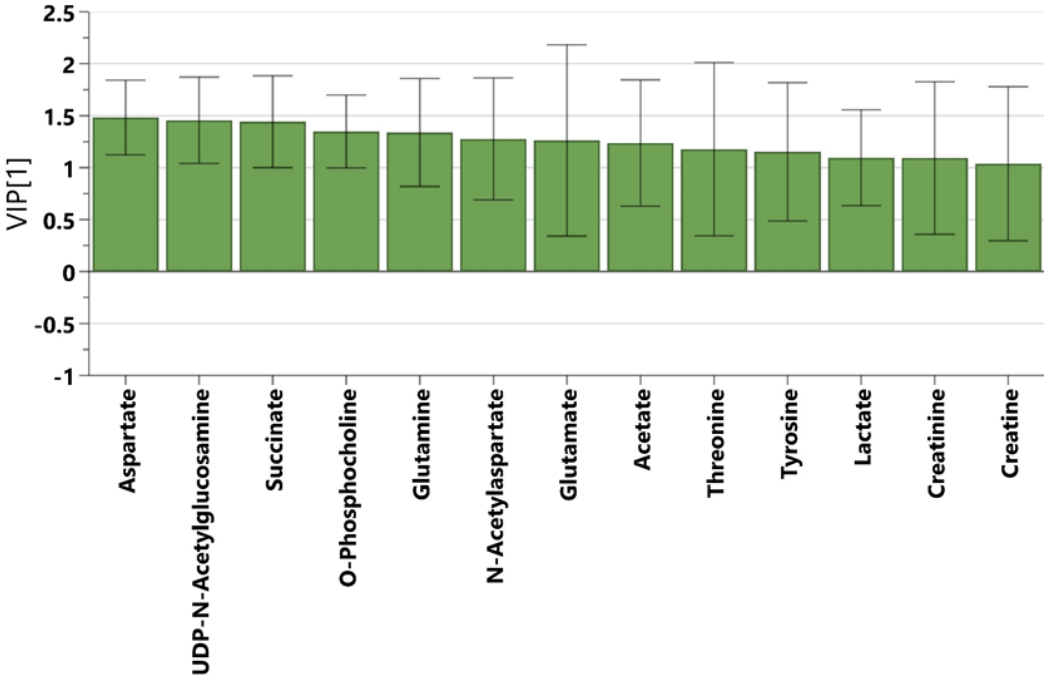
VIP[1]
2.5
2
1.5
1
0.5
0
-0.5
-1
Aspartate
UDP-N-Acetylglucosamine
Succinate
O-Phosphocholine
Glutamine
N-Acetylaspartate
Glutamate
Acetate
Threonine
Tyrosine
Lactate
Creatinine
Creatine

(**e**)

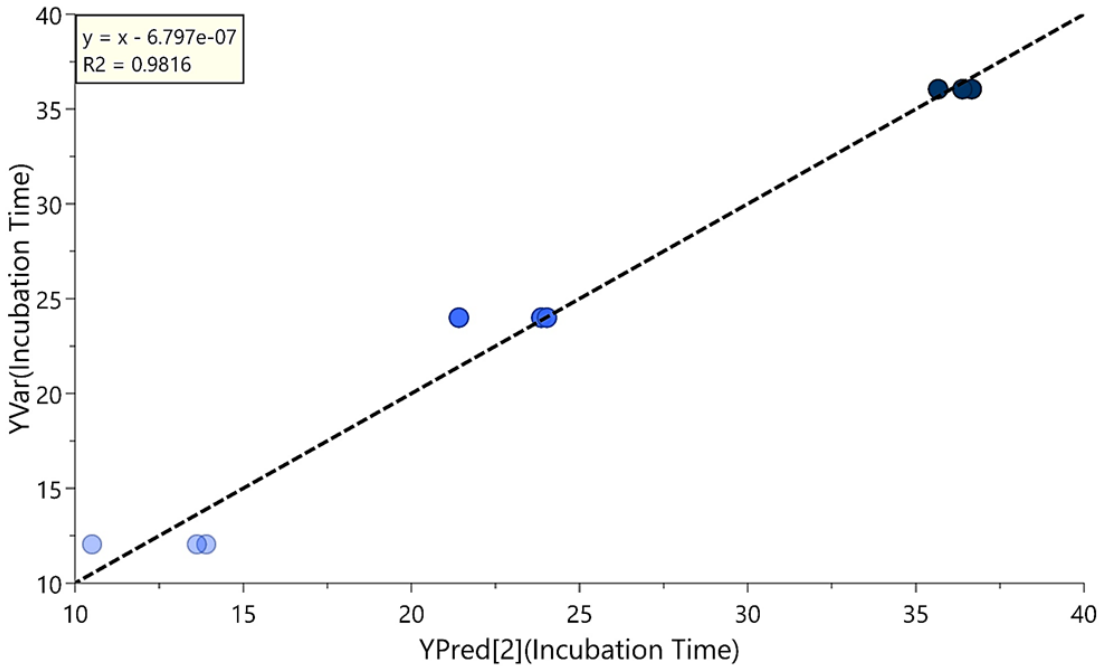
y = x - 6.797e-07
R2 = 0.9816
YVar(Incubation Time)
YPred[2](Incubation Time)
10
15
20
25
30
35
40

(f)

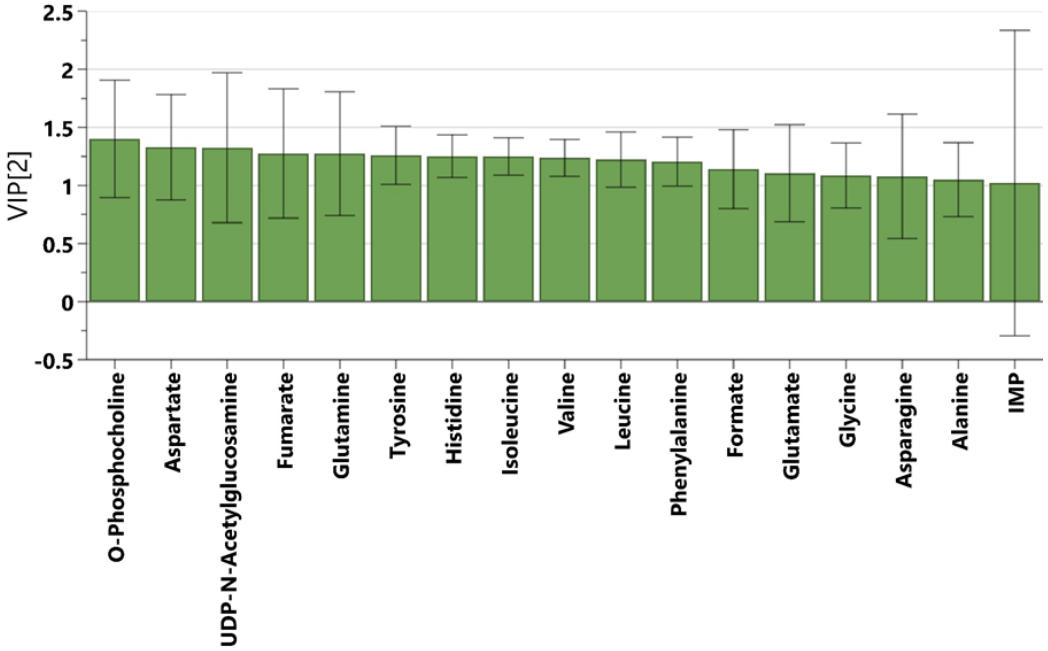

Figure 4. Graphical representation for ^{1}H-NMR relative intensity data driven models for HT1080 cells extracts (intercellular) at hypoxia 1%, normoxia 6% and hyperoxia 21% conditions after 12h, 24h and 36h incubation. (**a, c, e**) prediction plot from the partial least squares-regression model (PLS-R) built on relative intensity of ^{1}H-nuclear magnetic resonance spectra dataset at hypoxia 1%, normoxia 6% and hyperoxia 21%, respectively. (**b, d, f**) the Variable importance in projection (VIP) score plot for PLS-R model (VIP >1.00) at hypoxia 1%, normoxia 6% and hyperoxia 21%, respectively. Light green, normoxia 6% after 12h; green, normoxia 6% after 24h; dark green, normoxia 6% after 36h; Light blue, hyperoxia 21% after 12h; blue, hyperoxia 21% after 24h; dark blue, hyperoxia 21% after 36h.

The results from intracellular metabolome at hypoxia 1% showed that PCA overlapping between groups of 24h and 36h incubation time, and presence of outliers (**Figure** 3a). Therefore, we removed the one outlier for our further analysis. The loading plot in was created, displaying the explanatory pattern present in the dataset (**Figure** 3b).

The PLS regression model was created and validated at hypoxia 1% during 12h, 24h and 36h incubation time with R2 = 0.9887, by using just three PLS components the root-mean-square-error-of-cross-validation (RMSECV) was 2.64h and the cross-validated residuals (CV-ANOVA) of PLS-R model wasn't significant (**Table** 2). The 17 metabolites with VIP (variable importance in projection) value above 1.00 were selected such as (creatinine, glycine, lactate, leucine, UDP-N-acetylglucosamine, valine, phenylalanine, glutamine, O-phosphocholine, choline, threonine, IMP,

tyrosine, creatine, hypoxanthine, alanine, aspartate) (**Figure** 4a, 4b), The selective metabolites with VIP value above 1 were tested by ANOVA, and showed just one regulation as follows:

1. Downregulation of creatinine, glycine, lactate, leucine, UDP-N-Acetylglucosamine, valine, phenylalanine, glutamine, O-phosphocholine, choline, threonine, IMP, tyrosine, creatine, hypoxanthine, alanine, aspartate by increasing of incubation time at hypoxia 1% (**Figure** 5).

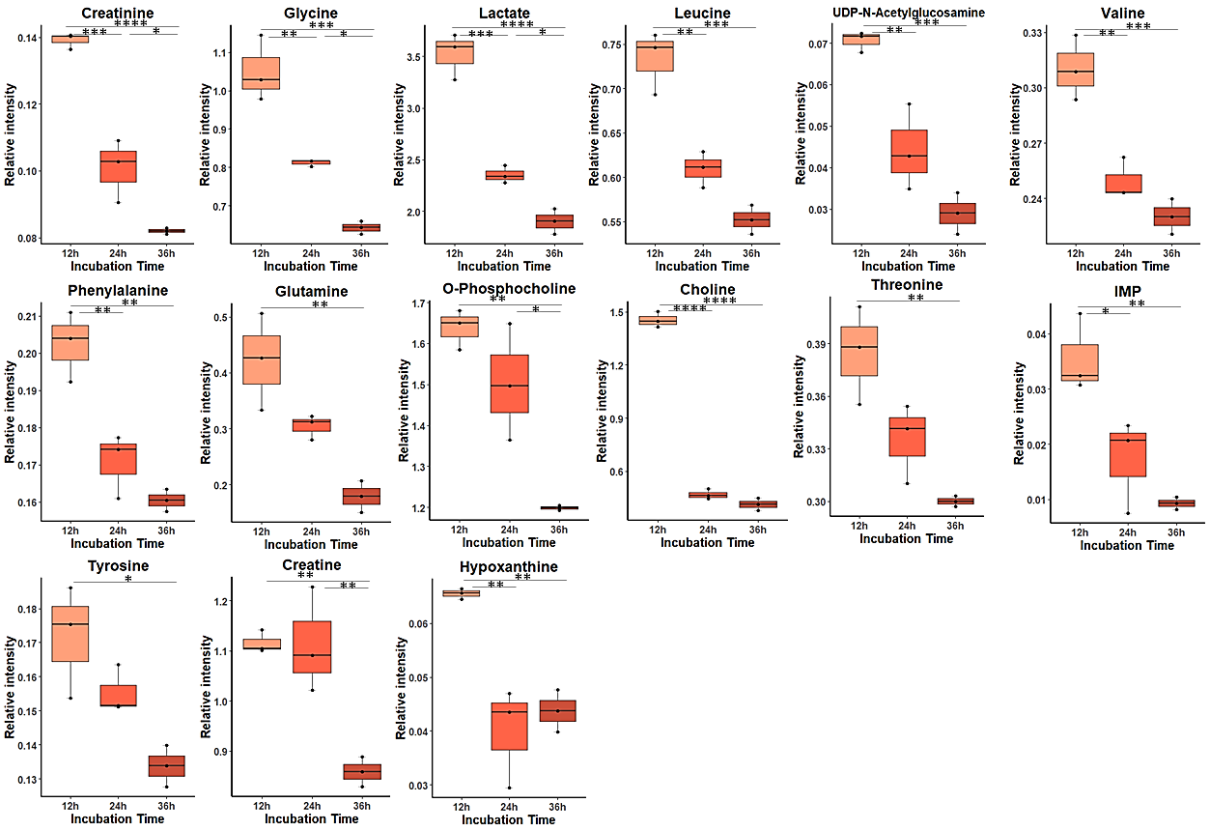

Figure 5. Boxplots for metabolites with VIP score above 1.00 identified by PLS-R model and pass the significant test after remove outliers, than the average recalculated and re-tested by one-way ANOVA analysis, for cells extraction (**intercellular**) samples at hypoxia 1% condition after 12h, 24h and 36h incubation time and after *p* value adjustment ($p < 0.05$). Whiskers—1.5 × interquartile range (IQR); bar—median; box—range between first quartile (Q1) and third quartile (Q3). Black points—data points. *Adjusted *p* value < 0.05.

By increasing the oxygen concentration to 6% (normoxia) the metabolomics profile of detected metabolites showed a separation between incubation times 12h, 24h and 36h among PCs, interestingly, the loading plot of PCA showed clear contributions of the metabolites and their regulation to incubation times (**Figure** 4c, 4d). In order to explore the metabolites regulations to incubation time, we built a PLS regression

model and we validated with R2 = 0.8913, by using just one PLS component and the RMSECV was 4.20h and the CV-ANOVA of PLS-R model was significant with $p < 0.05$ (**Table** 3), the 13 most important metabolites were obtained with VIP (variable importance in projection) value greater than 1.00 such as (aspartate, UDP-N-Acetylglucosamine, succinate, O-phosphocholine, glutamine, N-Acetylaspartate, glutamate, acetate, threonine, tyrosine, lactate, creatinine, creatine) (**Figure** 5c,5d), and their significance was tested by ANOVA, hence, we excluded non-significant ANOVA such as (tyrosine, creatinine, creatine, and IMP) from further analysis, and the results revealed the following trend:

1. All influential metabolites down-regulated with increased incubation time (**Figure** 6).

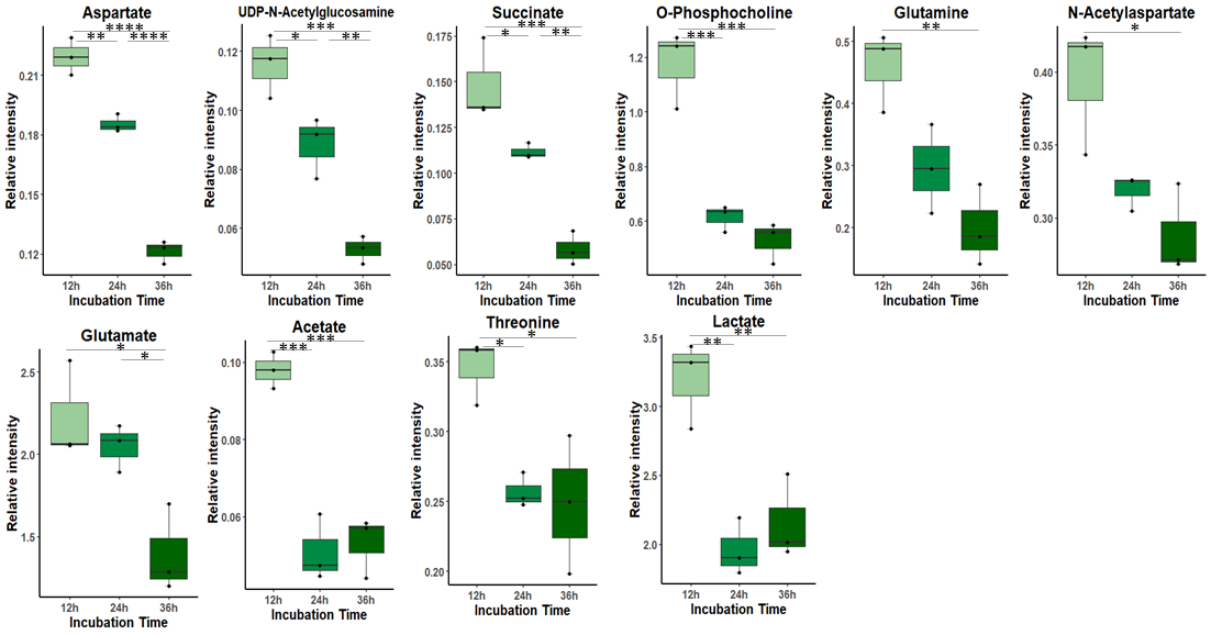

Figure 6. Boxplots for metabolites with VIP score above 1.00 identified by PLS-R model and statistically significant in one-way ANOVA test for HT1080 cells extracts (**intercellular**) samples at normoxia 6% condition after 12h, 24h and 36h incubation time and after p value adjustment ($p < 0.05$). Whiskers—1.5 × interquartile range (IQR); bar—median; box—range between first quartile (Q1) and third quartile (Q3). Black points—data points. *Adjusted p value < 0.05.

At hyperoxia 21% intracellular extracts revealed different trends from hypoxia 1% and normoxia 6% during the time of incubation, the natural separation between incubation time groups, we illustrate PCA by showing PC1 and PC2 coefficients of each interval time of incubation, we noticed a separation, we performed the loading plot in to displaying the explanatory pattern present in the dataset (**Figure** 4e, 4f). The correlation validation between incubation time at hyperoxia 21% was by the PLS

regression model, and we found a high correlation with R2 = 0.9816, by using just 2 PLS components and the RMSECV was 1.65h and the CV-ANOVA of PLS-R model was significant (**Table** 2), the 17 most important metabolites from PLS regression model were obtained with VIP (variable importance in projection) value above 1.00 such as (O-phosphocholine, aspartate, UDP-N-Acetylglucosamine, fumarate, glutamine, tyrosine, histidine, isoleucine, valine, leucine, phenylalanine, formate, glutamate, glycine, asparagine, alanine and IMP (**Figure** 5e,5f). We applied the ANOVA test to check their significance, hence, revealing different metabolic regulations as follows (**Figure** 7):

1. O-phosphocholine, aspartate, UDP-N-Acetylglucosamine, fumarate, glutamine and glutamate are downregulated with increased incubation time.
2. There weren't any significant differences between 24h and 36h, unlike, tyrosine, histidine, isoleucine, valine, leucine, phenylalanine, formate, glycine, asparagine and alanine showed up-regulation with time, especially after 36h, but was no significant difference between 12h and 24h.

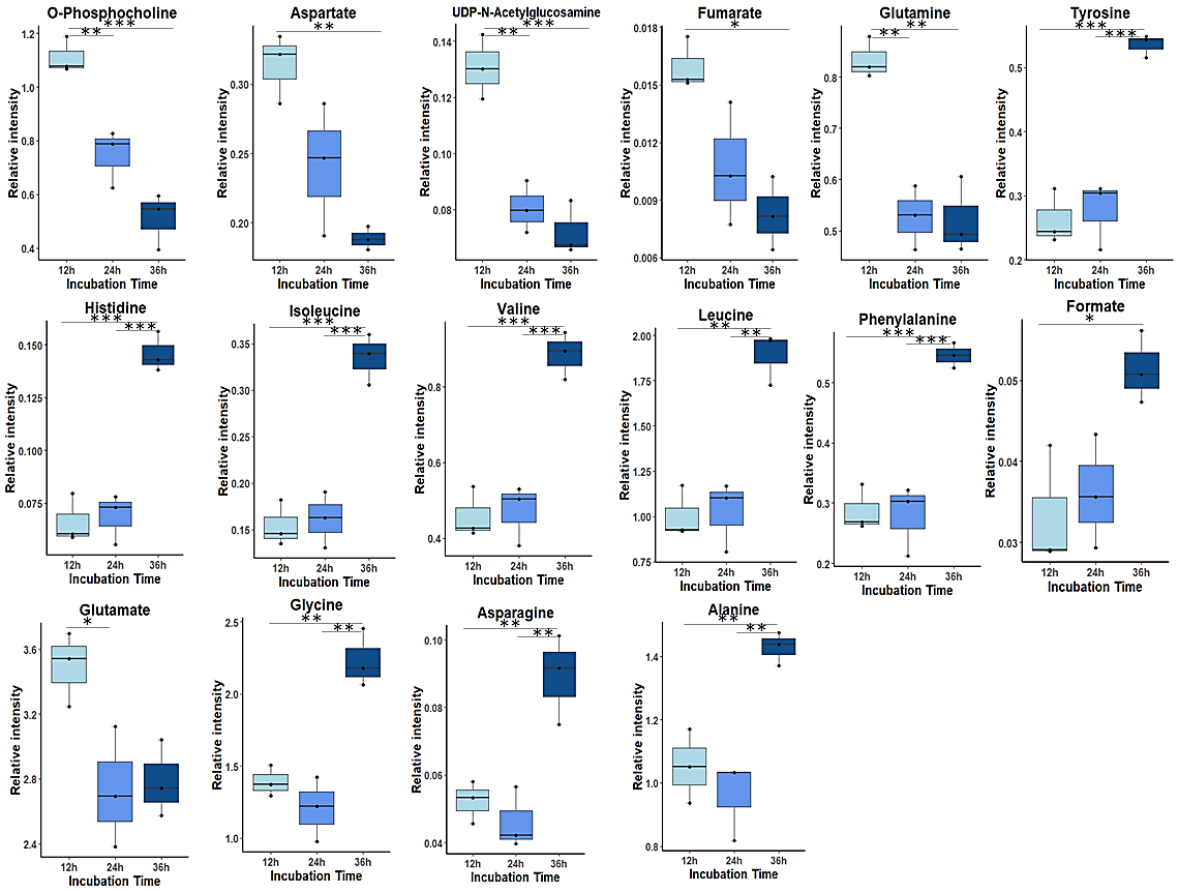

Figure 7. Boxplots for metabolites with VIP score above 1.00 identified by PLS-R model and statistically significant in one-way ANOVA test for HT1080 cells extracts (intercellular) samples at hyperoxia 21% condition after 12h, 24h and 36h incubation time and after *p* value adjustment ($p < 0.05$). Light blue— hyperoxia 21% after 12h; blue— hyperoxia 21% after 24h; dark blue— hyperoxia 21% after 36h. Whiskers—1.5 × interquartile range (IQR); bar—median; box—range between first quartile (Q1) and third quartile (Q3). Black points—data points. *Adjusted *p* value < 0.05.

Table 3. The direction of change summary of all significant metabolites in multivariate analysis with VIP > 1 and univariate analysis by ANOVA with *p* value < 0.05 from cell extract (intracellular) dataset at hypoxia 1%, normoxia 6% and hyperoxia 21%.

Nr	Hypoxia 1%	Normoxia 6%	Hyperoxia 21%
1	**UDP-GlcNAc**	**UDP-GlcNAc**	**UDP-GlcNAc**
2	**Glutamine**	**Glutamine**	**Glutamine**
3	**O-phosphocholine**	**O-phosphocholine**	**O-phosphocholine**
4	Lactate	Lactate	Histidine
5	Threonine	Threonine	Formate
6	Creatinine	Aspartate	Aspartate
7	Creatine	Glutamate	Glutamate
8	Choline	Succinate	Fumarate
9	IMP	N-Acetylaspartate	Isoleucine
10	Hypoxanthine	Acetate	Asparagine
11	Valine		Valine
12	Glycine		Glycine
13	Phenylalanine		Phenylalanine
14	Leucine		Leucine
15	Tyrosine		Tyrosine

Notes; Bold metabolites, cross common metabolites; red metabolites, up regulation; blue metabolites, down-regulation

3.2.1.2 The sensitivity of intracellular metabolome to hypoxia, normoxia and hyperoxia in function of time intervals

To understand the sensitivity of intracellular metabolome at each cultivation time, we built a PCA score loading plots of the ^{1}H NMR dataset and PLS regression model to predict the total scores of either in each incubation time points (12h, 24h and 36h) for hypoxic, normoxic and hyperoxic cells). Furthermore, the models were correctly validated, and obtained the R2X (cum), the total sum of variation in Y explained by the model R2Y (cum) and goodness of prediction Q2(cum) scores

and CV-ANOVA *p*-values for intracellular cell extracts in comparisons between oxygen concentrations groups.

Table 4. The multivariate analysis models summary of cells extract (intracellular) dataset for comparisons between 1%, 6% and 21% oxygen concentrations at each incubation time.

Time	O_2% Comparisons	Model Type	PC/ LV	N =	R2X (cum)	R2Y (cum)	Q2 (cum)	CV-ANOVA *p* value
12h	1% vs. 6% vs. 21%	PCA	2	9	0.821	–	–	–
	1% vs. 6% vs. 21%	PLS	3	9	0.898	0.989	0.939	7.41×10^{-2}
24h	1% vs. 6% vs. 21%	PCA	2	9	0.788	–	–	–
	1% vs. 6% vs. 21%	PLS	2	9	0.723	0.951	0.808	9.73×10^{-2}
36h	1% vs. 6% vs. 21%	PCA	3	9	0.962	–	–	–
	1% vs. 6% vs. 21%	PLS	2	9	0.927	0.985	0.975	**2.86×10^{-3}**

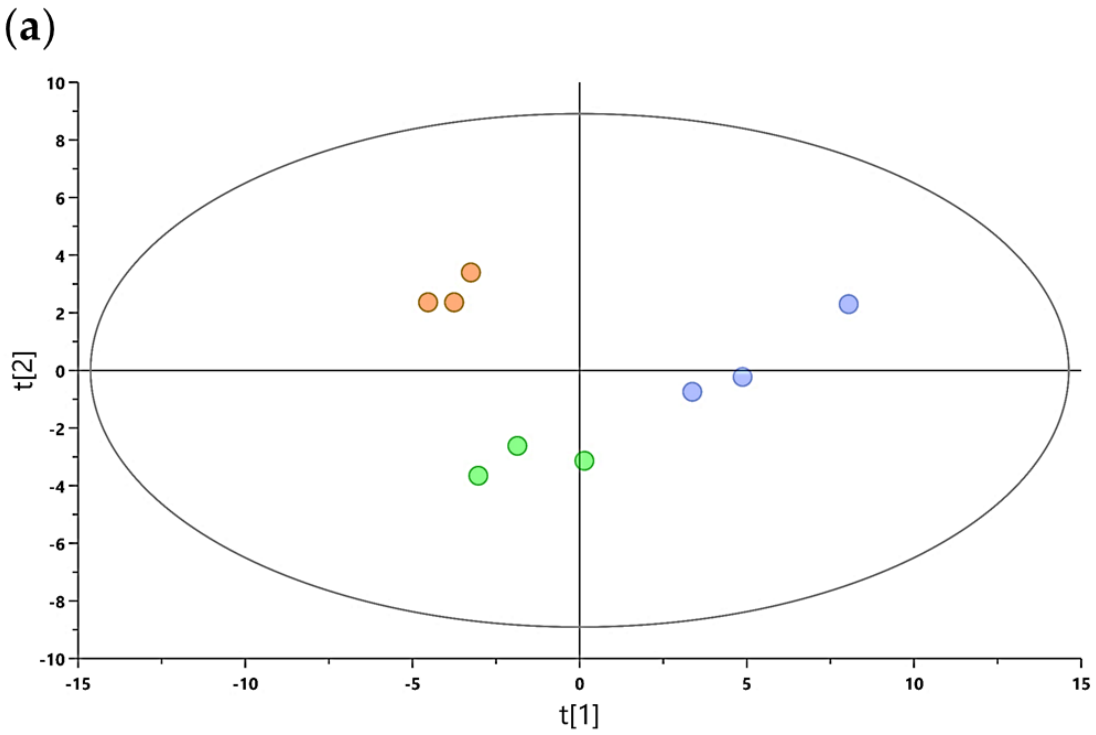

(b)

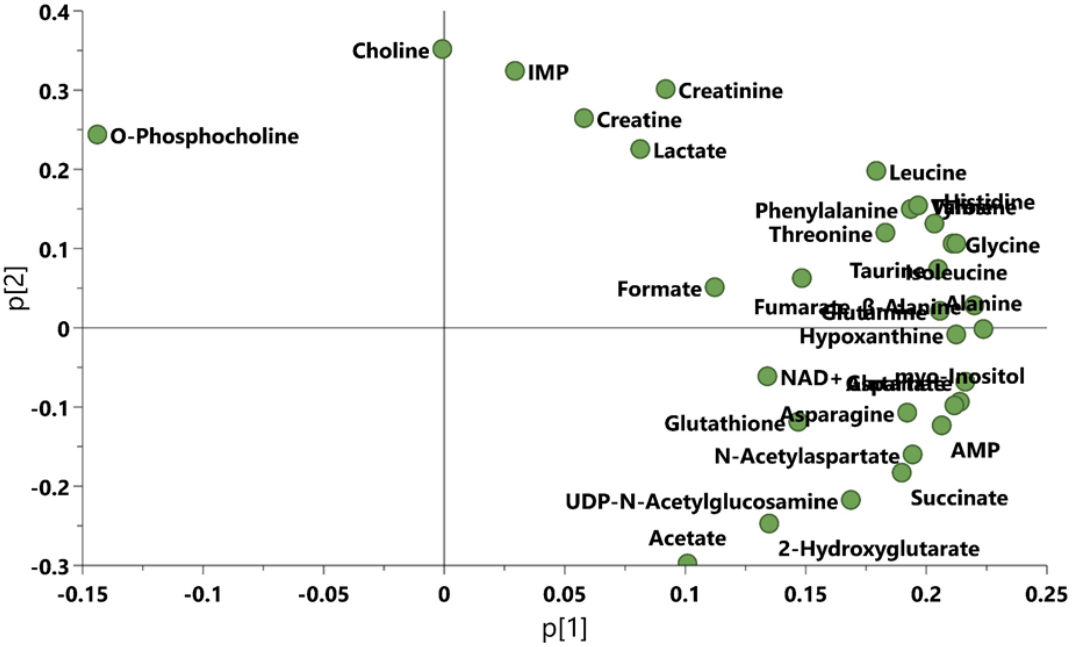
Choline
IMP
Creatinine
Creatine
Lactate
O-Phosphocholine
Leucine
Phenylalanine
Threonine
Glycine
Isoleucine
Formate
Alanine
Hypoxanthine
myo-Inositol
Asparagine
Glutathione
AMP
N-Acetylaspartate
Succinate
UDP-N-Acetylglucosamine
Acetate
2-Hydroxyglutarate
p[1]
p[2]

(c)

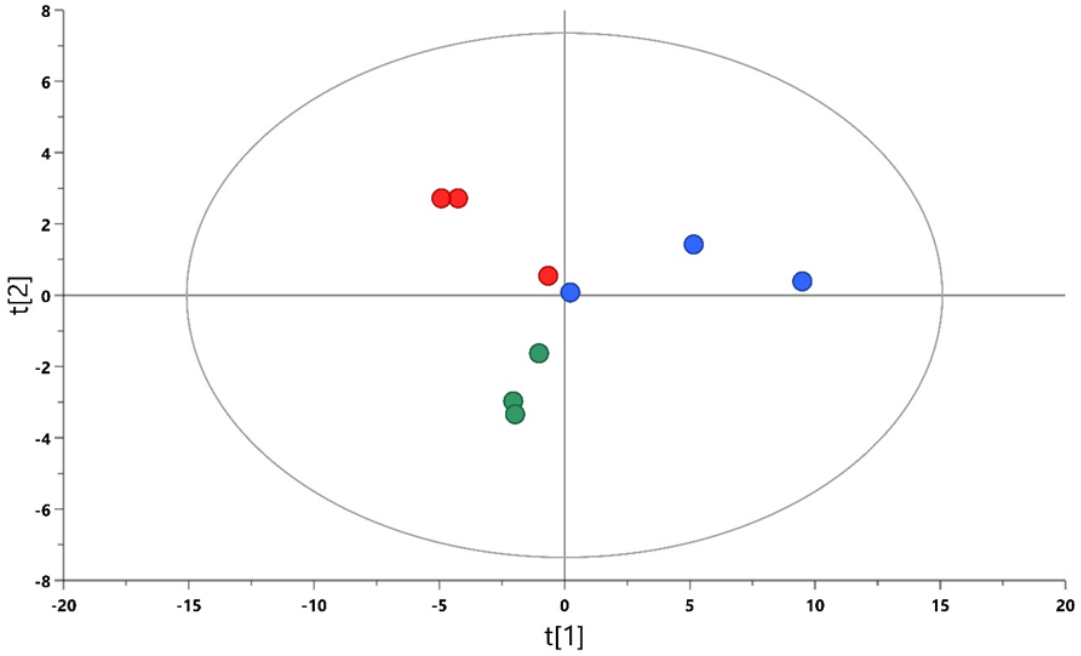
t[1]
t[2]

(d)

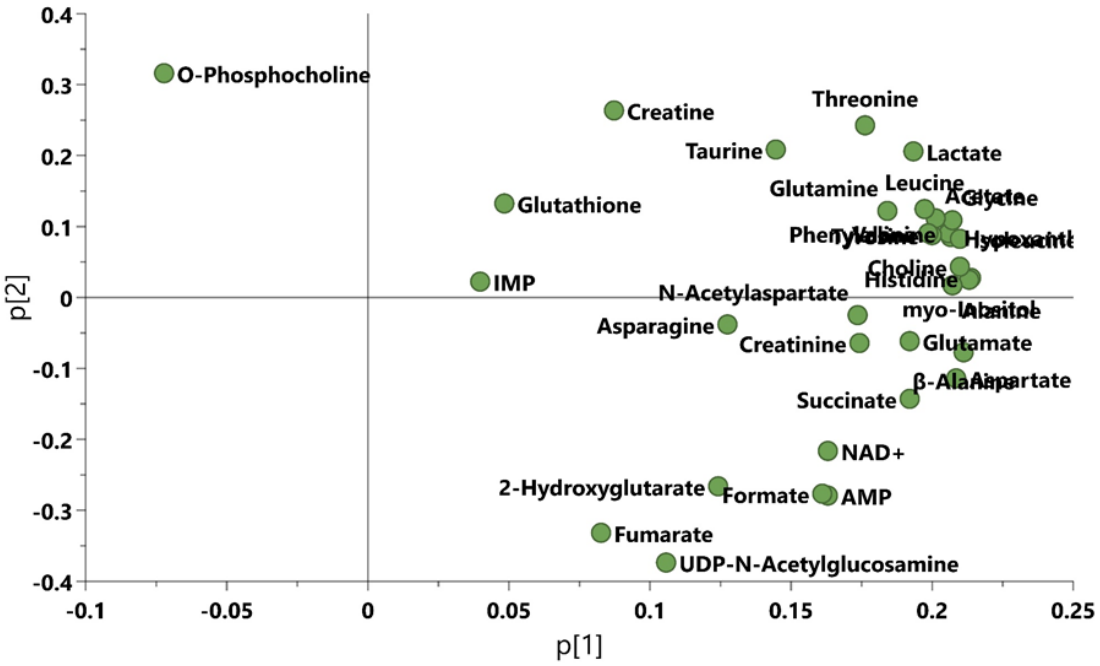
O-Phosphocholine
Creatine
Threonine
Taurine
Lactate
Glutamine
Leucine
Glutathione
IMP
Choline
Histidine
N-Acetylaspartate
Asparagine
Creatinine
Glutamate
Succinate
NAD+
2-Hydroxyglutarate
Formate
AMP
Fumarate
UDP-N-Acetylglucosamine
p[1]
p[2]

(e)

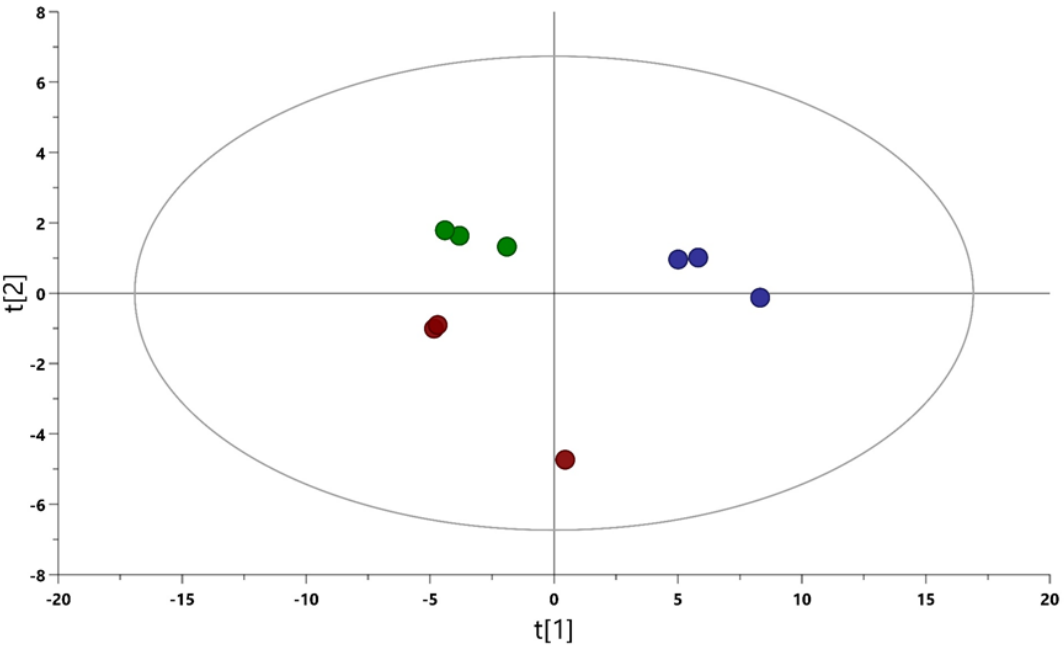
t[1]
t[2]

(f)

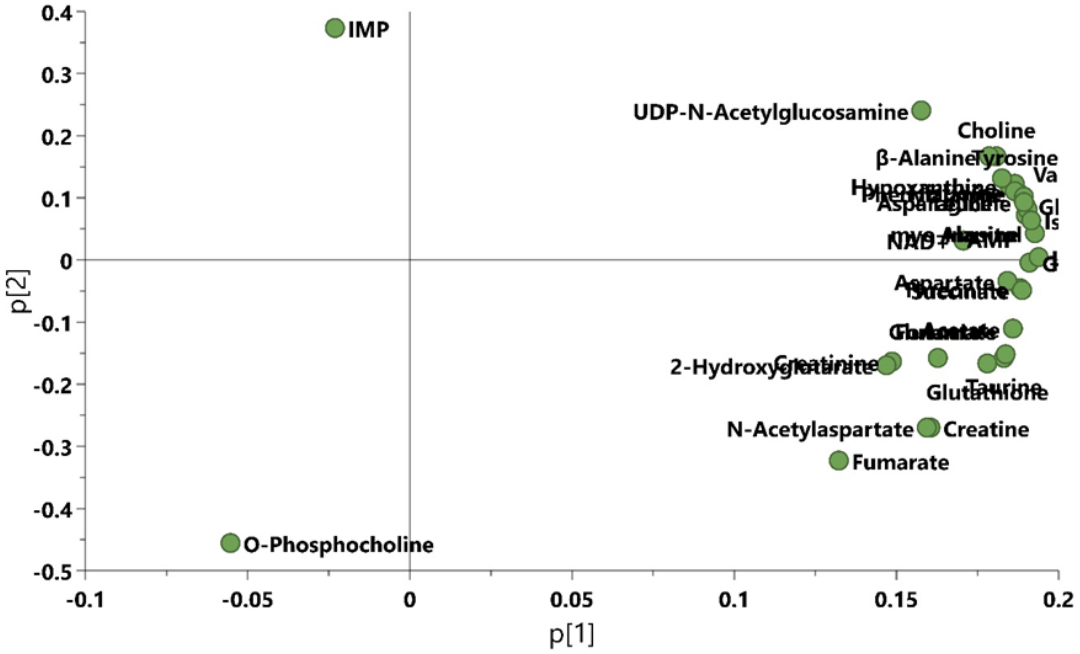

Figure 8. The Principal Component Analysis (PCA) scores plot and loadings plots for PCA model for ^{1}H-NMR relative intensity data driven models for HT1080 cells extracts (intracellular) during incubation time at hypoxia 1%, normoxia 6% and hyperoxia 21% conditions. (**a, b**) After 12h incubation; (**c, d**) After 24h incubation; (**e, f**) After 36h incubation. Light red, hypoxia 1% after 12h; red, hypoxia 1% after 24h; dark red, hypoxia 1% after 36h; Light green, normoxia 6% after 12h; green, normoxia 6% after 24h; dark green, normoxia 6% after 36h; Light blue, hyperoxia 21% after 12h; blue, hyperoxia 21% after 24h; dark blue, hyperoxia 21% after 36h.

(a)

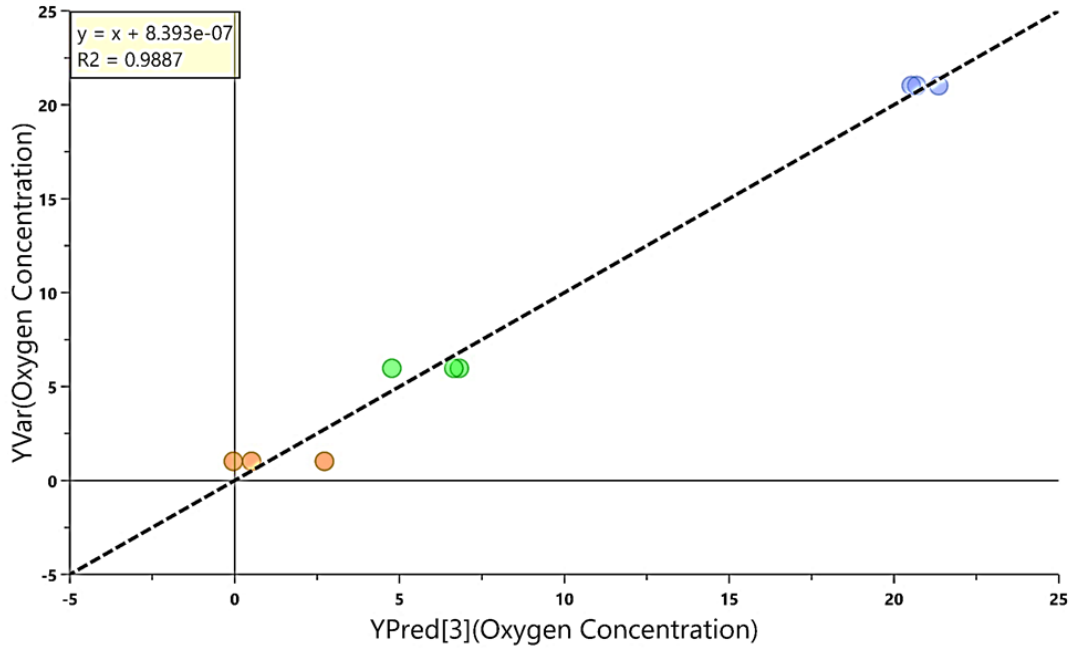

(**b**)

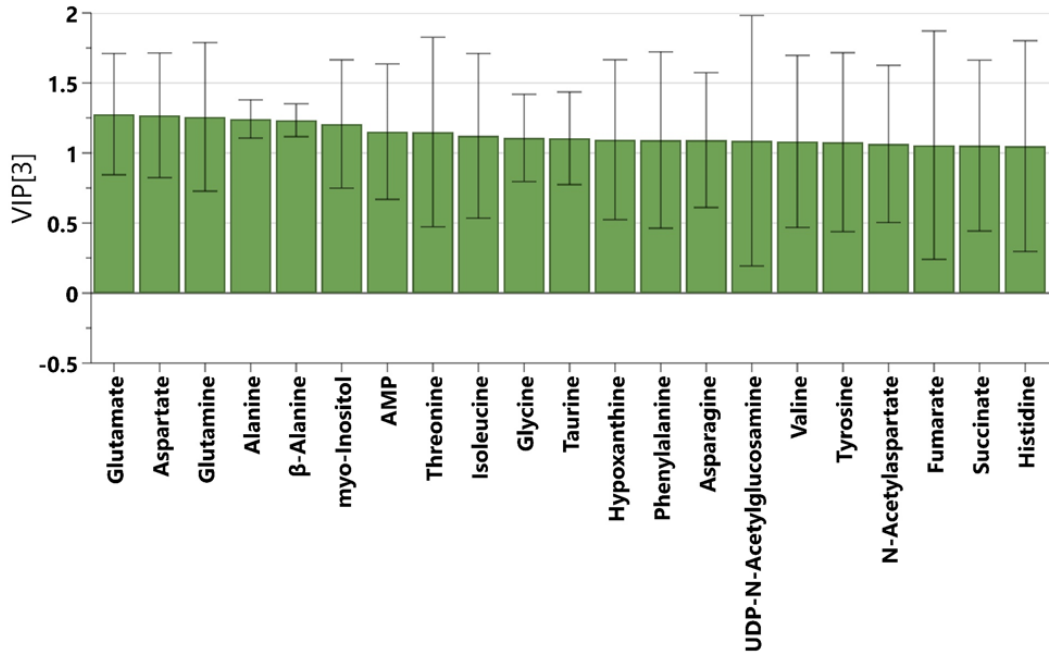
VIP[3]
2
1.5
1
0.5
0
-0.5
Glutamate
Aspartate
Glutamine
Alanine
β-Alanine
myo-Inositol
AMP
Threonine
Isoleucine
Glycine
Taurine
Hypoxanthine
Phenylalanine
Asparagine
UDP-N-Acetylglucosamine
Valine
Tyrosine
N-Acetylaspartate
Fumarate
Succinate
Histidine

(**c**)

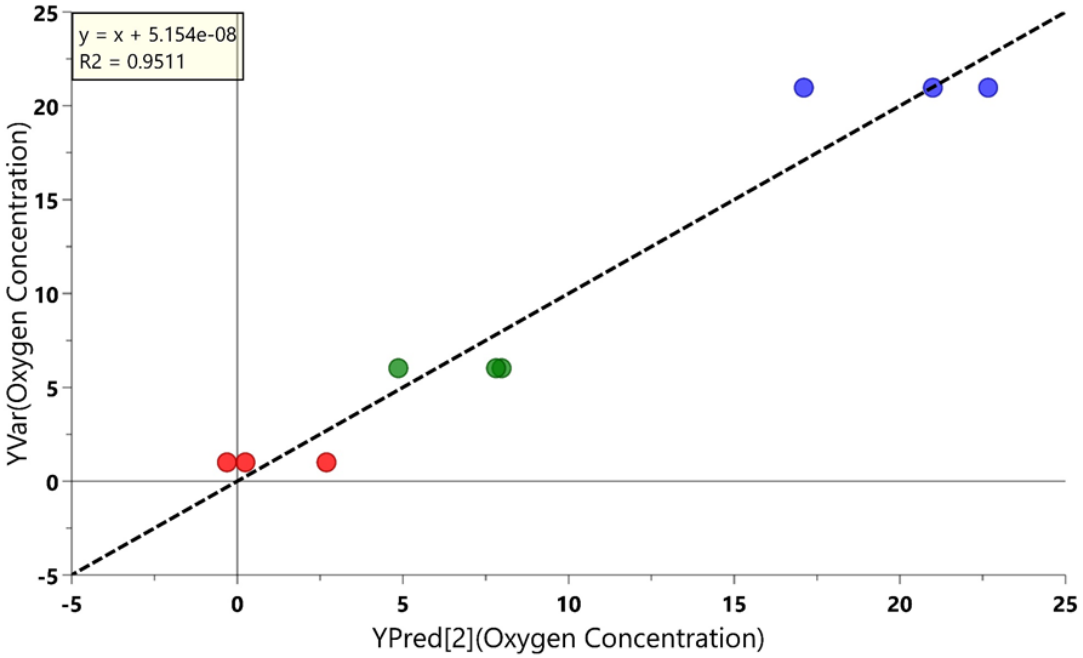
y = x + 5.154e-08
R2 = 0.9511
YVar(Oxygen Concentration)
YPred[2](Oxygen Concentration)
25
20
15
10
5
0
-5
-5
0
5
10
15
20
25

(**d**)

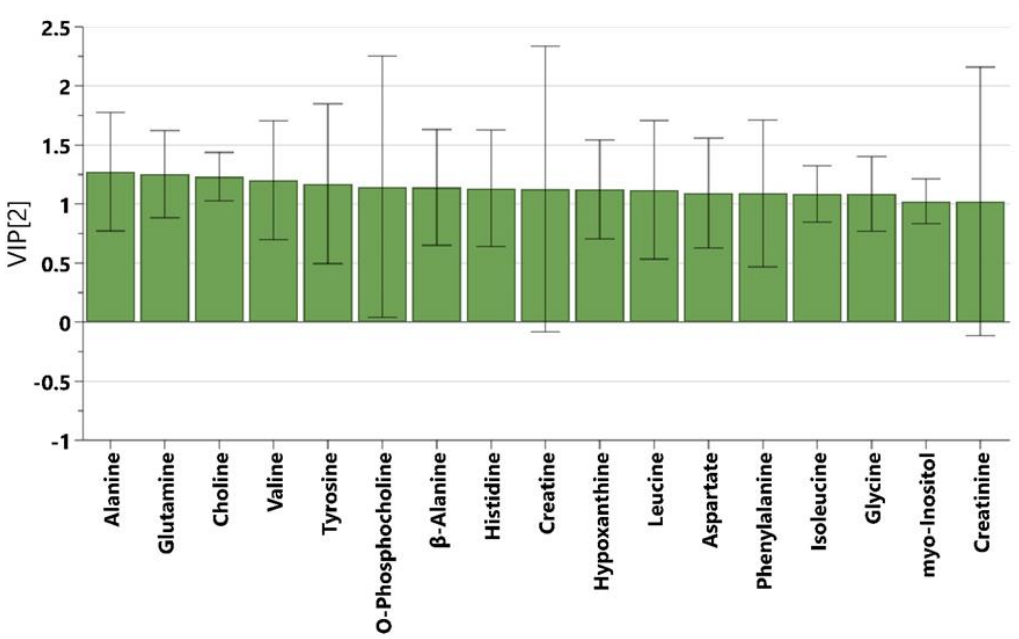
VIP[2]
2.5
2
1.5
1
0.5
0
-0.5
-1
Alanine
Glutamine
Choline
Valine
Tyrosine
O-Phosphocholine
β-Alanine
Histidine
Creatine
Hypoxanthine
Leucine
Aspartate
Phenylalanine
Isoleucine
Glycine
myo-Inositol
Creatinine

(**e**)

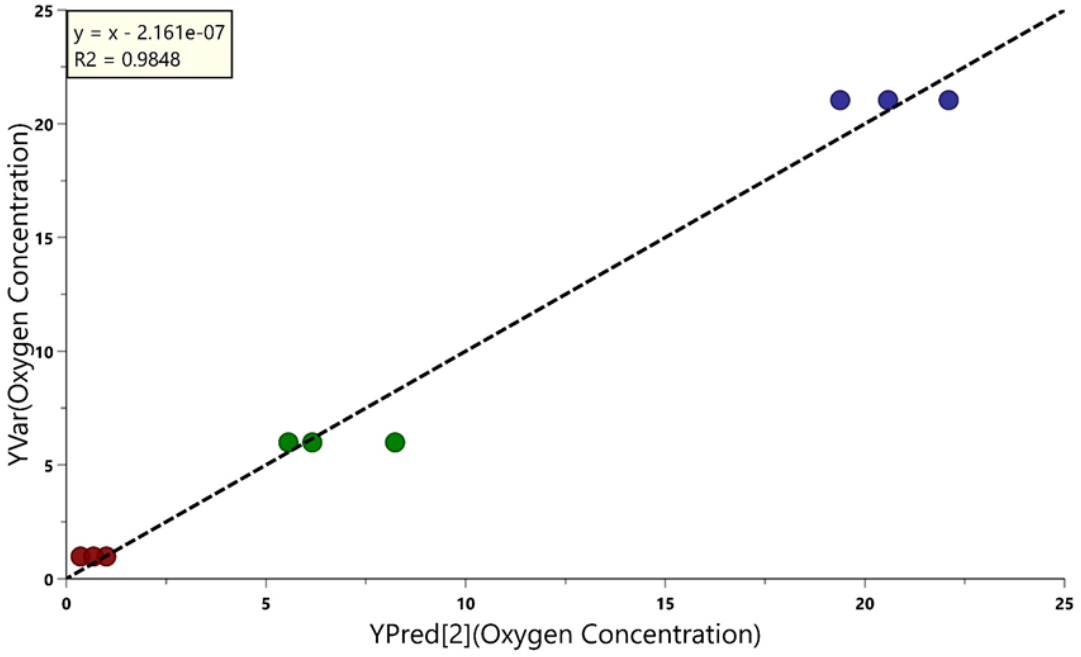
y = x - 2.161e-07
R2 = 0.9848
YVar(Oxygen Concentration)
YPred[2](Oxygen Concentration)
0
5
10
15
20
25

(f)

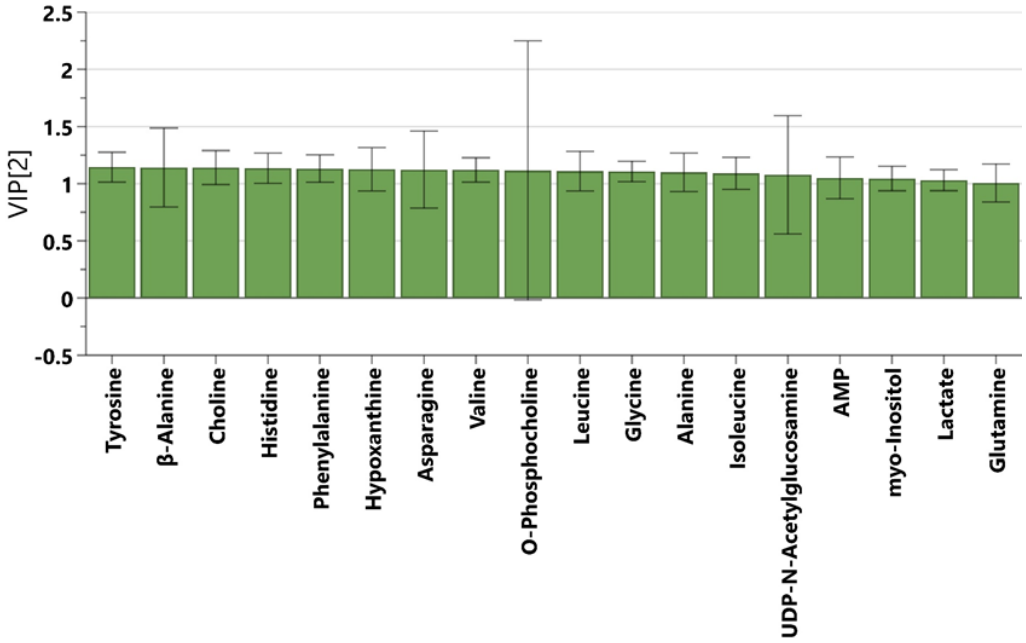

Figure 9. Graphical representation for ^{1}H-NMR relative intensity data driven models for HT1080 cells extracts (intercellular) after cultivation time at hypoxia 1%, normoxia 6% and hyperoxia 21% conditions. (**a, c, e**) Prediction plot from the partial least squares-regression model (PLS-R) built on relative intensity of ^{1}H-nuclear magnetic resonance spectra dataset after 12h, 24h and 36h, respectively. (**b, d, f**) The Variable importance in the projection (VIP) score plot for the PLSR model (VIP >1.00) after ,12h, 24h and 36h, respectively. Light red, hypoxia 1% after 12h; red, hypoxia 1% after 24h; dark red, hypoxia 1% after 36h; Light green, normoxia 6% after 12h; green, normoxia 6% after 24h; dark green, normoxia 6% after 36h; Light blue, hyperoxia 21% after 12h; blue, hyperoxia 21% after 24h; dark blue, hyperoxia 21% after 36h.

After 12h incubation, the PCA score of intracellular metabolome revealed a separation tendency among PC1 and PC2 between hypoxia 1%, normoxia 6% and hyperoxia 21% groups, and the loading plot was plotted which provided the explanatory pattern in the data set (**Figure** 8b). In order to explore the metabolites regulations to different oxygen concentrations, we have built a PLS regression model, and we found a high correlation between oxygen concentrations after 12h incubation with R2 = 0.9887 and by using just 3 PLS components, the RMSECV was 2.43%, but didn't reach statistically significant difference between groups by CV-ANOVA (**Table** 4), possibly due to the small nature of the differences after 12h of incubation between groups. The most influential intracellular metabolites with VIP (variable importance in projection) greater than 1.00 revealed 21 metabolites (glutamate, aspartate, glutamine, alanine, beta-Alanine, myo-Inositol, AMP, threonine, isoleucine,

glycine, taurine, hypoxanthine, phenylalanine, asparagine, UDP-N-Acetylglucosamine, valine, tyrosine, N-Acetylaspartate, fumarate, succinate, histidine), In addition, were tested by ANOVA, their tendency at different oxygen concentrations revealed overall commonly increased and upregulated to high oxygen concentration (hyperoxia 21%). However we noticed different metabolic regulation depend on their degree of sensitivity to oxygen concentration, for instance, 11 common cross significant metabolites with VIP value above 1.00 including glutamine, alanine, beta-alanine, myo-Inositol, isoleucine, glycine, hypoxanthine, phenylalanine, valine, tyrosine and histidine share the same trend of sensitivity with no significant differences between hypoxia 1% and normoxia 6% at each interval time point 12h, 24h and 36h. However, there were also another specific trends after 12h of incubation as follows (**Figure** 10):

1. The UDP-N-Acetylglucosamine, N-Acetylaspartate and succinate showed no significant differences between normoxia 6% and hyperoxia 21%.
2. Highly sensitive in concentration-dependent manner showed by glutamate, aspartate, myo-Inositol and AMP.

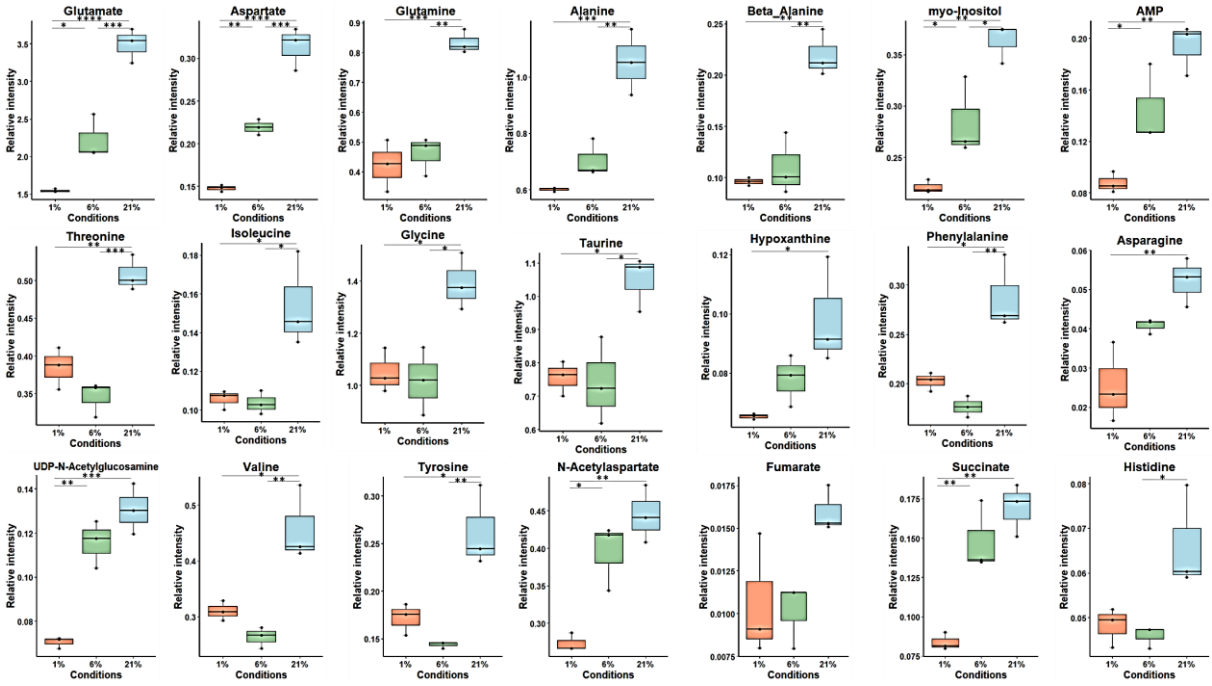

Figure 10. Boxplots for most important metabolites with VIP value above 1.00 identified by PLSR model and their significant was calculated by one-way ANOVA analysis for cells extraction (intracellular) samples after 12h incubation time at Hypoxia 1%, Normoxia 6% and Hyperoxia 21% conditions and after p value adjustment ($p < 0.05$). Whiskers—1.5 × interquartile range (IQR); bar—median; box—range between first quartile (Q1) and third quartile (Q3). Black points—data points. * Adjust *p* value < 0.05.

While the PCA model of the intracellular metabolome after 24h revealed clustering of three groups among both PC1 And PC2 (**Figure** 8c), the loading plot was plotted which provided the explanatory pattern in the data set (**Figure** 8d). While the PLS regression model revealed as well, a correlation fit between groups of oxygen concentrations with R2 = 0.9511 and by using just two PLS components the RMSECV value was 3.73% (**Figure** 9c) and the CV-ANOVA of PLS-R model wasn't significant (**Table** 4). The most influential intracellular metabolites with VIP (variable importance in projection) greater than 1.00 revealed 17 metabolites (alanine, glutamine, choline, valine, O-phosphocholine, beta-alanine, histidine, creatine, hypoxanthine, leucine, aspartate, phenylalanine, isoleucine, glycine, myo-inositol and creatinine), and were tested by ANOVA, their tendency at different oxygen concentrations which revealed all pass the ANOVA test, except, myo-inositol and creatinine didn't pass and we removed them from our calculations and were follow one specific trend:

1. All the remaining 15 metabolites commonly increased and upregulated to high oxygen concentration (hyperoxia 21%).
2. After 24h of incubation there wasn't any specific all of these metabolites act the same with no differences between hypoxia and normoxia. Except, O-phosphocholine was downregulated and showed no difference between normoxia 6% and hyperoxia 21% (**Figure** 11).

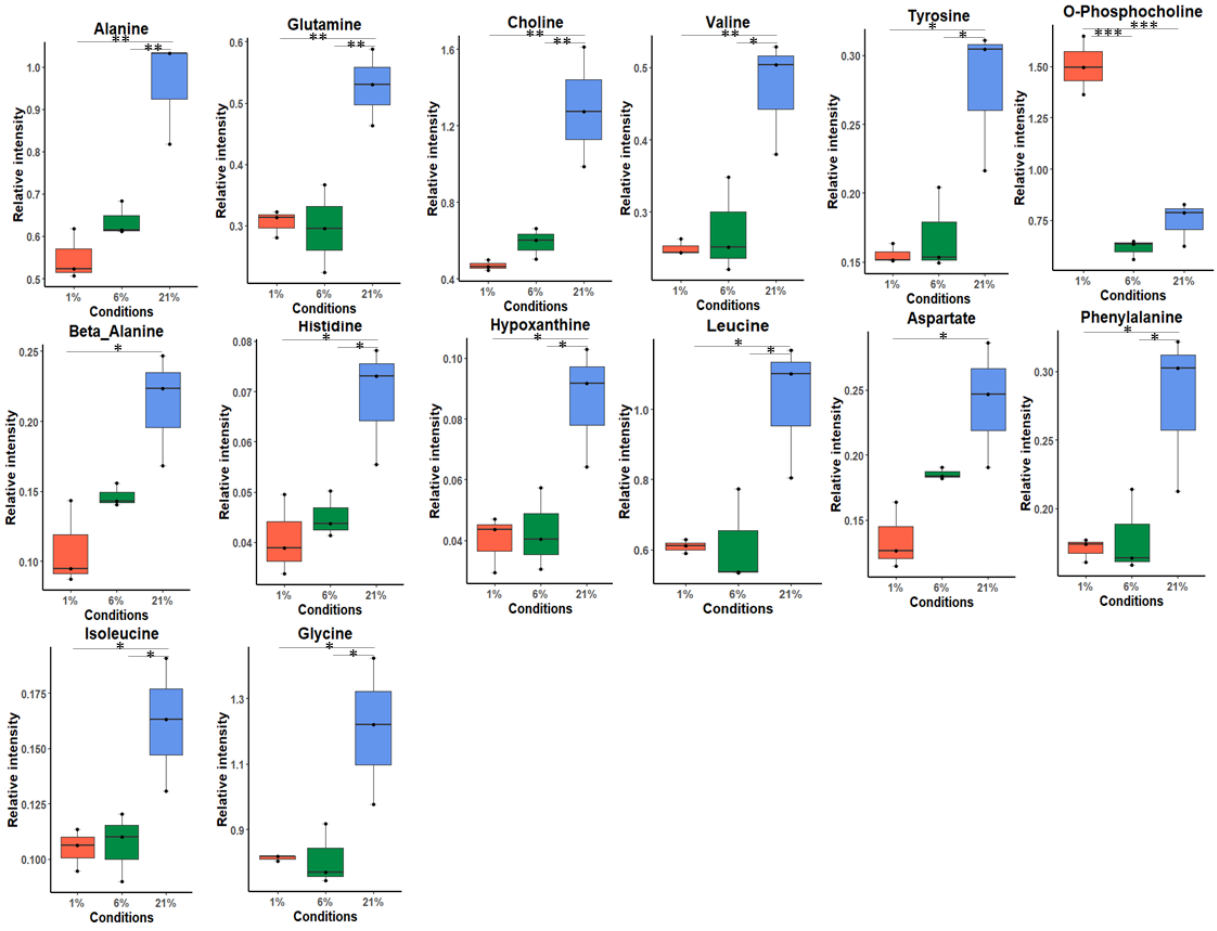

Figure 11. Boxplots for most important metabolites with VIP value above 1.00 identified by PLSR model and their significant was calculated by one-way ANOVA analysis for cells extraction (intracellular) samples after 24h incubation time at Hypoxia 1%, Normoxia 6% and Hyperoxia 21% conditions and after p value adjustment ($p < 0.05$). Whiskers—1.5 × interquartile range (IQR); bar—median; box—range between first quartile (Q1) and third quartile (Q3). Black points—data points. * Adjust *p* value < 0.05.

In addition, after 36h the PCA showed a trend of grouping toward oxygen concentrations differences, and the loading plot was plotted which provided the explanatory pattern in the data set (**Figure** 8e, 8f).

The regression model of PLS after 36h was validated between groups of oxygen concentrations with $R^2 = 0.9848$ and by using just two PLS components, the root-mean-square-error-of-cross-validation (RMSECV) was 1.67%, (**Figure** 9e) and the CV-ANOVA of PLS-R model was significant (**Table** 4). while, the most important metabolites with VIP above 1.00 was obtained with 18 metabolites (tyrosine, beta-alanine, choline, histidine, phenylalanine, hypoxanthine, asparagine, valine, O-phosphocholine, leucine, glycine, alanine, isoleucine, UDP-N-acetylglucosamine, AMP, myo-Inositol, lactate, glutamine) (**Figure** 9f) and were tested

by ANOVA and their tendency at different oxygen concentrations after 36h incubation as follows (**Figure** 12):

1. Showed no significant differences between hypoxia 1% and normoxia 6% for all influential metabolites, except, O-phosphocholine highly upregulated at hypoxia 1%, but no significant differences between normoxia 6% and hyperoxia 21%.
2. Both UDP-N-Acetylglucosamine and choline were high sensitive to oxygen concentration in concentration-depend manner.
3. Surprisingly, the significant inosine monophosphate (IMP) with VIP value equal to 0.578, showed a fluctuation behavior toward oxygen concentrations, with upregulation at normoxia 6%, nevertheless, at hypoxia 1% was down-regulated than hyperoxia 21%.

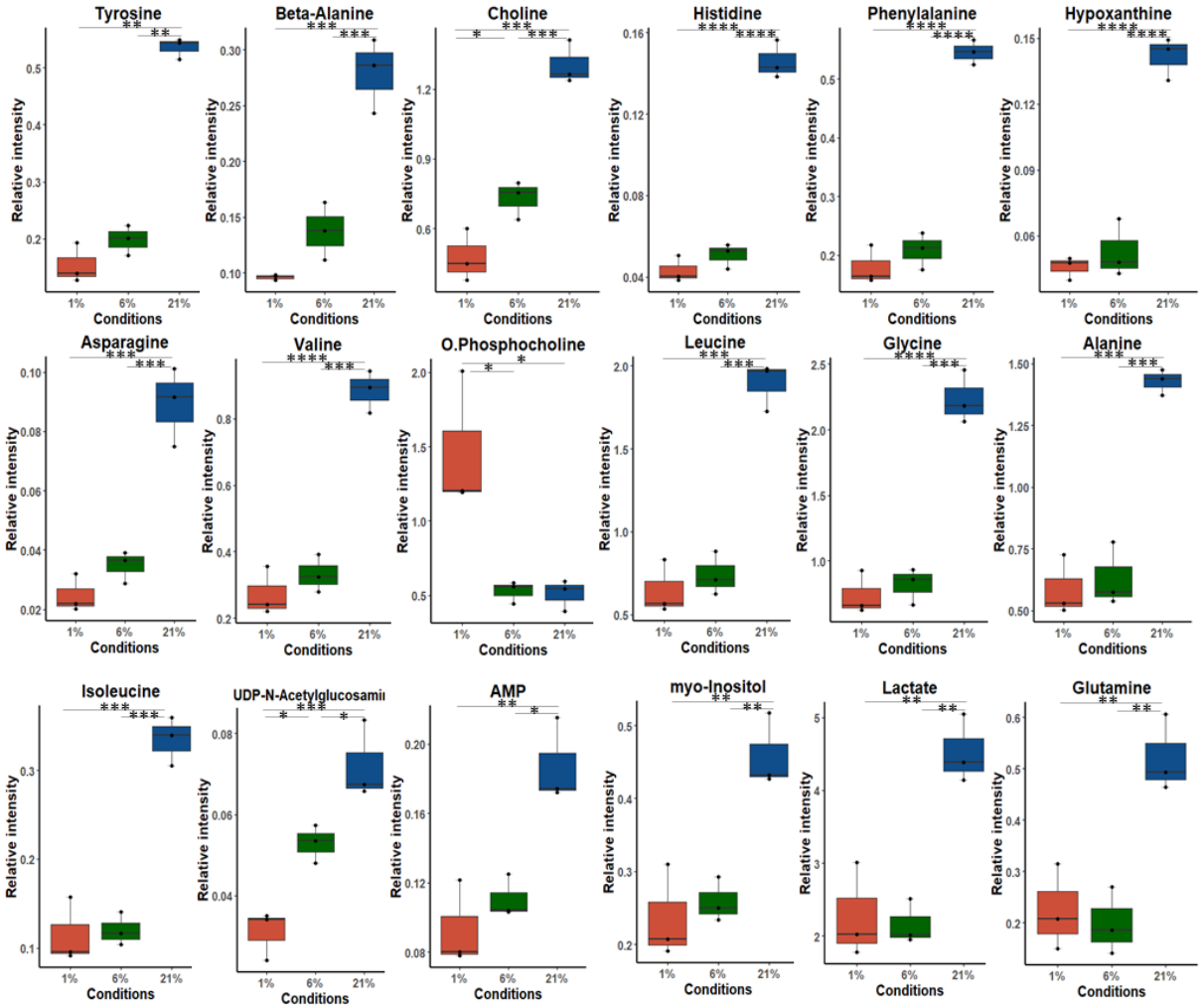

Figure 12. Boxplots for most important metabolites with VIP value above 1.00 identified by PLS-R model and their significant was calculated by one-way ANOVA analysis for cells extraction (intracellular) samples after 36h incubation time at Hypoxia 1%, Normoxia 6% and Hyperoxia 21% conditions and after p value adjustment ($p < 0.05$). Whiskers—1.5 × interquartile range

(IQR); bar—median; box—range between first quartile (Q1) and third quartile (Q3). Black points—data points. * Adjust *p* value < 0.05.

3.3.2. Extracellular results

The total sample set is 9 samples from post-cultured media, for each condition (1%, 6% and 21%), we conducted ^{1}H NMR-based metabolome analysis and 39 metabolites were successfully assigned in media respectively, (**Figure** 13, **Table** 5).

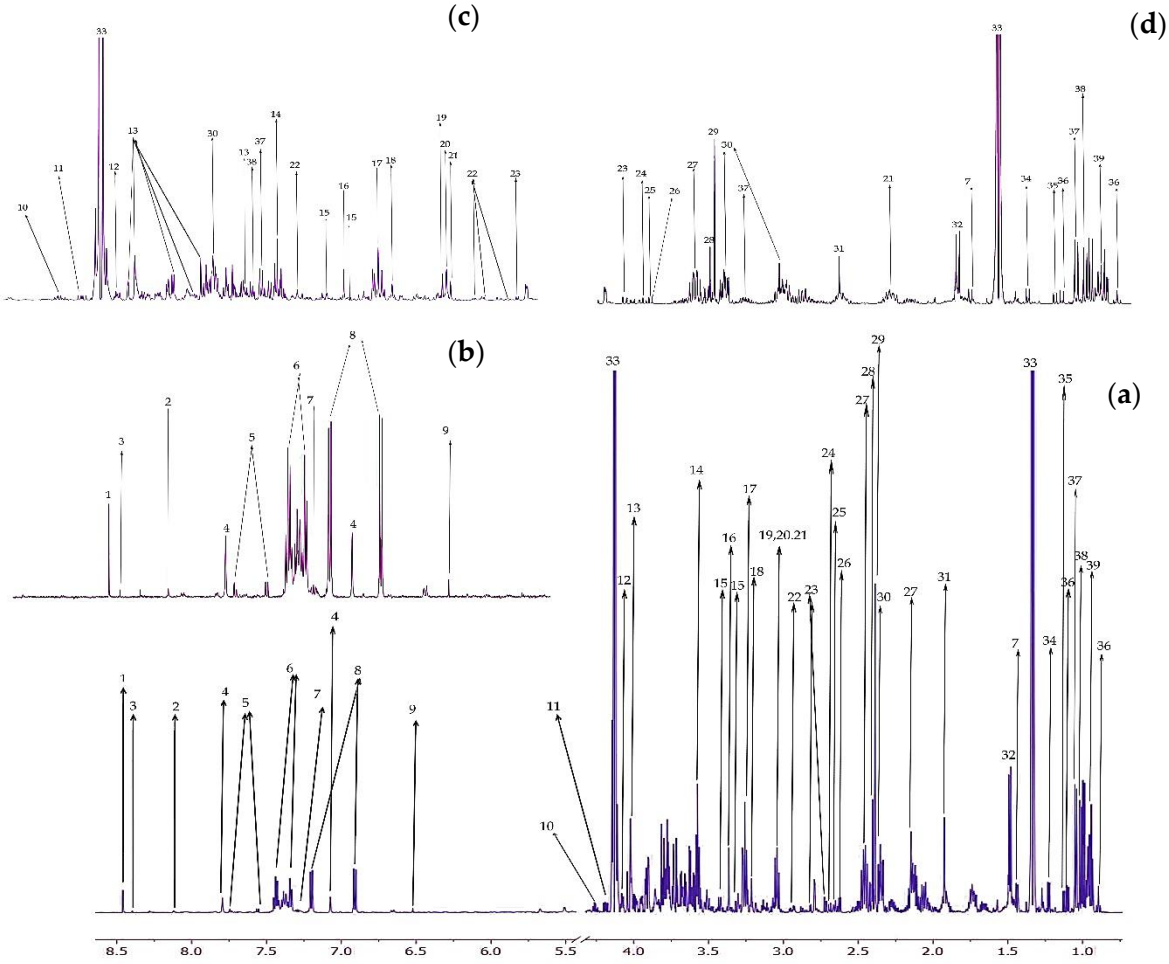

Figure 13. The representative 1H NMR spectrum obtained from cells extracts of HT1080. (a) Full 1H-NMR spectrum from δ 5.0 to δ 9.0; (b) Enlarged spectrum from δ 9.0 to δ 6.5; (c) Enlarged spectrum from δ 5.0 to δ 2.7; (d) Enlarged spectrum from δ 2.7 to δ 0.5. The metabolites were identified from 1- 39 as mentioned from Table 5 respectively.

Table 5. List of chemical shift values and proton assignments for HT1080 post-cultured medium extract metabolome identified by ^{1}H NMR spectroscopy with human metabolome database identification number (HMDB).

No	Metabolites	Peak Assignments	Peak Centers (ppm)	HMDB ID
1	Formate	s	8.44	HMDB0000142

2	Hypoxanthine	s	8.188, s (8.20)	HMDB0000157
3	S-Adenosylhomocysteine	s	8.38	HMDB0000939
4	Histidine	s	7.78	HMDB0000177
5	Tryptophan	m	7.543, m (7.722)	HMDB0000929
6	Phenylalanine	m	7.323, m (7.423), m (7.371)	HMDB0000159
7	2-Phenylpropionate	m	7.277, m (7.348), m (7.370),d (1.422)	HMDB0011743
8	Tyrosine	m	7.185, m (6.893)	HMDB0000158
9	Fumarate	s	6.506	HMDB0000134
10	Threonine	m	4.24, d (3.58), d (1.317)	HMDB0000167
11	Pyroglutamate	dd	4.171, m (2.407)	HMDB0000267
12	*myo*-Inositol	t	dd (4.065), 3.615, dd (3.544), t (3.287)	HMDB0000211
13	Fructose	d	m (4.016), m (4.00), m(3.895), m (3.818), 3.790, d (3.709), d (3.703)	HMDB0000660
14	Glycine	s	3.558	HMDB0000123
15	Proline	m	3.414	HMDB0000162
16	Methanol (residual solvent)	s	3.349	HMDB0001875
17	Arginine	m	3.241	HMDB0003416
18	Choline	s	3.198	HMDB0000097
19	Creatinine	s	3.039	HMDB0000562
20	Creatine	s	3.027	HMDB0000064
21	Lysine	t	3.027, tt (1.723)	HMDB0000182
22	Asparagine	t	2.928, t (2.849)	HMDB0000168
23	Aspartate	dd	2.689	HMDB0000191
24	Methionine	t	2.636	HMDB0000696
25	2-Oxoisocaproate	d	2.607	HMDB0000695
26	Methylamine	s	2.601	HMDB0000164
27	Glutamine	m	2.424, m (2.141)	HMDB0000641
28	Succinate	s	2.387	HMDB0000254
29	Pyruvate	s	2.37	HMDB0000243
30	Glutamate	m	2.35, m (2.039)	HMDB0060475
31	Acetate	s	1.9	HMDB0000042
32	Alanine	d	1.47	HMDB0000161
33	Lactate	d	1.318, q (4.112)	HMDB0000190
34	Methylmalonate	d	1.211	HMDB0000202
35	3-Hydroxybutyrate	d	1.109	HMDB0000011
36	3-Methyl-2-oxovalerate	d	1.084, t (0.879)	HMDB0000491
37	Valine	d	0.977, d (3.610), m (2.260), d (1.030)	HMDB0000883

38	Isoleucine	d	0.997, t (0.926)	HMDB0000172
39	Leucine	t	0.944	HMDB0000687

***s**, singlet; **d**, doublet; **t**, triplet; **q**, quartet; **m**, multiplet; **dd**, doublet of doublet; **ppm value underline**, the quantitative peak.*

We performed PCA score loading plots of the ^{1}H NMR dataset and PLS regression model to predict the total scores of either in each incubation time point, besides, in each oxygen concentration (hypoxia 1%, normoxia 6% and hyperoxia 21%). Furthermore, the PLS-R models were correctly validated, and obtained the R^2X (cum), good correlation R^2Y (cum) and goodness of prediction Q^2(cum) scores and significant CV-ANOVA *p*-values for extracellular media extracts in comparisons between oxygen concentrations groups and between incubation time groups without control samples.

3.3.2.1. The extracellular metabolic profile changes at hypoxia 1%, normoxia 6% and hyperoxia 21% in function of oxygen concentrations

Table 6. The multivariate analysis model summary of extracellular NMR- based metabolome in comparisons between 12h, 24h and 36h at 1%, 6% and 21% oxygen concentrations.

O_2%	Incubation Time Comparisons	Model Type	PC/ LV	N =	R^2X (cum)	R^2Y (cum)	Q^2 (cum)	CV-ANOVA *p* value
1%	12h vs. 24h vs. 36h	PCA	2	9	0.868	–	–	–
	12h vs. 24h vs. 36h	PLS	2	9	0.863	0.915	0.394	8.95×10^{-1}
6%	12h vs. 24h vs. 36h	PCA	2	9	0.804	–	–	–
	12h vs. 24h vs. 36h	PLS	2	9	0.804	0.98	0.971	**9.51×10^{-3}**
21%	12h vs. 24h vs. 36h	PCA	3	9	0.915	–	–	–
	12h vs. 24h vs. 36h	PLS	1	9	0.45	0.951	0.894	**1.19×10^{-3}**

(a)

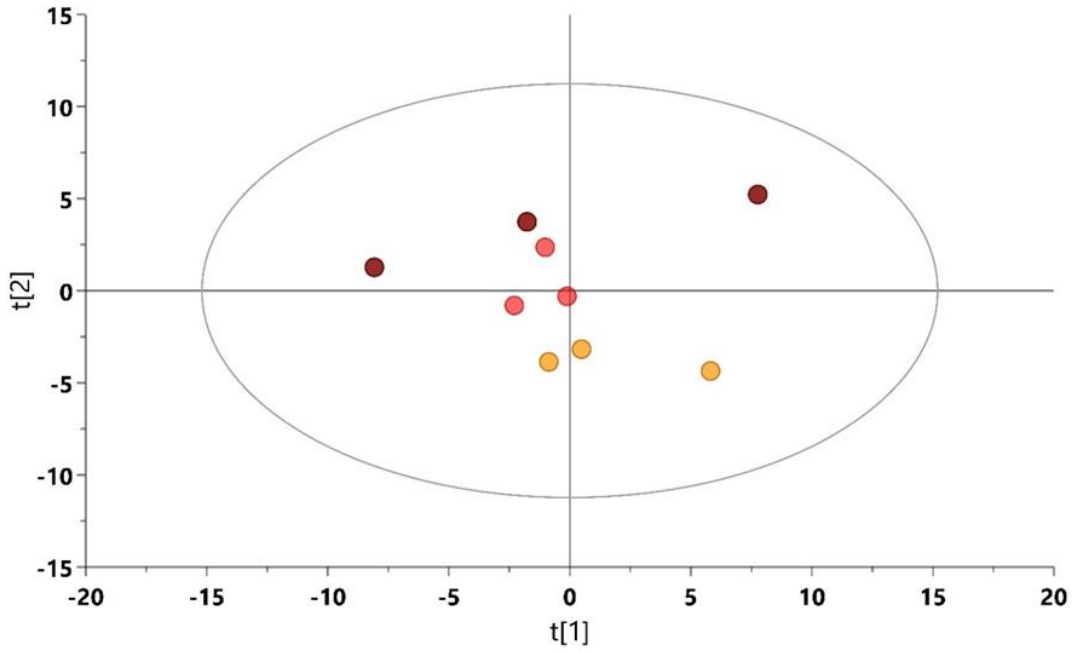
15
10
5
0
-5
-10
-15
t[2]
-20
-15
-10
-5
0
5
10
15
20
t[1]

(b)

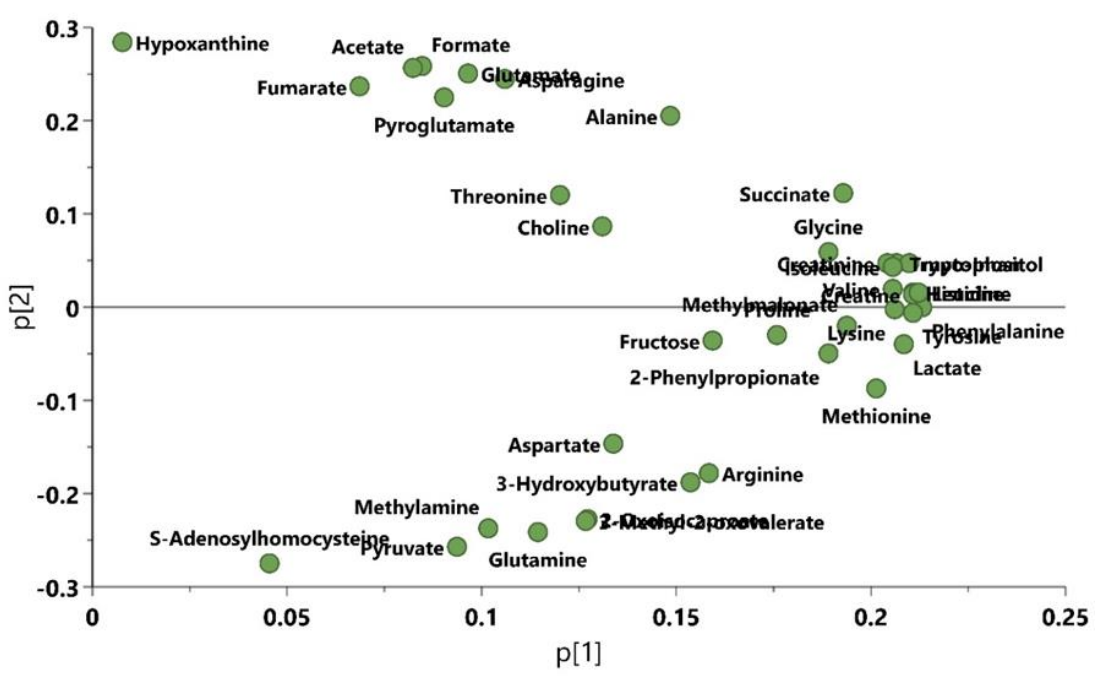
0.3
0.2
0.1
0
-0.1
-0.2
-0.3
p[2]
0
0.05
0.1
0.15
0.2
0.25
p[1]
Hypoxanthine
Acetate
Formate
Glutamate
Asparagine
Fumarate
Pyroglutamate
Alanine
Threonine
Choline
Succinate
Glycine
Methylmalonate
Proline
Lysine
Tyrosine
Phenylalanine
Fructose
2-Phenylpropionate
Lactate
Methionine
Aspartate
3-Hydroxybutyrate
Arginine
Methylamine
S-Adenosylhomocysteine
Pyruvate
Glutamine

(c)

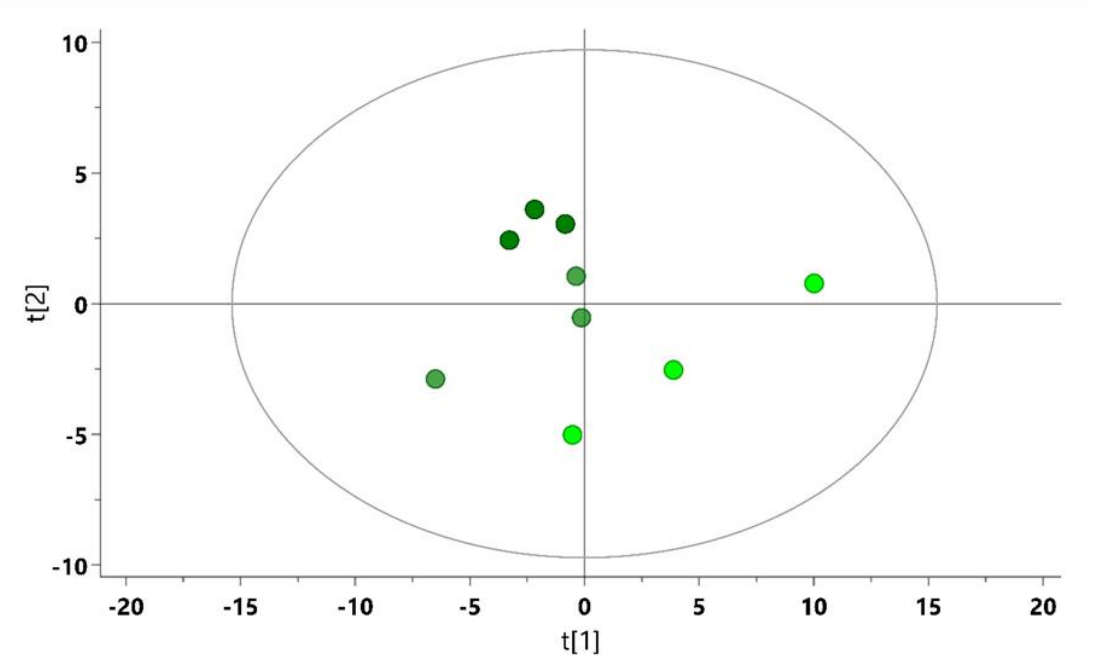
10
5
0
-5
-10
t[2]
-20
-15
-10
-5
0
5
10
15
20
t[1]

(d)

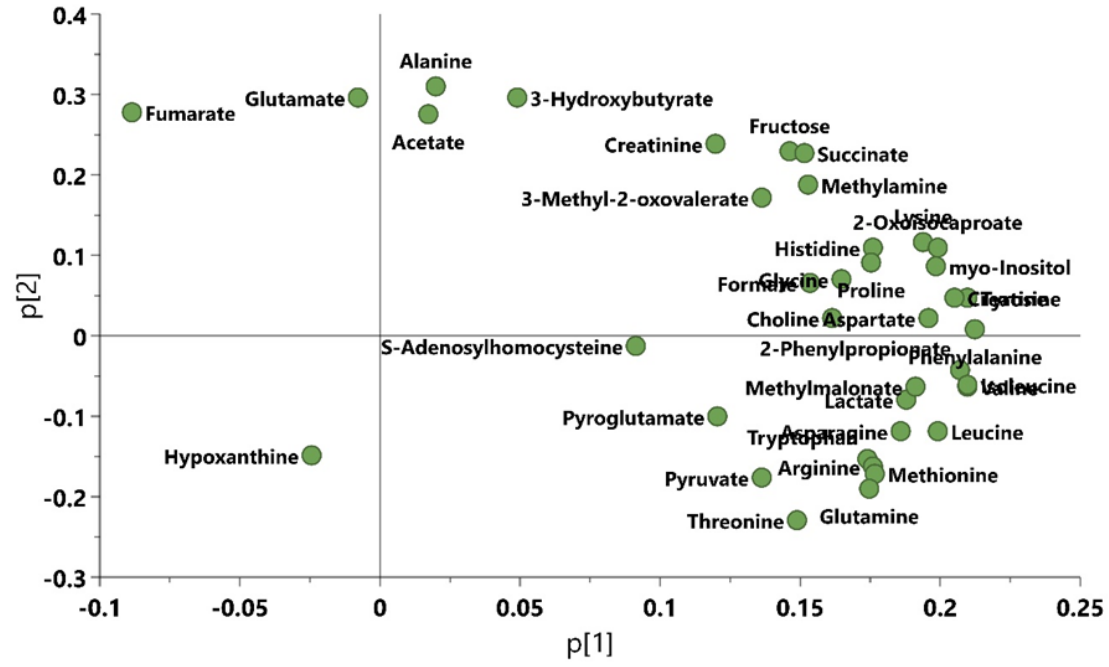
0.4
0.3
0.2
0.1
0
-0.1
-0.2
-0.3
p[2]
-0.1
-0.05
0
0.05
0.1
0.15
0.2
0.25
p[1]
Alanine
Glutamate
Fumarate
3-Hydroxybutyrate
Acetate
Creatinine
Fructose
Succinate
Methylamine
3-Methyl-2-oxovalerate
Histidine
myo-Inositol
Proline
Choline
Aspartate
S-Adenosylhomocysteine
2-Phenylpropionate
Phenylalanine
Methylmalonate
Lactate
Pyroglutamate
Leucine
Hypoxanthine
Arginine
Pyruvate
Methionine
Threonine
Glutamine

(e)

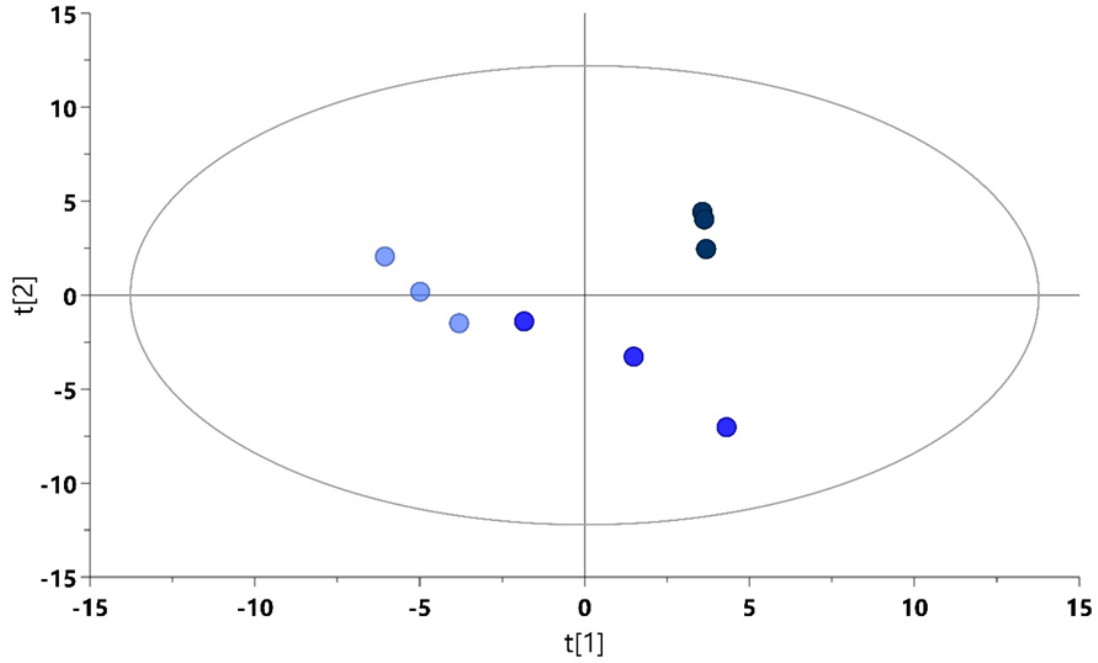

(f)

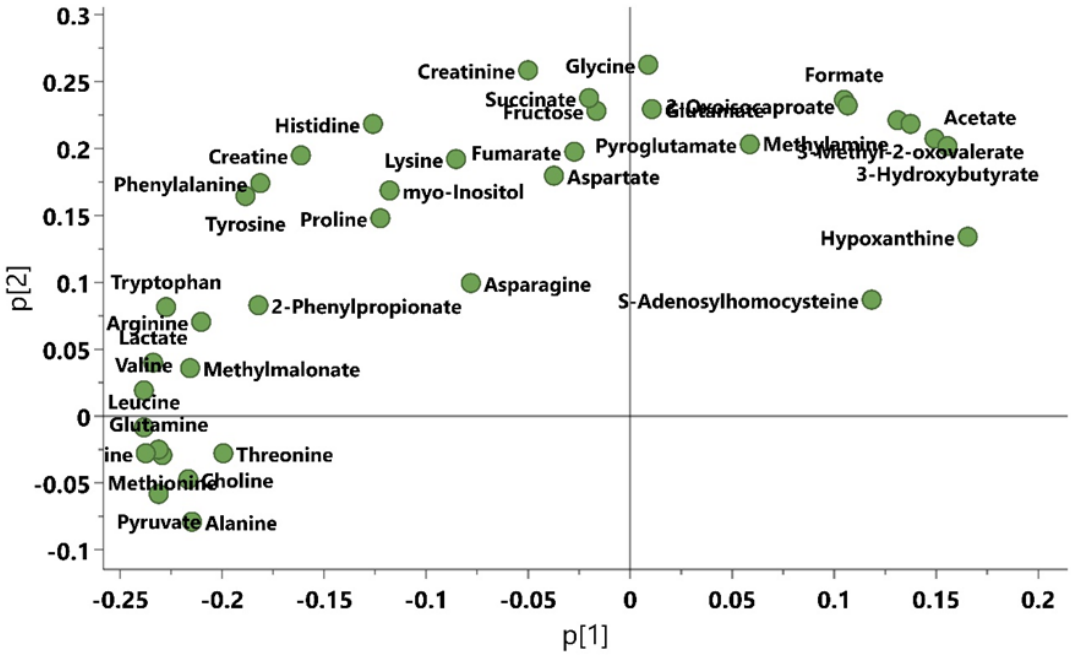

Figure 14. The Principal Component Analysis (PCA) scores plot and loadings plots for PCA model for ^{1}H-NMR relative intensity data driven models for HT1080 post culture medium extracts (extracellular) during incubation time at hypoxia 1%, normoxia 6% and hyperoxia 21% conditions. (**a, b**) a hypoxia 1%; (**c, d**) a normoxia 6%; (**e, f**) a hyperoxia 21%. Light red, hypoxia 1% after 12h; red, hypoxia 1% after 24h; dark red, hypoxia 1% after 36h; Light green, normoxia 6% after 12h; green, normoxia 6% after 24h; dark green, normoxia 6% after 36h; Light blue, hyperoxia 21% after 12h; blue, hyperoxia 21% after 24h; dark blue, hyperoxia 21% after 36h.

(a)

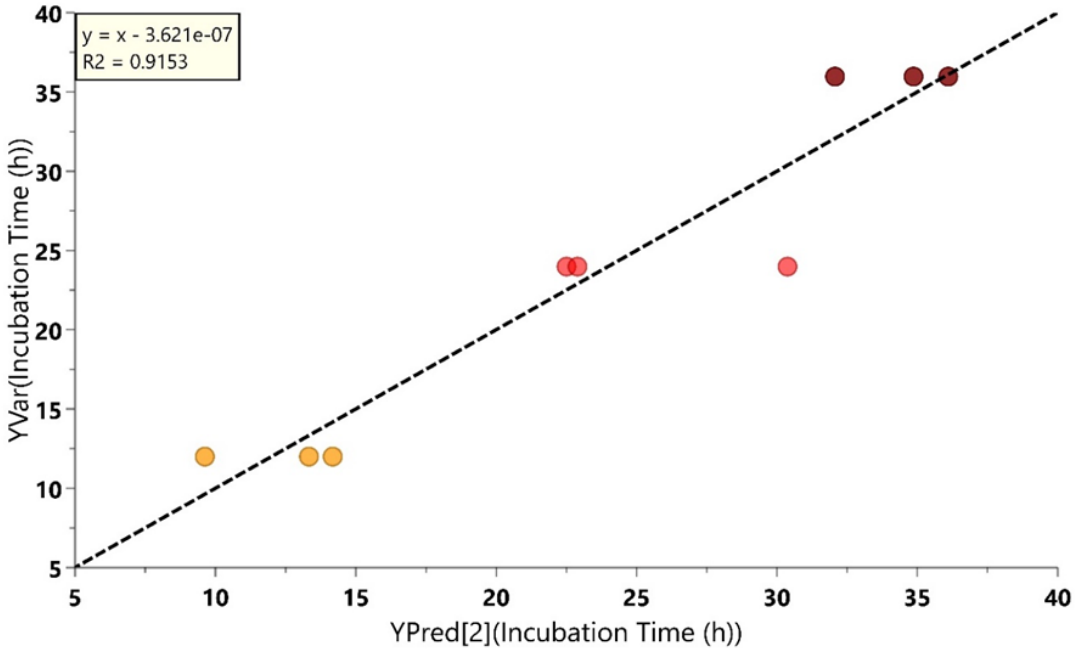
y = x - 3.621e-07
R2 = 0.9153
YVar(Incubation Time (h))
YPred[2](Incubation Time (h))
40
35
30
25
20
15
10
5
5
10
15
20
25
30
35
40

(b)

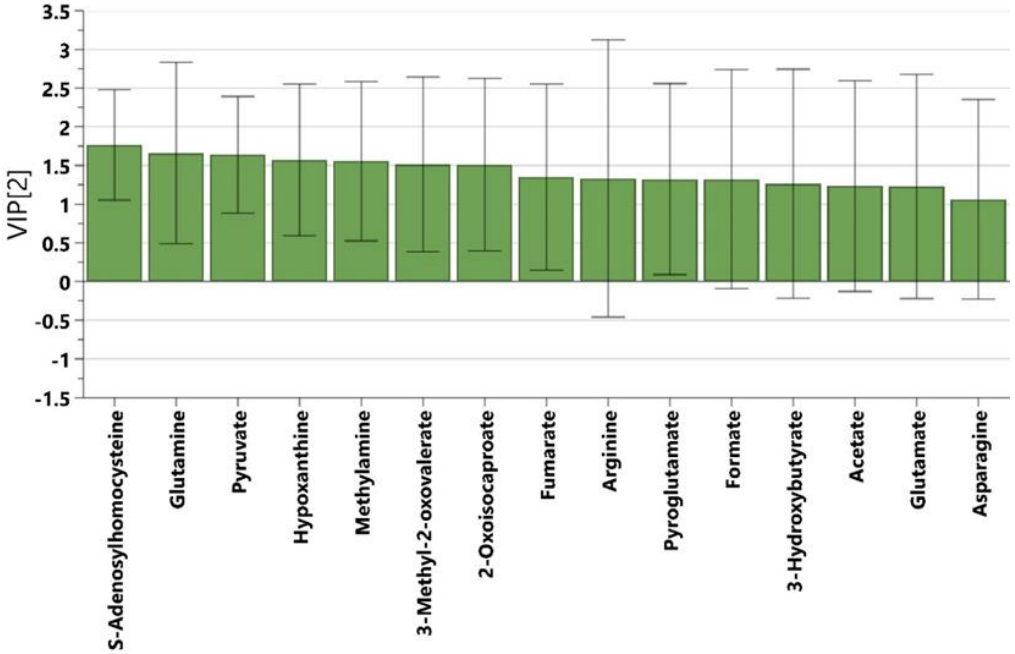
VIP[2]
3.5
3
2.5
2
1.5
1
0.5
0
-0.5
-1
-1.5
S-Adenosylhomocysteine
Glutamine
Pyruvate
Hypoxanthine
Methylamine
3-Methyl-2-oxovalerate
2-Oxoisocaproate
Fumarate
Arginine
Pyroglutamate
Formate
3-Hydroxybutyrate
Acetate
Glutamate
Asparagine

(c)

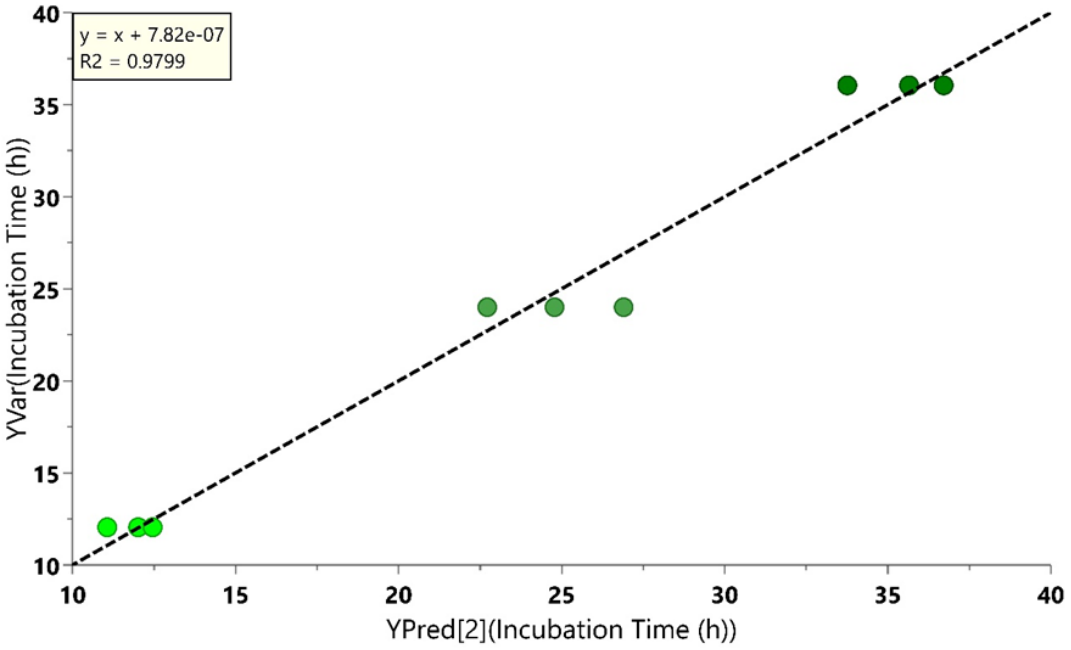
y = x + 7.82e-07
R2 = 0.9799
YVar(Incubation Time (h))
YPred[2](Incubation Time (h))
10
15
20
25
30
35
40

(d)

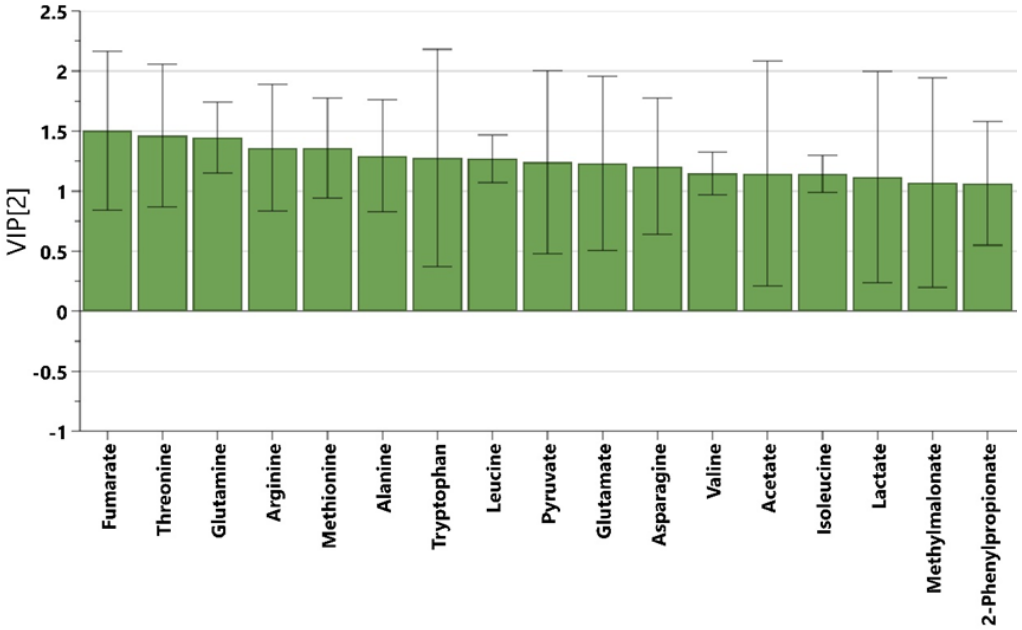
VIP[2]
2.5
2
1.5
1
0.5
0
-0.5
-1
Fumarate
Threonine
Glutamine
Arginine
Methionine
Alanine
Tryptophan
Leucine
Pyruvate
Glutamate
Asparagine
Valine
Acetate
Isoleucine
Lactate
Methylmalonate
2-Phenylpropionate

(e)

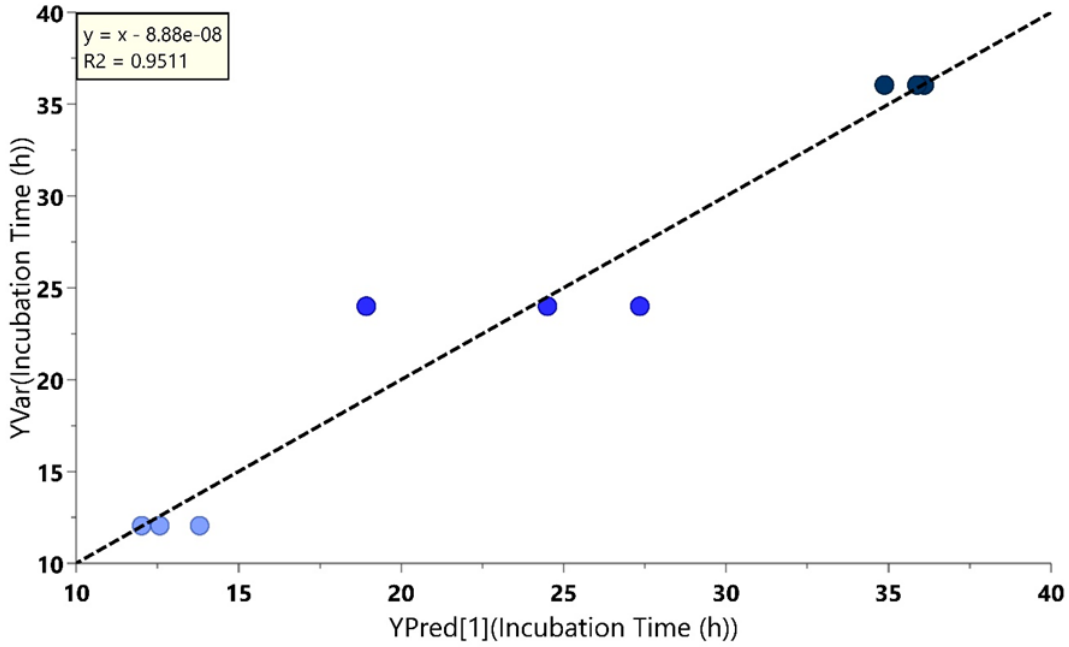

(f)

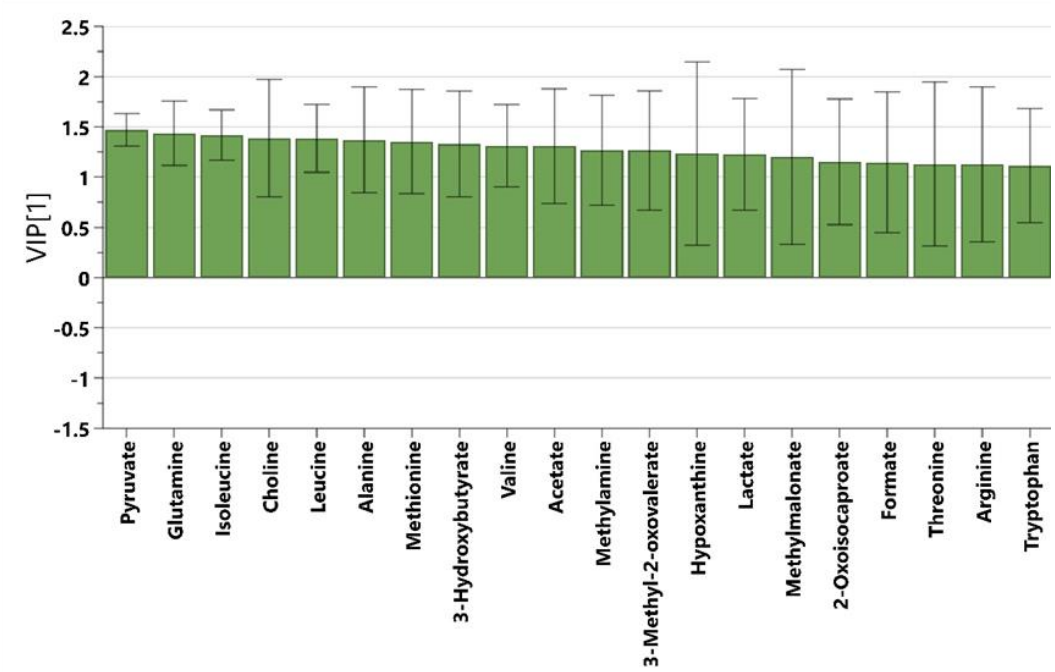

Figure 15. Graphical representation for ^{1}H-NMR relative intensity data driven models for HT1080 post culture media extracts (extracellular) at hypoxia 1% condition after 12h, 24h and 36h incubation. (**a, c, e**) Prediction plot from the partial least squares-regression model (PLS-R) built on relative intensity of ^{1}H-nuclear magnetic resonance spectra at hypoxia 1%, normoxia 6% and hyperoxia 21%, respectively. (**b, d, f**) The Variable importance in projection (VIP) score plot for PLSR model (VIP >1.00) at hypoxia 1%, normoxia 6% and hyperoxia 21%, respectively. Light red, hypoxia 1% after 12h; red, hypoxia 1% after 24h; dark red, hypoxia 1% after 36h; Light green, normoxia 6% after 12h;

green, normoxia 6% after 24h; dark green, normoxia 6% after 36h; Light blue, hyperoxia 21% after 12h; blue, hyperoxia 21% after 24h; dark blue, hyperoxia 21% after 36h.

The metabolomics profiles of medium extracts (extracellular) through different incubation times (12h, 24h and 36h) at hypoxia 1%, normoxia 6% and hyperoxia 21% were analyzed. We obtained the unsupervised multivariate analysis by PCA and showed slightly grouping and differences between incubation time point 12h vs. 24h vs. 36h among PCs at hypoxia 1%, normoxia 6% and hyperoxia 21% (**Figure** 12), Partial least squares regression (PLS-R) was applied to each comparison at hypoxia 1%, normoxia 6% and hyperoxia 21%, respectively, and were evaluated with R2 = 0.9153 for hypoxia 1%, R2= 0.9799 for normoxia 6% and R2= 0.9511 for hyperoxia 21% (**Figure** 13b, 13d, 13f), by using just 2, 2 and 1 PLS components, respectively, and RMSECV was 8.76h, 2.35h and 3.19h, respectively, the cross-validated residuals (CV-ANOVA) of PLS-R model wasn't significant with $p > 0.05$ at hypoxia 1% but was significant with normoxia 6% and hyperoxia 21% with $p < 0.05$ (**Table** 6).

At hypoxia, the combination between the most important metabolites from VIP (variable importance in projection) score with VIP value higher than 1.00 of PLS-R model as well as the univariate analysis significant by ANOVA revealed 9 common metabolites with four main regulations at hypoxia 1% (**Figure** 15b, 16):

1. Down-regulation with increasing cultivation time with significant differences between each incubation time point such as S-adenosylhomocysteine.
2. Down-regulation of glutamine, pyruvate, methylamine, 3-methyl-2-oxovalerate, 2-oxoisocaproate and 3-hydroxybutyrate after 12h but weren't showing any differences between 24h and 36h.
3. Up-regulations by increasing the cultivation time such as hypoxanthine.
4. Fumarate was up-regulation at 36h but did not show any significant difference between 12h and 24h.

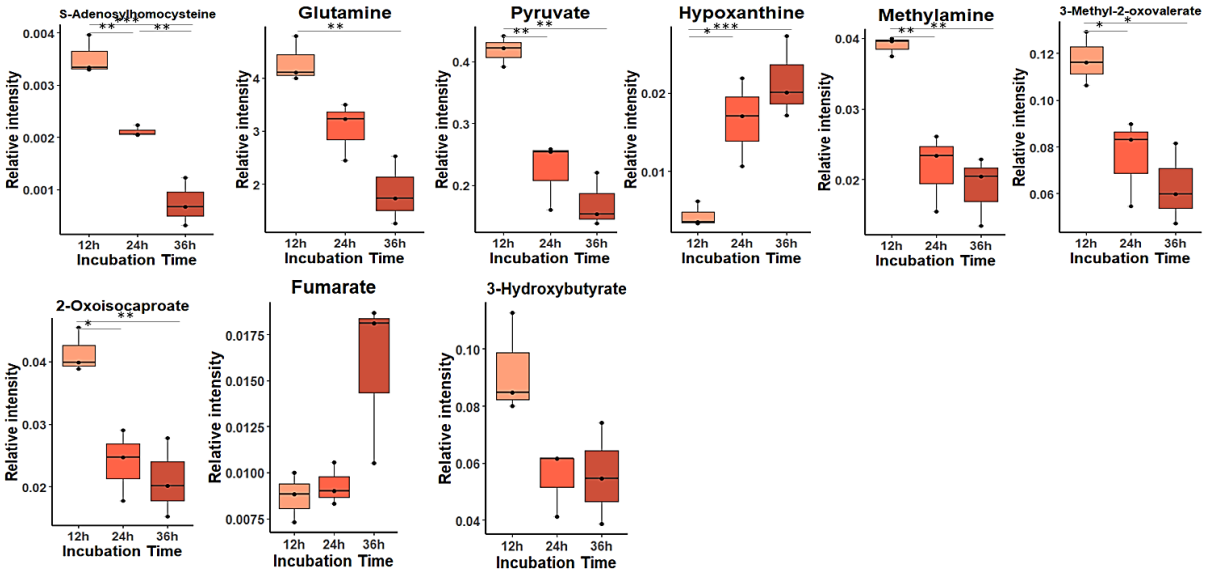

Figure 16. Boxplots for metabolites with VIP score above 1.00 identified by PLS-R model and statistically significant in one-way ANOVA test for HT1080 post culture media extracts (extracellular) samples at hypoxia 1% condition after 12h, 24h and 36h incubation time and after *p* value adjustment ($p < 0.05$). Whiskers—1.5 × interquartile range (IQR); bar—median; box—range between first quartile (Q1) and third quartile (Q3). Black points—data points. *Adjusted *p* value < 0.05.

On the other hand, at normoxia 6%, the VIP (variable importance in projection) revealed 17 most influential metabolites with VIP value above 1.00 such as (fumarate, threonine, succinate, glutamine, arginine, methionine, alanine, tryptophan, leucine, pyruvate, glutamate, asparagine, valine, acetate, isoleucine, lactate, methylmalonate and 2-phenylpropionate) (**Figure** 15d), and their significance was tested by ANOVA, hence, revealed 11 influential metabolites VIP > 1.00 with two main regulations (**Figure** 15d, 17):

1. Almost all downregulated with increased cultivation time (threonine, glutamine, arginine, methionine, tryptophan, leucine, pyruvate, asparagine, valine and 2-phenylpropionate).
2. Fumarate was up-regulated with increased time of incubation.

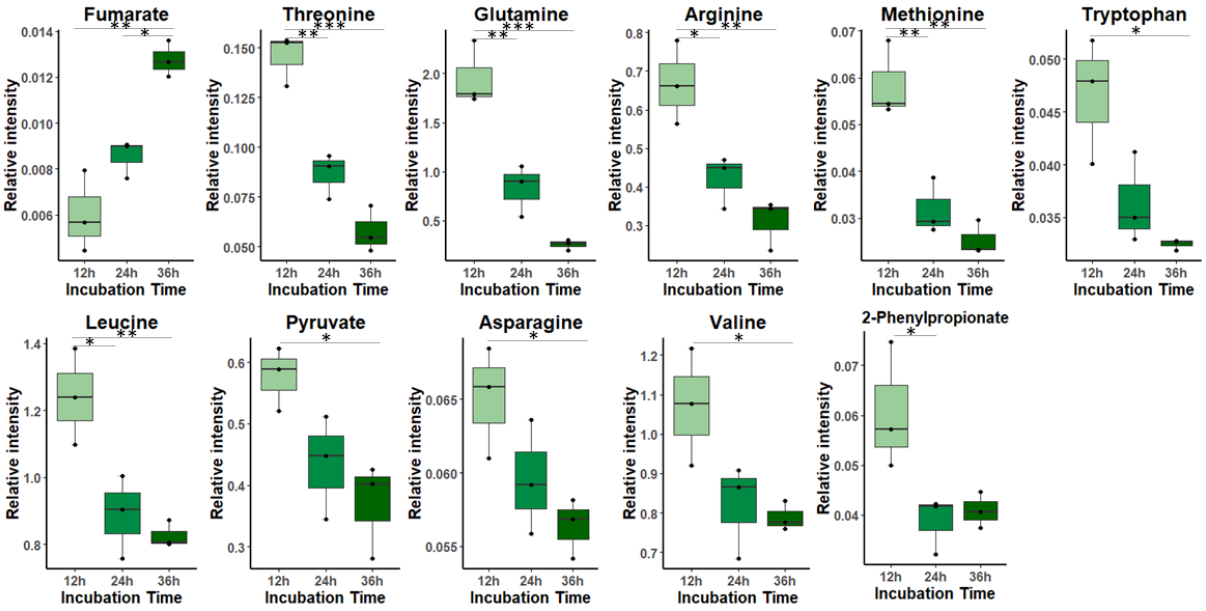

Figure 17. Boxplots for metabolites with VIP score above 1.00 identified by PLS-R model and statistically significant in one-way ANOVA test for HT1080 post culture media extracts (extracellular) samples at normoxia 6% condition after 12h, 24h and 36h incubation time and after p value adjustment ($p < 0.05$). Whiskers—1.5 × interquartile range (IQR); bar—median; box—range between first quartile (Q1) and third quartile (Q3). Black points—data points. *Adjusted p value < 0.05.

While, at hyperoxia 21%, 20 most important metabolites were obtained from the VIP (variable importance in projection) score with VIP value above 1.00 such as (pyruvate, glutamine, isoleucine, choline, leucine, alanine, methionine, 3-hydroxybutyrate, valine, acetate, methylamine, 3-methyl-2-oxovalerate, hypoxanthine, lactate, methylmalonate, 2-oxoisocaproate, formate, threonine, arginine and tryptophan) (**Figure** 15d), and their significance were tested by ANOVA, in which, revealed 19 influential metabolites with two main regulations (**Figure** 15f, 18):

1. Down-regulation of pyruvate, glutamine, isoleucine, choline, leucine, alanine, methionine, valine, lactate, methylmalonate, threonine, arginine and tryptophan with increased cultivation time.

2. Up-regulations with increased time of incubation especially at hyperoxia 21% and with no significant difference between 12h and 24h incubation time such as (3-hydroxybutyrate, acetate, methylamine, 3-methyl-2-oxovalerate, hypoxanthine, 2-oxoisocaproate, formate and threonine).

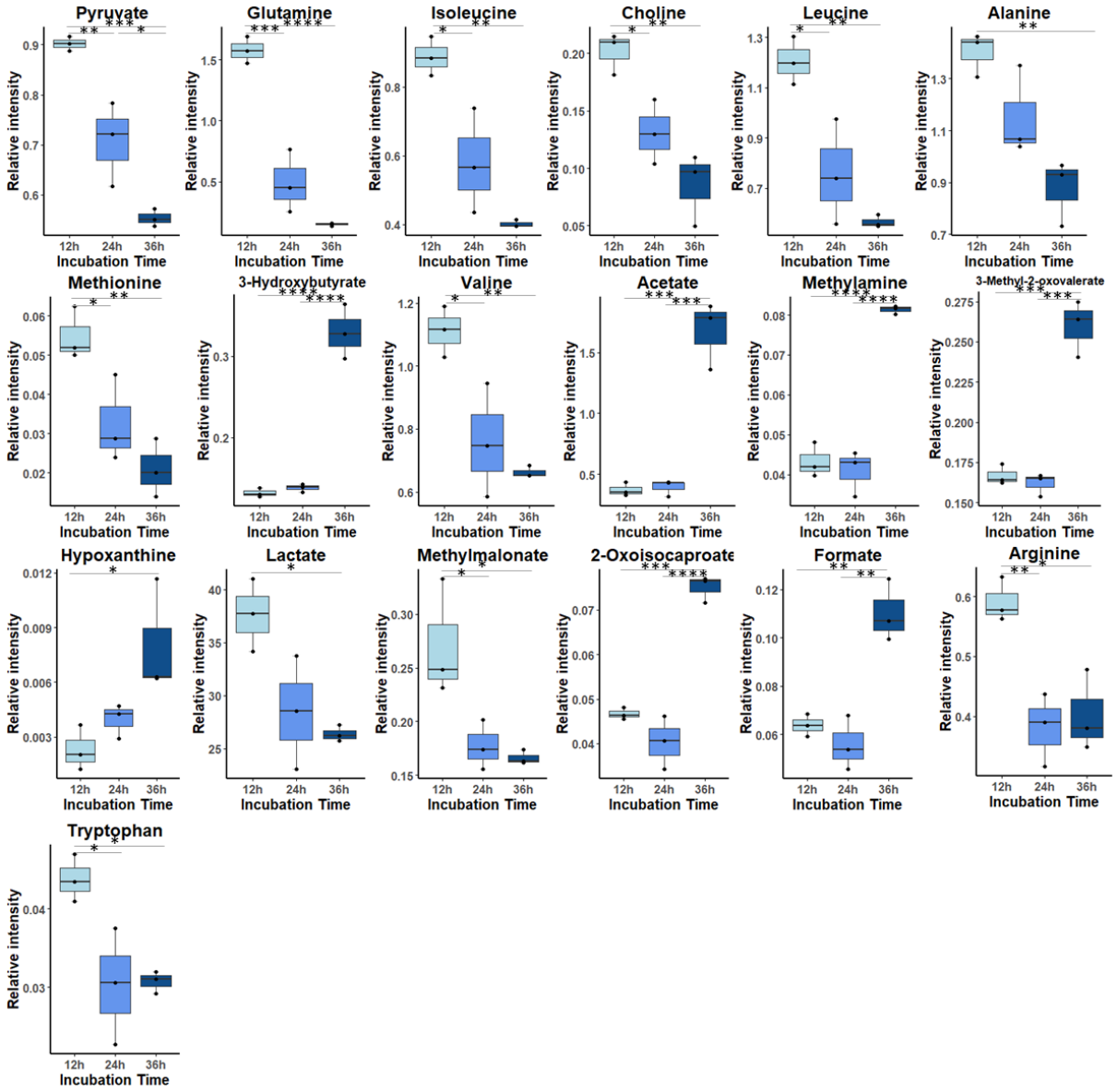

Figure 18. Boxplots for metabolites with VIP score above 1.00 identified by PLS-R model and statistically significant in one-way ANOVA test for HT1080 post culture media extracts (extracellular) samples at hyperoxia 21% condition after 12h, 24h and 36h incubation time and after *p* value adjustment ($p < 0.05$). Light blue— hyperoxia 21% after 12h; blue— hyperoxia 21% after 24h; dark blue— hyperoxia 21% after 36h. Whiskers—1.5 × interquartile range (IQR); bar—median; box—range between first quartile (Q1) and third quartile (Q3). Black points—data points. *Adjusted *p* value < 0.05.

Table 7. The summary of all significant metabolites in multivariate analysis with VIP > 1 and univariate analysis by ANOVA with *p* value < 0.05 from medium extract (Extracellular) dataset at hypoxia 1%, normoxia 6% and hyperoxia 21%.

Nr	Hypoxia 1%	Normoxia 6%	Hyperoxia 21%
1	**Pyruvate**	**Pyruvate**	**Pyruvate**
2	**Glutamine**	**Glutamine**	**Glutamine**
3	Fumarate	Fumarate	Isoleucine
4	S-Adenosylhomocysteine	Tryptophan	Tryptophan
5	Methylamine	Asparagine	Methylamine
6	3-methyl-2-oxovalerate	2-Phenylpropionate	3-methyl-2-oxovalerate
7	3-hydroxybutyrate	Threonine	3-hydroxybutyrate
8	2-oxoisocaproate	Leucine	2-oxoisocaproate
9	Hypoxanthine	Methionine	Hypoxanthine
10		Arginine	Leucine
11		Valine	Methionine
12			Arginine
13			Valine
14			Acetate
15			Alanine
16			Choline
17			Lactate
18			Methylmalonate
19			Formate

Notes; Bold metabolites, cross common metabolites; red metabolites, up-regulation; blue metabolites, down-regulation.

3.3.2.2. The metabolic sensitivity of the extracellular metabolome to various oxygen concentrations in the time interval function

The total sample set is 9 samples from post-cultured media, for each condition (1%, 6% and 21%), we conducted ^{1}H NMR-based metabolome analysis and 36 metabolites were successfully assigned in media respectively.

Table 8. The multivariate analysis models summary of medium extract (extracellular) dataset for comparisons between 1%, 6% and 21% oxygen concentrations at each incubation time.

Time	O_2% Comparisons	Model Type	PC/LV	N =	R2X (cum)	R2Y (cum)	Q2 (cum)	CV-ANOVA p value
12h	1% vs. 6% vs. 21%	PCA	2	9	0.835	–	–	–

	1% vs. 6% vs. 21%	PLS	3	9	0.884	0.993	0.933	6.01×10^{-2}
24h	1% vs. 6% vs. 21%	PCA	3	9	0.95	–	–	–
	1% vs. 6% vs. 21%	PLS	3	9	0.926	0.98	0.905	1.00×10^{-1}
36h	1% vs. 6% vs. 21%	PCA	2	9	0.925	–	–	–
	1% vs. 6% vs. 21%	PLS	3	9	0.95	0.997	0.989	**1.36×10^{-2}**

(a)

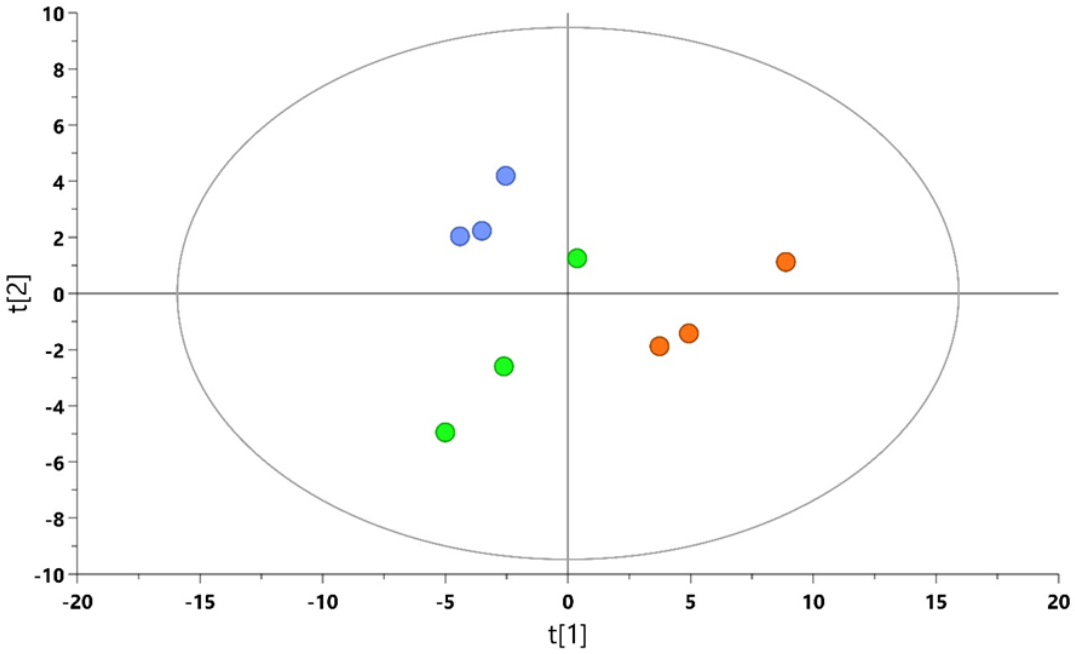

(b)

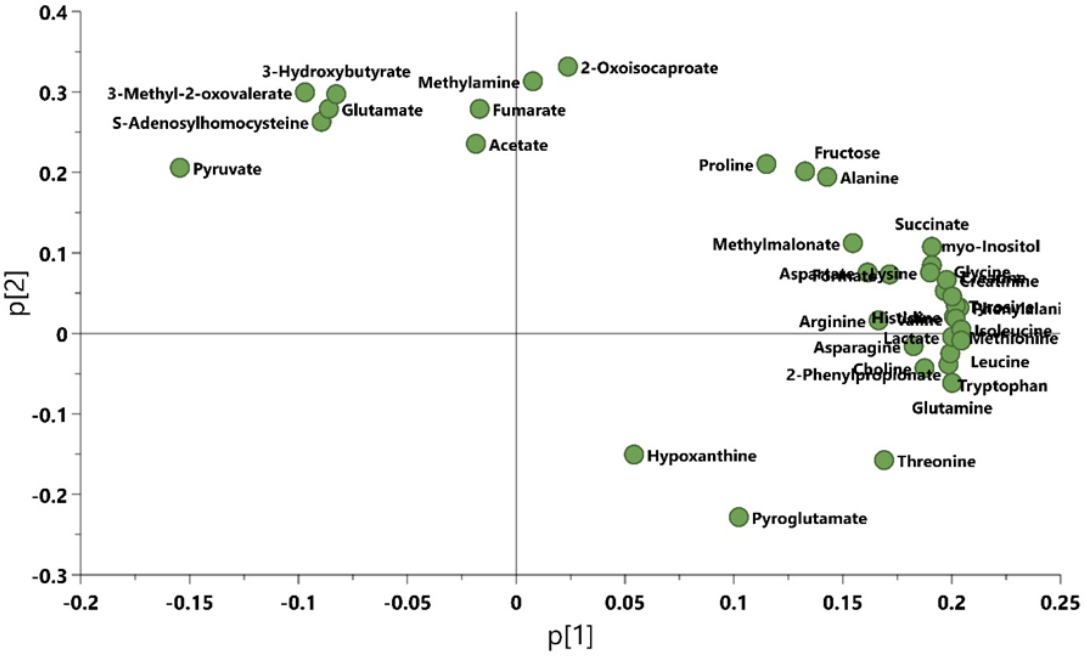

(c)

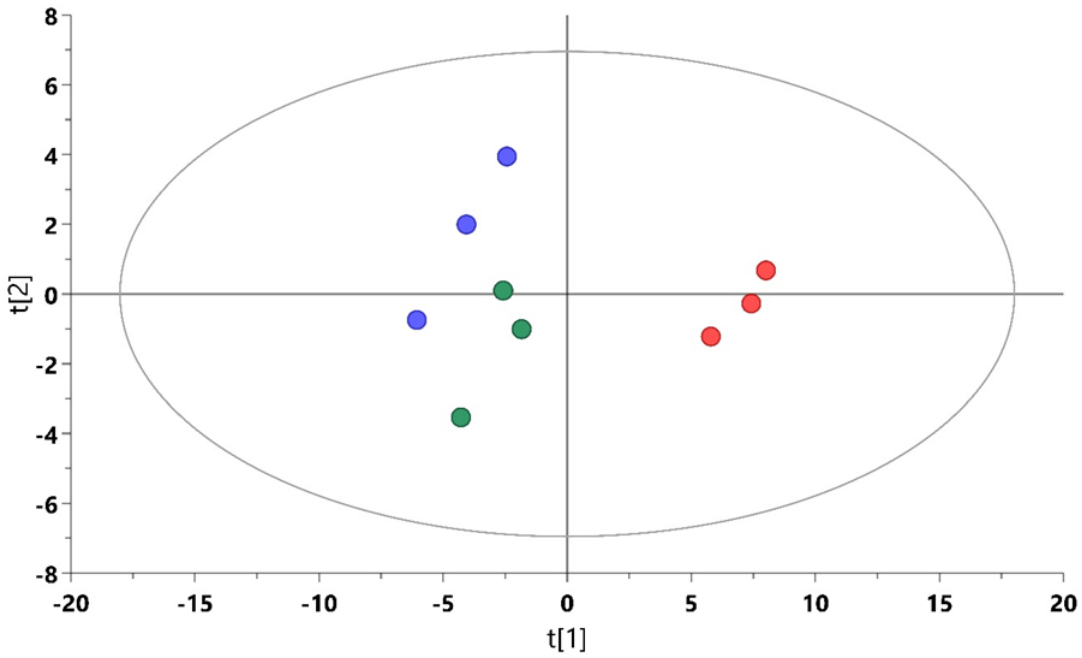
8
6
4
2
0
-2
-4
-6
-8
t[2]
-20
-15
-10
-5
0
5
10
15
20
t[1]

(d)

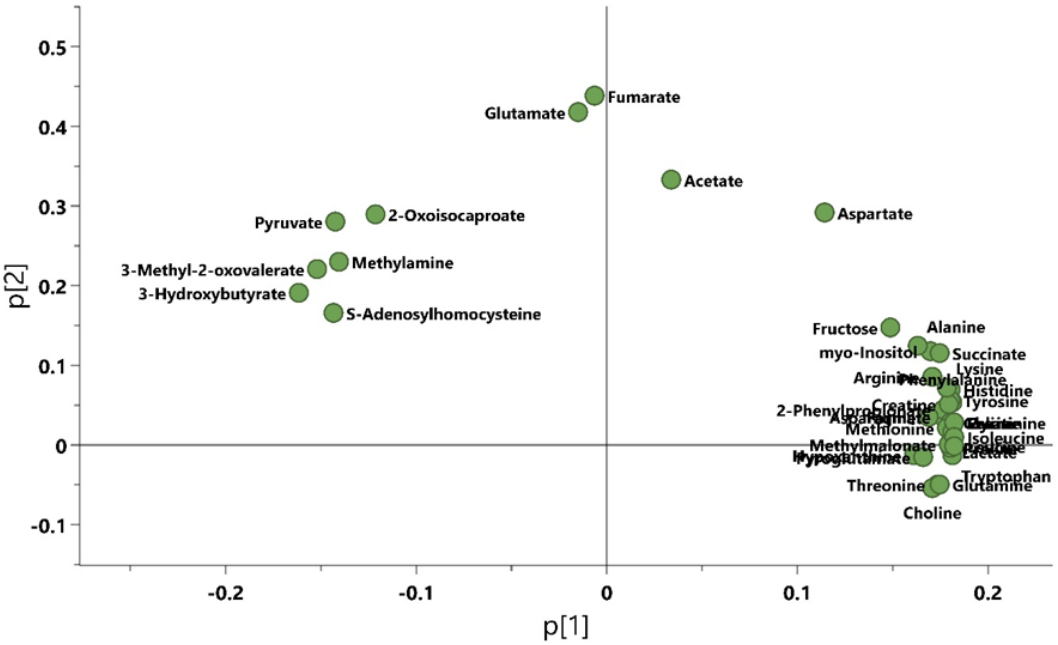
0.5
0.4
0.3
0.2
0.1
0
-0.1
p[2]
-0.2
-0.1
0
0.1
0.2
p[1]
Fumarate
Glutamate
Acetate
Aspartate
Pyruvate
2-Oxoisocaproate
3-Methyl-2-oxovalerate
Methylamine
3-Hydroxybutyrate
S-Adenosylhomocysteine
Fructose
Alanine
myo-Inositol
Succinate
Lysine
Histidine
Tyrosine
Methionine
Isoleucine
Methylmalonate
Tryptophan
Threonine
Glutamine
Choline

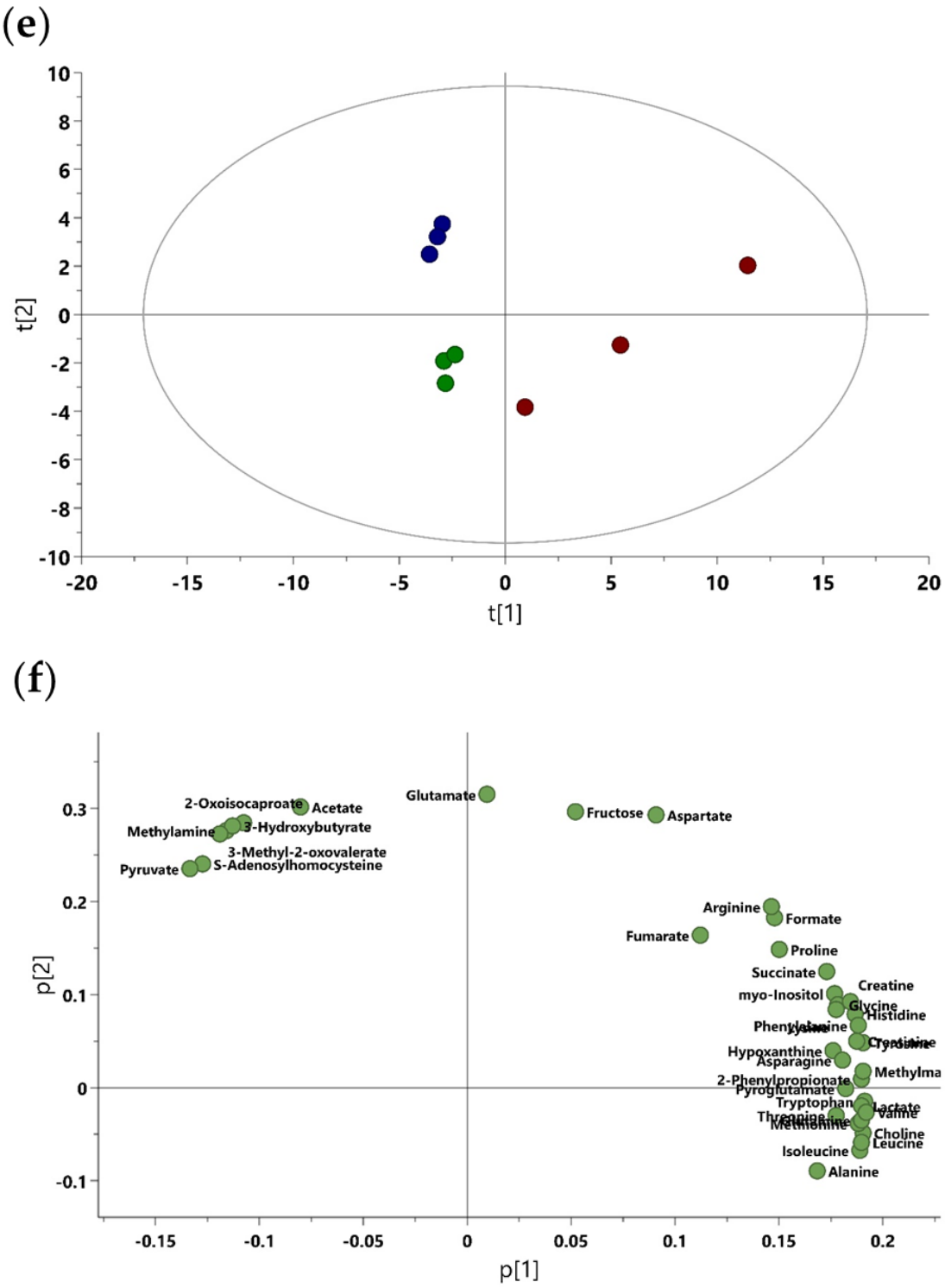

Figure 19. The Principal Component Analysis (PCA) scores plot and loadings plots for PCA model for ^{1}H-NMR relative intensity data driven models for HT1080 post culture medium extracts (extracellular) during incubation time at hypoxia 1%, normoxia 6% and hyperoxia 21% conditions. (**a, b**) After 12h incubation; (**c, d**) After 24h incubation; (**e, f**) After 36h incubation. Light red, hypoxia 1% after 12h; red, hypoxia 1% after 24h; dark red, hypoxia 1% after 36h; Light green, normoxia 6% after 12h; green, normoxia 6% after 24h; dark green, normoxia 6% after 36h; Light blue, hyperoxia 21% after 12h; blue, hyperoxia 21% after 24h; dark blue, hyperoxia 21% after 36h.

(a)

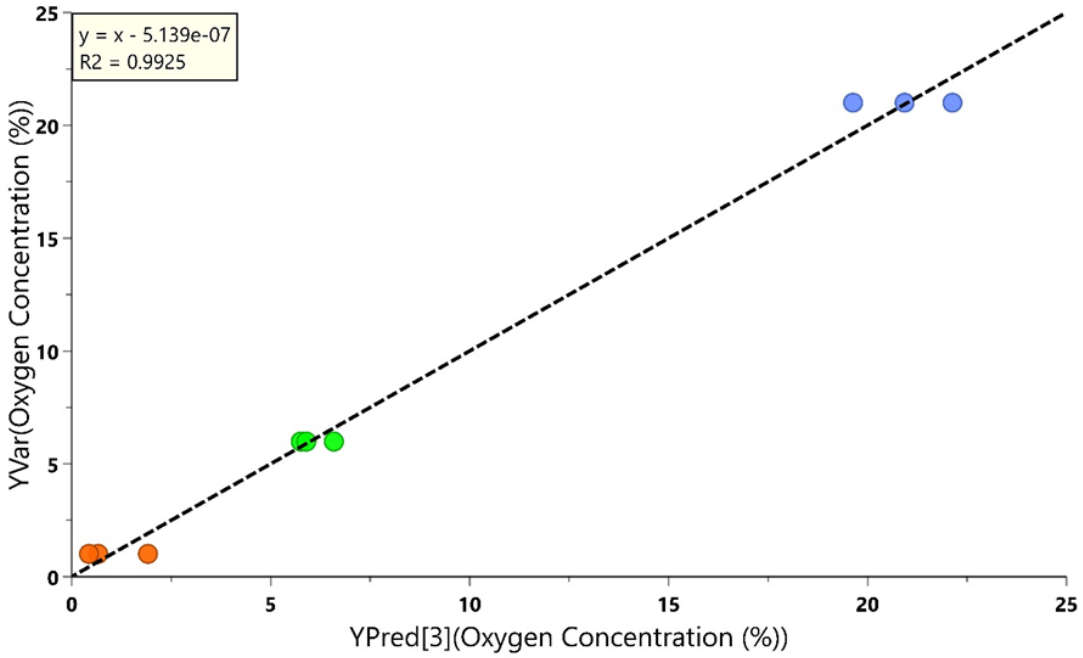
y = x - 5.139e-07
R2 = 0.9925
YVar(Oxygen Concentration (%))
YPred[3](Oxygen Concentration (%))
0
5
10
15
20
25

(b)

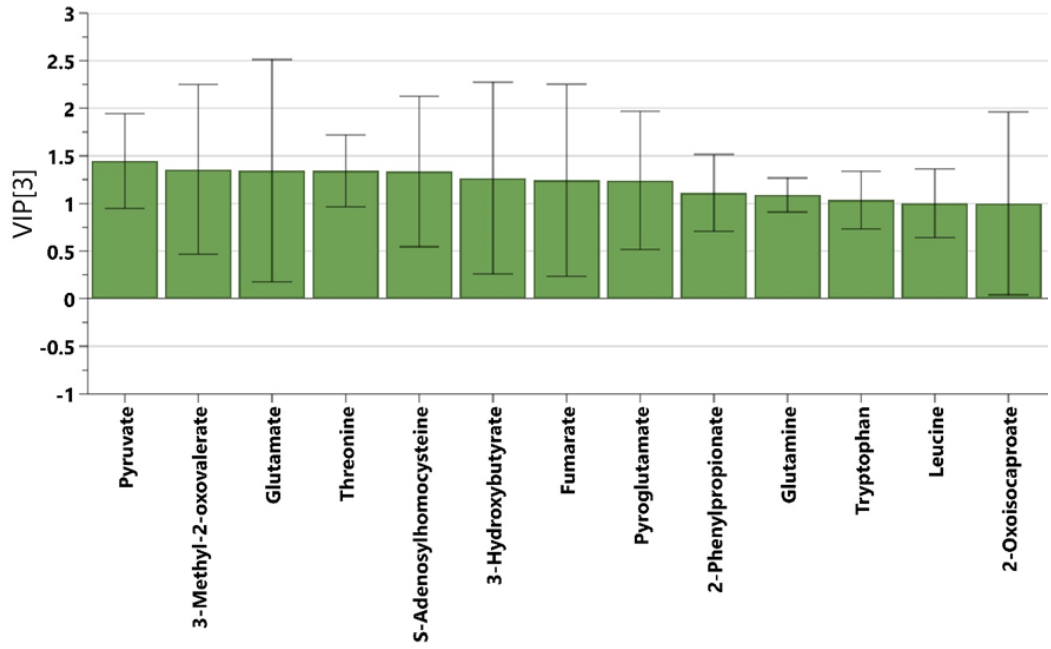
VIP[3]
3
2.5
2
1.5
1
0.5
0
-0.5
-1
Pyruvate
3-Methyl-2-oxovalerate
Glutamate
Threonine
S-Adenosylhomocysteine
3-Hydroxybutyrate
Fumarate
Pyroglutamate
2-Phenylpropionate
Glutamine
Tryptophan
Leucine
2-Oxoisocaproate

(c)

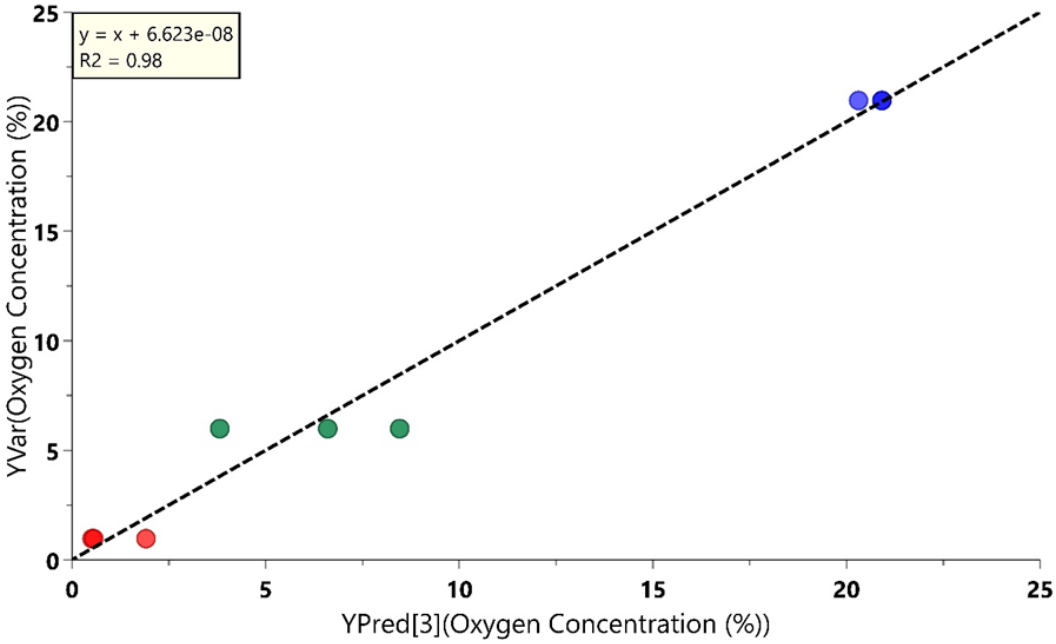
y = x + 6.623e-08
R2 = 0.98
YVar(Oxygen Concentration (%))
YPred[3](Oxygen Concentration (%))
0
5
10
15
20
25

(d)

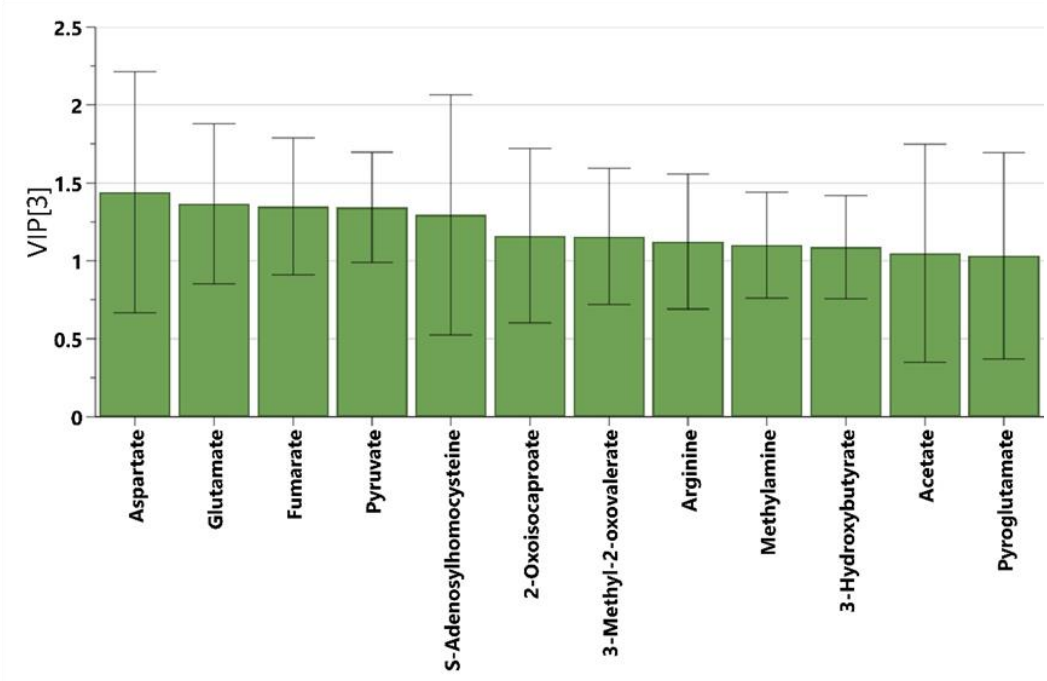
VIP[3]
2.5
2
1.5
1
0.5
0
Aspartate
Glutamate
Fumarate
Pyruvate
S-Adenosylhomocysteine
2-Oxoisocaproate
3-Methyl-2-oxovalerate
Arginine
Methylamine
3-Hydroxybutyrate
Acetate
Pyroglutamate

(e)

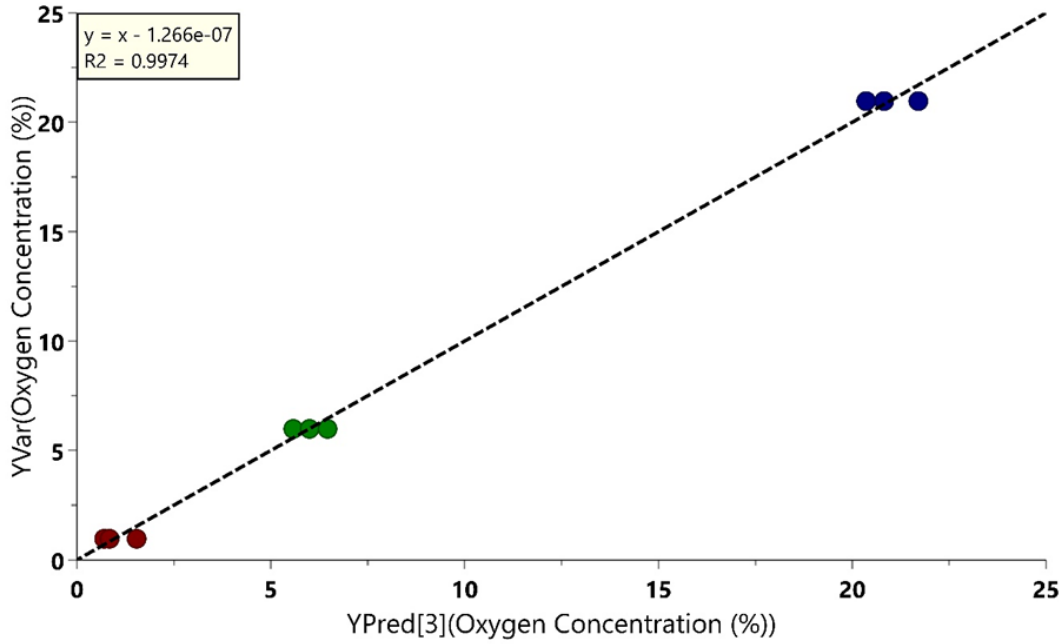

(f)

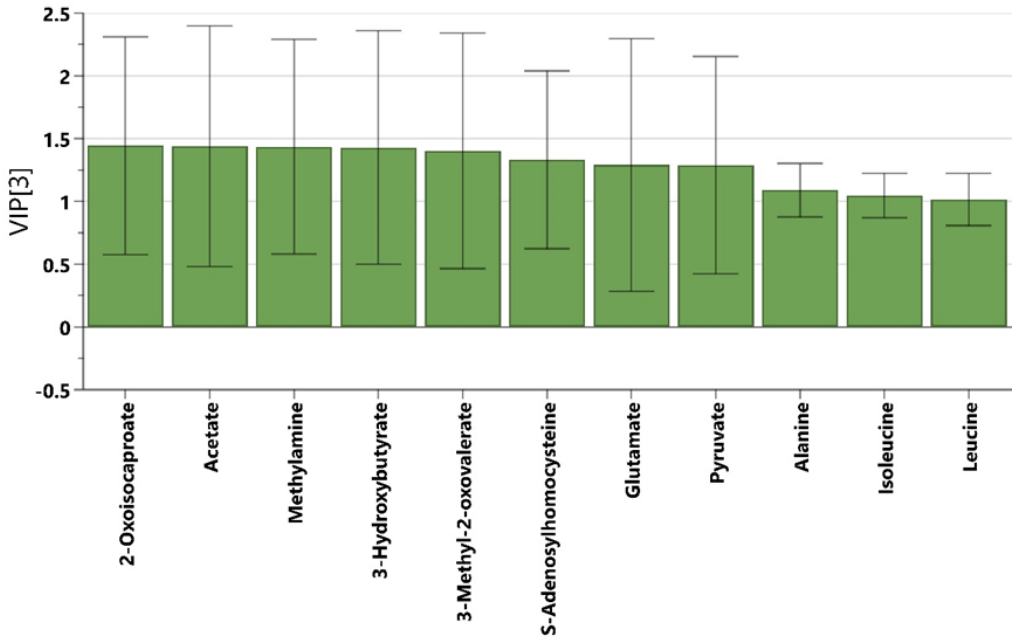

Figure 20. Graphical representation for ^{1}H-NMR relative intensity data driven models for HT1080 post cultured medium (extracellular) after cultivation time at hypoxia 1%, normoxia 6% and hyperoxia 21%. (**a, c, e**) Prediction plot from the partial least squares-regression model (PLS-R) built on relative intensity of ^{1}H-nuclear magnetic resonance spectra dataset after 12h, 24h and 36h, respectively. (**b, d, f**) The Variable importance in projection (VIP) score plot for PLSR model (VIP >1.00) after 12h, 24h and 36h, respectively.

We performed PCA score loading plots of the ^{1}H NMR dataset and PLS regression model to predict the total scores of each incubation time point to oxygen concentrations (hypoxia 1%, normoxia 6% and hyperoxia 21%). Furthermore, the PLS-R models were correctly validated and obtained the R^2X (cum), good correlation R^2Y (cum), goodness of prediction Q^2(cum) scores and significant CV-ANOVA *p*-values for extracellular media extracts in comparisons between oxygen concentrations groups.

To calculate the variations overview between hypoxia 1%, normoxia 6% and hyperoxia 21% after 12h incubation time, the PCA was created based on normalized an interval intensity data set obtained from ^{1}H NMR medium extracts (extracellular). The model showed a separation between groups of oxygen concentrations after 12h of incubation, among both PCs (**Figure** 19a). The loading plot was performed and showed the effect of oxygen concentrations on metabolites expression through PC1 and PC2 (**Figure** 19b). In addition, the Partial Least Squares - Regression (PLS-R) was generated and validated with R2 = 0.9925, by using just three PLS components. The RMSECV was 2.264% and the CV-ANOVA of PLS-R model wasn't significant with $p > 0.05$ (**Table** 8). The 13 most influential metabolites were selected from VIP (variable importance in projection) value above 1.00 such as (pyruvate, 3- methyl-2-oxovalerate, glutamate, threonine, s-adenosylhomocysteine, 3-hydroxybutyrate, fumarate, pyroglutamate, 2-phenylpropionate, glutamine, tryptophan, leucine and 2-oxoisocaproate) (**Figure** 19b), and were tested by one- way ANOVA. Afterward, 2-oxoisocaproate didn't pass ANOVA test and removed from further analysis. The remaining significant metabolites showed two significant trends: (**Figure** 21):

1. Up-regulation with increasing the oxygen concentrations for pyruvate, 3-Methyl-2-Oxovalerate, glutamate, S-adenosylhomocysteine and fumarate.
2. Down-regulation with increasing the oxygen concentrations for threonine, pyroglutamate, 2-phenylpropionate, glutamine, tryptophan and leucine.

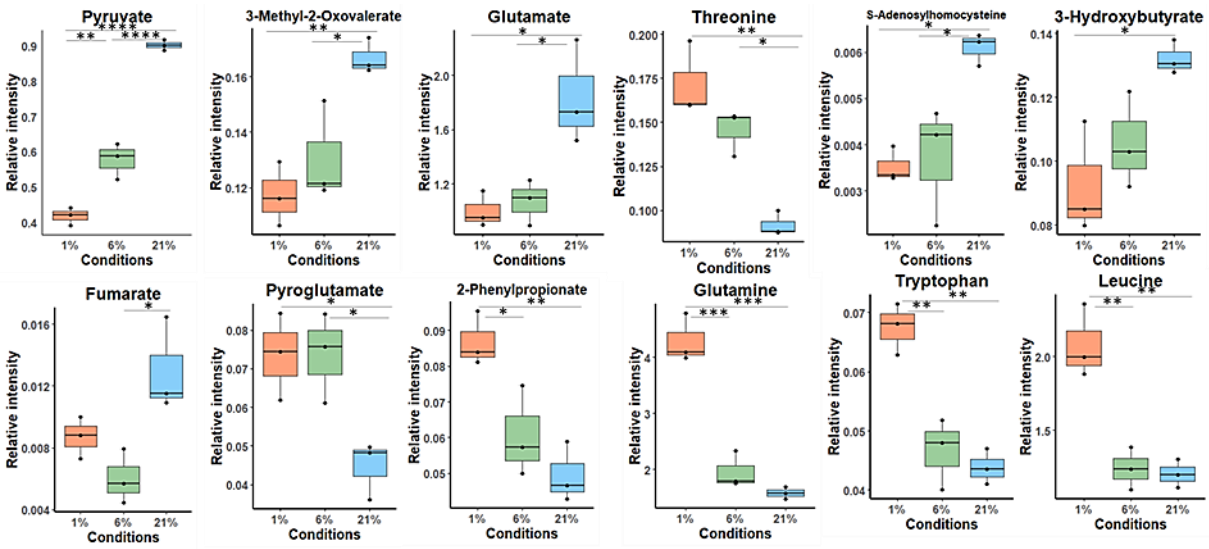

Figure 21. Boxplots for metabolites with VIP score above 1.00 identified by PLS-R model and statistically significant in one-way ANOVA test for HT1080 media extracts (extracellular) samples after 12h incubation time at hypoxia 1%, normoxia 6% and hyperoxia 21% conditions, and after *p* value adjustment. Whiskers—1.5 × interquartile range (IQR); bar—median; box—range between first quartile (Q1) and third quartile (Q3). Black points—data points. *Adjusted *p* value < 0.05.

The MVA after 24h of incubation, showed the variations between groups by principal component analysis (PCA) among PCs, and the influence of oxygen concentrations on metabolites distribution on the loading plot through PC1 and PC2 (**Figure** 19c, 19d), to estimate the relationship between metabolites and oxygen concentration. The Partial least squares-regression (PLS-R) was generated and validated by R2 = 0.98, and R2X, R2Y and O_2 parameters. The RMSECV was 2.71% and the CV-ANOVA of PLS-R model wasn't significant with $p > 0.05$ (**Table** 8) (**Figure** 20c). By VIP score, 12 most important metabolites were selected with VIP values greater than 1.00 (**Figure** 20d), and were tested by one way ANOVA. Afterward, glutamate, fumarate and acetate didn't pass ANOVA test and removed from further analysis The remaining significant metabolites showed two significant trends (**Figure** 22):

1. Up-regulation with increasing the oxygen concentrations for aspartate, pyruvate, S-adenosylhomocysteine, 2-oxoisocaproate, S-adenosylhomocysteine, 3-methyl-2-oxovalerate, methylamine and 3-hydroxybutyrate.

2. Down-regulation with increasing the oxygen concentrations for arginine and pyroglutamate.

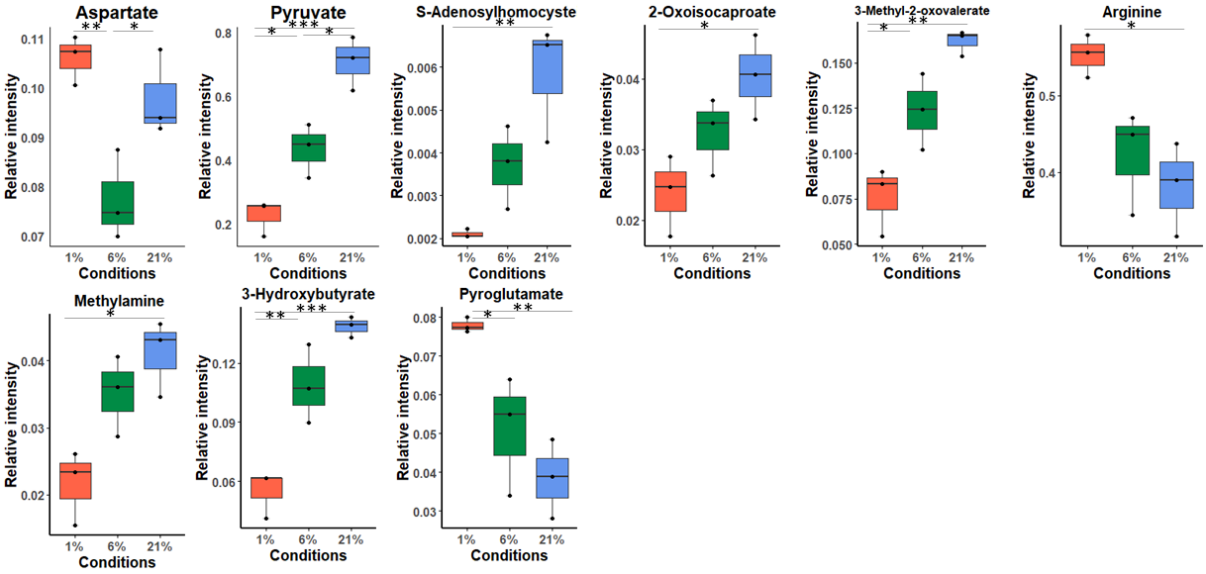

Figure 22. Boxplots for metabolites with VIP score above 1.00 identified by PLS-R model and statistically significant in one-way ANOVA test for HT1080 media extracts (extracellular) samples after 24h incubation time at hypoxia 1%, normoxia 6% and hyperoxia 21% conditions, and after *p* value adjustment. Whiskers—1.5 × interquartile range (IQR); bar—median; box—range between first quartile (Q1) and third quartile (Q3). Black points—data points. *Adjusted *p* value < 0.05.

Finally, the unsupervised multivariate method was obtained by PCA after 36h of incubation, showing the variations between groups among PCs (**Figure** 19e), and the loading plot was obtained which provided the explanatory pattern in the data set (**Figure** 19f). The Partial least squares - regression (PLS-R) was built and evaluated by R2 = 0.9974, and R2X(cum), R2Y(cum) and O_2(cum) parameters (**Table** 8), the RMSECV was 1.36% and the CV-ANOVA of PLS-R model was significant with $p < 0.05$ (**Table** 8). The 11 most important metabolites were selected from VIP (variable importance in projection) score, with VIP value greater than 1.00 (**Figure** 20f) and were tested by ANOVA, and these important metabolites showed three significant trends (**Figure** 23):

1. Up-regulation with increasing the oxygen concentrations for 2-oxoisocaproate, methylamine, 3-hydroxybutyrate, 3-methyl-2-oxovalerate and pyruvate.
2. Up-regulation at hyperoxia 21% but no differences between hypoxia 1% and normoxia 6% with acetate, S-adenosylhomocysteine and glutamate.

3. Alanine, isoleucine and leucine were down-regulation with increasing oxygen concentration.

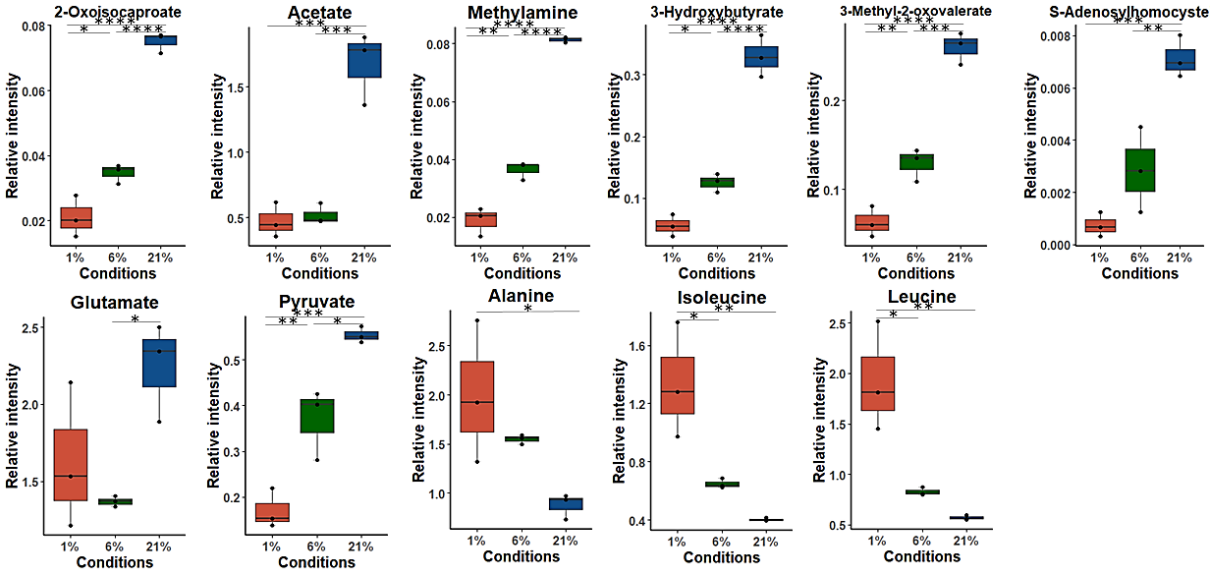

Figure 23. Boxplots for metabolites with VIP score above 1.00 identified by PLS-R model and statistically significant in one-way ANOVA test for HT1080 media extracts (extracellular) samples after 36h incubation time at hypoxia 1%, normoxia 6% and hyperoxia 21% conditions, and after *p* value adjustment. Whiskers—1.5 × interquartile range (IQR); bar—median; box—range between first quartile (Q1) and third quartile (Q3). Black points—data points. *Adjusted *p* value < 0.05.

Additionally, In this study, we assessed the metabolites sensitive (significant) regulation of the HT1080 cells intracellular and extracellular metabolome at hypoxia 1%, normoxia 6%, and hyperoxia 21%, during each interval time points. Here, we have noticed, by 72%, 93% and 83% of all intracellular significant metabolites after 12h, 24h and 36h of incubation, respectively, showed no sensitivity between hypoxia 1% and normoxia 6%, Moreover, by 14%, 7% and 6% of all significant metabolites after 12h, 24h and 36h of incubation, respectively, showed no sensitivity between normoxia 6% and hyperoxia 21% (**Table** 7).

Table 7. The degree of intracellular metabolites-sensitivity to O_2 concentration summary from total significant metabolites with VIP>1 and ANOVA *p*>0.05, after 12h (21 metabolites), after 24h (15 metabolites) and after 36h (18 metabolites).

Incubation time	Degree of Sensitivity to O_2 Concentration [%] *		
	High-sensitive $^{\Delta}$ (1%≠ 6% ≠ 21%)	Partial-sensitive (1% = 6% ≠ 21%)	Partial-sensitive (6% = 21% ≠ 1%)
12h	14	**72**	14
24h	0	**93**	7

36h	11	**83**	6

*≠ significantly different; = not significantly different; bold, highest value; Δ the highly sensitive refer to the significant between hypoxia and normoxia and hyperoxia as well as normoxia to hyperoxia; * the calculation was the number highly/partial-sensitive metabolites divide to total number of significant metabolites and multiple by 100.*

Moreover, we also assessed the extracellular oxygen-sensitive metabolites regulation of the HT1080 cells metabolome at hypoxia 1%, normoxia 6%, and hyperoxia 21%, during each interval time points showing that, after 12h 8% from all metabolites has highly sensitivity a cross all conditions, 50% of these metabolites were sensitive between normoxia and hyperoxia by their significant differences. Moreover, by 42% of all metabolites were significant between hypoxia and hyperoxia. However, after 24h of incubation we noticed that, the same number of metabolites by 11% were highly sensitive and partial sensitive, especially between normoxia and hyperoxia. However, was not significant between normoxia and hyperoxia by 78%. Surprisingly, after 36h incubation increased the sensitivity of the detected significant metabolites by 46% with no different between hypoxia and normoxia by 36%. Moreover, by 18% showed no significant between normoxia and hyperoxia (**Table** 8).

Table 8. The degree of extracellular metabolites-sensitivity to O_2 concentration summary from total significant metabolites with VIP>1 and ANOVA p>0.05, after 12h (21 metabolites), after 24h (9 metabolites) and after 36h (11 metabolites).

Incubation time	Degree of Sensitivity to O_2 Concentration [%] *		
	High-sensitive Δ (1%≠ 6% ≠ 21%)	Partial-sensitive (1% = 6% ≠ 21%)	Partial-sensitive (6% = 21% ≠ 1%)
12h	8	**50**	42
24h	11	11	**78**
36h	**46**	36	18

*≠ significantly different; = not significantly different; bold, highest value; Δ the highly sensitive refer to the significant between hypoxia and normoxia and hyperoxia as well as normoxia to hyperoxia; * the calculation was the number highly/partial-sensitive metabolites divide to total number of significant metabolites and multiple by 100.*

4. Discussion

An *in vitro* metabolomics is typically performed at standard oxygen concentration of 160 mmHg (21%), which is extremely high when compared to normal peripheral tissues. For this experiment, we proposed 21% as hyperoxia and 6% as the normoxia and compared to hypoxia 1%. We have found that, there

was a metabolic profile differences at 1%, 6%, and 21% O_2 and nutritional stress through cultivation time and showed a metabolite-sensitivity variations for extracellular and intracellular metabolome leading to produce metabolic phenotype of fibrosarcoma (HT1080) cell line, deliver more sufficient model of using a proper oxygen concentration as normoxia and a potential therapeutic approach by hyperoxia and starvation against cancer.

4.1. The metabolic changes of intracellular and extracellular metabolome at hypoxia, normoxia and hyperoxia through cultivation time.

The multivariate and univariate analysis of ^{1}H NMR spectra revealed the significant changes and correlations between cultivation time points on intra-extracellular metabolome that have been investigated.

The metabolic perturbation related to oxygen availability has been shown at hypoxia and causes an increasing glycolysis rate as a source of ATP production, even if it is insufficient to enhance intermediates metabolic building blocks for cells proliferation [14]. Moreover, the glucose deprivation which is much closer scenario to what's happens in the natural tumor environment including cellular stress and leads to switching to glutamine as an alternative source for nitrogen biosynthesis in cultured cancer cells [15,16], and as critical factor for *de novo* uridine-diphosphate-N-acetylglucosamine (UDP-GlcNAc) via hexosamine biosynthetic pathway. Herein, we showed that, a positive correlation between intra-UDP-GlcNAc and intra-extra glutamine in dependent manner to oxygen availability and cultivation time. Moreover, our data obtained revealed that, the UDP-GlcNAc act as metabolite-sensor of energy bioavailability. Recent studies suggested that, glutamine acquisition is related to increasing glutamine transporters (SLC38A1, SLC1A5, SLC38A2) expression to enter to the intracellular space, however, the linkage between glutamine and uridine diphosphate N-acetylglucosamine (UDP-GlcNAc) is associated with glutamine fructose-6-phosphate amidotransferase (GFAT), which converts glutamine and fructose-6-phosphate (F6P) to glucosamine-6-phosphate and glutamate followed up by multiple enzymatic reactions to uridine diphosphate N-acetylglucosamine (UDP-GlcNAc) [17] (**Figure** 22). As a consequence both intra-extracellular glutamine depletion showed a reduction in cellular uridine diphosphate N-acetylglucosamine

(UDP-GlcNAc) which is a cell-dependent nutrient state (glucose/glutamine) and cellular stress via hexosamine biosynthetic pathway (**Figure** 24) [18,19]. It is important to highlight the central role played by the hypoxia-inducible factor-1α (HIF-1α) in the metabolic adaptation process at pathological hypoxic microenvironments. Activation of HIF-1α serves to stabilize cellular demands in response to the restricted availability of oxygen and nutrients. The net outcome of HIF1 activation in hypoxic conditions is a shift in energy production, characterized by a heightened glycolytic rate and a decrease in mitochondrial function [20], through multiple enzymes and molecular targets such glucose transporters GLUT1/GLUT3 [21], hexokinase 2 (HK2) [22], PGI, PFK1, aldolase, TPI, GAPDH, PGK, PGM, enolase, PK, PFKFB1–4 [23], lactate dehydrogenase A [24], monocarboxylate transporter 4 (MCT4) [25], 3-phosphoinositide-dependent protein kinase 1/MAX interactor 1 (PDK1/MXI1) [26] and COX4I2, LON protease [27]. However, the stability of HIF1α in tumors effected by increasing the level of O_2 by-products (free radicals) or succinate and fumarate metabolites [20]. This is consistent with our findings that, both succinate and fumarate have been decreased at normoxia and hyperoxia.

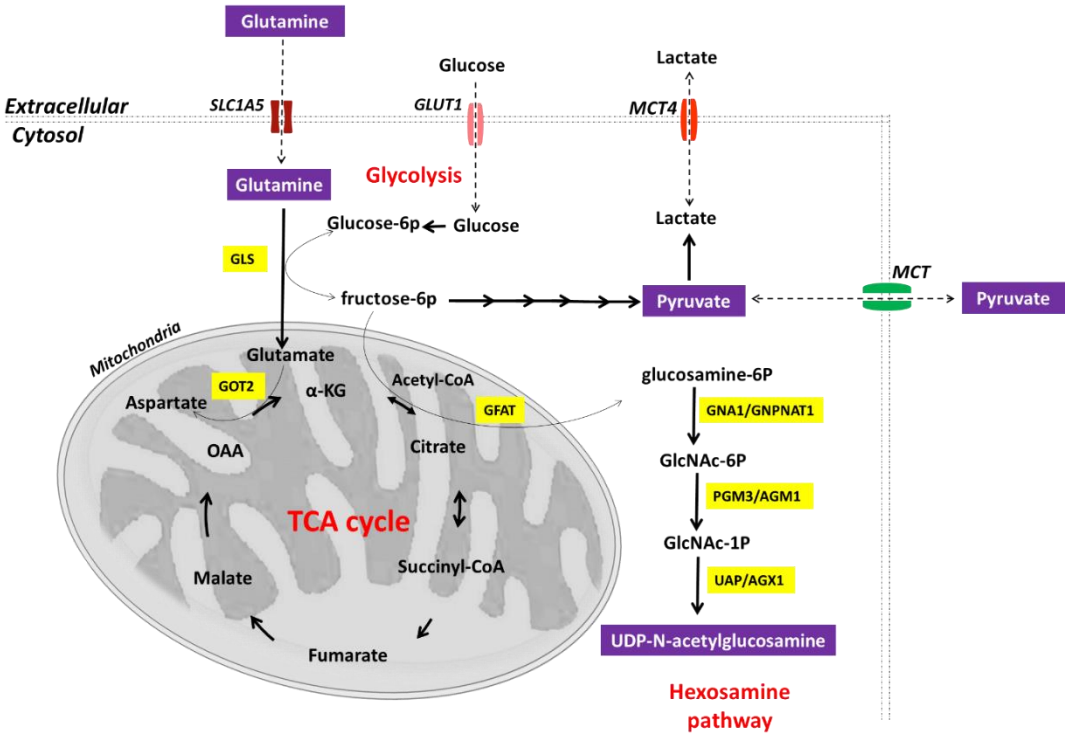

Figure 24. Metabolic pathways of HT1080 metabolome detected by ^{1}H NMR analysis, summarize the interactions of TCA cycle, glycolysis, hexosamine biosynthesis pathway; GLS, Glutaminase; GOT2, Glutamic-oxaloacetic transaminase 2; GFAT, glutamine:fructose-6-phosphate amidotransferase; GNA1/GNPNAT1, glucosamine-6-phosphate N-acetyltransferase; GlcNAc-6P, N-acetylglucosamine-6-Phosphate; GlcNAc-1P, N-acetylglucosamine 1-phosphate; UAP/AGX1, UDP-Nacetylhexosamine pyrophosphorylase; UDP-GlcNAc, uridine diphosphate N-acetylglucosamine. Purple color, significant metabolites detected by ^{1}H NMR; red color, metabolic pathways; yellow color, enzymes interactions.

Furthermore, It has been showed that, the o-phosphocholine plays an important role in choline phospholipid metabolism, which constitutes phosphatidylcholine membrane biosynthesis and characterized by total-choline compounds (choline, phosphocholine and glycerophosphocholine). Therefore, the total-choline compounds were classified as oncometabolite in several studies, which suggested that the correlation between malignant transformation and metabolic adaptation processes to tumor microenvironment causing choline metabolism perturbations and became a hallmark of cancer progression [28]. Moreover, at the most aggressive cancer phenotype was observed an accumulation of O-phosphocholine [29–32], which attributed mainly to induce choline phosphorylation through biosynthetic Kennedy pathway (**Figure** 23) via choline kinase (CK) activity in cancer cells including breast [33], colon [32], bladder [34] and epithelial ovarian [35], as well as partially from the degradation of phosphatidylcholine (PtdCho) via phosphatidylcholine-specific phospholipase C (PC-PLC) by 20%–50% in breast and ovarian cancer cells [36,37], and phosphatidylcholine-specific phospholipase D (PC-PLD) activity [38]. Most importantly, all these enzymes activity is controlled by oncogenic *Ras*-driven activation [39–44]. Herein, we have found that, at hypoxia and normoxia the level of intracellular choline showed a reduction through cultivation time with the same effect happened with O-phosphocholine at hypoxia, normoxia as well as hyperoxia. Obtained data stands in good agreement with other research in rat pheochromocytoma PC-12 cells by Bansal A et al. [45]. Moreover, other studies showed that, an inhibition of choline phosphorylation demonstrated under hypoxia mediated by HIF-1α in prostate cancer cell lines [46] and glioma cells [47]. That's might be associated to tumor-type of total-choline compounds regulation under hypoxia 1% and nutritional stress (starvation).

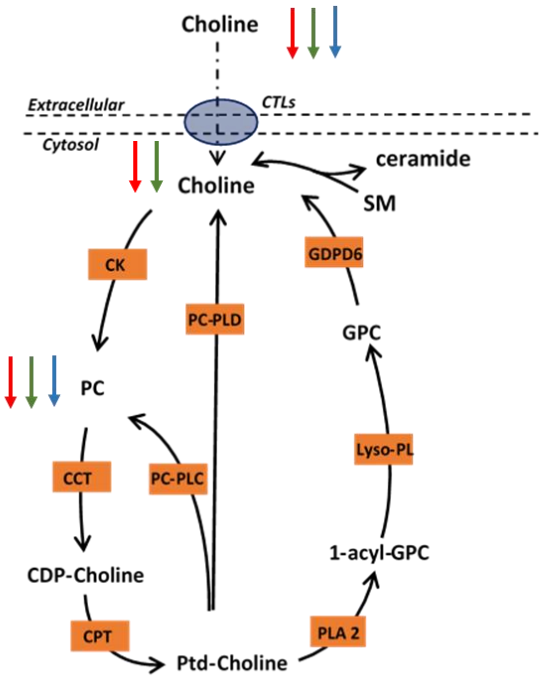

Figure 23. Choline metabolic pathway regulation on time-dependent manner, and the major enzymes involved in the cells, are shown, blue arrows represent the choline metabolism pathway and indicate the interconnection between compounds of choline network; phosphocholine (PC); cytidine 5′-diphosphocholine (CDP-Choline); phosphatidylcholine (Ptd-Choline); 1-acyl-glycerophosphocholine (1-acytl-GPC); glycerophosphocholine (GPC); choline transporter-like proteins (CTLs); Sphingomyelin (SM), and brown boxes indicate the regulation of enzymes activity in choline metabolism pathway, Choline kinase (CK); phosphocholine cytidylyltransferase (CCT); diacylglycerol choline phosphotransferase (CPT); phospholipase A2 (PLA2); lysophospholipase (Lyso-PL); glycerophosphodiester phosphodiesterase domain containing 6 (GDPD6); phospholipase C (PLC); phospholipase D (PLD). Red arrow, hypoxia 1%; green arrow, normoxia 6%; blue arrow, hyperoxia 21%. An arrow up; upregulation; arrow down, downregulation.

The amino acids transporter's activity and their metabolic enzymatic reactions are critical for metabolic reprogramming and adaptation processes [48]. For instance, the L-type amino acid transporters such as LAT1 (*SLC7A5*)) is among Na+ - and pH-independent that facilitate the influx of leucine, valine, phenylalanine and tyrosine into cells in exchange for efflux of other intracellular amino acids such as glutamine or other essential amino acids. Furthermore, the intracellular leucine and valine are catabolized by branched-chain aminotransferases (BCATs) to transfer nitrogen and carbon groups to α-KG to synthesize glutamate, besides other branched-chain α-ketoacids (BCKAs) which are highly expressed in many types of cancer to maintain cell proliferation and inhibit apoptosis [49,50]. Our results showed a reduction of the intracellular and extracellular of leucine, isoleucine and valine (BCAAs)

under hypoxia 1%. However, at hyperoxia 21%, especially after 36h showed an accumulation of BCAAs in intracellular space, considering the fact that, the extracellular of BCAAs at hyperoxia 21% were decreased through cultivation time. It was observed that, the BCAAs (leucine, isoleucine and valine) transporter (SLC7A5) activity and BCAT1 expression upregulated in glioblastoma by the effect of hypoxia-inducible factors (HIFs), in which has been proven that, the knockout of HIF-1α and HIF-2α or inhibition of BCAT, subsequently, inhibits GBM cells proliferation under hypoxia stress [51], which showed in our results an increase the BCAAs transporter (SLC7A5) activity and BCAT1 expression at hypoxia 1%. However, at hyperoxia 21% these amino acids accumulated in intracellular space after 36h incubation. This indication of this phenomena might be related at first for leucine, isoleucine and valine to BCAT1 inhibition or reducing BCAT1 activity. It was showed in other study that, BCAT1 knockdown will inhibit of PI3K/AKT/mTOR signaling as a key of cells viability and angiogenesis in gastric cancer [52], as well as inducing autophagy under various stress conditions such as starvation, hypoxia and oxidative stress [53]. However, still unclear the role of HIFs on BCAAs metabolism [54]. Meaning, under glucose starvation (fasting) and high oxygen concentration 21% lead of BCAAs accumulation in intracellular space and subsequently, could be triggered the apoptosis and cell-mediated cytotoxicity as a consequence of BCAT1 inhibition despite the BCAAs transporter (SLC7A5) activity. The same effect we noticed with accumulation of some essential amino acids such as phenylalanine and histidine and other non- essential amino acids such as glycine, asparagine and tyrosine in intracellular space could provide an evidence of toxic microenvironment of glucose deprivation-induced cytotoxicity [55–58], along with high oxygen concentration (hyperoxia) [59–61], as well as potential therapeutic combination strategy.

What's more, it was showed that, the process of BCAAs catabolism required two main steps as aforementioned above, first by BCATs transamination via a reversible reaction and the second is by branched-chain α-keto acid dehydrogenase complex (BCKDH) to yield branched-chain α-keto acids such as 2-keto-isocaproate/4-methyl-2-oxopentanoic acid (KIC), α-keto-β-methylvaleric acid/3-methyl-2-oxopentanoate (KMV), and 2-keto-isovalerate/3-methyl-2-oxobutanoic acid (KIV). Therefore, this oxidative decarboxylation is irreversibly reaction of BCKAs which allowed the cells to produce branched-chain acyl-CoA derivates such

as acetoacetate, propionyl-CoA and acetyl-CoA from leucine and isoleucine as well as propionyl-CoA from valine which metabolized through valine, leucine and isoleucine degradation pathway to generate 3-hydroxybutyrate, 3-methyl-2-oxovalerate and 2-oxoisocaproate [62,63]. Herein, we have found and for the first time, an increased levels of accumulation of 3-hydroxybutyrate, 3-methyl-2-oxovalerate and 2-oxoisocaproate a at the cellular space along with induced the efflux of these metabolites to extracellular milieu at hyperoxia 21% after 36h of incubation.

It has been demonstrated that, an increasing level of 2-oxoisocaproate to the culture media determines the intracellular catabolism capability of leucine in the glioma, glioblastoma, neuroblastoma cells, and suggested that, the part of 2-oxoisocaproate might enter the cellular energy metabolism via branched-chain alpha-keto acid dehydrogenase complex (BCKDH). Moreover, culture media supplement with high concentration of leucine will induce the cellular ketogenic reaction and release 3-hydroxybutyrate to extracellular space [64]. Additionally, 3-hydroxybutyrate is ketone body which produced as result of dehydrogenization of acetoacetate (AA) and degrades fatty acids via β-oxidation, which will be used as source of energy by the cells during starvation [65]. Also observed by others that, the 3-hydroxybutyrate (ketone body) significantly increased tumor growth by 2.5-fold, without any increases in tumor angiogenesis. In contrast, lactate increased experimental lung metastasis by 10-fold, but did not affect primary tumor growth. Furthermore, their findings revealed that both ketones and lactate stimulated the migration of MDA-MB-231 cells, acting as chemo-attractants. These results provide evidence for the "reverse Warburg effect," a phenomenon in which cancer cells utilize the metabolism of lactate and ketones for energy production rather than glucose [66]. Conversely, other *in vitro* studies showed that, 3-hydroxybutyrate during glucose starvation can significantly attenuated the tumor growth [67–69]. Interestingly, another evidence provided, the role of 3-hydroxybutyrate on class I histone deacetylases (HDACs) inhibition in cancer cells and increases histone acetylation as well as generation of lysine β-hydroxybutyrylation (Kbhb), which connected to the reduction of tumor suppressor gene p53 after Kbhb modification, therefore, reduces the cell growth arrest and apoptosis in cellular level [69]. With all these contradictions, we have found that, under hyperoxia 21% through glucose starvation, HT1080 cells increase of 3-hydroxybutyrate release to the media (extracellular).

This could be explained as under the glucose depletion and high oxygen concentration 21%, lead cells to reduce their proliferation potential and induce cell death as well as releasing intracellular components to the media as debris, which showed in our growth curve results after 36h at hyperoxia 21%. Additionally, It's well established that, the tumor microenvironment (TME) faces one critical stress with nutrient deficiency besides hypoxia, and acidosis [70]. This is due to the elevated demand for nutrients by rapidly proliferating tumors, which is not met by an adequate supply [70,71]. TME lacks multiple nutrients, with glucose deprivation being the most prevalent, caused by the high consumption of glucose by tumor cells through aerobic glycolysis [72]. Tumor cells adapt to glucose deprivation by using alternative fuel sources such as lactate, glutamine, and fatty acids, breaking down macromolecules via autophagy, or synthesizing glucose from lactate and amino acids [73–75]. Therefore, another scenario could be happened to fibrosarcoma cells through beta-oxidation which represents the breakdown of fatty acids to generate energy by involvement of acyl-CoA. To generate acetyl-CoA and serve as the substrate for the tricarboxylic acid (TCA) cycle, resulting in the generation of ATP highlights the interconnectivity between various metabolic pathways in regulating energy metabolism [76].

Intermediates in the beta-oxidation process, including 2-oxoisocaproate and 3-hydroxybutyrate, are formed from distinct precursors. 2-oxoisocaproate is produced during the oxidation of leucine via the branched-chain alpha-keto acid dehydrogenase complex, while 3-hydroxybutyrate arises from the oxidation of fatty acids catalyzed by 3-hydroxybutyrate dehydrogenase. Under conditions of glucose deprivation, cells may resort to beta-oxidation of fatty acids as an energy source, inducing metabolic pathways to enhance fatty acid availability and utilization through glycogen breakdown and *de novo* lipogenesis. In *in vitro* studies have demonstrated that low glucose levels trigger increased expression of genes involved in fatty acid uptake and beta-oxidation, as well as elevated activity of beta-oxidation enzymes such as carnitine palmitoyltransferase-1 (CPT-1) and acyl-CoA oxidase, which are crucial for fatty acid transport into the mitochondria and the initiation of beta-oxidation.

4.2.The sensitivity of the HT1080 cell's metabolome to hypoxia, normoxia and hyperoxia at each interval time point.

Since there isn't a particular study described the metabolic-sensitivity regulations term to various oxygen concentrations. However, It has been demonstrated that, culture cancer cells at high oxygen concentration (~18%) can effect reactive oxygen species (ROS) production [77], redox homeostasis [78], metabolism, mitochondrial networks [79], and therapy response [80], and showed differentially expressed genes (DEGs) on cell-type specific manner to 5% or 18% O2 for 14 days incubation on LNCaP, SH-SY5Y, Huh-7, and PC-3 cell lines [81]. Moreover, Alva, R et al. also suggested that, the hyper-physiological/non-physiological O_2 levels at standard cell culture hyperoxia, may affect experiments results and their interpretation compered to in vivo [81,82].

We already explained in details about uridine-diphosphate-N-Acetylglucosamine (UDP-GlcNAc) cellular mechanism and regulation during cultivation time in each oxygen concentration as nutrient-sensor metabolite in section 4.1.

Here, we have been found compered its regulation to the oxygen concentrations in each incubation time showed no sensitivity to oxygen concentration between 6% and 21% after 12h and highly sensitive after 36h of incubation. The uridine-diphosphate-N-Acetylglucosamine (UDP-GlcNAc) is a substrate for O-linked β-N-Acetylglucosamine (O-GlcNAc) transferase (OGT) [83]. Observed by others, elevating O-GlcNAcylation is directly affected by increasing the level of its substrate UDP-GlcNAc. Moreover, reducing O-GlcNAcylation in cancer cells will induced endoplasmic reticulum (ER) stress and cells apoptosis [83,84]. Our obtained results under normoxia and hyperoxia are cells well oxygenated showed an increase level of UDP-GlcNAc, therefore induce O- GlcNAcylation especially after 12h of incubation. However, the high sensitivity mechanism of the cells to oxygen concentration after 36h still unclear, which could be explained that after 12h under normoxia 6% with glucose availability and presence of oxygen, cells try to maximize the accumulation of UDP-GlcNAc and accelerate O- GlcNAcylation for installing N-Acetylglucosamine to proteins, lipids and proteoglycans as in hyperoxia 21%. Furthermore, after 36h with glucose starvation which reduced the HBP flux and UDP-GlcNAc accumulation,

thus, reduce O- GlcNAcylation may impair unfolded protein response (UPR) and trigger apoptosis through BCL2-family (CHOP) [84].

Furthermore, N-acetylasparate (NAA) play important role to maintain cells growth, suppressing ER stress and cell death through increasing the intracellular UDP-GlcNAc biosynthesis under low glucose concentration [85]. From our results we found, the intracellular N-acetylasparate (NAA) share the same trend as UDP-GlcNAc with no distinguish between 6% and 21% O_2 after 12h of incubation. It has been found that, the intracellular N-acetylaspartate (NAA) breakdown will limit the cells growth and leads to ER stress *in vivo*. Moreover, the main role of N-acetylasparate (NAA) to increase cells survival to glucose starvation [78]. Our indication showed the synergetic sensitivity of both UDP-GlcNAc and N-acetylasparate (NAA) under 6% or 21% after 12h of incubation [86].

In addition to choline and O-phosphocholine sensitivity under hypoxia, normoxia and hyperoxia. Here, we have found that, O-phosphocholine was significantly accumulated and sensitive at hypoxia than both normoxia and hyperoxia.. However, we have found no sensitivity to normoxia 6% and hyperoxia 21% after 24h and 36h of incubation. Moreover, From pervious section 4.1. which explored in more details the time-course effect in total choline compounds regulation at each oxygen concentrations (hypoxia, normoxia and hyperoxia) and their mechanism environmental stress. Our indication showed that the normoxia 6% and hyperoxia 21% didn't affect the enzymatic activity of via choline kinase (CK), phosphatidylcholine-specific phospholipase C (PC-PLC) and phosphatidylcholine-specific phospholipase D (PC-PLD) leading to produce at same level of intracellular O-phosphocholine. In contrast, were highly sensitive to hypoxia 1% by upregulation of intracellular O-phosphocholine.

Moreover, from MVA analysis revealed 4 common extracellular metabolites across incubation time points (12h, 24h and 36h) (**Figure** 19, 20, 21) and showed the extent of sensitivity of these metabolites to hypoxia 1%, normoxia 6% and hyperoxia 21% including pyruvate, 3-methyl-2-oxovalerate, S-Adenosylhomocysteine and 3-hydroxybutyrate by showing high sensitivity to the gradient of oxygen concentrations and define significant differences between hypoxia 1%, normoxia 6% and hyperoxia 21% through all incubation time point. It has been observed that, under hypoxia the pyruvate play a vital role to generate

lactate, suppresses AMPK activation and induce NAD^+/NADH ratio, moreover, mitigate ATP insufficiency for cells proliferation under hypoxia condition. Another piece of evidence provided that, even well oxygenated cells can release pyruvate in favor of hypoxic cells and use it as an oxygen surrogate [87]. Herein, we have found that, the level of extracellular pyruvate under hypoxia 1% was lowest compered to normoxia 6% and hyperoxia 21% and showing by high sensitivity presented an oxygen concentration and the time-dependent manners in HT1080 cells line. Additionally, we identified that the monocarboxylate transporter (MCT) plays a crucial role in regulating extracellular pyruvate levels under different oxygen conditions, acting as both a transporter and sensor for oxygen concentration. These findings provide new insights into the dynamic response of cells to changes in oxygen levels and the impact of oxygen levels on cellular metabolism. Further studies are needed to fully understand the underlying mechanisms and potential implications for cellular function and survival under different oxygen conditions. Similar affect showed the complexity of the pyruvate functions not just as a bridge between glycolysis and oxidative phosphorylation reactions but also as a key element between hypoxic and normoxic cells communication. Moreover, the crosstalk between hypoxic cells and cancer-associated fibroblasts "reverse Warburg effect "*in vitro* and *in vivo* by uptake of lactate which is produced from hypoxic cells and generates pyruvate to deliver it to hypoxic cells through tumor stroma [88]. In the microenvironment of cancer, cancer-associated fibroblasts (CAFs) exert a significant influence, playing a dominant role in shaping the homeostasis of the tumor microenvironment (TME). The complex interactions between cancer cells and surrounding CAFs have been shown to significantly impact cancer growth, metabolism, metastasis, and progression. This understanding has led to the development of the "dual-chamber" or "Reverse Warburg effect" model, highlighting the critical role of CAFs in the cancer microenvironment [89].

Additionally, methionine (Met), homocysteine (HCY), S-adenosylhomocysteine (SAH), and S-adenosylmethionine (SAM) are the main components of methionine metabolism in cancer cells [89]. It has been reported that, the total homocysteine (tHcy) elevation in the human plasma is associated with multiple diseases and cancer and correlated with elevation of cellular S-Adenosylhomocysteine (SAH) [90–95]. Moreover, the methionine is necessary

for S-adenosylmethionine (SAM) generation, thereafter, the SAM is predominant of methyl donor for methylation of DNA through catalysis reversible reaction to S-adenosylhomocysteine (SAH) via the methyltransferase nicotinamide N-methyltransferase (NNMT) [96]. However, a study showed that, under hypoxia condition (1% oxygen) compared to normoxia condition (20% oxygen) the methionine metabolism was induced in RCC Cells as a result of LAT1 upregulation and increase uptake of methionine [97]. Oppositely, we have found that, methionine was highly uptake under normoxia 6% and hyperoxia 21% compared to hypoxia 1%, in another hand, releasing S-Adenosylhomocysteine (SAH) to extracellular milieu in oxygen concentration-dependent manner. This indication could be related to the variation of hypoxia action to tumor types [97] at first, and more to the correlation to the GNMT that regulate the SAM/SAH ratio in cytosolic space [98] and/or the activity of S-adenosylhomocysteine hydrolase (SAHH) that contribute to tumorigenesis [99]. Therefore, the mechanism behind this phenomena might be connect to two scenarios, first, an increase the LAT1 activity to induce methionine uptake and releasing S-Adenosylhomocysteine to the media to restore the balance of cellular SAM/SAH ratio. While, the second scenario is S-adenosylhomocysteine hydrolase (SAHH) and downregulation or inactivation which leads to accumulate cellular S-Adenosylhomocysteine and effect DNA methylation and an excess of it released to extracellular space. It's worth to mention that, S-adenosylhomocysteine hydrolase (SAHH) inactivation might serve cancer cell proliferation showed by Leal J.F. et al. results which revealed an inactivation of SAHH will inhibit p53 transcriptional activity and impairs DNA damage-induced transcription of p21 [99].

5. Conclusion

In this chapter, we investigated the effect of oxygen concentrations on the extracellular and intracellular metabolome of HT1080 cells over time, using ^{1}H NMR. We found that hyperoxia had a distinct metabolic phenotype compared to hypoxia and normoxia, which could have implications for standardizing *in vitro* studies. Specifically:

1. Intracellular metabolites were downregulated at hypoxia and normoxia, while 60% of significant metabolites at hyperoxia were upregulated over time.

Comparison between different oxygen concentrations showed little sensitivity between hypoxia and normoxia after 12h, 24h, and 36h of incubation (72%, 93%, and 83% sensitivity, respectively).

2. Extracellular metabolites were mostly downregulated at hypoxia and upregulated at normoxia, except for fumarate which was upregulated at both. At hyperoxia, 30% of significant metabolites were upregulated over time. Sensitivity to oxygen concentration fluctuated among significant extracellular metabolites, with 50% showing no sensitivity between hypoxia and normoxia after 12h of incubation, 78% showing no difference between normoxia and hyperoxia after 24h, and almost 46% showing high sensitivity to all oxygen concentrations after 36h.

Our results suggest that oxygen concentration is a crucial factor to consider when studying the intracellular and extracellular metabolome, as it can result in significant metabolic variability. Therefore, researchers should pay attention to the oxygen concentration used in their experiments to avoid undesirable results that no connected to *in vivo* studies.

6. References

1. Al Tameemi, W.; Dale, T.P.; Al-Jumaily, R.M.K.; Forsyth, N.R. Hypoxia-Modified Cancer Cell Metabolism. *Frontiers in Cell and Developmental Biology* **2019**, *7*.
2. Yun, Z.; Lin, Q. Hypoxia and Regulation of Cancer Cell Stemness. In Proceedings of the Tumor Microenvironment and Cellular Stress; Koumenis, C., Hammond, E., Giaccia, A., Eds.; Springer: New York, NY, 2014; pp. 41–53.
3. Evans, S.M.; Koch, C.J. Prognostic Significance of Tumor Oxygenation in Humans. *Cancer Letters* **2003**, *195*, 1–16, doi:10.1016/S0304-3835(03)00012-0.
4. Moon, E.J.; Brizel, D.M.; Chi, J.A.; Dewhirst, M.W. The Potential Role of Intrinsic Hypoxia Markers as Prognostic Variables in Cancer. *Antioxidants & Redox Signaling* **2007**, *9*, 1237–1294, doi:10.1089/ars.2007.1623.
5. Horsman, M.R.; Mortensen, L.S.; Petersen, J.B.; Busk, M.; Overgaard, J. Imaging Hypoxia to Improve Radiotherapy Outcome. *Nat Rev Clin Oncol* **2012**, *9*, 674–687, doi:10.1038/nrclinonc.2012.171.
6. Muz, B.; Puente, P. de la; Azab, F.; Azab, A.K. The Role of Hypoxia in Cancer Progression, Angiogenesis, Metastasis, and Resistance to Therapy. *HP* **2015**, *3*, 83–92, doi:10.2147/HP.S93413.
7. Weljie, A.M.; Bondareva, A.; Zang, P.; Jirik, F.R. 1H NMR Metabolomics Identification of Markers of Hypoxia-Induced Metabolic Shifts in a Breast Cancer Model System. *J Biomol NMR* **2011**, *49*, 185–193, doi:10.1007/s10858-011-9486-4.

8. Kostidis, S.; Addie, R.D.; Morreau, H.; Mayboroda, O.A.; Giera, M. Quantitative NMR Analysis of Intra- and Extracellular Metabolism of Mammalian Cells: A Tutorial. *Analytica Chimica Acta* **2017**, *980*, 1–24, doi:10.1016/j.aca.2017.05.011.
9. Wenger, R.H.; Kurtcuoglu, V.; Scholz, C.C.; Marti, H.H.; Hoogewijs, D. Frequently Asked Questions in Hypoxia Research. *Hypoxia (Auckl)* **2015**, *3*, 35–43, doi:10.2147/HP.S92198.
10. Ulrich, E.L.; Akutsu, H.; Doreleijers, J.F.; Harano, Y.; Ioannidis, Y.E.; Lin, J.; Livny, M.; Mading, S.; Maziuk, D.; Miller, Z.; et al. BioMagResBank. *Nucleic Acids Research* **2008**, *36*, D402–D408, doi:10.1093/nar/gkm957.
11. Wishart, D.S.; Feunang, Y.D.; Marcu, A.; Guo, A.C.; Liang, K.; Vázquez-Fresno, R.; Sajed, T.; Johnson, D.; Li, C.; Karu, N.; et al. HMDB 4.0: The Human Metabolome Database for 2018. *Nucleic Acids Research* **2018**, *46*, D608–D617, doi:10.1093/nar/gkx1089.
12. Tomasi, G.; van den Berg, F.; Andersson, C. Correlation Optimized Warping and Dynamic Time Warping as Preprocessing Methods for Chromatographic Data. *Journal of Chemometrics* **2004**, *18*, 231–241, doi:10.1002/cem.859.
13. Savorani, F.; Tomasi, G.; Engelsen, S.B. Icoshift: A Versatile Tool for the Rapid Alignment of 1D NMR Spectra. *Journal of Magnetic Resonance* **2010**, *202*, 190–202, doi:10.1016/j.jmr.2009.11.012.
14. Paredes, F.; Williams, H.C.; San Martin, A. Metabolic Adaptation in Hypoxia and Cancer. *Cancer Letters* **2021**, *502*, 133–142, doi:10.1016/j.canlet.2020.12.020.
15. Gebregiworgis, T.; Purohit, V.; Shukla, S.K.; Tadros, S.; Chaika, N.V.; Abrego, J.; Mulder, S.E.; Gunda, V.; Singh, P.K.; Powers, R. Glucose Limitation Alters Glutamine Metabolism in MUC1-Overexpressing Pancreatic Cancer Cells. *J. Proteome Res.* **2017**, *16*, 3536–3546, doi:10.1021/acs.jproteome.7b00246.
16. Metallo, C.M.; Gameiro, P.A.; Bell, E.L.; Mattaini, K.R.; Yang, J.; Hiller, K.; Jewell, C.M.; Johnson, Z.R.; Irvine, D.J.; Guarente, L.; et al. Reductive Glutamine Metabolism by IDH1 Mediates Lipogenesis under Hypoxia. *Nature* **2012**, *481*, 380–384, doi:10.1038/nature10602.
17. Yoo, H.C.; Yu, Y.C.; Sung, Y.; Han, J.M. Glutamine Reliance in Cell Metabolism. *Exp Mol Med* **2020**, *52*, 1496–1516, doi:10.1038/s12276-020-00504-8.
18. Scalise, M.; Mazza, T.; Pappacoda, G.; Pochini, L.; Cosco, J.; Rovella, F.; Indiveri, C. The Human SLC1A5 Neutral Amino Acid Transporter Catalyzes a PH-Dependent Glutamate/Glutamine Antiport, as Well. *Frontiers in Cell and Developmental Biology* **2020**, *8*.
19. Akella, N.M.; Ciraku, L.; Reginato, M.J. Fueling the Fire: Emerging Role of the Hexosamine Biosynthetic Pathway in Cancer. *BMC Biology* **2019**, *17*, 52, doi:10.1186/s12915-019-0671-3.
20. Denko, N.C. Hypoxia, HIF1 and Glucose Metabolism in the Solid Tumour. *Nat Rev Cancer* **2008**, *8*, 705–713, doi:10.1038/nrc2468.
21. Chen, C.; Pore, N.; Behrooz, A.; Ismail-Beigi, F.; Maity, A. Regulation of Glut1 MRNA by Hypoxia-Inducible Factor-1: INTERACTION BETWEEN H-Ras AND HYPOXIA *. *Journal of Biological Chemistry* **2001**, *276*, 9519–9525, doi:10.1074/jbc.M010144200.
22. Mathupala, S.P.; Rempel, A.; Pedersen, P.L. Glucose Catabolism in Cancer Cells: IDENTIFICATION AND CHARACTERIZATION OF A MARKED ACTIVATION RESPONSE OF THE TYPE II HEXOKINASE GENE TO HYPOXIC CONDITIONS*. *Journal of Biological Chemistry* **2001**, *276*, 43407–43412, doi:10.1074/jbc.M108181200.
23. Iyer, N.V.; Kotch, L.E.; Agani, F.; Leung, S.W.; Laughner, E.; Wenger, R.H.; Gassmann, M.; Gearhart, J.D.; Lawler, A.M.; Yu, A.Y.; et al. Cellular and Developmental Control of O2 Homeostasis by Hypoxia-Inducible Factor 1α. *Genes Dev* **1998**, *12*, 149–162.
24. Firth, J.D.; Ebert, B.L.; Ratcliffe, P.J. Hypoxic Regulation of Lactate Dehydrogenase A: INTERACTION BETWEEN HYPOXIA-INDUCIBLE FACTOR 1 AND CAMP RESPONSE ELEMENTS (∗). *Journal of Biological Chemistry* **1995**, *270*, 21021–21027, doi:10.1074/jbc.270.36.21021.

25. Ullah, M.S.; Davies, A.J.; Halestrap, A.P. The Plasma Membrane Lactate Transporter MCT4, but Not MCT1, Is Up-Regulated by Hypoxia through a HIF-1α-Dependent Mechanism *. *Journal of Biological Chemistry* **2006**, *281*, 9030–9037, doi:10.1074/jbc.M511397200.
26. Papandreou, I.; Cairns, R.A.; Fontana, L.; Lim, A.L.; Denko, N.C. HIF-1 Mediates Adaptation to Hypoxia by Actively Downregulating Mitochondrial Oxygen Consumption. *Cell Metabolism* **2006**, *3*, 187–197, doi:10.1016/j.cmet.2006.01.012.
27. Fukuda, R.; Zhang, H.; Kim, J.; Shimoda, L.; Dang, C.V.; Semenza, G.L. HIF-1 Regulates Cytochrome Oxidase Subunits to Optimize Efficiency of Respiration in Hypoxic Cells. *Cell* **2007**, *129*, 111–122, doi:10.1016/j.cell.2007.01.047.
28. Sonkar, K.; Ayyappan, V.; Tressler, C.M.; Adelaja, O.; Cai, R.; Cheng, M.; Glunde, K. Focus on the Glycerophosphocholine Pathway in Choline Phospholipid Metabolism of Cancer. *NMR in Biomedicine* **2019**, *32*, e4112, doi:10.1002/nbm.4112.
29. Ackerstaff, E.; Pflug, B.R.; Nelson, J.B.; Bhujwalla, Z.M. Detection of Increased Choline Compounds with Proton Nuclear Magnetic Resonance Spectroscopy Subsequent to Malignant Transformation of Human Prostatic Epithelial Cells. *Cancer Res* **2001**, *61*, 3599–3603.
30. Smith, T. a. D.; Bush, C.; Jameson, C.; Titley, J.C.; Leach, M.O.; Wilman, D.E.V.; McCready, V.R. Phospholipid Metabolites, Prognosis and Proliferation in Human Breast Carcinoma. *NMR in Biomedicine* **1993**, *6*, 318–323, doi:10.1002/nbm.1940060506.
31. Aboagye, E.O.; Bhujwalla, Z.M. Malignant Transformation Alters Membrane Choline Phospholipid Metabolism of Human Mammary Epithelial Cells. *Cancer Res* **1999**, *59*, 80–84.
32. Nakagami, K.; Uchida, T.; Ohwada, S.; Koibuchi, Y.; Suda, Y.; Sekine, T.; Morishita, Y. Increased Choline Kinase Activity and Elevated Phosphocholine Levels in Human Colon Cancer†. *Japanese Journal of Cancer Research* **1999**, *90*, 419–424, doi:10.1111/j.1349-7006.1999.tb00764.x.
33. Eliyahu, G.; Kreizman, T.; Degani, H. Phosphocholine as a Biomarker of Breast Cancer: Molecular and Biochemical Studies. *International Journal of Cancer* **2007**, *120*, 1721–1730, doi:10.1002/ijc.22293.
34. Hernando, E.; Sarmentero-Estrada, J.; Koppie, T.; Belda-Iniesta, C.; Ramírez de Molina, V.; Cejas, P.; Ozu, C.; Le, C.; Sánchez, J.J.; González-Barón, M.; et al. A Critical Role for Choline Kinase-α in the Aggressiveness of Bladder Carcinomas. *Oncogene* **2009**, *28*, 2425–2435, doi:10.1038/onc.2009.91.
35. Iorio, E.; Ricci, A.; Bagnoli, M.; Pisanu, M.E.; Castellano, G.; Di Vito, M.; Venturini, E.; Glunde, K.; Bhujwalla, Z.M.; Mezzanzanica, D.; et al. Activation of Phosphatidylcholine Cycle Enzymes in Human Epithelial Ovarian Cancer Cells. *Cancer Research* **2010**, *70*, 2126–2135, doi:10.1158/0008-5472.CAN-09-3833.
36. Podo, F.; Paris, L.; Cecchetti, S.; Spadaro, F.; Abalsamo, L.; Ramoni, C.; Ricci, A.; Pisanu, M.E.; Sardanelli, F.; Canese, R.; et al. Activation of Phosphatidylcholine-Specific Phospholipase C in Breast and Ovarian Cancer: Impact on MRS-Detected Choline Metabolic Profile and Perspectives for Targeted Therapy. *Frontiers in Oncology* **2016**, *6*.
37. Spadaro, F.; Ramoni, C.; Mezzanzanica, D.; Miotti, S.; Alberti, P.; Cecchetti, S.; Iorio, E.; Dolo, V.; Canevari, S.; Podo, F. Phosphatidylcholine-Specific Phospholipase C Activation in Epithelial Ovarian Cancer Cells. *Cancer Research* **2008**, *68*, 6541–6549, doi:10.1158/0008-5472.CAN-07-6763.
38. Uchida, N.; Okamura, S.; Kuwano, H. Phospholipase D Activity in Human Gastric Carcinoma. *Anticancer Res* **1999**, *19*, 671–675.

39. Ramírez de Molina, A.; Penalva, V.; Lucas, L.; Lacal, J.C. Regulation of Choline Kinase Activity by Ras Proteins Involves Ral–GDS and PI3K. *Oncogene* **2002**, *21*, 937–946, doi:10.1038/sj.onc.1205144.
40. Janardhan, S.; Srivani, P.; Sastry, G.N. Choline Kinase: An Important Target for Cancer. *Current Medicinal Chemistry 13*, 1169–1186.
41. Ratnam, S.; Kent, C. Early Increase in Choline Kinase Activity upon Induction of the H-RasOncogene in Mouse Fibroblast Cell Lines. *Archives of Biochemistry and Biophysics* **1995**, *323*, 313–322, doi:10.1006/abbi.1995.9959.
42. Bj, G.; Aud; Diaz-Meco, M.T.; Moscat, J.; Johansen, T. Evidence for a Bifurcation of the Mitogenic Signaling Pathway Activated by Ras and Phosphatidylcholine-Hydrolyzing Phospholipase C (∗). *Journal of Biological Chemistry* **1995**, *270*, 21299–21306, doi:10.1074/jbc.270.36.21299.
43. Cai, H.; Erhardt, P.; Troppmair, J.; Diaz-Meco, M.T.; Sithanandam, G.; Rapp, U.R.; Moscat, J.; Cooper, G.M. Hydrolysis of Phosphatidylcholine Couples Ras to Activation of Raf Protein Kinase during Mitogenic Signal Transduction. *Molecular and Cellular Biology* **1993**, *13*, 7645–7651, doi:10.1128/mcb.13.12.7645-7651.1993.
44. Jiang, H.; Lu, Z.; Luo, J.-Q.; Wolfman, A.; Foster, D.A. Ras Mediates the Activation of Phospholipase D by V-Src (∗). *Journal of Biological Chemistry* **1995**, *270*, 6006–6009, doi:10.1074/jbc.270.11.6006.
45. Prabhakar, N.R. Invited Review: Oxygen Sensing during Intermittent Hypoxia: Cellular and Molecular Mechanisms. *Journal of Applied Physiology* **2001**, *90*, 1986–1994, doi:10.1152/jappl.2001.90.5.1986.
46. Bansal, A.; Shuyan, W.; Hara, T.; Harris, R.A.; DeGrado, T.R. Biodisposition and Metabolism of [18F]Fluorocholine in 9L Glioma Cells and 9L Glioma-Bearing Fisher Rats. *Eur J Nucl Med Mol Imaging* **2008**, *35*, 1192–1203, doi:10.1007/s00259-008-0736-y.
47. Bansal, A.; Harris, R.A.; DeGrado, T.R. Choline Phosphorylation and Regulation of Transcription of Choline Kinase α in Hypoxia [S]. *Journal of Lipid Research* **2012**, *53*, 149–157, doi:10.1194/jlr.M021030.
48. Lieu, E.L.; Nguyen, T.; Rhyne, S.; Kim, J. Amino Acids in Cancer. *Exp Mol Med* **2020**, *52*, 15–30, doi:10.1038/s12276-020-0375-3.
49. Wei, Z.; Liu, X.; Cheng, C.; Yu, W.; Yi, P. Metabolism of Amino Acids in Cancer. *Frontiers in Cell and Developmental Biology* **2021**, *8*.
50. Possemato, R.; Marks, K.M.; Shaul, Y.D.; Pacold, M.E.; Kim, D.; Birsoy, K.; Sethumadhavan, S.; Woo, H.-K.; Jang, H.G.; Jha, A.K.; et al. Functional Genomics Reveal That the Serine Synthesis Pathway Is Essential in Breast Cancer. *Nature* **2011**, *476*, 346–350, doi:10.1038/nature10350.
51. Zhang, B.; Chen, Y.; Shi, X.; Zhou, M.; Bao, L.; Hatanpaa, K.J.; Patel, T.; DeBerardinis, R.J.; Wang, Y.; Luo, W. Regulation of Branched-Chain Amino Acid Metabolism by Hypoxia-Inducible Factor in Glioblastoma. *Cell. Mol. Life Sci.* **2021**, *78*, 195–206, doi:10.1007/s00018-020-03483-1.
52. Shu, X.; Zhan, P.-P.; Sun, L.-X.; Yu, L.; Liu, J.; Sun, L.-C.; Yang, Z.-H.; Ran, Y.-L.; Sun, Y.-M. BCAT1 Activates PI3K/AKT/MTOR Pathway and Contributes to the Angiogenesis and Tumorigenicity of Gastric Cancer. *Frontiers in Cell and Developmental Biology* **2021**, *9*.
53. Luo, L.; Sun, W.; Zhu, W.; Li, S.; Zhang, W.; Xu, X.; Fang, D.; Grahn, T.H.M.; Jiang, L.; Zheng, Y. BCAT1 Decreases the Sensitivity of Cancer Cells to Cisplatin by Regulating MTOR-Mediated Autophagy via Branched-Chain Amino Acid Metabolism. *Cell Death Dis* **2021**, *12*, 1–13, doi:10.1038/s41419-021-03456-7.

54. Ananieva, E.A.; Wilkinson, A.C. Branched-Chain Amino Acid Metabolism in Cancer. *Current Opinion in Clinical Nutrition & Metabolic Care* **2018**, *21*, 64–70, doi:10.1097/MCO.0000000000000430.
55. Spitz, D.R.; Sim, J.E.; Ridnour, L.A.; Galoforo, S.S.; Lee, Y.J. Glucose Deprivation-Induced Oxidative Stress in Human Tumor Cells. A Fundamental Defect in Metabolism? *Ann N Y Acad Sci* **2000**, *899*, 349–362, doi:10.1111/j.1749-6632.2000.tb06199.x.
56. Ahmad, I.M.; Aykin-Burns, N.; Sim, J.E.; Walsh, S.A.; Higashikubo, R.; Buettner, G.R.; Venkataraman, S.; Mackey, M.A.; Flanagan, S.W.; Oberley, L.W.; et al. Mitochondrial O 2 ⋅ ¯ and H2O2 Mediate Glucose Deprivation-Induced Stress in Human Cancer Cells *. *Journal of Biological Chemistry* **2005**, *280*, 4254–4263, doi:10.1074/jbc.M411662200.
57. Simons, A.L.; Mattson, D.M.; Dornfeld, K.; Spitz, D.R. Glucose Deprivation-Induced Metabolic Oxidative Stress and Cancer Therapy. *J Cancer Res Ther* **2009**, *5 Suppl 1*, S2-6, doi:10.4103/0973-1482.55133.
58. Kalimuthu, K.; Kim, J.H.; Park, Y.S.; Luo, X.; Zhang, L.; Ku, J.-L.; Choudry, M.H.A.; Lee, Y.J. Glucose Deprivation-Induced Endoplasmic Reticulum Stress Response Plays a Pivotal Role in Enhancement of TRAIL Cytotoxicity. *Journal of Cellular Physiology* **2021**, *236*, 6666–6677, doi:10.1002/jcp.30329.
59. Moen, I.; Stuhr, L.E.B. Hyperbaric Oxygen Therapy and Cancer—a Review. *Targ Oncol* **2012**, *7*, 233–242, doi:10.1007/s11523-012-0233-x.
60. Chen, S.-Y.; Tsuneyama, K.; Yen, M.-H.; Lee, J.-T.; Chen, J.-L.; Huang, S.-M. Hyperbaric Oxygen Suppressed Tumor Progression through the Improvement of Tumor Hypoxia and Induction of Tumor Apoptosis in A549-Cell-Transferred Lung Cancer. *Sci Rep* **2021**, *11*, 12033, doi:10.1038/s41598-021-91454-2.
61. Qi, Y.; Ruan, J.; Wang, M.; Dai, Y.; Zhou, Q.; Gui, S.; Zhang, S.; Wang, Y. Effects of Hyperbaric Oxygen Treatment on Gastric Cancer Cell Line SGC7901. *Biomedical Reports* **2017**, *6*, 475–479, doi:10.3892/br.2017.869.
62. Mann, G.; Mora, S.; Madu, G.; Adegoke, O.A.J. Branched-Chain Amino Acids: Catabolism in Skeletal Muscle and Implications for Muscle and Whole-Body Metabolism. *Frontiers in Physiology* **2021**, *12*.
63. Hutson, S.M. The Case for Regulating Indispensable Amino Acid Metabolism: The Branched-Chain α-Keto Acid Dehydrogenase Kinase-Knockout Mouse. *Biochemical Journal* **2006**, *400*, e1, doi:10.1042/BJ20061506.
64. Gondáš, E.; Kráľová Trančíková, A.; Baranovičová, E.; Šofranko, J.; Hatok, J.; Kowtharapu, B.S.; Galanda, T.; Dobrota, D.; Kubatka, P.; Busselberg, D.; et al. Expression of 3-Methylcrotonyl-CoA Carboxylase in Brain Tumors and Capability to Catabolize Leucine by Human Neural Cancer Cells. *Cancers* **2022**, *14*, 585, doi:10.3390/cancers14030585.
65. Huang, S.; Wang, Z.; Zhao, L. <p>The Crucial Roles of Intermediate Metabolites in Cancer</P>. *CMAR* **2021**, *13*, 6291–6307, doi:10.2147/CMAR.S321433.
66. Martinez-Outschoorn, U.E.; Prisco, M.; Ertel, A.; Tsirigos, A.; Lin, Z.; Pavlides, S.; Wang, C.; Flomenberg, N.; Knudsen, E.S.; Howell, A.; et al. Ketones and Lactate Increase Cancer Cell "Stemness," Driving Recurrence, Metastasis and Poor Clinical Outcome in Breast Cancer. *Cell Cycle* **2011**, *10*, 1271–1286, doi:10.4161/cc.10.8.15330.
67. Woolf, E.C.; Syed, N.; Scheck, A.C. Tumor Metabolism, the Ketogenic Diet and β-Hydroxybutyrate: Novel Approaches to Adjuvant Brain Tumor Therapy. *Frontiers in Molecular Neuroscience* **2016**, *9*.
68. Shimazu, T.; Hirschey, M.D.; Newman, J.; He, W.; Shirakawa, K.; Le Moan, N.; Grueter, C.A.; Lim, H.; Saunders, L.R.; Stevens, R.D.; et al. Suppression of Oxidative Stress by β-Hydroxybutyrate, an Endogenous Histone Deacetylase Inhibitor. *Science* **2013**, *339*, 211–214, doi:10.1126/science.1227166.

69. Liu, K.; Li, F.; Sun, Q.; Lin, N.; Han, H.; You, K.; Tian, F.; Mao, Z.; Li, T.; Tong, T.; et al. P53 β-Hydroxybutyrylation Attenuates P53 Activity. *Cell Death Dis* **2019**, *10*, 1–13, doi:10.1038/s41419-019-1463-y.
70. Carmona-Fontaine, C.; Deforet, M.; Akkari, L.; Thompson, C.B.; Joyce, J.A.; Xavier, J.B. Metabolic Origins of Spatial Organization in the Tumor Microenvironment. *Proceedings of the National Academy of Sciences* **2017**, *114*, 2934–2939, doi:10.1073/pnas.1700600114.
71. Finicle, B.T.; Jayashankar, V.; Edinger, A.L. Nutrient Scavenging in Cancer. *Nat Rev Cancer* **2018**, *18*, 619–633, doi:10.1038/s41568-018-0048-x.
72. Hirayama, A.; Kami, K.; Sugimoto, M.; Sugawara, M.; Toki, N.; Onozuka, H.; Kinoshita, T.; Saito, N.; Ochiai, A.; Tomita, M.; et al. Quantitative Metabolome Profiling of Colon and Stomach Cancer Microenvironment by Capillary Electrophoresis Time-of-Flight Mass Spectrometry. *Cancer Research* **2009**, *69*, 4918–4925, doi:10.1158/0008-5472.CAN-08-4806.
73. Pavlova, N.N.; Thompson, C.B. The Emerging Hallmarks of Cancer Metabolism. *Cell Metab* **2016**, *23*, 27–47, doi:10.1016/j.cmet.2015.12.006.
74. Kimmelman, A.C.; White, E. Autophagy and Tumor Metabolism. *Cell Metabolism* **2017**, *25*, 1037–1043, doi:10.1016/j.cmet.2017.04.004.
75. Grasmann, G.; Smolle, E.; Olschewski, H.; Leithner, K. Gluconeogenesis in Cancer Cells – Repurposing of a Starvation-Induced Metabolic Pathway? *Biochimica et Biophysica Acta (BBA) - Reviews on Cancer* **2019**, *1872*, 24–36, doi:10.1016/j.bbcan.2019.05.006.
76. Harris, F.T.; Rahman, S.M.J.; Hassanein, M.; Qian, J.; Hoeksema, M.D.; Chen, H.; Eisenberg, R.; Chaurand, P.; Caprioli, R.M.; Shiota, M.; et al. Acyl-Coenzyme A Binding Protein Regulates Beta Oxidation Required for Growth and Survival of Non-Small Cell Lung Cancer. *Cancer Prev Res (Phila)* **2014**, *7*, 748–757, doi:10.1158/1940-6207.CAPR-14-0057.
77. Maddalena, L.A.; Selim, S.M.; Fonseca, J.; Messner, H.; McGowan, S.; Stuart, J.A. Hydrogen Peroxide Production Is Affected by Oxygen Levels in Mammalian Cell Culture. *Biochemical and Biophysical Research Communications* **2017**, *493*, 246–251, doi:10.1016/j.bbrc.2017.09.037.
78. Ferguson, D.C.J.; Smerdon, G.R.; Harries, L.W.; Dodd, N.J.F.; Murphy, M.P.; Curnow, A.; Winyard, P.G. Altered Cellular Redox Homeostasis and Redox Responses under Standard Oxygen Cell Culture Conditions versus Physioxia. *Free Radical Biology and Medicine* **2018**, *126*, 322–333, doi:10.1016/j.freeradbiomed.2018.08.025.
79. Moradi, F.; Moffatt, C.; Stuart, J.A. The Effect of Oxygen and Micronutrient Composition of Cell Growth Media on Cancer Cell Bioenergetics and Mitochondrial Networks. *Biomolecules* **2021**, *11*, 1177, doi:10.3390/biom11081177.
80. Yan, H.-M.; Ramachandran, A.; Bajt, M.L.; Lemasters, J.J.; Jaeschke, H. The Oxygen Tension Modulates Acetaminophen-Induced Mitochondrial Oxidant Stress and Cell Injury in Cultured Hepatocytes. *Toxicological Sciences* **2010**, *117*, 515–523, doi:10.1093/toxsci/kfq208.
81. Alva, R.; Moradi, F.; Liang, P.; Stuart, J.A. Culture of Cancer Cells at Physiological Oxygen Levels Affects Gene Expression in a Cell-Type Specific Manner. *Biomolecules* **2022**, *12*, 1684, doi:10.3390/biom12111684.
82. Alva, R.; Gardner, G.L.; Liang, P.; Stuart, J.A. Supraphysiological Oxygen Levels in Mammalian Cell Culture: Current State and Future Perspectives. *Cells* **2022**, *11*, 3123, doi:10.3390/cells11193123.
83. Ferrer, C.M.; Lynch, T.P.; Sodi, V.L.; Falcone, J.N.; Schwab, L.P.; Peacock, D.L.; Vocadlo, D.J.; Seagroves, T.N.; Reginato, M.J. O-GlcNAcylation Regulates Cancer Metabolism and Survival Stress Signaling via Regulation of the HIF-1 Pathway. *Molecular Cell* **2014**, *54*, 820–831, doi:10.1016/j.molcel.2014.04.026.
84. Walter, L.A.; Lin, Y.H.; Halbrook, C.J.; Chuh, K.N.; He, L.; Pedowitz, N.J.; Batt, A.R.; Brennan, C.K.; Stiles, B.L.; Lyssiotis, C.A.; et al. Inhibiting the Hexosamine Biosynthetic

Pathway Lowers O-GlcNAcylation Levels and Sensitizes Cancer to Environmental Stress. *Biochemistry* **2020**, *59*, 3169–3179, doi:10.1021/acs.biochem.9b00560.
85. Palorini, R.; Cammarata, F.P.; Balestrieri, C.; Monestiroli, A.; Vasso, M.; Gelfi, C.; Alberghina, L.; Chiaradonna, F. Glucose Starvation Induces Cell Death in K-Ras-Transformed Cells by Interfering with the Hexosamine Biosynthesis Pathway and Activating the Unfolded Protein Response. *Cell Death Dis* **2013**, *4*, e732–e732, doi:10.1038/cddis.2013.257.
86. Alkan, H.F.; Walter, K.E.; Hackl, H.; Heiden, M.G.V.; Madl, T.; Bogner-Strauss, J.G. N-Acetylaspartate Improves Cell Survival When Glucose Is Limiting 2020, 2020.05.28.114629.
87. Yin, C.; He, D.; Chen, S.; Tan, X.; Sang, N. Exogenous Pyruvate Facilitates Cancer Cell Adaptation to Hypoxia by Serving as an Oxygen Surrogate. *Oncotarget* **2016**, *7*, 47494–47510, doi:10.18632/oncotarget.10202.
88. Pavlides, S.; Whitaker-Menezes, D.; Castello-Cros, R.; Flomenberg, N.; Witkiewicz, A.K.; Frank, P.G.; Casimiro, M.C.; Wang, C.; Fortina, P.; Addya, S.; et al. The Reverse Warburg Effect: Aerobic Glycolysis in Cancer Associated Fibroblasts and the Tumor Stroma. *Cell Cycle* **2009**, *8*, 3984–4001, doi:10.4161/cc.8.23.10238.
89. Pascale, R.M.; Simile, M.M.; Calvisi, D.F.; Feo, C.F.; Feo, F. S-Adenosylmethionine: From the Discovery of Its Inhibition of Tumorigenesis to Its Use as a Therapeutic Agent. *Cells* **2022**, *11*, 409, doi:10.3390/cells11030409.
90. Xu, C.; Wu, Y.; Liu, G.; Liu, X.; Wang, F.; Yu, J. Relationship between Homocysteine Level and Diabetic Retinopathy: A Systematic Review and Meta-Analysis. *Diagnostic Pathology* **2014**, *9*, 167, doi:10.1186/s13000-014-0167-y.
91. Zhang, D.; Wen, X.; Wu, W.; Guo, Y.; Cui, W. Elevated Homocysteine Level and Folate Deficiency Associated with Increased Overall Risk of Carcinogenesis: Meta-Analysis of 83 Case-Control Studies Involving 35,758 Individuals. *PLOS ONE* **2015**, *10*, e0123423, doi:10.1371/journal.pone.0123423.
92. Hsieh, R.-L.; Huang, Y.-L.; Chen, W.-J.; Chen, H.-H.; Shiue, H.-S.; Lin, Y.-C.; Hsueh, Y.-M. Associations between Plasma Folate and Vitamin B12, Blood Lead, and Bone Mineral Density among Adults and Elderly Who Received a Health Examination. *Nutrients* **2022**, *14*, 911, doi:10.3390/nu14040911.
93. Homocysteine Studies Collaboration Homocysteine and Risk of Ischemic Heart Disease and StrokeA Meta-Analysis. *JAMA* **2002**, *288*, 2015–2022, doi:10.1001/jama.288.16.2015.
94. Seshadri, S.; Beiser, A.; Selhub, J.; Jacques, P.F.; Rosenberg, I.H.; D'Agostino, R.B.; Wilson, P.W.F.; Wolf, P.A. Plasma Homocysteine as a Risk Factor for Dementia and Alzheimer's Disease. *New England Journal of Medicine* **2002**, *346*, 476–483, doi:10.1056/NEJMoa011613.
95. Dai, Y.; Zhu, J.; Meng, D.; Yu, C.; Li, Y. Association of Homocysteine Level with Biopsy-Proven Non-Alcoholic Fatty Liver Disease: A Meta-Analysis. *Journal of Clinical Biochemistry and Nutrition* **2016**, *58*, 76–83, doi:10.3164/jcbn.15-54.
96. Butler, M.; Meer, L.T. van der; Leeuwen, F.N. van Amino Acid Depletion Therapies: Starving Cancer Cells to Death. *Trends in Endocrinology & Metabolism* **2021**, *32*, 367–381, doi:10.1016/j.tem.2021.03.003.
97. Xu, Q.; Liu, Y.; Sun, W.; Song, T.; Jiang, X.; Zeng, K.; Zeng, S.; Chen, L.; Yu, L. Blockade LAT1 Mediates Methionine Metabolism to Overcome Oxaliplatin Resistance under Hypoxia in Renal Cell Carcinoma. *Cancers* **2022**, *14*, 2551, doi:10.3390/cancers14102551.
98. Bhandari, V.; Hoey, C.; Liu, L.Y.; Lalonde, E.; Ray, J.; Livingstone, J.; Lesurf, R.; Shiah, Y.-J.; Vujcic, T.; Huang, X.; et al. Molecular Landmarks of Tumor Hypoxia across Cancer Types. *Nat Genet* **2019**, *51*, 308–318, doi:10.1038/s41588-018-0318-2.

99. Leal, J.F.; Ferrer, I.; Blanco-Aparicio, C.; Hernández-Losa, J.; Ramón y Cajal, S.; Carnero, A.; LLeonart, M.E. S-Adenosylhomocysteine Hydrolase Downregulation Contributes to Tumorigenesis. *Carcinogenesis* **2008**, *29*, 2089–2095, doi:10.1093/carcin/bgn198.

CHAPTER 3

The effect of hypoxia-reoxygenation and normoxia-deoxygenation in HT1080 cell line metabolome by 1H NMR analysis

Contents

1 Introduction 120

2 Materials and Methods 120

2.1. Cell Culturing medium (MEM) preparation 120

2.2. Experimental design 121

2.3. Culture media extraction 122

2.4. Cells extraction 122

2.5. Cell Growth measurement 123

2.6. NMR data acquisition 123

2.7. Metabolites Identification 124

2.8. Processing for Data Analysis 124

2.9. Data Analysis 125

2.9.1. Univariate Analysis 125

2.9.2. Multivariate Data Analysis (MVA) 125

3 Results 126

3.1. Cell growth curves 126

3.2. Time-dependent effect on HT1080 cell line metabolome during oxygen concentrations reverse approaches 127

3.2.1. The metabolic profiling of the normoxia-deoxygenation (DNC) approach 131

3.2.2. The metabolic profiling of the hypoxia-reoxygenation (RHC) treatment 139

4 Discussion 147

4.1. The post normoxia deoxygenation impact on of HT1080 cells metabolome 147

4.1.1 Conclusion 165

4.2. The post hypoxia reoxygenation impact on of HT1080 cells metabolome 167

4.2.1 Conclusion 175

5 References 178

1. Introduction

The common form of cancer is solid tumors, and tumor hypoxia occurs in all human malignant tumors [1–3]. Hypoxia develops within tumors as a consequence of rapid and uncontrolled tumor cell proliferation with abnormal mass and dysfunction of the tumor vasculature [4], leading to quick depletion of oxygen and nutrient supply. Hence, tumors develop different approaches to facilitate oxygen delivery, for instance, by inducing angiogenesis proteins and forming new vessels by releasing hypoxia-inducible angiogenic factors like endothelial growth factor (VEGF) and increasing diffusion exchange of nutrients and oxygen reperfusion [4,5]. Moreover, the tumors acquisition of cell migration characteristics and metastasis via the epithelial-to-mesenchymal transition (EMT) phenotype allows the cell to relocate to more sufficient sources of nutrients and oxygen [6]. We believe that during cancer cells uncontrolled proliferation the normoxic cells become hypoxic, the same situation happened, when the hypoxic cells induce hypoxic-angiogenic factors for nutrients and oxygen supply will become normoxic, and both transitions develop different phenotypes of cancer cells (hypoxic-normoxic transitions).

In this study, we aimed to establish an *in vitro* model of hypoxia and normoxia transitions by inducing hypoxia-reoxygenation (RHC) and normoxia-deoxygenation (DNC) to investigate the intracellular and extracellular metabolic profiling on the HT1080 cell line.

2. Materials and Methods

2.1. Cell Culturing in MEM

The HT1080 (human fibrosarcoma cell line) were purchased from American Type Culture ((ATCC® CCL-121™). Cells were kept for 72 h in T 75 cm^2 tissue culture flasks, in particular MEM culture medium. All the cells were used within the first 10 passages from unfreezing. The experiments start first by harvest the amount of cells required for all experiments. The cells were cultivated in Minimum Essential Medium Eagle (MEM) culture medium (Sigma Life Science, Sigma-Aldrich, Gillingham, UK) with 10% fetal bovine serum (FBS) (Biowest, origin South America, Riverside, MO, USA), 1% penicillin/streptomycin solution (HyClone, GE Healthcare Life Sciences,

Wien, Austria), 1% L-glutamine solution (Trypsin-EDTA solution, Sigma-Aldrich, SL, USA), 1% MEM Non-essential Amino Acid Solution (100x) (Sigma-Aldrich, SL, USA).

2.2.Experimental design

The HT1080 cells line was seeded in 75 cm^2 flasks at a density of 1 $x10^7$ cells per plate, For each plate we added 10 mL of media. The culture plates were incubated at hypoxia 1% and normoxia 6% O_2, in CO_2 –incubator with O_2 control (Binder, Tuttlingen, Germany) 5% CO_2 conditions at 37 °C. For the reverse to hypoxia (normoxia-deoxygenation) samples were conducted by 9 flasks and were kept at normoxia 6% for 12h in triplicate for cells and medium extraction as normoxia 6% after 12h of incubation is the baseline. The remaining 6 flasks transferred from normoxia 6% after 12h to hypoxia 1% for an addition time 12h and 24h, then we collected samples for each period of incubation time for cells and medium extraction. Likewise for the reverse to normoxia (hypoxia-reoxygenation). The 9 flasks were kept at hypoxia 1% for 12h in triplicate for cells and medium extraction as hypoxia 1% after 12h of incubation is the baseline. The remaining 6 flasks transferred from hypoxia 1% after 12h to normoxia 6% for an addition time 12h and 24h. Then we collected samples for each period of incubation time from normoxia for cells and medium extraction (**Figure** 1).

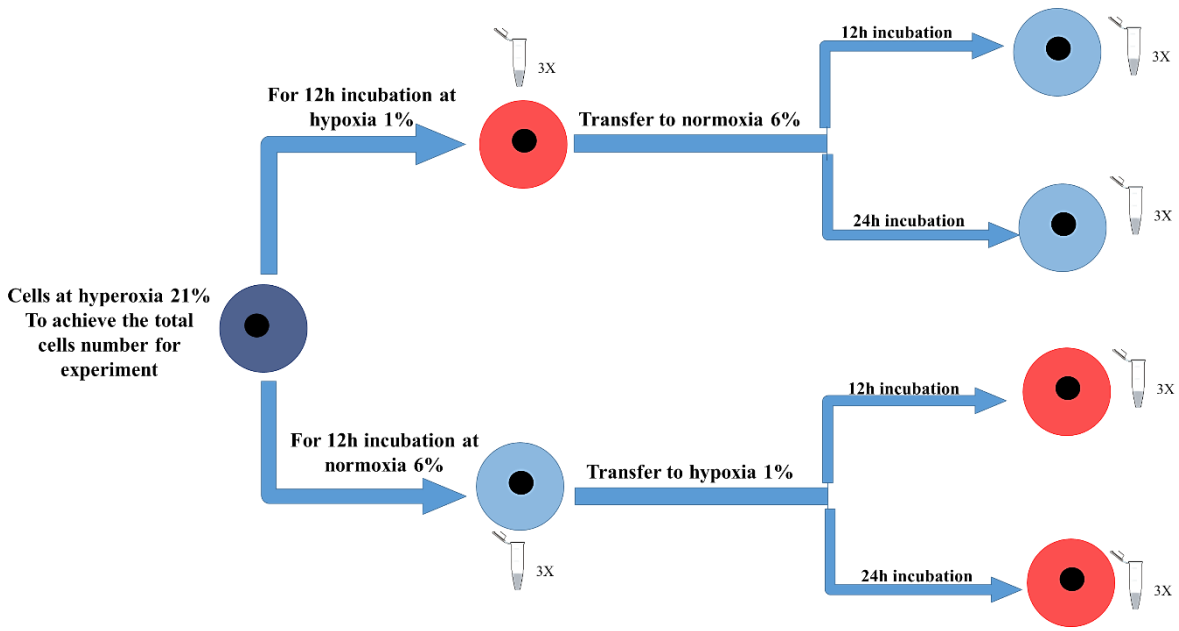

Figure 1. Experimental graphical design for all samples and methodology for NMR experiments. Blue, normoxia; red, hypoxia.

2.3. Culture medium extraction

Each time interval point at normoxia for 12h and deoxygenized normoxic cells condition (DNCs) at hypoxia for 12h and 24h. Moreover, at hypoxia for 12h and reoxygenized hypoxic cells (RHCs) for 12h and 24h, and was collected 1 mL from each culturing flask, then immediately stored at −80 °C. At the beginning of the analysis the medium was thawed out at room temperature and vortexed. Transfer 400 μL medium from each sample to a new Eppendorf tube with methanol 1.2 mL (LC-MS grade, Merck, Darmstadt, Germany). The mixture of medium-methanol was shaken for 10 min at 30 Hz (Tissiulyzer LT, Qiagen, Germantown, MD, USA), then incubated at −20 °C for 20 min and centrifuged for 30 min at 4 °C, 12000 rpm. Supernatant in 1 mL was transferred to a new Eppendorf tube and evaporated to dryness under a vacuum centrifuge (JWElectronic WP-03, Warsaw, Poland) at 40 °C, 1405 rpm. After evaporation, the samples were resuspended in 600 μL PBS buffer (pH, 7.3, 20% D_2O, 3mM TSP). Finally, 550 μL was transferred to an NMR cuvette (5 mm, SP type, ARMAR Chemicals, Döttingen, Switzerland). Prepared samples were stored at 4 °C until NMR spectra acquisition.

2.4.Cells extraction

After we reached 85-90% confluence at each time interval point mentioned above, the medium was removed from each flask, and the cells were washed with PBS (Phosphate Buffered Saline, Sigma-Aldrich, SL, USA). After that, the cells were detached by adding 5 mL of trypsin-EDTA (Trypsin-EDTA solution, Sigma-Aldrich, SL, USA), and incubated for 5 min at 5% CO_2 conditions at 37 °C. The cells suspension was centrifuged for 5 min at 21 °C, 1940 rpm. The supernatant was discarded and the cell pellet was washed with PB (Phosphate buffered saline, Sigma-Aldrich, SL, USA), and centrifuged once again. Finally, the supernatant was removed and the cells were kept at −80 °C before extraction. The cell pellet was thawed at room temperature 25 °C and, the pallet was mixed with 1.5 mL of cold methanol (LC-MS grade, Merck, Darmstadt, Germany) together with 7mm stainless steel beads (Qiagen GmbH, Hilden, Germany), and was homogenized for 10 min at 30 Hz (Tissiulyzer LT, Qiagen, Germantown, MD, USA), then incubated at −20 °C for 20 min, then the samples were centrifuged for 30 min at 4 °C, 12000 rpm. 1mL

of Supernatant was transferred to a new Eppendorf tube and evaporated the samples to dryness under a vacuum centrifuge (JWElectronic WP-03, Warsaw, Poland) at 40 °C, 1500 rpm. After evaporation, the samples were kept at -80 °C until NMR analysis. Evaporated samples were thawed at room temperature 25 °C and re-suspended in 600 µL PBS buffer (pH, 7.4, 20% D_2O, 0.33 mM of TSP). Finally, 550 µL was transferred to an NMR tube (5 mm, SP type, ARMAR Chemicals, Döttingen, Switzerland). The prepared samples were stored at 4 °C until NMR spectra acquisition.

2.5.Cells counting measurement

The cells growth was conducted separately, HT1080 cell lines were plated into a 6-wells plate at a cell density of 1 x 10^6 cells per well. The plates were cultivated in 12h normoxia 6% and the transferred plates from normoxia 6% after 12h to hypoxia 1% for 3h, 6h, 12h and 24h. Also after 12h hypoxia 1% and transferred plates from hypoxia 1% to normoxia 6% for 3h, 6h, 12h and 24h, in CO_2 –incubator with O_2 control (Binder, Tuttlingen, Germany) 5% CO_2 conditions at 37 °C. For cell viability, the cells were first trypsinzed and then stained with 0.4% Trypan Blue (Sigma, USA) in PBS for 1-3 min at room temperature, then counted by a hemocytometer (Brand, Wertheim, Germany). The growth curve was plotted. The population doubling time and growth rate were calculated during the exponential growth phase of the cells using the equations:

1. Cell doubling time (h):

$$T_d = (T2 - T1) . \frac{\ln(2)}{\ln(\frac{q2}{q1})}$$

2. Growth rate cells (h):

$$gr = \frac{\ln\left(\frac{q2}{q1}\right)}{\Delta t}$$

T_d = Doubling period (time it takes for object to double in number)
gr = Growth rate
$(T_2\text{-}T_1)$ or Δt = Duration time at the exponential growth.
q_2 = the number of cells at time T_2.
q_1 = the number of cells at time T_1.

2.6. NMR data acquisition

The ^{1}H NMR spectra of cells and post-cultured medium samples were recorded at 300 K using the Avance II spectrometer (Bruker, GmBH, Bremen, Germany). The proton operation frequency was set at 600.58 MHz. The 1D ^{1}H NMR spectra were recorded using a CPMG pulse sequence with water presaturation (cpmgpr1d in Bruker notation). For each sample, the spectra parameters were set respectively, width, 20.01 ppm; 128 scans; spin-echo delay of 400 μs; 80 loops; time domain of 64k, acquisition time of 2.73 s, and relaxation delay of 3.5s.

2.7. Metabolites Identification NMR

The identification of resonance signals was obtained by assignments published in the literature, Chenomx software (v 8.5 Chenomx Inc., Edmonton, Canada), and online database Biological Magnetic Resonance Data Bank [7], and Human Metabolome Database [8]. For intracellular metabolome 39 metabolites were identified (**Table** 1).

2.8. Processing for Data Analysis

The spectra were manually phased, than baseline-corrected with MestReNova software (Mestrelab Research v 14.1.1), and referenced to TSP signal group (δ = 0.000 ppm) for both types of samples. The spectra a prior were normalized to the constant sum of TSP resonance signal. The signals of water was removed from analysis. The icoshift algorithm and correlation optimized warping algorithm (COW) (if needed) was used for the alignment of resonance signals both implemented in MATLAB (v R2014a, MathWorks Inc., Natick, MA, USA) [9,10]. The sum of data points of the overlapping and non-overlapping resonances was obtained for calculation of relative intensity of identified metabolites resonance signals for Intracellular, however, for extracellular the data matrix was calculated individually for each spectra to obtain relative intensity of NMR measured metabolites. Before statistical analysis the relative intensity values of identified metabolites were normalized to respective cell number that was determined by each incubation time point after 12h in normoxia and reverse to hypoxia after 12h and 24h. In addition, after 12h in hypoxia and reverse to normoxia after 12h and 24h. Finally, quantified relative intensity of post-culture

media extracts and cells extracts for further analysis were prepared as a separate data matrices.

2.9.Data analysis

2.9.1. Univariate Analysis

The univariate analysis was calculated by using Statistica Software v.13 on relative intensity values of assigned intracellular and extracellular metabolites datasets with respect of interval time point for 12h normoxia (referred as 0h) and DNCs for 12h and 24h at hypoxia. In addition for 12h hypoxia (referred as 0h) and RHCs for 12h and 24h at normoxia. Multiple comparisons based on incubation time were tested by one-way ANOVA, Tukey's multiple-comparison posttest and multiplicity adjusted p value was calculated to account for multiple comparisons with family-wise significance and confidence level at $\alpha = 0.05$ (95% confidence interval). The boxplots were obtained by Rstudio (Rstudio Ver.R 3.0.1,Inc., Boston, NA, USA) based on triplicates for each cultivation time point from normoxia to hypoxia and from hypoxia to normoxia.

2.9.2. Multivariate Analysis (MVA)

The multivariate data analysis was performed using SIMCA software (Ver. 17.0, Sartorius, Göttingen, Germany). The relative intensity values of assigned intracellular and extracellular metabolites were prepared as separate data matrices. A priori multivariate analysis variables were UV scaled and sample order was randomized. The MVA was divided into two parts unsupervised exploratory analysis and supervised regression analysis, by The Principal Component Analysis (PCA) was used to show the overall clustering of data and determine potential outliers and the partial least squares regression model (PLS-R) with X block containing metabolites relative intensity and Y -block as incubation time points for reoxygenation hypoxic cells (RHCs) and deoxygenation of normoxic cells (DNCs) to build a linear model and predict the models parameters, such as the goodness-of-fit parameter R2 which, used to evaluate the quality of the model together with the predictive validation parameter Q^2.

The most important metabolites identified by PLS-R model were selected based on variable importance in projection (VIP) score above 1.00. The analysis of variance of cross-validated residuals (CV-ANOVA) for the partial least squares

regression model (PLS-R) used a significance level at alpha= 0.05 to assess model fit quality.

3. Results

3.1. Cell growth curves

The cells growth was assessed by differences in the cells number calculated to determine the growth ratio, which, was done separately in 6 wells plate, without changing the media during all experiments.

Our direct counting assay revealed variations in the growth of HT1080 cells under deoxygenation and reoxygenation conditions. These growth differences are illustrated in (**Figure** 2). We observed that under hypoxia (1% O_2) and normoxia (6% O_2) during a 12h of incubation, the cells entered an exponential growth phase, with a population-doubling time (PDT) of 36.6h, 35.6h and a growth rate of 0.019, 0.019 cell per hour, respectively. However, during RHC condition the cells went through stationary phase for 6h instantaneously entered once again the an exponential growth phase, with a population-doubling time (PDT) of 73.4h and a growth rate of 0.009 per hour. Unlike DNC condition leads to a deterioration in cell growth.

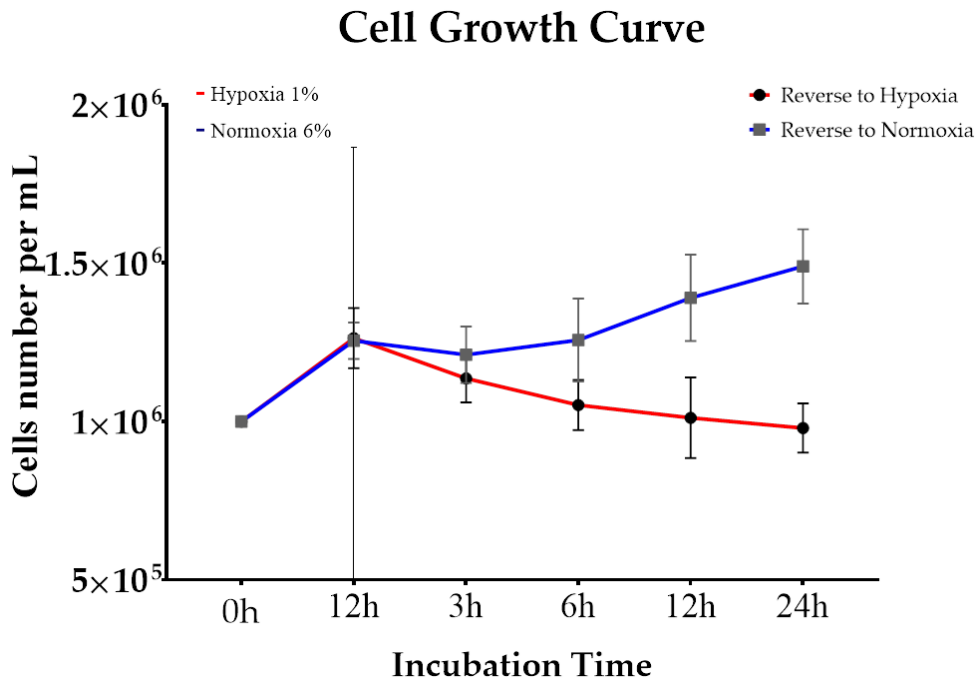

Figure 2. The HT1080 cell growth curve for studied time intervals points to RHC and DNC conditions. The line points error bars were obtained from the standard error of the mean (SEM). Red line— hypoxia 1%; red line — normoxia 6%; Blue line.

3.2. Time-dependent effect on HT1080 cell line metabolome during oxygen concentrations reverse approaches

Our results of 9 samples in total from cells extraction and 9 samples from post-cultured medium extraction at each incubation time point for RHC and DNC cell conditions were studied. We conducted a ^{1}H NMR-based metabolomics analysis and 41 metabolites were successfully assigned in cells extraction respectively (**Figure** 3, **Table** 1). 36 metabolites were successfully assigned from post-cultured medium extraction, besides 3 unknown metabolites (**Figure** 4, **Table** 2).

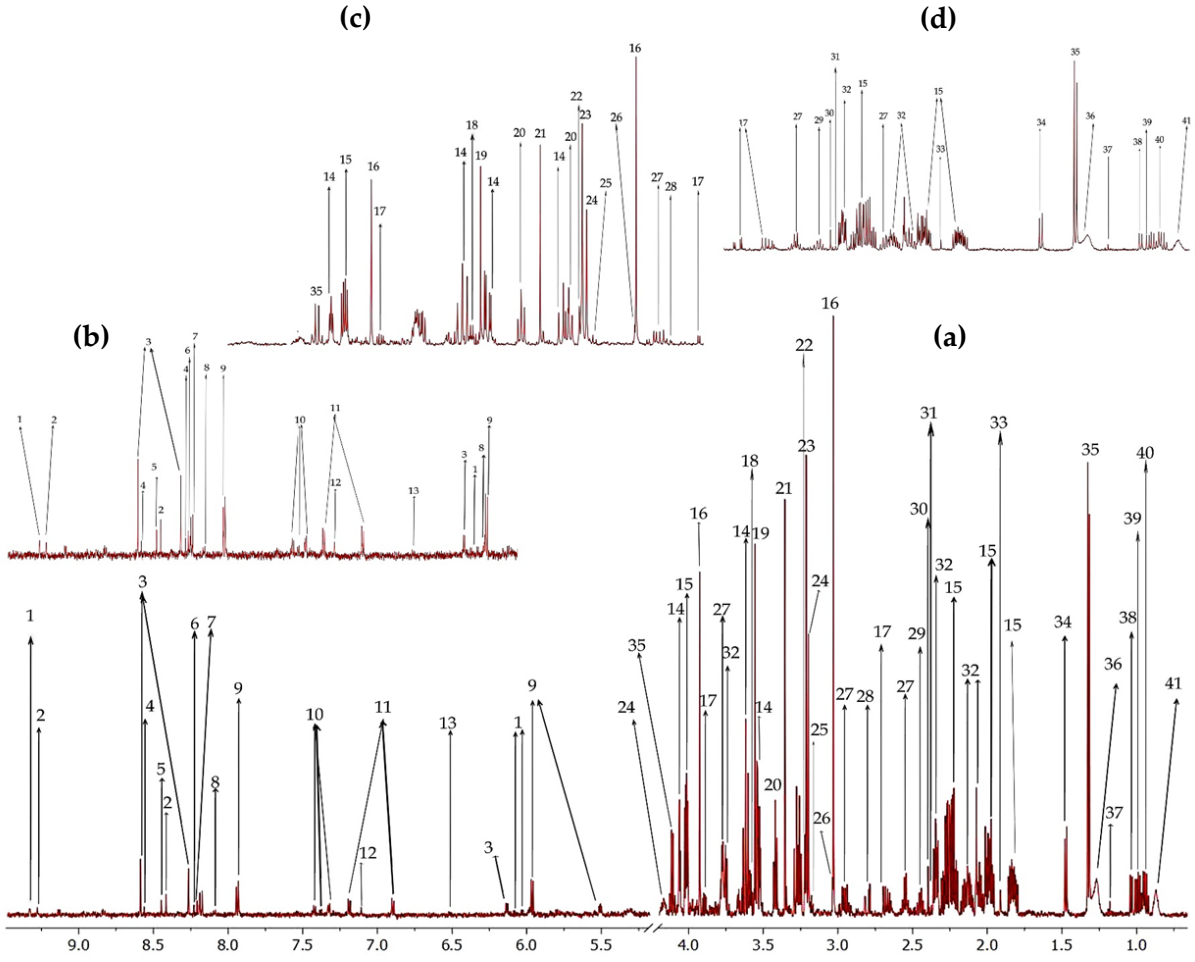

Figure 3. The representative ^{1}H NMR spectrum obtained from cells extracts (intracellular) of HT1080 after RHC and DNC. (a) Full 1H-NMR spectrum from δ 0.5 to δ 10.00; (b) Enlarged spectrum from δ 10.00 to δ 6.5; (c) Enlarged spectrum from δ 5.0 to δ 2.7; (d) Enlarged spectrum from δ 2.7 to δ 0.5. The metabolites were identified from 1- 41 as mentioned from Table 1 respectively.

Table 1. The chemical shifts and signal multiplicity of HT1080 cells extract metabolome identified by ^{1}H NMR spectroscopy.

No	Metabolites	Peak Assignments	Peak Centers (ppm)	HMDB ID
1	NAD+	s	8.409, d (9.127), d (8.827), s (9.321), m (8.167)	HMDB0000902
2	1-Methylnicotinamide	s	s (9.271), d (9.126), 8.827, s (8.185), s (4.470)	HMDB0000699
3	AMP	s	8.581, s (8.258)	HMDB0000058
4	IMP	s	8.555, s (8.222)	HMDB0000175
5	Formate	s	8.44	HMDB0304356
6	Oxypurinol	s	8.201	HMDB0000786
7	Hypoxanthine	s	s (8.187), 8.182	HMDB0000157
8	UMP	d	8.085, m (5.980)	HMDB0060282
9	UDP-N-Acetylglucosamine	d	7.932, d (5.967), dd (5.502), dd (4.350), m (4.274),s (2.066)	HMDB0000290
10	Phenylalanine	m	7.419, m (7.367), d (7.320)	HMDB0000159
11	Tyrosine	m	7.182, d (6.890)	HMDB0000158
12	π-Methylhistidine	s	7.101, s (3.738)	HMDB0000479
13	Fumarate	s	6.506	HMDB0000134
14	myo-Inositol	m	4.055, t (3.612), dd (3.525)	HMDB0000211
15	2-Hydroxyglutarate	m	4.01	HMDB0059655
16	Creatine	s	3.919	HMDB0000064
17	Aspartate	dd	3.889	HMDB0000191
18	Threonine	d	3.58	HMDB0000167
19	Glycine	s	3.549	HMDB0000123
20	Taurine	t	3.413, t (3.252)	HMDB0000251
21	Methanol (residual of extraction)	s	3.348	HMDB0001875
22	sn-Glycero-3-phosphocholine	s	3.216	HMDB0000086
23	O-Phosphocholine	s	3.207	HMDB0001565
24	Choline	s	3.192	HMDB0000097
25	β-Alanine	t	3.17	HMDB0000056
26	Creatinine	s	3.029	HMDB0000562
27	Glutathione	dd	2.972, dd (2.926)	HMDB0000125
28	Asparagine	t	2.851	HMDB0000168
29	Glutamine	m	2.462	HMDB0000641
30	Succinate	s	2.391	HMDB0000254
31	Pyruvate	s	2.368	HMDB0000243
32	Glutamate	m	t (3.748), 2.354, m (2.117), m (2.041)	HMDB0000148
33	Acetate	s	1.906	HMDB0000042
34	Alanine	d	1.467	HMDB0000161
35	Lactate	t	1.315, q (4.103)	HMDB0000190
36	L-1	LDL&VLDL	1.259	CH3−(CH2)n−

37	Ethanol	t	1.172	HMDB0000108
38	Valine	d	0.977, d (1.029)	HMDB0000883
39	Isoleucine	d	0.998, t (0.927)	HMDB0000172
40	Leucine	t	0.955	HMDB0000687
41	L-2	LDL&VLDL	0.867	CH3–(CH2)n–

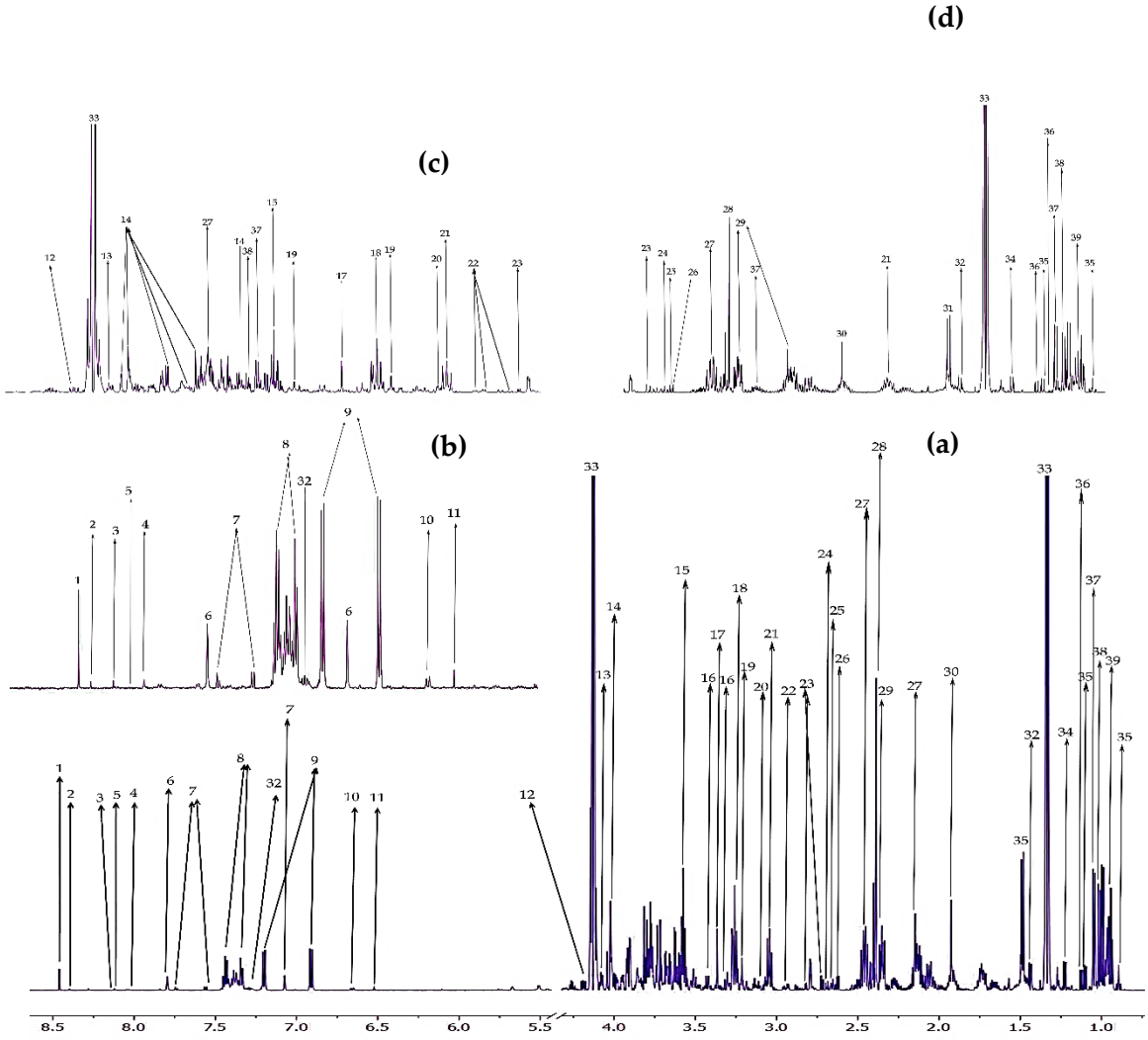

Figure 4. The representative ^{1}H NMR spectrum obtained from post cultured medium (extracellular) extracts of HT1080 RHC and DNC. (a) Full 1H-NMR spectrum from δ 0.5 to δ 10.00; (b) Enlarged spectrum from δ 8.5 to δ 6.5; (c) Enlarged spectrum from δ 5.0 to δ 2.7; (d) Enlarged spectrum from δ 2.7 to δ 0.5. The metabolites were identified from 1- 41 as mentioned from Table 2 respectively.

Table 2. The chemical shifts and signal multiplicity of HT1080 post cultured medium extract metabolome identified by ^{1}H NMR spectroscopy.

No	Metabolites	Peak Assignments	Peak Centers (ppm)	HMDB ID
1	Formate	s	8.44	HMDB0304356

2	S-Adenosylhomocysteine	s	8.38, s (8.27)	HMDB0000939
3	ATP	s	8.264	HMDB0000538
4	Unknown_1	s	8.104, s (7.289)	-
5	Hypoxanthine	s	8.188, s (8.20)	HMDB0000157
6	Histidine	s	8.012, s (7.058)	HMDB0000177
7	Tryptophan	d	7.543, d (7.722)	HMDB0000929
8	Phenylalanine	m	7.323, m (7.423), m (7.371)	HMDB0000159
9	Tyrosine	m	7.185, m (6.893)	HMDB0000158
10	Unknown_2	d	6.64	-
11	Fumarate	s	6.506	HMDB0000134
12	Pyroglutamate	dd	4.171, m (2.407)	HMDB0000267
13	*myo*-Inositol	dd	4.065, t (3.615), dd (3.544), t (3.287)	HMDB0000211
14	Fructose	d	m (4.016), m (4.00), m (3.895), m (3.818), 3.790, d (3.709), d (3.703)	HMDB0000660
15	Glycine	s	3.558	HMDB0000123
16	Proline	m	3.414	HMDB0000162
17	Methanol (residual solvent)	s	3.349	HMDB0001875
18	Arginine	m	3.241	HMDB0003416
19	Choline	s	3.198	HMDB0000097
20	Ornithine	t	3.054	HMDB0000214
21	Lysine	t	3.027, m (1.723)	HMDB0000182
22	Asparagine	t	2.928, t (2.849)	HMDB0000168
23	Aspartate	dd	2.689	HMDB0000191
24	Methionine	t	2.636	HMDB0000696
25	2-Oxoisocaproate	d	2.607	HMDB0000695
26	Methylamine	s	2.601	HMDB0000164
27	Glutamine	m	2.424, m (2.141)	HMDB0000641
28	Pyruvate	s	2.37	HMDB0000243
29	Glutamate	m	2.35, m (2.039)	HMDB0060475
30	Acetate	s	1.9	HMDB0000042
31	Alanine	d	1.47	HMDB0000161
32	2-Phenylpropionate	d	m (7.277), m (7.348), m (7.370), 1.123	HMDB0011743
33	Lactate	t	1.318, q (4.112)	HMDB0000190
34	Methylmalonate	d	1.211	HMDB0000202
35	3-Methyl-2-oxovalerate	d	1.084, t (0.879)	HMDB0000491
36	Unknown_3	d	1.109	-
37	Valine	d	0.977 , d (3.610), m (2.260), d (1.030)	HMDB0000883
38	Isoleucine	d	0.997, t (0.926)	HMDB0000172
39	Leucine	t	0.944	HMDB0000687

3.2.1. The metabolic profiling of the normoxia-deoxygenation (DNC) approach

For exploring the changes of the intracellular and extracellular metabolome, we built a PCA score and loading plots based on the ^{1}H NMR dataset, also the PLS-regression model was constructed to predict the behavior of dependent variables at each incubation time points. It must be mentioned that 12h at normoxia condition is referred to 0h, and DNC for 12h and 24h at hypoxia. Furthermore, the models were correctly validated and within obtained parameters the R^2X (cum), R^2Y (cum) Q^2(cum) for score plot and CV-ANOVA *p*-values for intracellular cells and extracellular post-culture medium extracts for all chosen comparison and time point are collected in (**Table** 3 and 4).

Table 3. The multivariate analysis models summary of cells extract (intracellular) NMR-based metabolome in comparisons between 0h (after 12h in normoxia 6%), 12h and 24h at DNC.

O_2 %	Incubation Time Comparison	Model Type	PC/LV	N =	R^2X (cum)	R^2Y (cum)	Q^2 (cum)	CV-ANOVA *p* value
Reverse to hypoxia	0h vs 12h vs. 24h	PCA	2	9	0.0.73	–	–	–
	0h vs 12h vs. 24h	PLS	3	9	0.929	0.991	0.969	$\mathbf{2.38 \times 10^{-2}}$

0h =12h at normoxia (Reverse to hypoxia)

Table 4. The multivariate analysis models summary of post cultured medium (extracellular) NMR- based metabolome in comparisons between 0h, 12h and 24h at DNC.

O_2 %	Incubation Time Comparison	Model Type	PC/LV	N =	R^2X (cum)	R^2Y (cum)	Q^2 (cum)	CV-ANOVA *p* value
Reverse to hypoxia	0h vs 12h vs. 24h	PCA	3	9	0.876	–	–	–
	0h vs 12h vs. 24h	PLS	4	9	0.92	0.989	0.963	$\mathbf{3.48 \times 10^{-2}}$

0h =12h at normoxia (Reverse to hypoxia)

From normoxic cells deoxygenation, the PCA score of cells extract (intracellular) metabolome revealed a separation tendency among PC1 and PC2 between normoxia 6% after 12h and reverse to hypoxia 1% after 12h and 24h groups (**Figure** 5a). The PCA loading plots was built and ascribed to the contributions of the intracellular metabolites among PC1 and PC2 (**Figure** 5b). On the other hand, the PCA score of post-cultured medium (extracellular) metabolome revealed a slightly separation tendency among PC1 and PC2 between normoxia 6% after 12h and reverse to hypoxia 1% after 12h and 24h groups (**Figure** 6a). The PCA loading plots was built

and showed the contributions of the extracellular metabolites among PC1 and PC2 (**Figure** 6b).

In order to explore the metabolites regulations to different oxygen concentrations through incubation time points. We build PLS regression model, and we found a high correlation between DNC groups through incubation time points for intracellular and extracellular datasets, with R^2 = 0.9905 and R^2 = 0.9887 by using just three PLS components (**Figure** 5c), and four PLS components (**Figure** 6c), respectively. The root-mean-square error of cross-validation (RMSECV) was 3.19h and 2.45h for intracellular and extracellular datasets, respectively, and did reach a statistically significant difference between groups by cross-validated predictive residuals of the PLS-R (CV-ANOVA) (**Table** 3, 4).

(a)

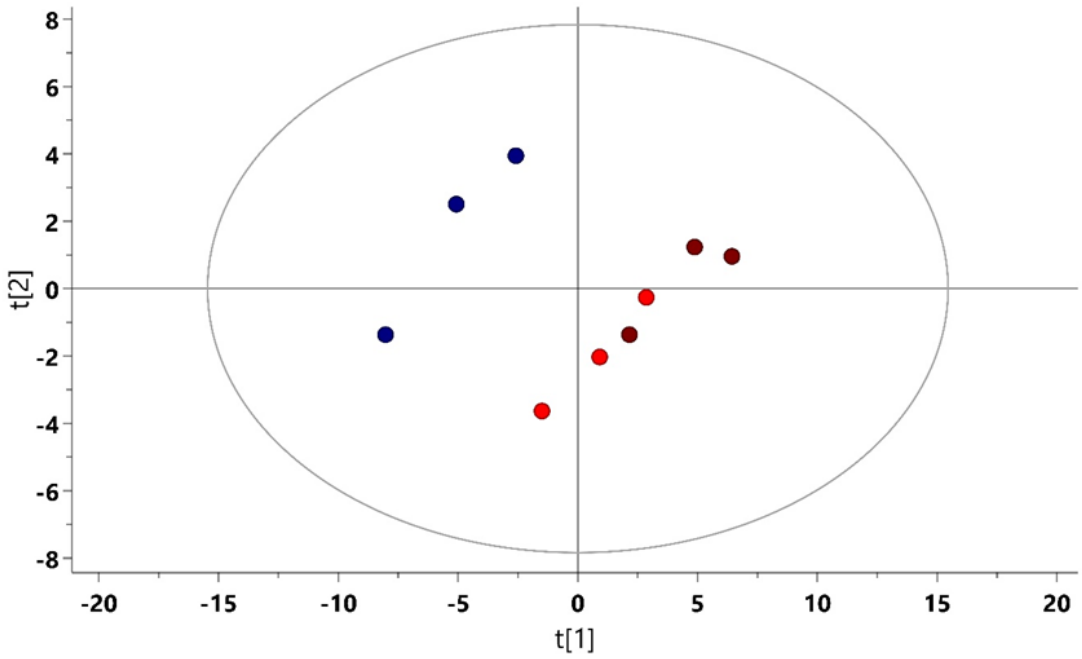

(b)

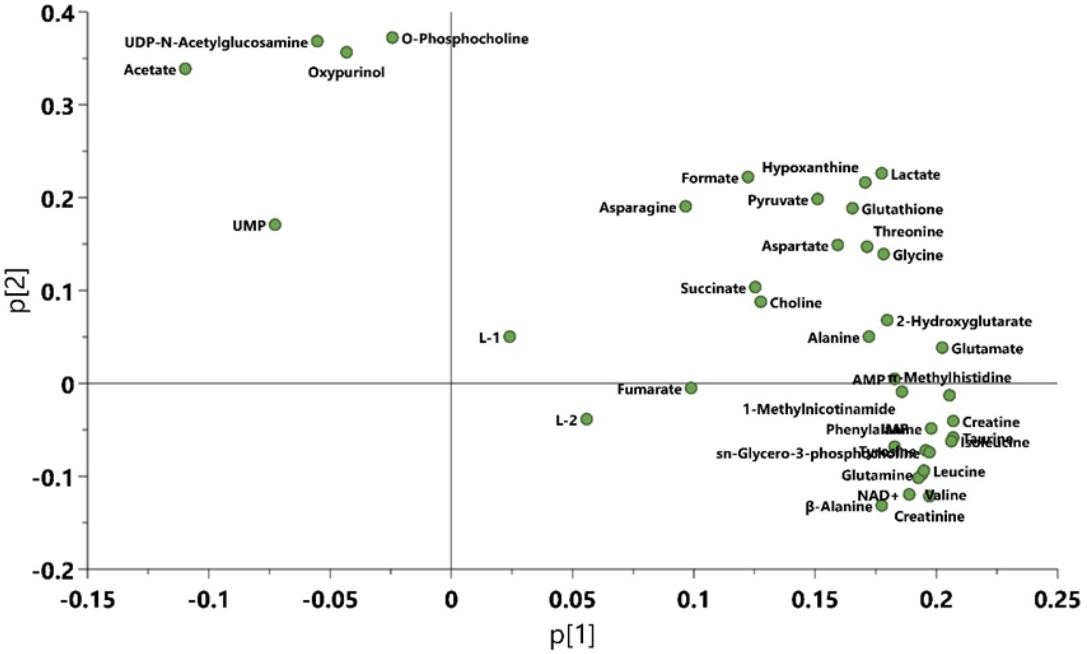
UDP-N-Acetylglucosamine
O-Phosphocholine
Acetate
Oxypurinol
UMP
Formate
Hypoxanthine
Lactate
Asparagine
Pyruvate
Glutathione
Threonine
Aspartate
Glycine
Succinate
Choline
2-Hydroxyglutarate
L-1
Alanine
Glutamate
Fumarate
1-Methylnicotinamide
L-2
Creatine
Taurine
Leucine
Glutamine
NAD+
Valine
β-Alanine
Creatinine
p[2]
p[1]
0.4
0.3
0.2
0.1
0
-0.1
-0.2
-0.15
-0.1
-0.05
0
0.05
0.1
0.15
0.2
0.25

(c)

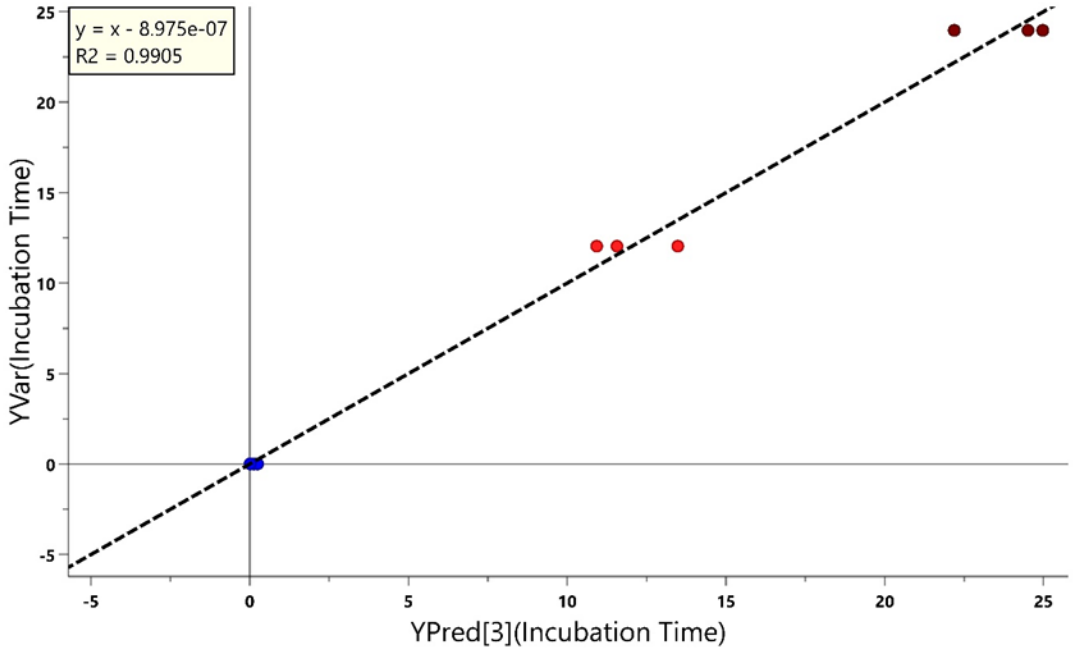
y = x - 8.975e-07
R2 = 0.9905
YVar(Incubation Time)
YPred[3](Incubation Time)
25
20
15
10
5
0
-5
-5
0
5
10
15
20
25

(**d**)

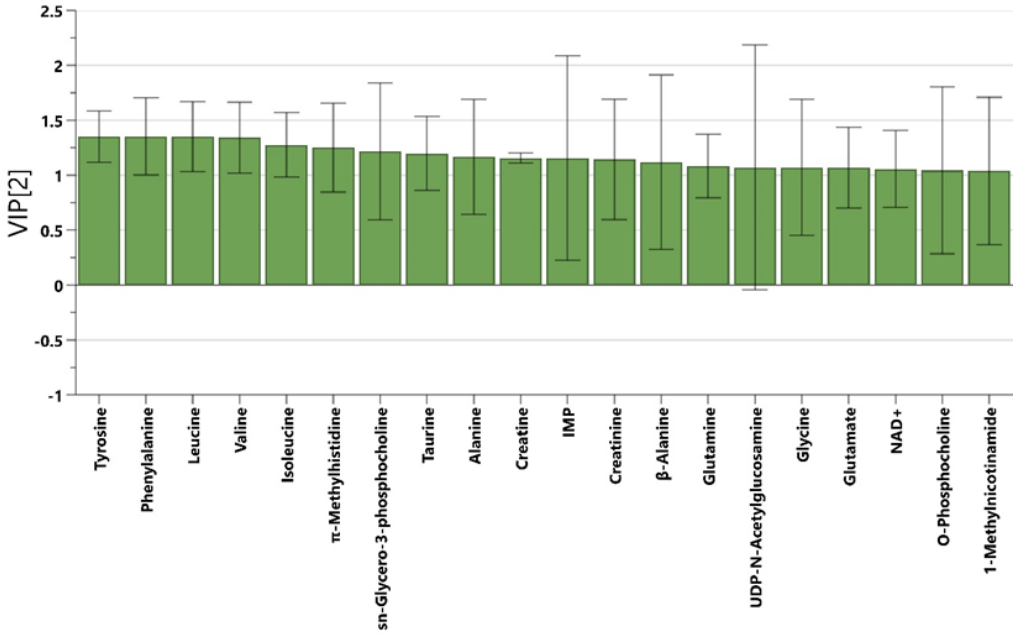

Figure 5. Graphical representation for ^{1}H-NMR relative integral data driven models from HT1080 cells extracts (intercellular) after 12h normoxia (0h) (blue color) and DNC samples after 12h (red color) and 24h (dark red color). (**a**) The Principal Component Analysis (PCA) scores plot. (**b**) The Loadings plots for PCA model (**c**) Prediction plot from the partial least squares-regression model (PLS-R). (**d**) The Variable importance in projection (VIP) score plot for PLS-R model (VIP >1.00).

The most influential intracellular metabolites in DNC with VIP (variable importance in projection) greater than 1.00 revealed 19 metabolites (UDP-N-acetylglucosamine, leucine, tyrosine, valine, isoleucine, IMP, alanine, creatinine, taurine, creatine, phenylalanine, NAD+, π-methylhistidine, β-alanine, glycine, glutamine, sn-glycero-3-phosphocholine, glutamate, AMP) (**Figure** 5d). However, for extracellular revealed 15 metabolites (fumarate, ornithine, alanine, aminoimidazol, acetate, methylmalonate, asparagine, arginine, formate, glycine, histidine, tryptophan, unknown-1, glutamine and phenylalanine) (**Figure** 6d).

(a)

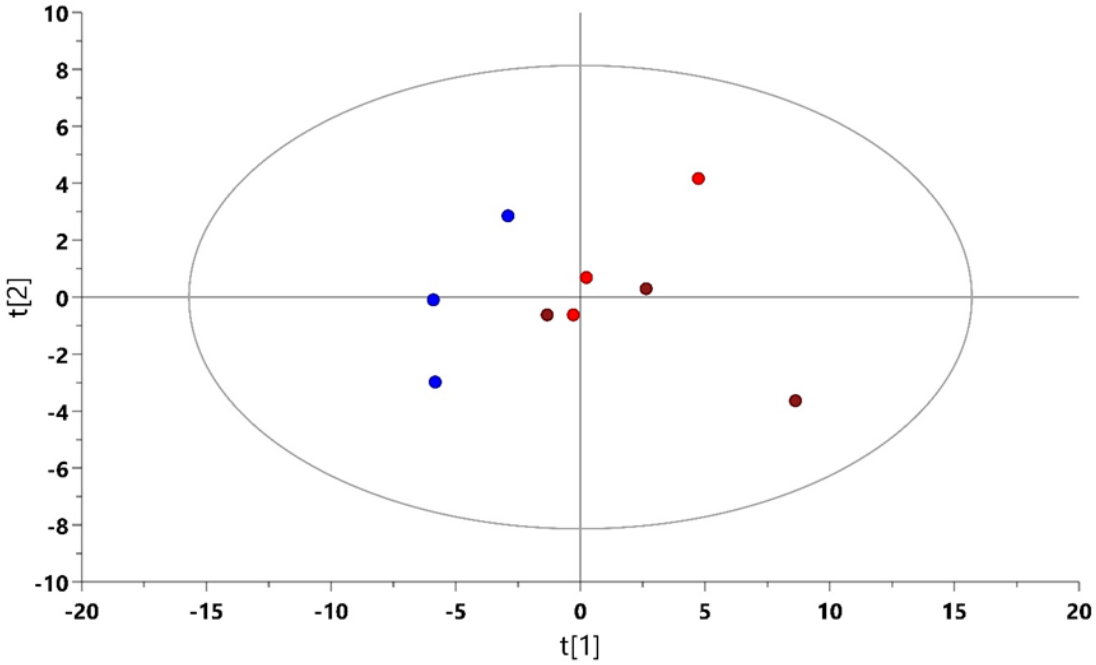
t[2]
t[1]

(b)

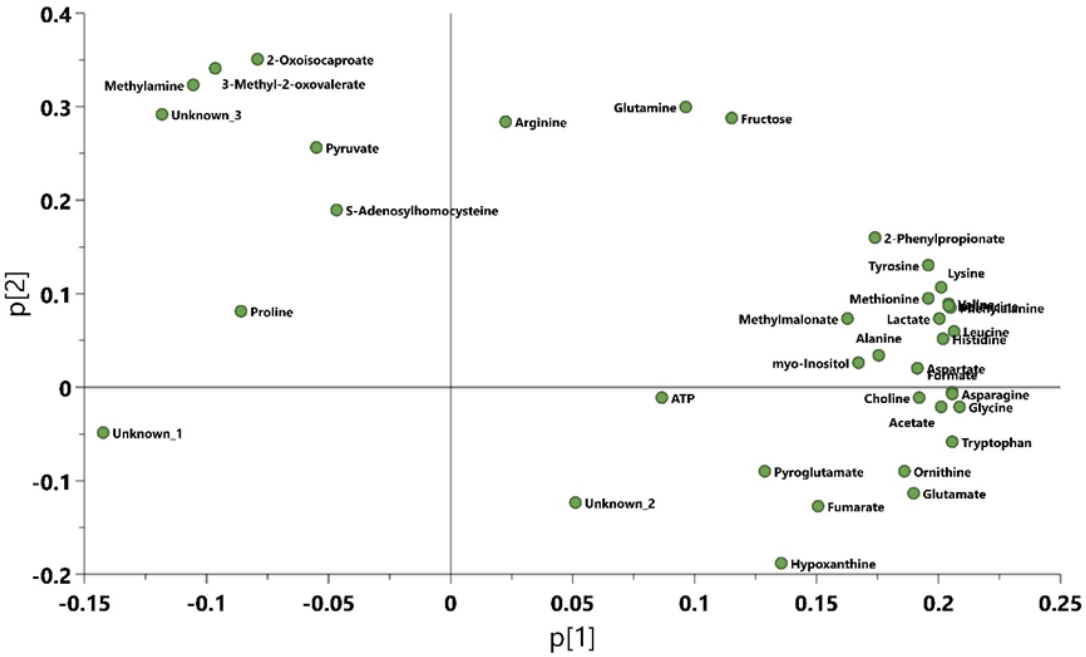
p[2]
p[1]
2-Oxoisocaproate
Methylamine
3-Methyl-2-oxovalerate
Unknown_3
Pyruvate
S-Adenosylhomocysteine
Proline
Unknown_1
Arginine
Glutamine
Fructose
ATP
Unknown_2
Hypoxanthine
2-Phenylpropionate
Tyrosine
Lysine
Methionine
Methylmalonate
Lactate
Leucine
Alanine
Histidine
myo-Inositol
Aspartate
Formate
Choline
Asparagine
Glycine
Acetate
Tryptophan
Pyroglutamate
Ornithine
Glutamate
Fumarate

(c)

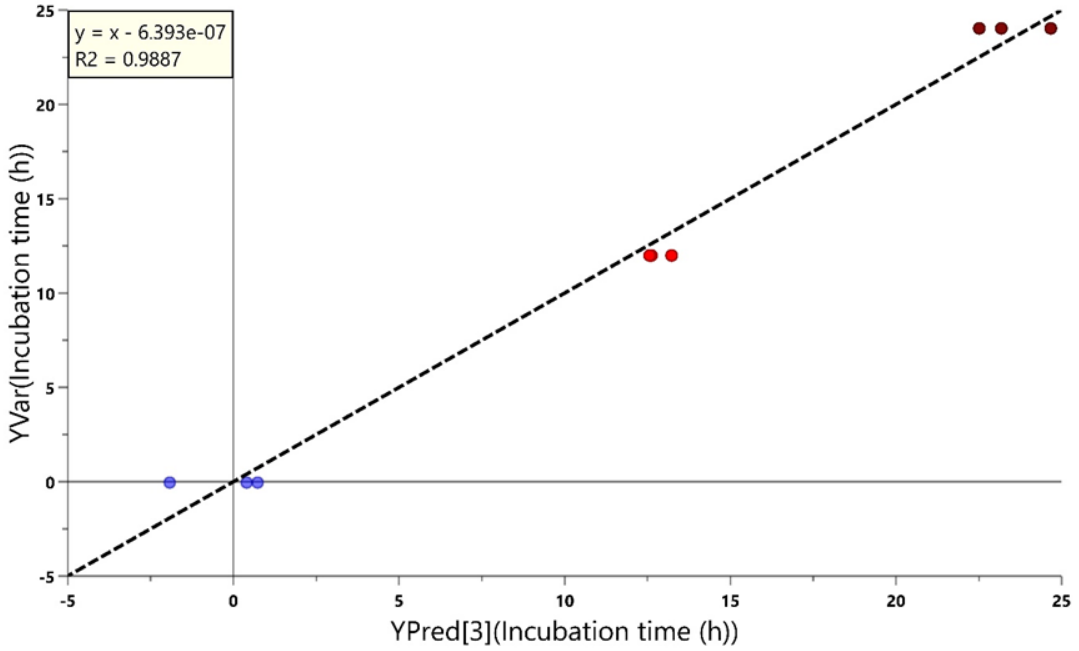

(d)

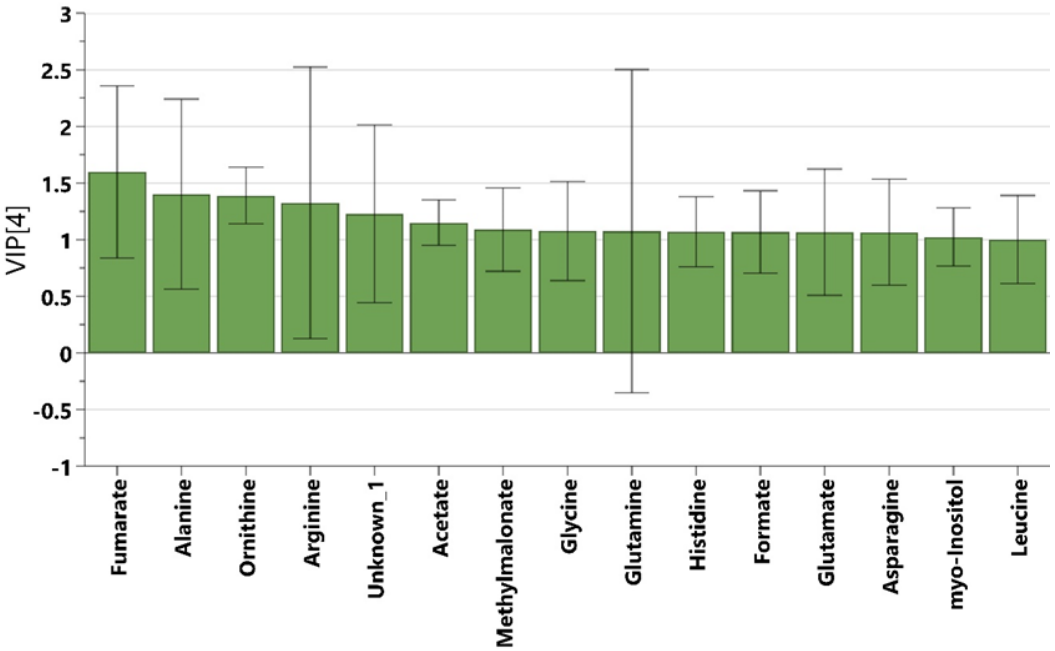

Figure 6. Graphical representation for ^{1}H-NMR relative integral data-driven models from HT1080 post cultured medium (extracellular) after 12h normoxia (0h) (blue color) and DNC samples after 12h (red color) and 24h (dark red color). (**a**) The Principal Component Analysis (PCA) scores plot. (**b**) The Loadings plots for PCA model (**c**) Prediction plot from the partial least squares-regression model (PLS-R). (**d**) The variable importance in projection (VIP) score plot for PLS-R model (VIP >1.00).

In addition, from 19 significant and important intracellular metabolites for DNC with VIP above 1.00, we removed glutamate and O-phosphocholine from further calculation because didn't pass the ANOVA test. The 17 remain significant intracellular metabolites revealed with three DNC states after 12h and 24h compared to normoxic cells after 12h (0h) as follows (**Figure** 7):

1. Gradation of upregulation including tyrosine, phenylalanine, leucine and valine.
2. Slow upregulation-state of glycine and alanine with no significant difference between normoxic cells after 12h (referred as 0h) and reversed normoxic cells after 12h at hypoxia, thereafter, upregulated after 24h.
3. Fast upregulation–state of the reversed normoxic cells after 12h and 24h at hypoxia for the remaining metabolites.

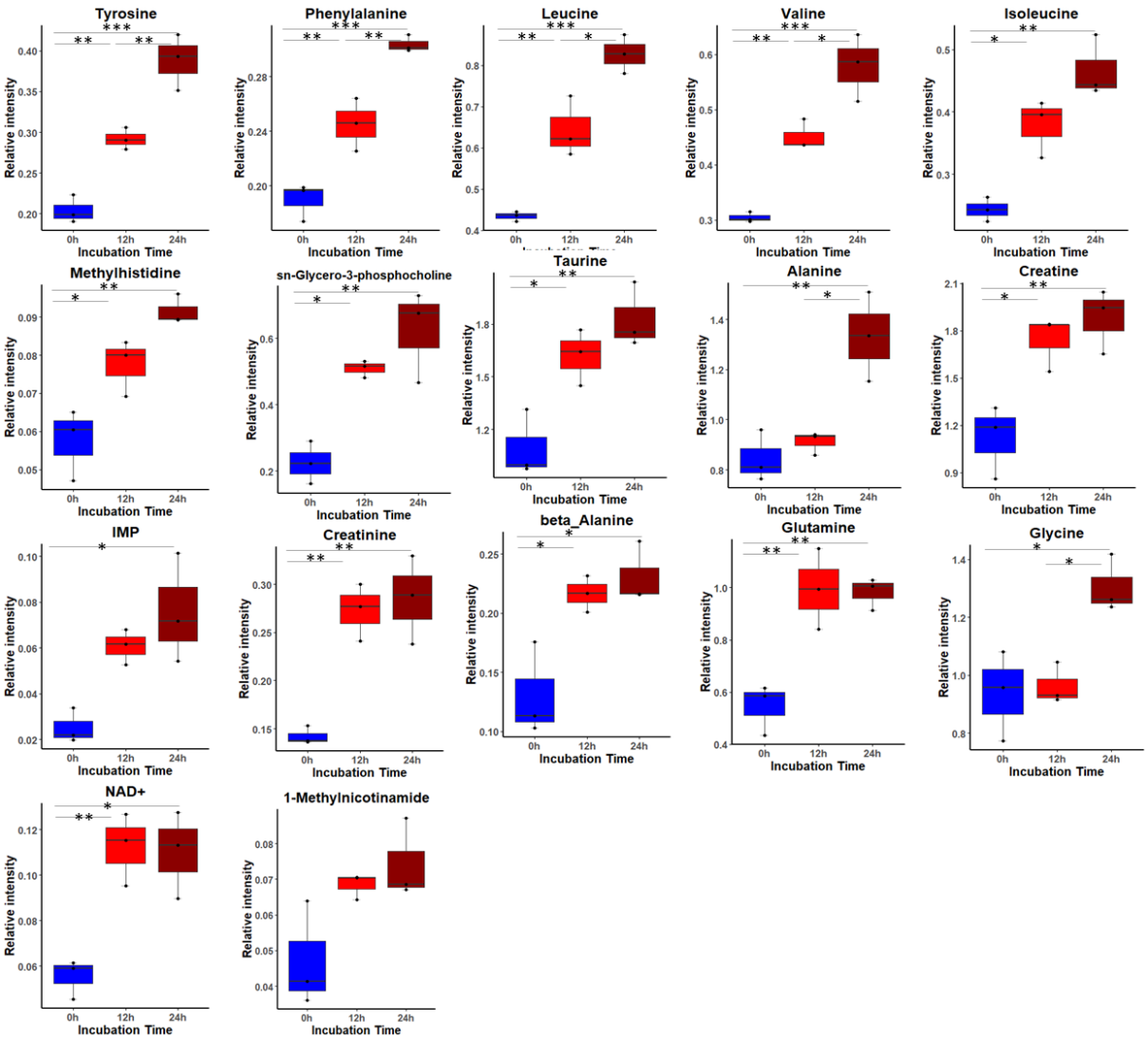

Figure 7. Boxplots for metabolites with VIP score above 1.00 identified by PLS-R model and statistically significant in one-way ANOVA test from cells extract (intracellular) samples after 12h normoxia (0h) and DNC after 12h and 24h. Whiskers—1.5 × interquartile range (IQR); bar—median; box—range between first quartile (Q1) and third quartile (Q3). Black points—data points. *Adjusted *p* value < 0.05.

On the other hand, the combination between the multivariate and univariate analysis for DNC revealed 12 important extracellular metabolites with two main type of regulations (**Figure** 8):

1. Upregulation between normoxic cells 6% after 12h and deoxygenized normoxic cells at hypoxia 1% after 12h and 24h such as fumarate, alanine, ornithine, acetate, methylmalonate, glycine, histidine, formate and asparagine.
2. Surprisingly, unknown_1 showed an abnormal trend, we didn't obtain any significant difference between deoxygenized normoxic cells at hypoxia after 12h and 24h. However, the deoxygenized normoxic cells at hypoxia 1% after 12h and 24h were extremely decreased.

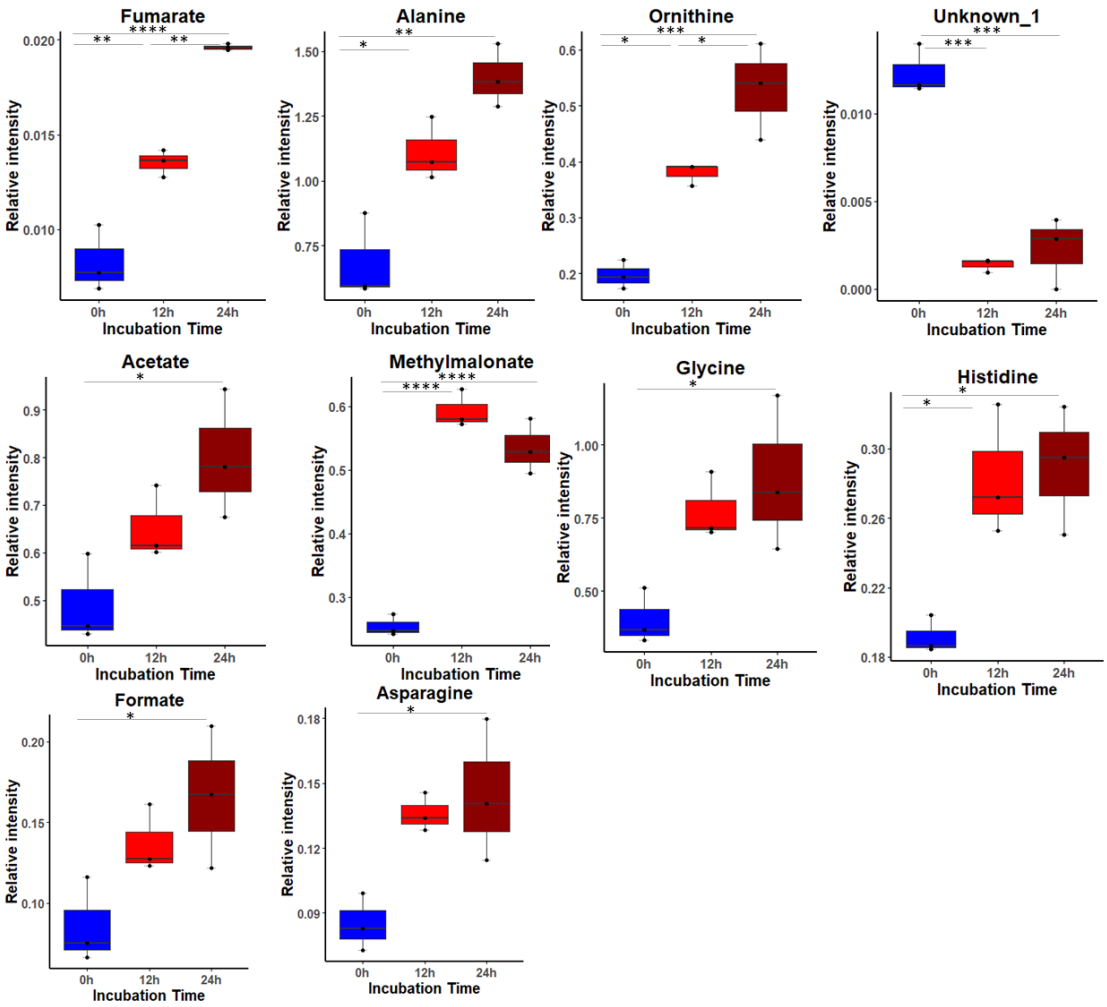

Figure 8. Boxplots for metabolites with VIP score above 1.00 identified by PLS-R model and statistically significant in one-way ANOVA test from post cultured medium extract (extracellular) samples after 12h normoxia (0h) and DNC samples after 12h and 24h. Whiskers—1.5 × interquartile range (IQR); bar—median; box—range between first quartile (Q1) and third quartile (Q3). Black points—data points. *Adjusted *p* value < 0.05.

3.2.2 The metabolic profiling of the hypoxia-reoxygenation (RHC) treatment

This part includes our results from a total of 15 samples from cells extract and 15 samples from post-cultured medium extract at each cultivation time points for hypoxic cells after 12h referred as (0h) and RHCs after 12h and 24h at normoxia.

We conducted a ^{1}H NMR-based metabolomics analysis and 39 metabolites were successfully assigned in cells extraction respectively, and 37 metabolites were successfully assigned from post-cultured medium extraction within 2 unknown metabolites. For exploring the changes of the intracellular and extracellular metabolome, we built a PCA score and loading plots of the ^{1}H NMR dataset and PLS-regression model to predict the total scores in each incubation time points (0h, 12h and 24h). Furthermore, the models were correctly validated and obtained the R^2X (cum), good correlation R^2Y (cum) and goodness of prediction Q^2(cum) scores and CV-ANOVA *p*-values for intracellular cells and extracellular post-culture medium extracts in comparisons between incubation time groups (**Table** 5, 6).

Table 5. The multivariate analysis models summary of cells extract (intracellular) NMR-based metabolome in comparisons between 0h, 12h and 24h at RHC.

O_2 %	Incubation Time Comparison	Model Type	PC/LV	N =	R^2X (cum)	R^2Y (cum)	Q^2 (cum)	CV-ANOVA *p* value
Reverse to normoxia	0h vs 12h vs. 24h	PCA	2	9	0.939	–	–	–
	0h vs 12h vs. 24h	PLS	5	9	0.972	0.996	0.877	7.88×10^{-1}

0h =12h at hypoxia (Reverse to normoxia)

Table 6. The multivariate analysis models summary of post-cultured medium (extracellular) NMR- based metabolome in comparisons between 0h, 12h and 24h at RHC.

O_2 %	Incubation Time Comparison	Model Type	PC/LV	N =	R^2X (cum)	R^2Y (cum)	Q^2 (cum)	CV-ANOVA *p* value
Reverse to normoxia	0h vs 12h vs. 24h	PCA	3	9	0.666	–	–	–
	0h vs 12h vs. 24h	PLS	3	9	0.932	0.997	0.985	$\mathbf{1.74 \times 10^{-2}}$

0h =12h at hypoxia (Reverse to normoxia)

From RHC results, the PCA score of intracellular metabolome revealed a no clustering and poor separation among PC1 and PC2 between hypoxia 1% after 12h and reverse to normoxia 6% after 12h and 24h groups (**Figure** 9a). PCA loading plot was built and showed no contributions of the intracellular metabolites among PC1 and PC2 (**Figure** 9b).

On other hand, the PCA score of extracellular metabolome revealed a slight clustering among PC1 and PC2 between extracellular hypoxic cells after 12h and reoxygenized hypoxic cells at normoxia 6% after 12h and 24h groups (**Figure** 10a). Moreover, the PCA loading plot was built and showed contributions of the extracellular metabolites among PC1 and PC2 (**Figure** 10b).

Furthermore, in order to explore the metabolites correlation between hypoxic cells after 12h and RHCs at normoxia condition after 12h and 24h. We build PLS regression model, and obtained correlation between hypoxic cells and RHCs at normoxia condition groups through incubation time points with $R^2 = 0.9957$ (**Figure** 9c) and $R^2 = 0.9965$ (**Figure** 10c) by using five and three PLS components for both intracellular and extracellular datasets, respectively. Moreover, the RMSECV of the last component of intracellular dataset was equal to 4.51h which is high, thereby, didn't reach statistically significant difference between groups by cross-validated predictive residuals of the PLS-R (CV-ANOVA) (**Table** 5). On the other hand, the RMSECV of the last component of extracellular dataset was 1.70h and pass statistically significant difference between groups by cross-validated predictive residuals of the PLS-R (CV-ANOVA) (**Table** 6).

(**a**)

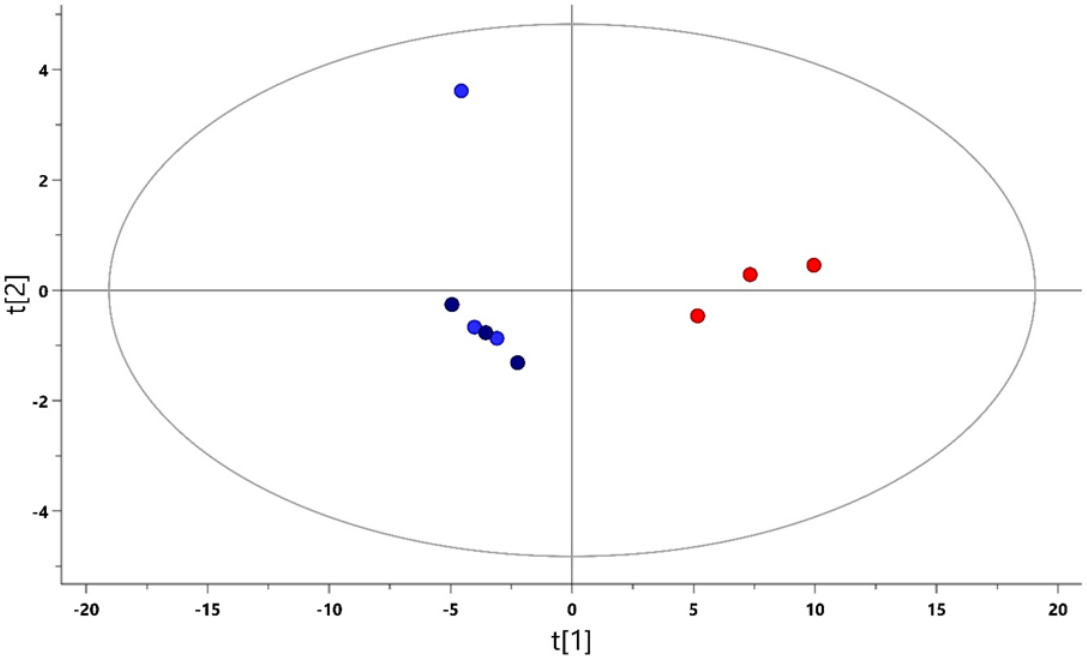
t[2]
t[1]
4
2
0
-2
-4
-20
-15
-10
-5
0
5
10
15
20

(**b**)

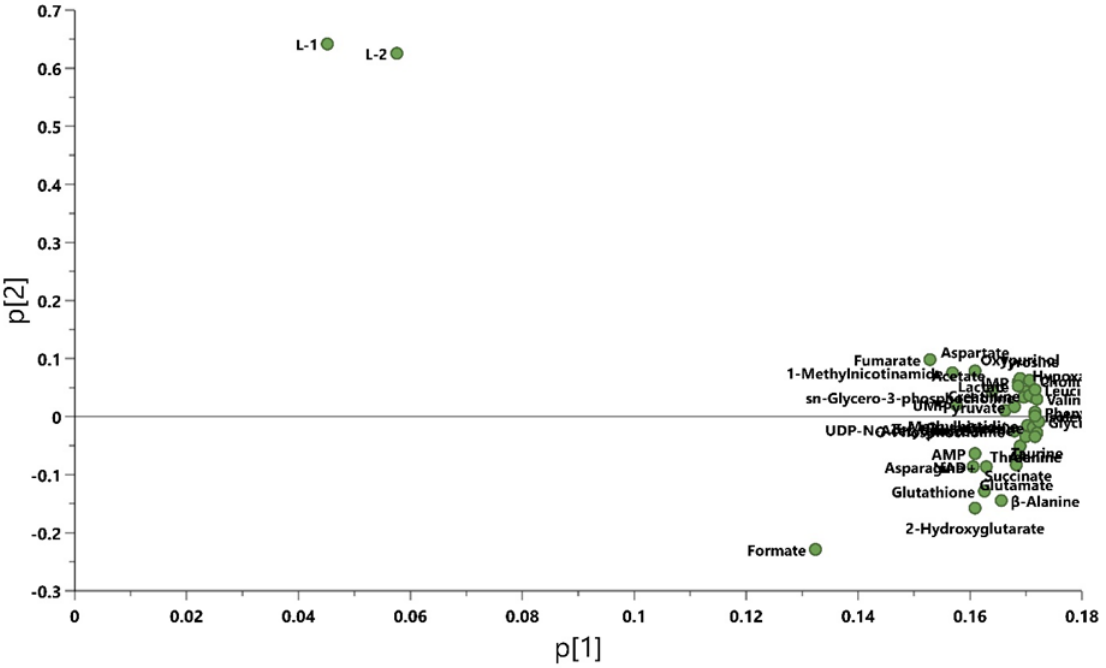
p[2]
p[1]
L-1
L-2
Fumarate
Aspartate
1-Methylnicotinamide
Acetate
AMP
Lactate
sn-Glycero-3-phosphocholine
UMP
Pyruvate
UDP-N-Acetylglucosamine
AMP
Asparagine
NAD+
Succinate
Glutathione
Glutamate
β-Alanine
2-Hydroxyglutarate
Formate
0.7
0.6
0.5
0.4
0.3
0.2
0.1
0
-0.1
-0.2
-0.3
0
0.02
0.04
0.06
0.08
0.1
0.12
0.14
0.16
0.18

(c)

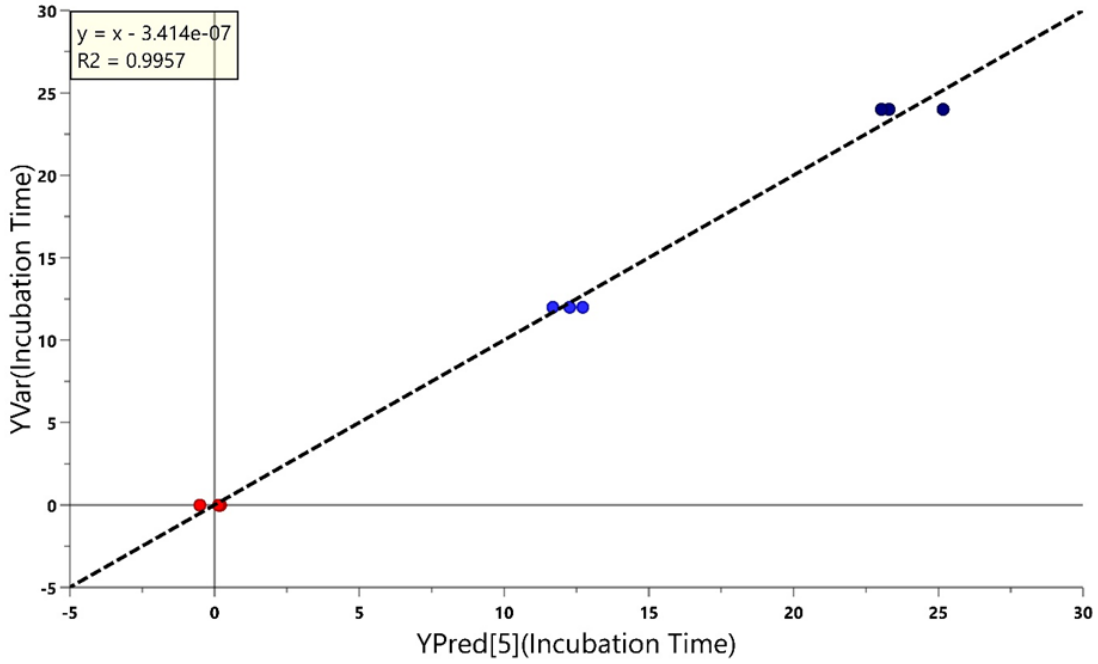

(d)

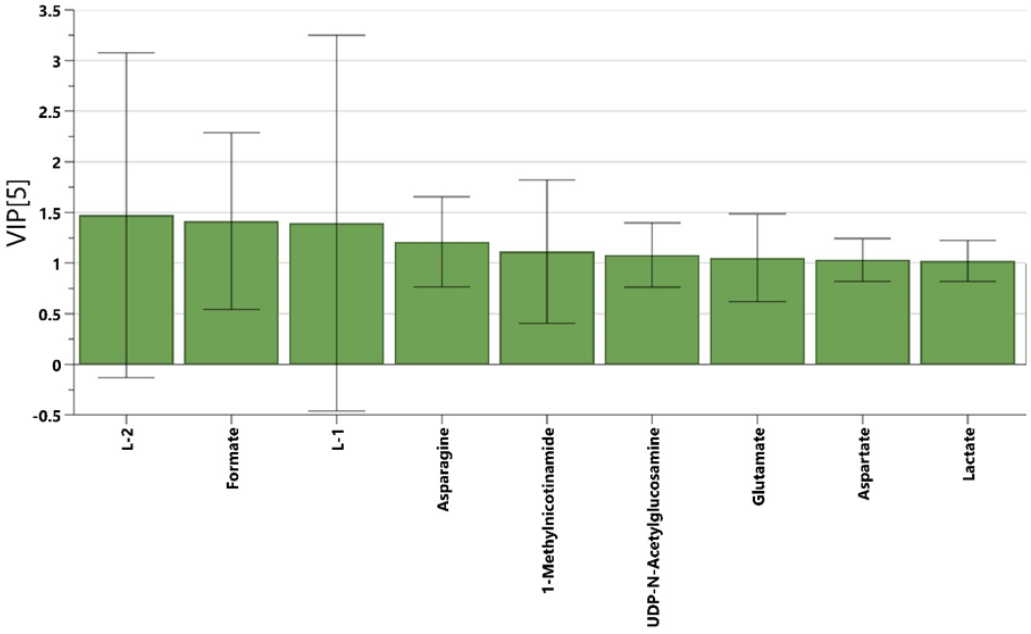

Figure 9. Graphical representation for 1H-NMR relative intensity data driven models from HT1080 cells extracts (intercellular) after 12h hypoxia (0h) (red colors) and RHC samples after 12h (blue colors) and 24h (dark blue colors). (a) The Principal Component Analysis (PCA) scores plot. (b) The Loadings plots for PCA model (c) Prediction plot from the partial least squares-regression model (PLS-R). (d) The Variable importance in projection (VIP) score plot for PLSR model (VIP >1.00).

(a)

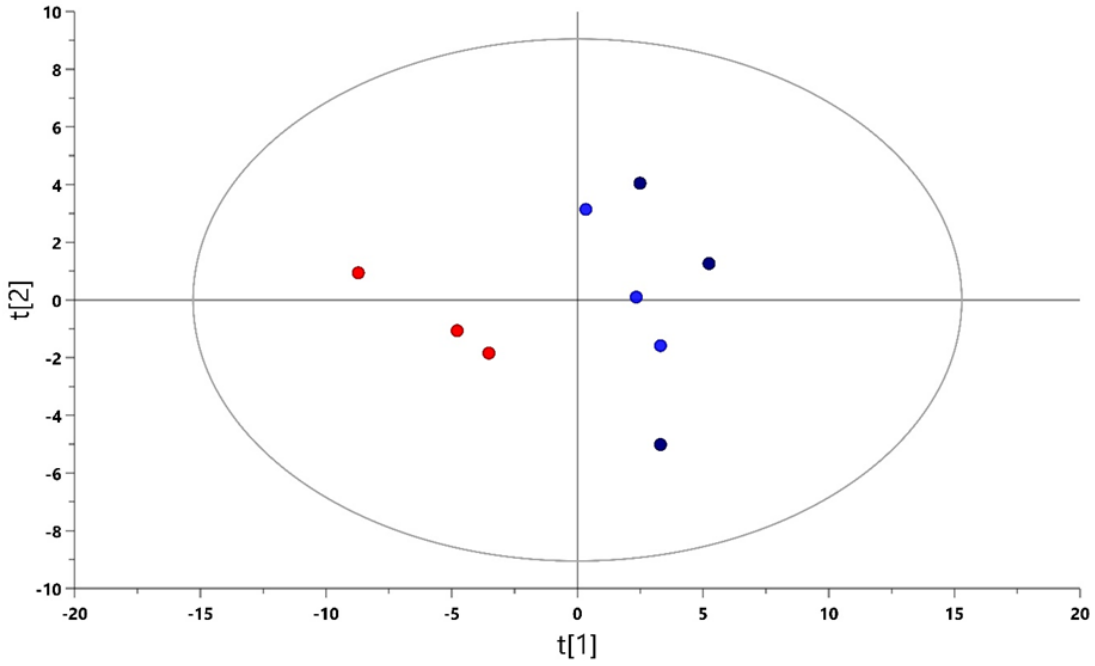
t[2]
t[1]
10
8
6
4
2
0
-2
-4
-6
-8
-10
-20
-15
-10
-5
0
5
10
15
20

(b)

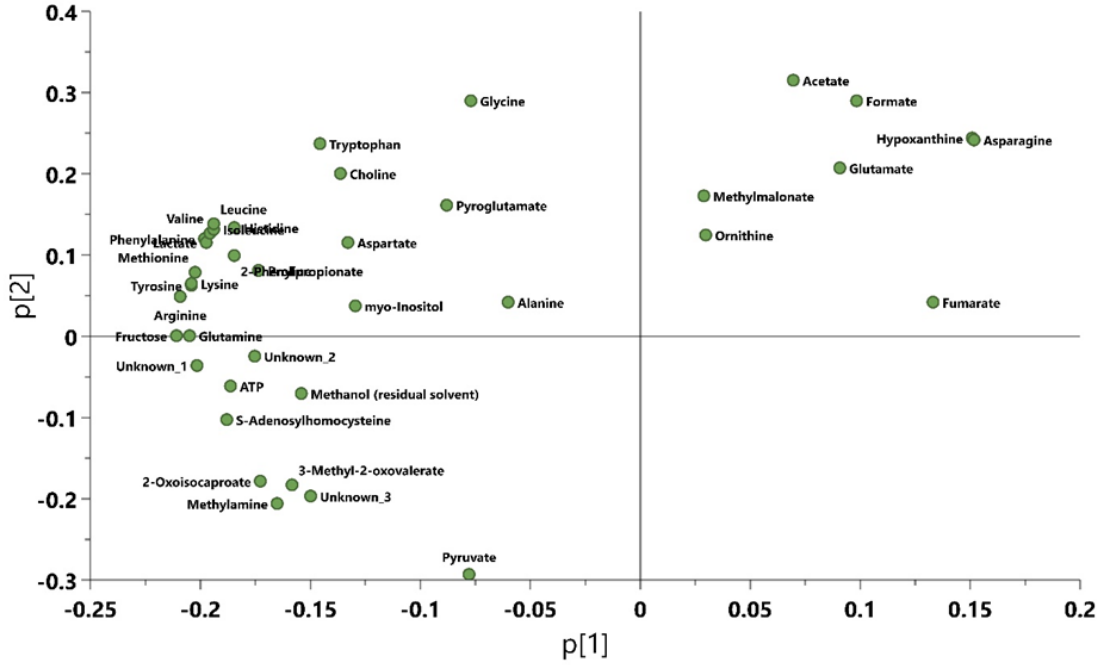
p[2]
p[1]
0.4
0.3
0.2
0.1
0
-0.1
-0.2
-0.3
-0.25
-0.2
-0.15
-0.1
-0.05
0
0.05
0.1
0.15
0.2
Glycine
Tryptophan
Choline
Pyroglutamate
Aspartate
Alanine
myo-Inositol
Valine
Leucine
Methionine
Tyrosine
Lysine
Arginine
Fructose
Glutamine
Unknown_1
Unknown_2
ATP
Methanol (residual solvent)
S-Adenosylhomocysteine
2-Oxoisocaproate
3-Methyl-2-oxovalerate
Methylamine
Unknown_3
Pyruvate
Acetate
Formate
Hypoxanthine
Asparagine
Glutamate
Methylmalonate
Ornithine
Fumarate

(c)

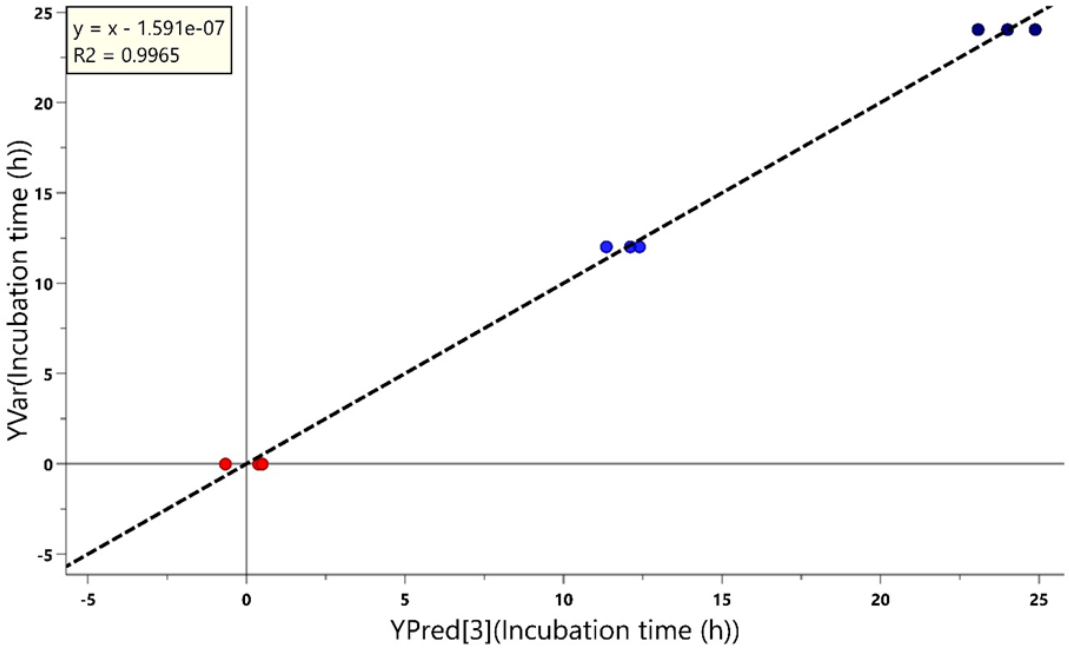

(d)

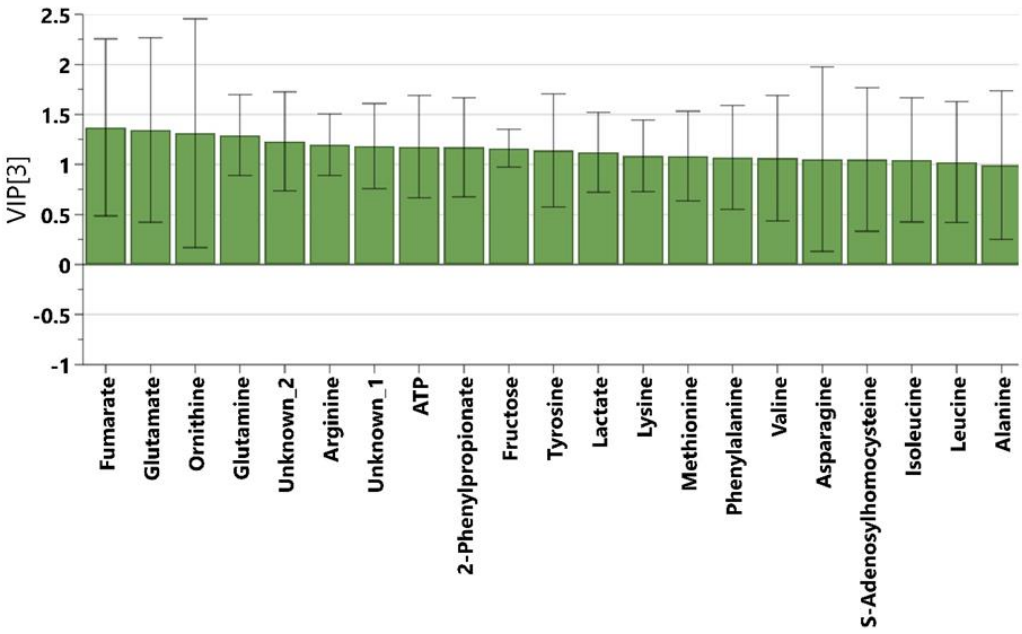

Figure 10. Graphical representation for 1H-NMR relative intensity data driven models from HT1080 post cultured medium (extracellular) after 12h hypoxia (0h) (red color) and RHC samples after 12h (blue colors) and 24h (dark blue colors). (a) The Principal Component Analysis (PCA) scores plot. (b) The Loadings plots for PCA model (c) Prediction plot from the partial least squares-regression model (PLS-R). (d) The Variable importance in projection (VIP) score plot for PLSR model (VIP >1.00).

From MVA analysis, we obtained 9 influential intracellular metabolites with VIP value above 1.00 including L-1, formate, L-2, Asparagine, 1-methylnicotinaamide, UDP-N-Acetylglucosamine, glutamate, aspartate and lactate (**Figure** 9d), thereafter, we tested their significant by on-way ANOVA which revealed only 6 important and significant metabolites (asparagine, 1-methylnicotinaamide, UDP-N-Acetylglucosamine, glutamate, aspartate and lactate) with one major regulation by down-regulation between 12h at hypoxia and RHCs after 12h and 24h (**Figure** 11).

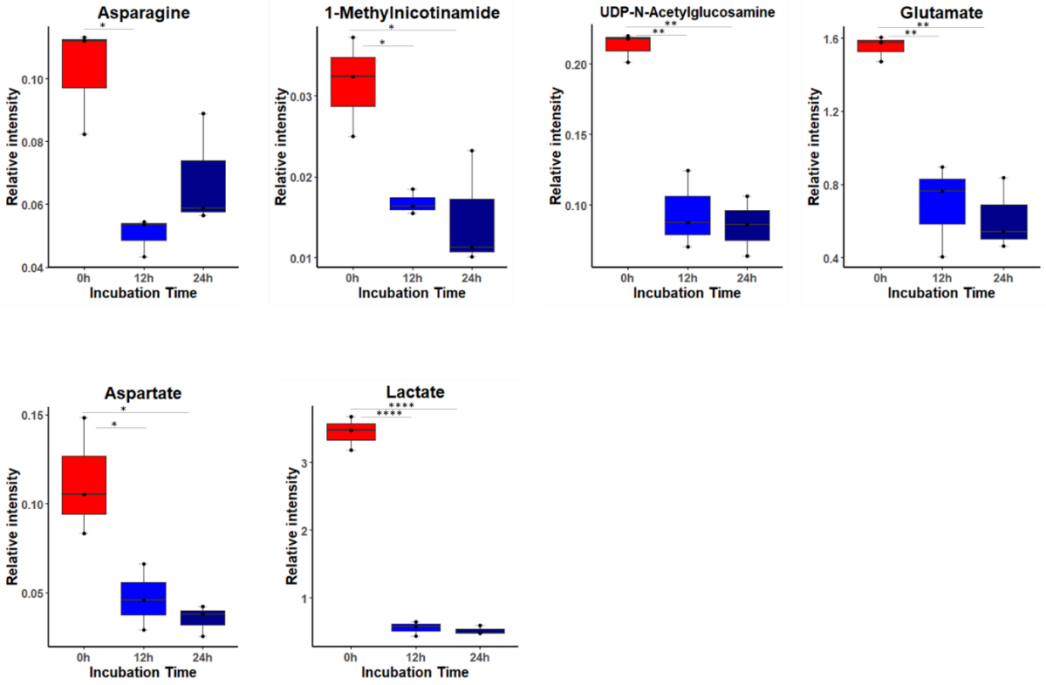

Figure 11. Boxplots for metabolites with VIP score above 1.00 identified by PLS-R model and statistically significant in one-way ANOVA test from cells extract (intracellular) samples after 12h hypoxia (0h) and RHCs samples after 12h and 24h. Whiskers—1.5 × interquartile range (IQR); bar—median; box—range between first quartile (Q1) and third quartile (Q3). Black points—data points. *Adjusted p value < 0.05.

The extracellular hypoxic cells after 12h referred as (0h) and extracellular RHCs after 12h and 24h, the most important extracellular metabolites form VIP (variable importance in projection) score with VIP value above 1.00 of PLS-R model we obtained 20 influential metabolites (fumarate, glutamate, ornithine, glutamine, unknown_2, arginine, unknown_1, ATP, 2-phenylpropionate, fructose, tyrosine, lactate, lysine, methionine, phenylalanine, valine, asparagine, S-Adenosylhomocysteine, isoleucine and leucine) (**Figure** 10d) and then tested their significant by on-way ANOVA test revealed 17 important and significant metabolites, however we exclude the following metabolites such as glutamate, ornithine

and S-Adenosylhomocysteine because their lack of significant by ANOVA. The remaining 17 metabolites showed with two main type of regulations (**Figure** 12):

1. Downregulation of extracellular reversed hypoxic cells at normoxia 6% including glutamate, ornithine, glutamine, unknown_2, arginine, unknown_1, ATP, 2-phenylpropionate, fructose, tyrosine, lactate, lysine, methionine, phenylalanine, valine, S-Adenosylhomocysteine, isoleucine and leucine.
2. Upregulation of the extracellular reversed hypoxic cells at normoxia 6% including fumarate and asparagine.

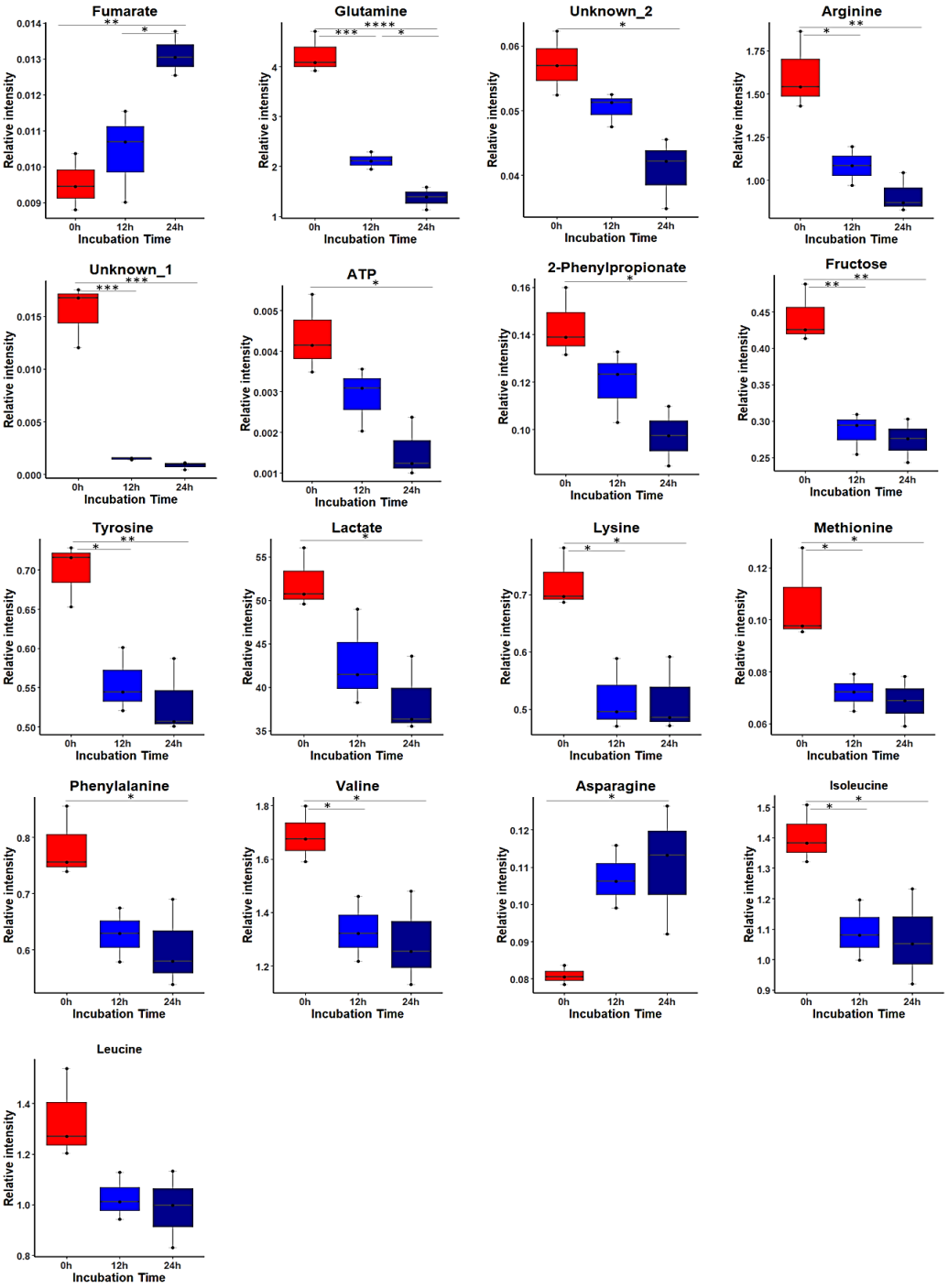

Figure 12. Boxplots for metabolites with VIP score above 1.00 identified by PLS-R model and statistically significant in one-way ANOVA test from post cultured medium extract (extracellular) samples after 12h hypoxia (0h) and RHCs samples after 12h and 24h. Whiskers—1.5 × interquartile range (IQR); bar—median; box—range between first quartile (Q1) and third quartile (Q3). Black points—data points. *Adjusted p value < 0.05.

4. Discussion

The tumor microenvironment involves a complex interplay of oxygen diffusion gradients and nutrient availability that shape the metabolic reprogramming and adaptation of cancer cells. This results in a dynamic cell-metabolite phenotype in response to deoxygenation and reoxygenation processes, as well as rapid cell proliferation and angiogenesis, ultimately driving cancer progression.

4.1.The post normoxia deoxygenation impact on of HT1080 cells metabolome

For the first time in this study, we have investigated by ^{1}H NMR the varieties of intracellular and extracellular metabolic profile of HT1080 cell line during RHC and DNC conditions through a period of interval time points. Our results demonstrate that after 12h and 24h of incubation for DNCs at hypoxia 1% O_2, there was a significant increase of various intracellular and extracellular metabolites compared to normoxic cells. These findings indicate that even short-term oxygen deprivation can have a significant impact on cellular metabolism and the accumulation of metabolites inside and outside of the cells. These observations have important implications for understanding the metabolic changes that occur in response to oxygen deprivation and availability and the potential impact on cellular function and survival.

It has been showed that, the adaptive metabolic responses to hypoxia involved the hypoxia-inducible factors (HIFs) as a bridge between adaptation to low O_2 tension, therefore, regulate metabolic enzymes and glycolysis components, oxidative phosphorylation and redox status [11]. Moreover, HIF-1 arrests mitochondrial oxidative metabolism by reducing oxygen consumption [12]. However, the mechanism and interaction between these metabolites and their accumulation in the intracellular space in relation to oxygen concentration effect are complex and involve multiple metabolic pathways and regulatory mechanisms. It also might be affected by other factors such as the type of cancer or tissue and the presence of other metabolic stresses.

For instance, among most important metabolites were tyrosine and phenylalanine which both play important roles in the function of cells system.

The primary metabolic pathway of phenylalanine is converted to tyrosine, a precursor for the synthesis of a range of biologically significant compounds including the catecholamines (epinephrine, norepinephrine, and dopamine), thyroid hormones, and the pigment melanin. Tyrosine is an integral component of proteins, highlighting its crucial role in cellular metabolism [13] (**Figure** 13).

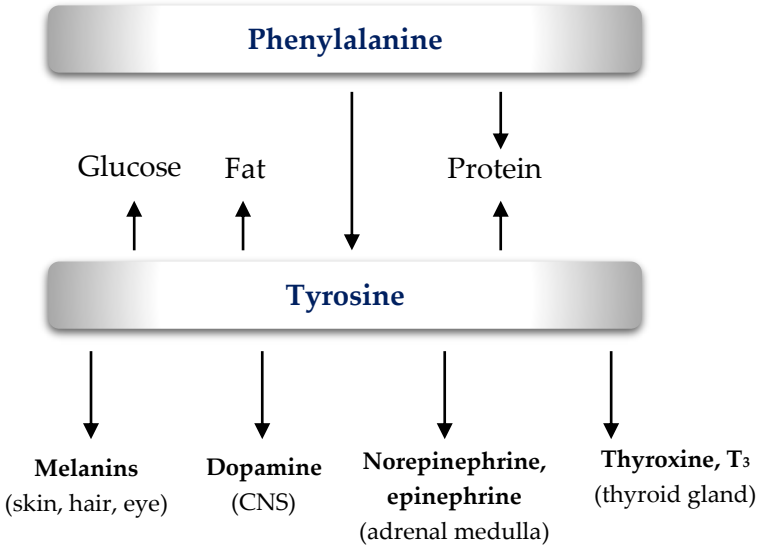

Figure 13. Overview of phenylalanine and tyrosine metabolism

The metabolic degradation of phenylalanine is primarily accomplished through its conversion to tyrosine via phenylalanine hydroxylation at the para position. This irreversible reaction is facilitated by the coenzyme biopterin, specifically in its active form of tetrahydrobiopterin (H4-biopterin), which undergoes oxidation to dihydrobiopterin (H2-biopterin) during the reaction. This reduction is then replenished by NADPH-dependent dihydrobiopterin reductase. Phenylalanine hydroxylation occurs in the liver and involves the incorporation of molecular oxygen (O_2) into the para position of phenylalanine and its reduction to water [14]. Moreover, it has been demonstrated that, the metabolism of aromatic amino acids (tyrosine and phenylalanine) may be impaired in cases of gastroesophageal cancer [15], and any changes in phenylalanine hydroxylase activity have been observed in instances of inflammation or malignancy [16,17]. This highlights that the tyrosine and phenylalanine, as well as tryptophan are elevated in both gastric content

and tissues of individuals diagnosed with gastroesophageal cancer. Elevated levels of tyrosine and phenylalanine were also noted in the urine of these patients. Conversely, the majority of studies examining serum (or plasma) concentrations indicate that these amino acids are reduced in the serum (or plasma) of individuals with gastroesophageal cancer [16,17], however is very difficult to compare the changes occurring in the cell colony with complex organism machinery. Recent research has suggested that the increased concentrations of aromatic amino acids in gastric content may be due to various mechanisms. One possibility involves the increased production of enzymes by invasive cancer cells [18]. These enzymes are able to degrade the basement membrane and extracellular matrix, with certain matrix metalloproteinase enzymes being upregulated in aggressive cancer cells [19]. As a result, these aromatic amino acids may be released into the gastric content, leading to their increased concentrations [20]. Additionally, increased protein synthesis within rapidly growing malignant tissues may also lead to their release into the gastric content [21]. Here we have found that, increased levels of intracellular tyrosine and phenylalanine after DNCs at hypoxia 1%. This finding is supported by previous studies that have shown several mechanisms including reduced their degradation by inhibiting the activity of phenylalanine hydroxylase and tyrosine hydroxylase enzymes, resulting in higher levels of these amino acids [21,22], besides, increasing expression and activity of amino acid transporters, such as LAT1 and ASCT2, can increase the uptake of these amino acids into cancer cells [23]. Our findings suggest that under hypoxic conditions, activation of genes associated with the inhibition of degradation and increased uptake of phenylalanine and tyrosine can lead to elevated levels of these amino acids in cancer cells under hypoxic conditions. However, our understanding of the role of tyrosine in cancer biology remains limited [24].

Under hypoxic conditions, several interrelated mechanisms contribute to the increased levels of branched-chain amino acids (BCAAs) such as leucine, isoleucine, and valine in cancer cells. Here, we have found increase the level of intracellular BCAAs of DNCs. Observed by others that, under hypoxia, the expression and activity of transporters, such as the system L amino acid transporter 1 (LAT1), are upregulated, leading to elevated levels of branched-chain amino acids (BCAAs) in cancer cells [25]. These transporters play a crucial role in the uptake of BCAAs into the cells and their increased activity in a hypoxic environment drives

higher BCAA levels, thereby fostering tumor growth and progression for example in human glioblastoma (GBM) cell lines and primary GBM cells [25]. Moreover, the decreased activity of enzymes involved in the degradation of branched-chain amino acids (BCAAs) can result in elevated levels of these amino acids in cancer cells under hypoxic conditions. This reduction of BCAA catabolism has been observed in several types of human cancers [26,27], including hepatocellular carcinoma [27], breast cancer [28], leukemia [29], early pancreatic ductal adenocarcinoma [30], and clear renal cell carcinoma [31]. Other studies suggest that BCAA accumulation in cancer cells is driven by the decreased activity of enzymes such as branched-chain alpha-ketoacid dehydrogenase and an increase in reamination of BCAAs through the enzyme BCAT1 [32]. The molecular mechanistic of elevated BCAA levels have been linked to the activation of rapamycin complex 1 (mTORC1) pathway [33], which regulates cellular processes such as autophagy, lipid synthesis, nucleotide synthesis, and protein synthesis, providing a potential target for therapeutic intervention [34]. Our findings suggested that the combination of these mechanisms can result in increased levels of BCAAs, particularly leucine, isoleucine, and valine, in cancer cells under hypoxic conditions compared to post-normoxic cells, which can provide important insights into the biology of cancer and potential therapeutic targets for the treatment.

Another pathways that involved on DNCs regulations were glutamate metabolism as well as nitrogen metabolism. The metabolic differences between cancer cells and normal cells have been well-documented for nearly a century [35]. In addition to their reliance on elevated rates of aerobic glycolysis, thereby, cancer cells are characterized by a disrupted uptake and utilization of amino acids [36]. Among the primary metabolites required to support tumor proliferation is glutamine, a non-essential amino acid, which holds a prominent position [37]. Its significance lies not only in its ability to provide nitrogen and carbon atoms for various pathways that promote growth [38], but also in its crucial role in chromatin modification, cell signaling regulation, and anti-oxidative defense [39]. Moreover, glutamine can be synthesized from glutamate *de novo* and can become a conditionally essential nutrient during times of stress or excessive growth [37, 39]. However, in the core of solid tumors, where a heterogeneous microenvironment and deficient vasculature are commonly observed, excessive glutamine consumption can deplete local supplies.

As glutamine deprivation may coexist with other microenvironmental abnormalities, such as hypoxia, the adaptive mechanisms in response may be more complex [37,40–43]. Here we have found that, the intracellular glutamine and glutamate have been upregulated in comparisons between DNCs and normoxic cells. Observed by others that, an increase in glutamine consumption when A549 cells were cultured under low oxygen levels (1%) [44]. This was evidenced by the unchanged secretion of glutamate, indicating that the net consumption of glutamine was elevated and potentially being utilized for biosynthesis [44]. Moreover, the incorporation of glutamine-derived carbon into lipids was observed in proliferating cells under both normoxic and hypoxic conditions, whereas glutamine can contribute carbon to the biosynthesis of Acetyl coenzyme A (Ac-CoA) through two mechanisms. The first involves the oxidative metabolism of glutamine-derived α-ketoglutarate (αKG) in the tricarboxylic acid cycle, leading to the generation of pyruvate from malate by glutaminolysis [43]. The second pathway involves the reductive carboxylation of αKG to produce citrate [45,46]. As recent studies have indicated that the isocitrate dehydrogenase-1 (IDH1) reaction is highly reversible [47–49]. Therefore, literature examples indicated by using stable isotopic tracers that, the net flux of reductive glutamine significantly increased in reductive carboxylation activity under hypoxia in cell culture to palmitate synthesis in A549 cells growing under hypoxic conditions. Approximately 80% of the carbon utilized for *de novo* lipogenesis was derived from the reductive carboxylation of glutamine-derived αKG [44]. Moreover, an increase activity of glutamine transporters such as SLC1A5 and SLC38A2 can meet the demand of this transition to glutamine [50]. Hence, this phenomena might be explained that, the transition conditions from normoxia to hypoxia leads to increase the uptake of glutamine due to the elevated levels of glutamine transporters and redirects glutamine from the oxidative pathway towards the reductive carboxylation pathway, which is crucial given the reduced the entry of pyruvate into the tricarboxylic acid (TCA) cycle and increased lactate secretion in hypoxia, therefore, this metabolic adjustment enables cells to continuously produce TCA metabolites, like α-ketoglutarate (αKG) and citrate, which are then converted to cytosolic acetyl-CoA for lipid synthesis.

Nicotinamide adenine dinucleotide (NAD) synthesis in mammalian cells occurs through three pathways, namely *de novo* pathway (Kynurenine pathway), Preiss-Handler, and salvage pathways [51]. The key enzymes that regulate the salvage

pathway and control intracellular NAD levels are nicotinamide phosphoribosyltransferase (Nampt) and nicotinamide mononucleotide adenylyltransferase (Nmnat) [51]. Nampt converts NAM and PRPP to nicotinamide mononucleotide (NMN), and Nmnat generates NAD by adenylylating NMN from ATP [52]. Additionally, Nampt is primarily found in the cytoplasm, and its suppression can impede glycolysis [53]. The Preiss-Handler pathway involves nicotinate phosphoribosyltransferase (Naprt) generating NAMN from nicotinic acid and PRPP, followed by Nmnat conjugating ATP to NAMN [54]. The *de novo* pathway uses tryptophan as the source for NAD synthesis and is mediated by tryptophan 2,3-dioxygenase or indoleamine 2,3-dioxygenase. The degradation of NAD is coupled with NAM recycle through enzymes such as poly ADP-ribose polymerase (PARP), sirtuins, CD38, and CD157 [55,56]. Nmnat isozymes Nmnat1-3 have different subcellular localizations and tissue distributions, with Nmnat1 primarily in the nucleus, Nmnat2 in the Golgi apparatus, and Nmnat3 in mitochondria. Overexpression of Nmnat3 has been shown to increase mitochondrial NAD levels and enhance energy metabolism [57,58]. Herein, we have found that, NAD has been increased in the DNCs after 12h and 24h at hypoxia condition compered to normoxic cells.

Our findings that NAD levels increase in DNCs under hypoxic conditions are consistent with previous studies indicating that, the coenzyme nicotinamide adenine dinucleotide (NAD) plays a key role in redox reactions across multiple metabolic pathways, such as glycolysis, the tricarboxylic acid (TCA) cycle, oxidative phosphorylation, and serine biosynthesis. The sustained replenishment of NAD is essential for the proliferation and survival of rapidly growth of cancer cells. This is due to the fact that elevated NAD levels increase glycolysis through glyceraldehyde 3-phosphate dehydrogenase (GAPDH) and lactate dehydrogenase (LDH), which require NAD as a cofactor at hypoxia [51,53,57]. Therefore, Therefore, our findings support the notion that NAD plays a crucial role in cancer cell metabolism and survival, particularly under hypoxic conditions. Further research is needed to fully understand the mechanisms underlying the effects of NAD on cancer cell metabolism.

Alanine is an amino acid primarily synthesized in the mitochondrial matrix via the conversion of pyruvate [59]. The competition for pyruvate between alanine aminotransferase (ALAT) and pyruvate dehydrogenase (PDH), which converts

pyruvate to acetyl-CoA, suggests that lower PDH activity in conditions such as hypoxia may result in increased alanine synthesis [60]. That's revealed from our results that showed an increase in the level of intracellular in the DNCs compered to normoxic cells after 12h and 24h of incubation. Likewise, was with extracellular alanine. This finding is in line with recent evidence suggesting that amino acid synthesis, including alanine synthesis, is regulated by a complex interplay between demand for α-ketoglutarate and pyruvate uptake in the microenvironment [61]. The fate of the alanine produced under these conditions is not clear, but it is likely to be excreted into the extracellular space and potentially taken up by stromal cells [60]. However, this system demonstrates a reversal from the previously described process in pancreatic ductal adenocarcinoma (PDAC), where stromal cells secrete alanine that is taken up by cancer cells as a significant carbon source [62]. Therefore, this indication not only increases oxygen consumption in hypoxic tumors, but also spares glucose for other cell types or for the synthesis of macromolecular substrates, including serine and glycine [60]. This finding highlights the importance of alanine metabolism in cancer cells and suggests that it plays a critical role in maintaining the energy balance required for cancer cell proliferation and survival under hypoxic conditions. However, further research is needed to fully understand the underlying mechanisms.

β-Alanine is a non-proteogenic amino acid formed in the body from the degradation of carnosine, anserine, balenine, and dihydrouracil and work as intracellular buffer which has been suggested to possess multiple anti-tumor properties [63]. It is also the precursor of the carnosine dipeptide, which acts as an intracellular buffer [64]. Here we have found an upregulation of intracellular β-Alanine on the DNCs after 12h and 24h. It has been showed that, carnosine, a dipeptide composed of β-alanine and histidine, has been shown to have beneficial effects in inhibiting cancer cell proliferation. Numerous studies have reported that carnosine accumulation can significantly inhibit tumor cell growth and proliferation [65,66]. Additionally, it has been demonstrated that carnosine's accumulation can significantly inhibit glycolysis and energy production and the its anti-cancer effects in human cervical tumor cells [67], and its ability to decrease ATP production in glioma cells [68]. Hence, the observed upregulation of β-Alanine in DNCs under hypoxic conditions may be a favorable response to counteract cancer cell proliferation

and glycolysis, as indicated by the increased growth rate of DNCs. However, the exact mechanisms behind these effects are still unclear and appear to vary based on the type of tissue. Our results emphasize the importance of conducting additional research to better understand the mechanism.

With regard to taurine, it's worth to noticed about the taurine mechanism in cancer cells. The efficacy of taurine was rigorously evaluated using an ATP assay, which revealed a significant reduction in the OGD-induced upregulation of endoplasmic reticulum stress markers and pro-apoptotic proteins. This findings demonstrate the capacity of taurine to mitigate cellular damage and promote cellular survival in the face of hypoxia or oxygen/glucose deprivation on human neuroblastoma cell culture and colorectal cancer (CRC) [69]. Conversely, observed by others on human colon cancer cells showed a significant evidence of taurine antiproliferative effect, as well as its potent induction of apoptosis. Moreover, the molecular investigations revealed that taurine exerts its antiproliferative effect via two distinct pathways: (i) stimulation of increased PUMA expression and (ii) regulation of pro- and anti-apoptotic gene expression. Specifically, a significant upregulation of the pro-apoptotic gene *Bax* and a corresponding downregulation of the anti-apoptotic gene *Bcl-2*, resulting in elevated caspase-3/9 activity. These results provide a compelling argument for taurine as a potential therapeutic target in the fight against colon cancer [70]. Likewise, we have found the level of taurine was elevated after DNCs at hypoxia 1%. This controversy might be due the type of tumors and organism.

What's more, the cholinic phenotype, characterized by elevated phosphocholine (PCho) and total choline-containing compounds (tCho), was first discovered through magnetic resonance spectroscopy studies of tumors in the 1980s [71,72]. Initially, the elevated PCho levels in cancer cells were believed to be a result of rapid cell proliferation [73]. However, subsequent studies showed that even rapidly proliferating non-malignant breast and prostate epithelial cells still had significantly lower PCho and tCho levels, indicating that malignant transformation, is not just cell proliferation, but the cause of abnormal choline metabolism in cancers [74]. Observed by us that, an increase of sn-glycero-3-phosphocholine after 12h and 24h incubation of DNCs compered to normoxic cells. This finding is consistent with previous studies that, the abnormal physiological conditions including hypoxia and acidic extracellular

pH affect choline levels [75]. For instance, acidic extracellular pH significantly increases glycerophosphocholine (GPC) levels and decreases PCho levels with perfused mammalian cells [76]. Moreover, hypoxia was found to increase total choline-containing compounds (tCho) and phosphocholine (PCho) in a human prostate cancer model, with a correlation observed between high tCho and hypoxia due to regulation of choline kinase-α (CHKα) expression by HIF1 [77]. Additionally, conditioned growth medium from cancer cells was shown to increase PCho levels in human vascular endothelial cells, indicating that cancer cells can impact the stromal cells in the tumour environment [78]. Another mechanism should be mentioned here is the choline uptake process and the role of choline transport system. It has been showed that abnormal choline metabolism in multiple cancers have been linked to changes in various enzymes, including choline kinase-α, ethanolamine kinase-α, phosphatidylcholine-specific phospholipase C and -D, glycerophosphocholine phosphodiesterases, and activity of choline transporters, such as choline transporter-like protein 1 (CTL1) [79–82]. Additionally, high expression of the choline transporter, CTL1, has been observed in several cancer cell lines. The detection of increased tCho levels through ^{1}H magnetic resonance spectroscopy is being explored as a diagnostic marker for various cancers [80,83]. Taken together, the upregulation of sn-glycero-3-phosphocholine in DNCs under hypoxic conditions may indicate altered choline metabolism that could be relevant for cancer diagnosis and treatment.

Another significant intercellular metabolite was creatine. Creatine metabolism has a link between creatine metabolism and the process of metastatic dissemination, where it is believed that creatine kinase provides the energy necessary for the migration of cancer cells [84]. Creatine is synthesized in the kidneys and liver through a two-step process involving l-arginine: glycine amidinotransferase and N-guanidinoacetate methyltransferase. The first enzyme, l-arginine: glycine amidinotransferase, is predominantly expressed in the kidney and pancreas which catalyzes the transamidation of arginine to glycine. The second enzyme, N-guanidinoacetate methyltransferase, is predominantly expressed in the liver which methylates the resulting guanidinoacetic acid to yield creatine. Creatine then enters the blood circulation and reaches various tissues that require it including muscle, brain, and heart as well as others organ [85–87]. Cancer cells have been found to utilize creatine to sustain their energy metabolism, enabling their survival through exploit

phosphocreatine to ensure their survival in the liver microenvironment on colorectal cancer cells [88]. Herein, we showed that, HT1080 cell line increase the level of intracellular creatine after 12h and 24h of DNCs at hypoxia compered to normoxic cells. Our observation is consistent with other studies implicating SLC6A8 activity and showed that, the upregulation of intracellular creatine levels in hypoxic TNBC cells in vitro is caused by the transcriptional activation of the SLC6A8 gene by p65/NF-κB. Under hypoxic conditions, the activation of p65/NF-κB leads to an increase in the expression of SLC6A8, which results in an accumulation of creatine. The increased levels of creatine support cell survival and inhibit apoptosis by maintaining redox homeostasis and enhancing cellular antioxidant defenses. Intracellular creatine reduces mitochondrial activity and oxygen consumption, thereby decreasing the accumulation of reactive oxygen species and activating the AKT-ERK signaling pathway, which protects the viability of hypoxic triple negative breast cancer (TNBC) cells. Thereby, this activation protected the viability of hypoxic TNBC cells through upregulating Ki-67 and Bcl-2 and downregulating Bax and cleaved Caspase-3 [89]. Additionally, *in vivo* studies have investigated the presence of creatine-related metabolites in the serum and urine of cancer patients, with the findings suggesting that elevated levels of creatine in most cancer types are correlated with accelerated cancer progression [90]. In hepatocellular carcinoma patients, the higher levels of creatine and creatinine in urine have been found linked to advanced stages of the disease [91,92]. Women with higher levels of these substances in fasting plasma have an increased risk of breast cancer [93]. Moreover, magnetic resonance studies have also demonstrated that higher levels of creatine within no non-enhancing tumors correspond with subsequent growth in glioblastoma [94]. What's more, elevated levels of serum creatine and creatinine in patients with invasive vulvar cancer have been linked to both poor disease-specific and overall survival in a retrospective cohort study. Moreover, a comparison of human pancreatic ductal adenocarcinoma and benign adjacent tissue found that tumor tissue had higher phosphorylation levels of creatine [95]. However, the relationship between creatine levels and cancer progression is not clear cut, as in some cases, higher levels of creatine have been associated with suppressed cancer cell growth, while in others, the levels have gradually decreased with malignancy progression [96]. Therefore, our finding on the HT1080 cell line are consistent with both *in vitro* and *in vivo* studies

from our finding showing that under hypoxia increases intracellular creatine levels enabling their survival and inhibiting apoptosis through SLC6A8 upregulation and AKT-ERK signaling pathway activation.

Likewise as creatine was noticed an increase of intracellular creatinine level DNCs compared to normoxic cells. Demonstrated by others that, the *in vitro* treatment of prostate cancer cells with cyclocreatine, a creatine analog, resulted in a significant decrease in intracellular levels of creatine, phosphocreatine, and creatinine and a suppression of cellular proliferation [97]. Others suggested that serum creatinine levels might be an important biomarker of cancer cachexia-associated muscle wasting [98]. Therefore, both in vitro and in vivo studies have shown that creatinine, a metabolite closely related to creatine, may also play a role in cancer progression. This further highlights the potential significance of creatine-related metabolites in cancer progression and the need for further investigation.

The growth and proliferation of cancer cells necessitates depend on the availability of ample amounts of serine and glycine, two non-essential amino acids, through either intracellular synthesis or uptake from the environment as diet. While most non-transformed cells in the body have lower demands for these amino acids, certain cancer subtypes have been found to hyperactivate the anabolic serine and glycine synthesis and become dependent on *de novo* production [99]. It well established that, glycine is synthesized from glucose through the serine synthesis pathway, which diverts the glycolytic intermediate 3-phosphoglycerate (3PG) into serine and then converts it to glycine. The initial step in this process is the oxidation of 3PG to 3-phosphohydroxypyruvate (pPYR) by the enzyme PHGDH [100]. pPYR is then transaminated by phosphoserine aminotransferase (PSAT) using glutamate as a nitrogen donor to generate phosphoserine (pSER) and alpha-ketoglutarate (αKG). pSER is then dephosphorylated by phosphoserine phosphatase (PSPH) to produce serine, which can be directly converted to glycine via transfer of a carbon into the folate pool by cytoplasmic serine hydroxymethyltransferases 1 and 2 (cytoplasmic SHMT1 and mitochondrial SHMT2) [101,102]. Here, we have found an increase in the level of intracellular and extracellular of glycine on the DNCs compered to normoxic cells.

It has been suggested that, the glycine cleavage system (GCS), located in mitochondria, oxidatively catabolizes glycine to serve as a source of one-carbon

units by cleaving the methylene group from glycine and accepting it by tetrahydrofolate (THF) to form methylene-THF. This process also results in the regeneration of NADH from NAD+ and releases CO_2 and ammonia. The upregulation of the core enzyme of GCS, glycine decarboxylase, in lung tumor-initiating cells [103], and glioblastoma-derived cells [104], suggests that glycine and GCS may promote cancer cell growth. This hypothesis is supported by the dependency of the cancer cells upon this metabolic pathway [105]. Take into account the fact some studies mentioned that, "An excessive amount of glycine has been shown to hinder cancer cell proliferation and limit tumor growth [106,107]. Herein, we have found that, increased the level of glycine on DNCs specifically, after 24h of incubation at hypoxia. Our results might be related to the fact that, the high expression activity of SHMT1 and SHMT2 occurs after 24 hours of incubation of DNCs in a manner that sheds light on the underlying mechanisms of glycine in cancer cell metabolism. However, the excess accumulation of intracellular glycine leads to its release into the extracellular milieu, suggesting a role in maintaining cell growth. Additionally, the inhibition of serine metabolism through serine starvation, deletion of the SHMT2 gene, or knockdown of SHMT2 expression via RNA interference leads to an accumulation of precursors upstream of inosine monophosphate (IMP). This results in a depletion of one-carbon units for purine biosynthesis, which in turn restricts cancer cell proliferation [104,108,109].

The synthesis of serine and glycine involves numerous enzymatic steps and the utilization of various amino acids and energy sources, such as glutamine, ATP, and formate. Purine metabolism in rapidly growing cancer cells is reliant on these substrates, which are vital for the production of inosine monophosphate (IMP). While the complementary salvage pathway satisfies most cellular demands for purine nucleotides, the magnesium-dependent enzyme hypoxanthine-guanine phosphoribosyltransferase (HPRT) plays a crucial role in purine biosynthesis by catalyzing the transfer of a phosphoribosyl group to hypoxanthine and guanine, leading to the production of IMP and guanine monophosphate, respectively [110, 111].

In this study, we observed a higher level of inosine monophosphate (IMP) in DNCs compared to normoxic cells. Observed by others, given the metabolic changes that occur in response to hypoxia, including the upregulation of glycolysis and pentose phosphate pathway, and the correlation between purinosome formation and elevated

de novo purine biosynthesis, they hypothesized that hypoxia would drive an increase in purinosome assembly in cells. This increase would allow cells to synthesize the key molecules required for cell proliferation by utilizing increased metabolites from glycolysis and PPP [112,113]. From other studies have revealed that HIF-1 activates the bifunctional glycolytic enzyme 6-phospho-2-kinase/fructose-2,6-biphosphatase (PFKFB) [114,115]. Among the four PFKFB members, PFKFB3 is crucial for regulating the cellular levels of PRPP and *de novo* nucleic acid synthesis in tumor cells. This is because PFKFB3 activation controls the level of fructose 2,6-bisphosphate (F2,6BP), a potent activator of the glycolytic rate-limiting enzyme PFK-1. This in turn directs the flow of carbon from glycolysis into the non-oxidative branch of the pentose phosphate pathway (PPP) [116]. These findings suggest that inhibiting the non-oxidative PPP may selectively target nucleotide biosynthesis in tumors that exhibit constant HIF-1α activation. Therefore, the DNCs exhibit a higher level of IMP compared to normoxic cells, likely due to hypoxia-induced upregulation of glycolysis and pentose phosphate pathway.

Another significant metabolites was π-methylhistidine (1-methylhistidine). Histidine can be methylated at either the N1 or N3 position of its imidazole ring, resulting in the formation of two isomers: 1-methylhistidine (also known as π-methylhistidine) or 3-methylhistidine (also referred to as τ-methylhistidine) via methyltransferase (METTL9), which is the primary enzyme responsible for the formation of 1-methylhistidine in mouse and human proteins [117]. In this study, we observed a upregulation of 1-methylhistidine expression in DNCs compared to normoxic cell. It has been showed that, the elevated levels of creatine and 3-methylhistidine were observed in the gastrocnemius muscle of rats with tumors, indicating a strong correlation between muscle wasting and intense protein breakdown [118]. In another study, increased levels of tyrosine, phenylalanine, and methylhistidine were found in the gastrocnemius muscle of a murine model of gastric cancer, indicating their involvement in metabolic wasting [119]. Previous *in vivo* research has demonstrated that π-methylhistidine and τ-methylhistidine are directly linked to muscle protein degradation [120–122]. In another *in vivo* study, they found that despite no significant change in τ-methylhistidine, the concentration of π-methylhistidine in the skeletal muscle was elevated, with a trend of up to 3.3 times increase in all stages of tumor growth, indicating that tumor progression can directly

impact the human skeletal muscle [123,124]. There is a limitation of knowledge about 1-methylhistidine regulations *in vitro* studies and its mechanism in cancer progression. However, our observation is consistent with the aforementioned *in vivo* results.

The accumulation of fumarate is one of the most distinctive biochemical features of fumarate hydratase (FH) deficient cells, with a potential role in tumorigenesis [125]. It was initially believed that the stabilization of the hypoxia-inducible factor (HIF) transcription factor due to the accumulation of fumarate played a critical role in the tumorigenesis of FH-deficient renal cancer [125–127]. However, the importance of HIF as a tumor driver has been challenged recently, with the observation that the genetic elimination of HIF in Fh1-deficient mice not only failed to abolish cyst formation but actually worsened this phenotype [128]. A new connection between fumarate accumulation and tumorigenesis was later proposed, with fumarate found to modify cysteine residues of kelch-like ECH-associated protein 1 (Keap1), which regulates the nuclear factor (erythroid-derived 2)-like 2 (Nrf2), suggesting a role for a dysregulated antioxidant response in the formation of FH-deficient tumors [129]. Moreover, other studies mentioned both succinate dehydrogenase (SDH) and fumarate hydratase (FH) play a critical role in the energy production processes of normal cells, but also act as tumor suppressors [130,131]. Additionally, the exposure to fumarate showed to be profoundly more cytotoxic and genotoxic than succinate. Therefore, the cytotoxicity seems to be due to the activation of an apoptotic pathway. Although it has been reported that fumarate can accumulate to between 200 and 300 times the normal concentration [126,132]. What's more, both succinate and fumarate result in a change in the global DNA methylation pattern, causing significant hypermethylation of DNA. This change in the epigenetic profile may play important role in the oncogenesis observed in cells exposed to elevated levels of these metabolites [132]. Here, we have found an increase of extracellular fumarate in DNCs compared to normoxic cell after 12h and 24h of incubation at hypoxia. From our finding the cancer cells release fumarate to the extracellular space during hypoxia might be as a survival mechanism. Under low oxygen conditions (hypoxia), cancer cells are unable to produce energy through oxidative phosphorylation and must switch to anaerobic metabolism. This leads to the accumulation of metabolic intermediates, including fumarate, which

can accumulate to toxic levels within the cell. To prevent cellular damage, cancer cells may release excess fumarate into the extracellular space, thereby reducing its intracellular concentration. This process may contribute to the growth and progression of the cancer cells, as well as the surrounding tissue. Further research is needed to fully understand the mechanisms and effects of fumarate release in cancer cells during hypoxia.

Another important extracellular metabolite was acetate. Acetate produced in the colon during digestion of fermentable carbohydrates, has an impact on normal metabolism, including mitochondrial function and fatty acid oxidation [133]. It has been reported that, the effects of acetate on colon cancer have not yet been fully established. The metabolic effects of acetate were investigated on HT29 and HCT116 colon cancer cell lines, including its effect on mitochondrial proliferation, reactive oxygen species, cellular bioenergetics, gene expression, and lipid levels [134]. Their results showed that acetate reduced proliferation and glycolysis in both cell lines under normal oxygen conditions, and increased oxygen consumption and ROS levels. The observed cell death was not dependent on acetyl-CoA synthetase 1 (ACSS1) and 2 (ACSS2) expression. However, under hypoxia, reduced proliferation was maintained in HT29 but not HCT116. Increased acetyl-CoA synthetase 2 expression and lipid levels in both cell lines under hypoxia may protect cells from the anti-proliferative effects of acetate. These findings suggest that acetate's impact on proliferation is due to its effect on mitochondrial metabolism and is independent of ACCS1/2 expression under normal oxygen conditions [134]. In this study we showed that, an increase level of extracellular acetate in DNCs compared to normoxic cell after 12h and 24h of incubation at hypoxia. It has been reported that, in normoxia, glucose and glutamine are the main sources of acetyl-CoA. However, in hypoxia, these sources decline the flux from glucose to citrate and cells utilize alternative sources for acetate production [44,135]. Therefore, the exogenous acetate, which is present in mammalian serum, could be incorporated into acetyl-CoA and used for lipid biosynthesis in some cell lines in hypoxia. They also discovered that acetate contributes significantly to lipid biosynthesis in hypoxic cells, suggesting that it is produced locally in the microenvironment [135]. Other study raises the possibility that cells could produce acetate used by neighboring cells, and it highlights the importance of understanding acetate's role in acetyl-CoA generation and its impact

on tumor growth [136]. The conclusion of the upregulation of extracellular acetate is that acetate may play a significant role in providing acetyl-CoA for lipid biosynthesis in hypoxic cells. This may suggests that cancer cells may rely on locally produced acetate as a major source to support cell-cell communication during hypoxia, potentially due to slower metabolism in these cells and highlight the complex interplay between cancer cell metabolism and communication pathways, which may contribute to tumor progression.

Another metabolic pathway that requires functional mitochondria is the oxidation of the third carbon of serine to formate. The formate produced in the mitochondria is released into the cytosol where it is used for nucleotide synthesis. Additionally, the formate can be reused to resynthesize serine through the cytosolic one-carbon metabolism process [109,137,138]. Our results showed that, an increase level of extracellular formate in DNCs compared to normoxic cell after 12h and 24h of incubation at hypoxia. This aligns with other findings suggested that, the process of serine catabolism, leading to formate production, often takes place at a higher rate than required for nucleotide synthesis. This results in an overflow of formate which is released from the cells, a phenomenon referred to as "formate overflow". This was predicted and confirmed through *in vitro* and *in vivo* experimental verification [139]. Another study indicated that elevated serine catabolism leading to increased formate production is a common feature of intestinal adenomas and mammary carcinomas *in vivo*. This is reflected in the elevated serum formate levels observed in these transformed tissues. However, inhibiting formate production through genetic interference significantly decreases cancer cell invasion, a phenotype that can be rescued by adding exogenous formate. Other findings suggest that elevated formate overflow is a defining characteristic of oxygenated cancers and plays a role in promoting invasion through an undetermined mechanism [140]. Additionally, has been reported that, under normoxic laboratory standard (21% O_2) and hypoxia (1% O_2), the formate overflow was observed to be higher in aggressive cancer cells compared to non-aggressive. However, under hypoxia, aggressive cells showed a preference for being more energetically efficient, while under normoxia, they favored fatty acid biosynthesis when compared to non-aggressive cells [141].

Here, we found that, the extracellular asparagine was higher with DNCs compared to normoxic cell after 12h and 24h of incubation at hypoxia. It's well known

that, cancer cells often require certain non-essential amino acids, like glutamine and asparagine, to function properly. This is due to the high demand for such amino acids in cancer cells for various metabolic processes, including glutaminolysis [142], hexosamine biosynthesis, glutathione biosynthesis, proline biosynthesis, and nucleotide biosynthesis. In response to this high demand, cancer cells extract TCA cycle intermediates, particularly oxaloacetate, to generate aspartate [142]. Glutamine acts as a source of replenishment for the TCA cycle in cancer cells, while asparagine can also fulfill some of these roles but at the cost of large amounts of acetyl-CoA being converted into the TCA cycle. A study showed that while asparagine prevented cell death during glutamine depletion, it did not restore fully TCA cycle metabolites, this suggests that glutaminolysis is a more straightforward pathway that is not as affected by the loss of certain molecules as the TCA cycle [143,144]. Moreover, asparagine has a vital function as a mediator for the transport other amino acids, mainly glycine, histidine, threonine, and serine. The main function of intracellular asparagine is to be exported for the import of these amino acids. A decrease in asparagine, for example in cells with low expression of asparagine synthetase, leads to a reduction in amino acid import and protein synthesis. The presence of intracellular asparagine can also suppress the mTOR signaling pathway by directly reducing the phosphorylation of the protein initiation complex, which in turn can also enhance nucleotide synthesis [144–146]. A recent study highlights the role of asparagine in protecting against apoptosis during nutrient stress in response to KRAS signaling in non-small-cell lung cancer. This protection is achieved through the KRAS-Akt-Nrf2-ATF4 axis, where glutamine restriction leads to an increase in ATF4 expression, which in turn leads to an upregulation of ASNS to support cellular proliferation. The study found that targeting asparagine through L-asparaginase can almost completely stop tumor growth in cells that lack ASNS, highlighting the vulnerability of KRAS-driven ASNS activity during nutrient deprivation. The combination of an AKT inhibitor and L-asparaginase was found to significantly reduce the growth of H460 xenografts, compared to control or single agent treatment [147]. Based on our observation of increased intracellular glutamine and aspartate under hypoxia, it appears that hypoxic cancer cells may rely on producing aspartate from glutamine via glutamic oxaloacetic transaminase (GOT) [23], as a way to replenish the TCA cycle. This pathway can be fulfilled through glutaminolysis, even in the absence of acetyl-

CoA, instead of relying on asparagine. Therefore, hypoxic cancer cells prioritize using glutamine over asparagine to meet their metabolic needs. Additionally, increase the activity of exchange transporters, such as ASCT2 (SLC1A5), can facilitate the release of asparagine and uptake of other amino acids such as serine and glutamine. Hence, the accumulation is essential for the functioning of other cellular pathways [148]. Hence, the DNCs releases of asparagine to extrcellular space as priority mechanism to meet their metabolic needs of the cells for the other NEAAs, which is essential for the functioning of other cellular pathways. Moreover, targeting asparagine through L-asparaginase has been shown to be effective in stopping tumor growth in cells that lack ASNS, highlighting the vulnerability of KRAS-driven ASNS activity during nutrient deprivation.

Ornithine is a non-essential and non-proteinoceus amino acid involved in various metabolic pathways. It is converted into citrulline, proline, and polyamines by the enzymes ornithine transcarbomylase (OTC), ornithine aminotransferase (OAT), and ornithine decarboxylase (ODC), respectively [149]. Citrulline plays a crucial role in the urea cycle and low levels can lead to hyperammonemia [150]. Herein, our results showed an increased level of extracellular ornithine in DNCs compared to normoxic cell after 12h and 24h of incubation at hypoxia. It has been reported by *in vivo* study that, the association between ornithine levels and breast cancer in females with 735 breast cancer cases and 735 controls were included in the 1:1 age-matched case-control study. Fasting blood samples were used to measure ornithine levels. Each increase in ornithine levels was associated with a 12% decrease in breast cancer risk. Higher ornithine levels were found to be linked to a lower risk of breast cancer in females [151]. Thus, the initial step of polyamine synthesis involves the decarboxylation of ornithine by ODC, which produces putrescine and CO2. Polyamines, however, play a crucial role in regulating hypoxia-induced apoptosis of endothelial cells via the PI3K/AKT pathway, thereby exerting a significant influence on neovascularization under hypoxia [152]. Previous study have shown that the depletion of polyamines resulting from reduced expression of spermidine/spermine N(1)-acetyltransferase (SSAT) leads to significant inhibition of p-Akt, p-GSK3β, and β-catenin nuclear translocation, resulting in the reduced growth, migration, and invasion of human hepatocarcinoma and colon cancer cell models [153]. Therefore, our observations might be linked to the inhibition of ornithine decarboxylase (ODC), which is the substrate

for the synthesis of urea and polyamines. This observation aligns with our findings on the growth curve after DNCs and the accumulation of extracellular ornithine, which results from ODC inhibition.

Aging-related increases in serum methylmalonate have been implicated in driving the aggressive behavior of cancer cells. Hence, elevated levels of the metabolite methylmalonic acid (MMA) - a by-product of propionate metabolism - coincides with the increased risk of cancer during normal ageing. This increase in MMA has been linked to the induction of the EMT phenotype and the promotion of cancer cell aggressiveness [154]. Here, we have noticed an increase of methylmalonate levels in DNCs compared to normoxic cell after 12h and 24h of incubation at hypoxia. It has been shown that, there is a direct correlation between systemic aging and an increase in methylmalonate levels, which leads to a poor prognosis and increased mortality in elderly cancer patients [154]. This emphasizes the crucial role that metabolic changes play in determining the progression of tumors [154]. What's more, it has reported that, the enzyme propionyl-CoA carboxylase (PCC) plays a crucial role in the regulation of the propionate metabolic pathway. Propionyl-CoA carboxylase (PCC) catalyzes the transformation of branched-chain amino acids (BCAA) and odd-chain fatty acids (OCFA)-derived propionyl-CoA into dimethylmalonyl-CoA. The overexpression of PCC resulted in a heightened propionyl-CoA concentration, leading to a boosted flux through the propionate metabolic pathway. This was evidenced by an increased presence of methylmalonate and succinate, as well as intensified levels of intermediates within the tricarboxylic acid cycle. Moreover, overexpression of PCC was observed to enhance pro-metastatic markers in HCC1806, MCF-10A, and A549 cell lines. The results showed that while the migratory capacity of cells was not significantly impacted, PCC overexpression significantly increased the invasiveness of MDA-MB231 cells [155].

4.1.1. Conclusion

In summary, this is the list of our findings from all significant metabolites as follows:

1. Hypoxia activates genes that inhibit degradation and increase uptake of phenylalanine and tyrosine, leading to elevated levels of these amino acids in cancer cells.

2. Mechanisms such as upregulation of L amino acid transporter 1 activity, decreasing activity of enzymes involved in the degradation of branched-chain amino acids, and decreasing activity of the branched-chain alpha-ketoacid dehydrogenase enzyme result in increased levels of BCAAs, particularly leucine, isoleucine, and valine, in cancer cells under hypoxic conditions.
3. Glutamine uptake increases under hypoxia due to elevated levels of glutamine transporters and redirection towards the reductive carboxylation pathway, enabling cells to produce TCA metabolites.
4. NAD levels increase in DNCs under hypoxic conditions, promoting cancer cell survival and proliferation by increasing glycolysis.
5. Alanine levels increase in DNCs under hypoxia, highlighting the importance of understanding the alanine complex interplay between cancer cells and their microenvironment in tumor metabolism.
6. Upregulation of β-Alanine in DNCs under hypoxia may be a favorable response to counteract cancer cell proliferation and glycolysis.
7. Taurine levels show a controversy in our findings compared to some other literature observations, which may be due to the type of tumors and organism.
8. Upregulation of sn-glycero-3-phosphocholine in DNCs under hypoxic conditions indicates altered choline metabolism that could be relevant for cancer diagnosis and treatment.
9. HT1080 cell line increases intracellular creatine levels under hypoxia, enabling survival and inhibiting apoptosis through SLC6A8 upregulation and AKT-ERK signaling pathway activation.
10. Intracellular creatinine levels increase in DNCs, suggesting a potential role in cancer progression.
11. Increased glycine levels in DNCs specifically after 24h of incubation at hypoxia due to high expression activity of SHMT1 and SHMT2, shedding light on the underlying mechanisms of glycine in cancer cell metabolism.
12. DNCs exhibit a higher level of IMP compared to normoxic cells due to upregulation of glycolysis and pentose phosphate pathway in response to hypoxia.

13. Upregulation of 1-methylhistidine expression in DNCs compared to normoxic cell, the limitation knowledge of 1-methylhistidine regulations *in vitro* studies. However, most of in vivo studies were in consistence with our finding.
14. Extracellular fumarate levels increase in DNCs as a survival mechanism under hypoxic conditions, reducing cytotoxicity effect and the activation of an apoptotic pathway, which may contribute to the growth and progression of cancer cells and surrounding tissue.
15. Extracellular acetate levels increase in DNCs, playing a crucial role in providing acetyl-CoA for lipid biosynthesis and supporting cell-cell communication during hypoxia.
16. Induced formate overflow in DNCs highlights the important role of formate in cancer cell metabolism and suggests targeting formate production and utilization as a promising avenue for developing new cancer therapies.
17. Extracellular asparagine levels increase in DNCs, supporting cell proliferation and metastasis.
18. An increased level of extracellular ornithine in DNCs as results from ornithine decarboxylase (ODC) inhibition leading to reduced growth, migration, and invasion cancer cells.
19. An increase of methylmalonate levels in DNCs as consequence of increased PCC overexpression and induce invasiveness of cancer cells

Overall, the findings suggest that cancer cells undergo significant metabolic adaptations under hypoxic conditions, which allow them to survive and even thrive in a low oxygen environment. These adaptations include changes in amino acid metabolism, upregulation of glycolysis and pentose phosphate pathway, redirection of glutamine metabolism, and alterations in the production and utilization of various metabolites. Therefore, understanding these metabolic adaptations may provide important insights into the biology of cancer and potential therapeutic targets for the treatment of hypoxic tumors. However, it is important to note that some of the observed changes in metabolite levels may vary depending on the specific tumor type and microenvironment, highlighting the need for further research in this area. Additionally, this chapter also underscores the importance of using multiple

approaches, including *in vitro* and *in vivo* findings, to gain a comprehensive understanding of cancer cell metabolism under DNC condition.

4.2. The post hypoxia reoxygenation impact on HT1080 cells metabolic phenotype

The hallmark characteristics of malignant cells include the ability to invade surrounding tissues, uncontrolled self-sufficient growth, resistance to apoptosis induction, and manipulation of their microenvironment through multiple processes, for instance, angiogenesis [156]. The progression of tumors is contingent upon angiogenesis and lymphangiogenesis, which are stimulated by chemical signals produced by rapidly growing tumor cells [157]. Team of researchers compared the growth behavior of cancer cells in different regions of an organ with and without blood circulation. Cancer cells grew to 1-2 mm^3 and stopped in the absence of circulation, but grew beyond 2 mm^3 in an area with angiogenesis. Angiogenesis was found to be an important factor in the progression of cancer as tumors without vascular support can become necrotic or apoptotic [158–160]. Moreover, in human cancers, the rapid proliferation of cancer cells often leads to a limited oxygen (O_2) diffusion within the tumor, due to outgrowing their vascular network. Abnormal tumor blood vessel structure and function can cause perfusion defects, resulting in hypoxic stress. This leads to higher levels of hypoxia-inducible factor (HIF) in the tumor tissues compared to normal tissue [161,162]. In addition, in experimental studies, experiments have shown that elevating HIF-1α expression leads to a growth in tumors, as well as an increase in angiogenesis and metastasis. Conversely, reducing HIF activity has been linked to the opposite outcomes and provides the opportunity to observe transitions in oxygen levels within the cells from hypoxia to normoxia [163]. In light of this, we aim to investigate the cell-oxygen transition deoxygenation and, in this case, reoxygenation approach in the HT1080 cell intracellular and extracellular metabolome.

Noteworthy, from our results obtained, we showed a reductions of one influencer intracellular metabolites that sustained its level as normoxic cells after RHC treatment such as amino sugar uridine diphosphate N-acetylglucosamine (UDP-GlcNAc). The regulation of metabolic processes and maintenance of cellular

homeostasis are significantly influenced by nutrient sensing. The hexosamine biosynthetic pathway (HBP) and its end product, uridine diphosphate N-acetyl glucosamine (UDP-GlcNAc), play a crucial role in cellular signaling and can promote tumorigenesis. Imbalances in nutrient uptake homeostasis can result in cellular stress and disrupt cellular energetics [164]. In cancer cells, increased glucose and glutamine uptake, as well as oncogenic signals such as Ras, mTORC2, and TGF-β, result in an upregulation of the hexosamine biosynthetic pathway (HBP) and higher levels of UDP-GlcNAc. This important regulatory pathway in cell signaling promotes tumor growth. The HBP can also regulate N-linked and O-linked glycosylation through nutrient sensing, which impacts downstream cellular signaling [165–169]. However, the correlation between depletion of the extracellular glucose and glutamine levels altered the UDP-GlcNAc levels has been demonstrated in various cancer cell types, including cervical and pancreatic cancer [170], colon cancer [171], breast cancer [172], large B-cell lymphoma and hepatocellular carcinoma [173]. These findings highlight the importance of nutrient sensing in regulating cellular processes and the role of UDP-GlcNAc as a key regulator in tumor promotion [174]. This observation was consistent with our findings that showed the limitations of intracellular and extracellular of glucose and downregulation of glutamine on RHCs after 12h and 24h incubation at normoxia. Moreover, our previous results on the DNC approach have shown that asparagine and aspartate regulations are dependent on glutamine availability. Here, we have noticed that, the downregulation of glutamine has positive correlation on intracellular asparagine and aspartate levels. The conditionally essential amino acid asparagine is normally expressed at low levels in most cells [175,176], but can be rapidly induced when the availability of glucose, asparagine, leucine, isoleucine, or glutamine is limited, or when the dietary amino acid composition is imbalanced. This *de novo* synthesis of asparagine is mediated by the enzyme asparagine synthetase (ASNS). Other observation suggested that, in certain cancers have been associated with low serum levels of asparagine [177]. Moreover, cancer cells often overexpress the enzyme asparagine synthetase (ASNS) to cope with nutrient deprivation and/or hypoxia [175], this enzyme responsible for the conversion of aspartate and glutamine to asparagine and glutamate in an ATP-dependent manner [175]. Observed by others, the vital role of asparagine in cancer cell proliferation and adaptation to glutamine depletion. It has been observed that a defective asparagine

synthetase (ASNS) gene inhibited cells at the G1 step of the cell cycle, and can induce apoptosis [178]. However, we noticed also an upregulation of extracellular asparagine after RHCs after 12h and 24h of incubation at normoxia. This may related to the selective advantage of using extracellular asparagine and asparagine transporter *SLC1A5* activity under normoxia over using glutamine via glutaminolysis for aspartate synthesis and act as primary amino acid over extracellular asparagine to provide carbon and nitrogen to other pathways. Therefore, could be explain the intracellular aspartate downregulation as well.

Finally, among the most important metabolites that was identified by MVA was 1-methylnicotinamide. According to research, nicotine and its metabolites play a significant influence in the development of oral squamous cell carcinoma (OSSC) [179]. Cancer cells' metabolic adaptability is thought to allow them to use methyl-donor S-adenosylmethionine (SAM) for non-epigenetic functions such as nicotinamide and nicotine methylation. This SAM channeling to make 1-methylnicotinamide (1-MNA) and methylated nicotine products is regarded to be a critical step in cancer formation because it induces DNA hypomethylation, which helps to create favorable epigenetic states [179]. herein, we have found that, a reduction on 1-methylnicotinamide levels with RHCs after 12h and 24h of incubation at normoxia. It has been reported that, pancreatic adenocarcinoma (PAAD) is characterized by desmoplasia, which results in a harsh hypoxic microenvironment that forces PAAD cells to adapt. This adaptation is driven by the HIF-1 pathway and the Sonic Hedgehog (SHh) signaling pathway [180]. To thrive under these conditions, PAAD cells activate specific metabolic pathways, such as increased glucose and glutamine metabolism, that are driven by the *KRAS* oncogene [181]. The levels of N-methyltransferase (NNMT) in PAAD are significantly higher than those in normal pancreatic tissue, which is correlated with poor clinical outcomes and is proposed as an independent predictor of patient survival [182]. This aligns with our findings in the previous section (**Section** 4.1.) and also her which showed at hypoxia cells expressed high concentration of 1-methylnicotinamide and downregulated with increase oxygen concentration.

Additionally, in cancer cells, pyruvate generated from glycolysis is transformed into lactate by lactate dehydrogenase A (LDHA) instead of being converted to acetyl-CoA [183]. This is referred to as the "Warburg effect" [184]. Abnormal regulation of glycolysis leads to high lactate levels, which are transported

out of the cell via the plasma membrane transporters, MCTs (monocarboxylic acid solute transporters) [185]. Lactate is a prevalent metabolite in the human circulatory system [186]. It is produced from the final product of glycolysis, pyruvate, by lactate dehydrogenase (LDH). In aerobic conditions, pyruvate can be transported into mitochondria to support biosynthetic pathways and the production of ATP. Under hypoxia, pyruvate is transformed into lactate, a reaction that replenishes NAD+, which is crucial for the maintenance of glycolysis [187]. Even in the presence of adequate oxygen, cells may still convert pyruvate into lactic acid [184]. Moreover, lactate can be transported through monocarboxylate transporters (MCT 1-4), which also have bidirectional capabilities [188]. The conversion of lactate to lactic acid occurs due to the acquisition of a proton from NADH. Lactic acid dissociates in aqueous solution at physiological pH, resulting in lactate and hydrogen ions (H+), leading to acidification of the extracellular microenvironment. Alternatively, lactate can also be used to produce lactyl-CoA and regulate gene transcription through histone lactylation [189]. The expression of the lactate dehydrogenase (LDH) enzyme is regulated by two subunits, LDHA and LDHB, encoded by the ldha and ldhb genes, respectively. The five isoforms of LDH (LDH 1-5) are differentially overexpressed in various tissues. The LDHA isoform is known to be overexpressed in several cancer types, including pancreatic, osteosarcoma, lung adenocarcinoma, non-small-cell lung cancer, oral squamous cell carcinoma, and head and neck cancers. The LDHA catalyzes the conversion of pyruvate to lactate, whereas the backward reaction is catalyzed by LDHB [190]. Others showed, lactate dehydrogenase B (LDHB) plays a crucial role in controlling key cellular processes, including lysosomal acidification, vesicle maturation, and intracellular proteolysis. By catalyzing the conversion of lactate to pyruvate, LDHB is essential for basal autophagy and cancer cell proliferation, in both oxidative and glycolytic cancer cells [191]. This mechanism aligned with our observation under normoxia with a reduction on the intracellular and extracellular lactate related to the overexpression of lactate dehydrogenase B (LDHB) enzyme.

Additionally, in cancer cells, the availability of amino acids can play a crucial role in their survival and proliferation, especially in adverse conditions such as genotoxic, oxidative, and nutritional stress [192]. Amino acids can be divided into two categories essential amino acids and nonessential amino acids as well as some

amino acids are conditional and their classification is based on the requirement for growth and survival in organisms, including cancer cells. An amino acid is considered to be metabolically essential if its carbon structure cannot be synthesized in the body and must be obtained from the diet. The growth of cancer cells can be arrested by removing a specific amino acid from their growth medium. It is important to determine the net requirement of amino acids by the growing cancer cells and compare it to the capacity of their transport system. The transport of amino acids is facilitated by a group of transporters, including uniporters, symporters, and antiporters [193]. Here, we have showed that, nearly all extracellular metabolites showed a reduction in RHCs compered to hypoxic cells. including choline, lysine, alanine, leucine, isoleucine, methionine, valine, methylamine, and lactate.

Cells' demand for amino acids requires the coordinated and finely regulated activity of plasma membrane transporters to ensure proper uptake, distribution to tissues or cells, as well as reabsorption from kidney ultrafiltration. This network maintains homeostasis in physiological conditions [194]. Cancer cells utilize glutamine through the glutaminolysis pathway to obtain building blocks and energy for anabolic purposes. This highlights the critical role of glutamine transporters in cancer growth and the potential for these transporters to be targeted in chemotherapy [195]. To date, 14 plasma membrane transporters in mammalian cells have been identified at the molecular level to transport glutamine. It is crucial to note that none of these transporters have specific selectivity for glutamine and not all of them facilitate glutamine influx into cells. The transporters exhibit varying substrate selectivity, with some accepting only neutral amino acids, others accepting neutral and cationic amino acids, and still others accepting neutral, cationic, and anionic amino acids [196]. In addition, some of these transporters facilitate the release of intracellular glutamine into the extracellular environment under normal physiological conditions, while most of them mediate the entry of extracellular glutamine into cells [196]. Moreover, It has been reported that, the presence of a suite of glutamine transporters (influx/efflux), including SNAT1 (SLC38A1), mediating the net uptake of specific amino acid transporters (AATs) [197], ASCT2 (SLC1A5) and LAT1 (SLC7A5) and they are amino acid transporter harmonisers, which rapidly exchange various amino acids to ensure their presence in the cytosol, and rescue amino acid transporters including SNAT4

(SLC38A4), as well as SNAT2 (SLC38A2) which provide redundant capacity and are upregulated in response to stress [193,195].

In human cervical adenocarcinoma epithelial cells (HeLa) and human thymidine kinase-negative osteosarcoma cells 143B and the net glutamine uptake was dependent on SNAT1 and SNAT2. However, the absence of ASCT2 resulted in an amino acid starvation response and increased expression of SNAT1. Suppressing GCN2 in this scenario led to further reduction in cell growth, implying that a multiple glutamine transporter that induce glutamine-dependent cancer cell growth "addicted cells" [195]. In this study, we have found that, a significant decrease of extracellular glutamine (increase glutamine consumption) in RHCs after 12h and 24h of incubation at normoxia compered to hypoxic cells. moreover, the same effect was observed in DNC condition. Observed by others that, in K-Ras mutant cells, the presence of glutamine increases both oxygen consumption rate and ATP generation, contributing to the development of tumorigenesis [198]. It has been reported that the activation of K-Ras and Akt in transformed cells results in 60% of the total FADH2 and NADH2 being synthesized from glutamine, with only 30% derived from glucose [199]. This highlights the significant contribution of glutamine to ATP generation and oxygen consumption in these cells, further supporting its role in tumorigenesis, and heightened the expression of glutamine transporters.

Moreover, the large amino acid transporter 1 (LAT1) mediates the uptake of several essential amino acids (EAAs), including leucine, isoleucine, valine, phenylalanine, tyrosine, tryptophan, methionine, and histidine into the cell [200], and the expression of LAT1 increases in various cancers during their progression [201]. Herein, we have found that, a reduction in the levels of extracellular leucine, isoleucine, valine, tyrosine, phenylalanine and methionine (increase essential amino acids consumption) with RHCs after 12h and 24h of incubation at normoxia compered to hypoxic cells. It has been demonstrated from *in vitro* study that, LAT1 (SLC7A5) has high affinity for bulky branched-chain and aromatic amino acids, thus providing a source of energy through their contribution to the TCA cycle [202]. The LAT1 (SLC7A5) have been implicated in various cancer-associated traits such as protection against cell death, promotion of cell proliferation, activation of invasion and metastasis, induction of angiogenesis, evasion of immune response, and disruption of cellular energy homeostasis [203]. Therefore, the increase in demand for leucine, isoleucine,

valine, tyrosine, phenylalanine and methionine may contributes to the expression of LAT1 (SLC7A5), promoting the development of tumorigenesis.

Moreover, the cationic amino acid transporter-1 (CAT-1) is mainly located in the basolateral membrane, However, it can also be exist in intracellular membranes. There are two variants of CAT2, known as CAT2-A and CAT2-B. CAT2-A is mostly found in the liver, skeletal muscle, and pancreas, while CAT2-B expression is inducible in multiple cell types [204]. Others suggest a high demand for arginine by tumor cells and indicates that either inhibiting transport or reducing extracellular arginine could be a promising therapeutic approach. The strong impact of reducing CAT-1 on chronic lymphocytic leukemia (CLL) cell viability and tumor growth may also be partially caused by decreased uptake of the essential amino acid including lysine, which is also a substrate for CAT-1 [205]. Here, we have found a reduction of the extracellular arginine and lysine levels with RHCs after 12h and 24h of incubation at normoxia compered to hypoxic cells. It has been demonstrated that, the potential roles of CATs in metabolic reprogramming are multiple and may involve: (i) facilitating the buildup of arginine and lysine to drive the TCA cycle; (ii) providing arginine for nitric oxide biosynthesis; and (iii) supporting ornithine utilization for polyamine synthesis [206]. Therefore, the elevated arginine and lysine consumption within the tumors highlights its central importance for tumor cell survival [207], and importance of inducing the expression of cationic amino acid transporter-1 (CAT-1).

The metabolic fate of fructose is diverse and complex. However, certain metabolic pathways overlap with those of glucose metabolism and are integral to cell growth and survival. Thus, it is expected that, analogous to glucose, fructose can impact the growth, proliferation, and survival of cancer cells [208,209]. Recent studies have established a link between the fructose transporter GLUT5 (encoded by SLC2A5) and cancer development and progression [210]. Upregulation of GLUT5 has been found to be associated with poor prognosis in patients with lung adenocarcinoma. Therefore, demonstrate that depletion of GLUT5 diminished cell proliferation and invasion and increased apoptosis, while increased GLUT5 expression enhanced cell proliferation, migration, invasion, and tumorigenic potential [210]. Here, we have observed that, a downregulation of extracellular fructose with RHCs after 12h and 24h of incubation at normoxia compered to hypoxic cells. Several studies has been shown that, the enhanced uptake of fructose led to increased cell proliferation, colony

growth, and boosted migration and invasion. Consequently, high GLUT5 expression and increased fructose utilization are linked to unfavorable outcomes and exacerbate cancerous phenotypes. What's more, GLUT5 overexpression has been observed in various types of cancer, including glioblastoma, colon, liver, lung, breast, and prostate [211–213]. This aligned with our observation on the level of extracellular fructose downregulation as reflection of high expression of fructose transporter GLUT5.

Adenosine triphosphate (ATP) is an essential biochemical component of the tumor microenvironment (TME), which can have either tumor-promoting or tumor-suppressing effects depending on its concentration and the specific ecto-nucleotidases and receptors expressed by immune and cancer cells [1]. ATP can be released from cells via both regulated and non-regulated pathways, such as exocytotic granules and plasma membrane-derived microvesicles, as well as various membrane channels and transporters, such as ATP-binding cassette (ABC) transporters, connexin hemichannels, pannexin 1 (PANX1), calcium homeostasis modulator 1 (CALHM1), volume-regulated anion channels (VRACs) and maxi-anion channels (MACs). Unregulated ATP release, on the other hand, occurs from dying and damaged cells [214,215]. Observed by us a reduction on the extracellular ATP with RHCs after 12h and 24h of incubation at normoxia compered to hypoxic cells.

In recent years, study has provided a growing body of evidence that cancer cells utilize extracellular nutritional/energy molecules [36], including ATP, to meet their nutritional and energetic requirements. Moreover, the finding of extracellular ATP's roles in cancer metabolism expands the list of functionally significant extracellular molecules and provides a new target for prospective anticancer therapeutics [216]. Our finding is also consistent with these observations shown the importance of extracellular ATP for cancer cells energy demand requirements by inducing the expression of it transporters under normoxia conditions. Additionally, we have noticed that, fumarate was accumulated in extracellular space in which already explained in details in the previous section about the mechanism of fumarate overflow in normoxia and hypoxia (**Section** 4.1).

4.2.1. Conclusion

In summary , we found that, the intracellular and extracellular metabolome of hypoxic cells and reoxygenized hypoxic cells at normoxia after 12h and 24h showed an increase of the catabolic capacity and induced amino acids influx into cells to sustain energy production and building blocks of intermediaries amino acids for biosynthesis process through various mechanisms including the following:

- The downregulation of all significant intracellular metabolites including asparagine, aspartate, glutamate, 1-methylnicotinamide, UDP-GlcNAc and lactate deliver different metabolic mechanisms as follows:
    1. The depletion of the extracellular glucose and glutamine levels downregulate the UDP-GlcNAc level via oncogenic signals such as Ras, mTORC2, and TGF-β as well as downregulated the hexosamine biosynthetic pathway (HBP).
    2. The reduction of glutamine has positive correlation on intracellular asparagine and aspartate. Moreover, upregulation of extracellular asparagine after RHCs after 12h and 24h of incubation at normoxia via selective advantage mechanism of using extracellular asparagine and asparagine transporter *SLC1A5* activity under normoxia over using glutamine via glutaminolysis for aspartate synthesis and act as primary amino acid over extracellular asparagine to provide carbon and nitrogen to other pathways.
    3. The reduction on 1-methylnicotinamide levels with RHCs after 12h and 24h of incubation at normoxia was driven via reducing of HIF-1 pathway and the sonic hedgehog (SHh) signaling pathway as well as a reduction on N-methyltransferase (NNMT) enzyme activity to adept the transition condition from hypoxia to normoxia.
    4. This mechanism of our observation under normoxia with a reduction on the intracellular and extracellular lactate related to the overexpression of lactate dehydrogenase B (LDHB) enzyme.

- Under normoxia conditions, most significant extracellular metabolites are downregulated compared to hypoxia, except for fumarate which is explained in chapter 2, and asparagine which is discussed in section 4.1. This reduction is attributed to the upregulation of amino acid transporters under normoxia

compared to hypoxia, which play a crucial role in various cellular mechanisms for cancer development and progression, including the following:

1. SNAT1 (SLC38A1), ASCT2 (SLC1A5) and LAT1 (SLC7A5) for extracellular glutamine.
2. LAT1 (SLC7A5) for extracellular leucine, isoleucine, valine, tyrosine, phenylalanine and methionine.
3. The cationic amino acid transporter-1 (CAT-1) for extracellular arginine and lysine.
4. The fructose transporter GLUT5 (encoded by SLC2A5) for extracellular fructose.
5. Through membrane channels and transporters, such as ATP-binding cassette (ABC) transporters, connexin hemichannels, pannexin 1 (PANX1), calcium homeostasis modulator 1 (CALHM1), volume-regulated anion channels (VRACs) and maxi-anion channels (MACs) for ATP.

The presented results provide novel insights into the impact of oxygen concentration and oxygen transition on HT1080 cells by NMR, shedding light on their responses to deoxygenation and reoxygenation. Specifically, under deoxygenation, normoxic cells experience stress and cease their degradation process, leading to the accumulation of intracellular amino acids. Therefore, this triggers the induction of amino acid transporters, which release amino acids into the extracellular space to maintain homeostasis and energy reserves for relevant pathways under hypoxia. Conversely, under reoxygenation, hypoxic cells experience an increase in the degradation and transformation process, coupled with the induction of transporter expression to increase uptake of significant amino acids aided by the oxygen supplied under normoxia. Overall, the findings provide crucial insights into understanding the both terms physiological and pathological implications of hypoxia in HT1080 cells, highlighting the importance of oxygen transition in restoring cellular processes. These findings represent a significant contribution to the literature and hold great potential for advancing our understanding of hypoxic responses in various cell types.

5. References

1. Semenza, G.L. Hypoxia-Inducible Factors: Mediators of Cancer Progression and Targets for Cancer Therapy. *Trends in Pharmacological Sciences* **2012**, *33*, 207–214, doi:10.1016/j.tips.2012.01.005.
2. Eales, K.L.; Hollinshead, K.E.R.; Tennant, D.A. Hypoxia and Metabolic Adaptation of Cancer Cells. *Oncogenesis* **2016**, *5*, e190–e190, doi:10.1038/oncsis.2015.50.
3. Hong, B.-J.; Kim, J.; Jeong, H.; Bok, S.; Kim, Y.-E.; Ahn, G.-O. Tumor Hypoxia and Reoxygenation: The Yin and Yang for Radiotherapy. *Radiat Oncol J* **2016**, *34*, 239–249, doi:10.3857/roj.2016.02012.
4. Muz, B.; Puente, P. de la; Azab, F.; Azab, A.K. The Role of Hypoxia in Cancer Progression, Angiogenesis, Metastasis, and Resistance to Therapy. *HP* **2015**, *3*, 83–92, doi:10.2147/HP.S93413.
5. Folkman, J. History of Angiogenesis. In *Angiogenesis: An Integrative Approach From Science to Medicine*; Figg, W.D., Folkman, J., Eds.; Springer US: Boston, MA, 2008; pp. 1–14 ISBN 978-0-387-71518-6.
6. Rankin, E.B.; Giaccia, A.J. Hypoxic Control of Metastasis. *Science* **2016**, *352*, 175–180, doi:10.1126/science.aaf4405.
7. Ulrich, E.L.; Akutsu, H.; Doreleijers, J.F.; Harano, Y.; Ioannidis, Y.E.; Lin, J.; Livny, M.; Mading, S.; Maziuk, D.; Miller, Z.; et al. BioMagResBank. *Nucleic Acids Research* **2008**, *36*, D402–D408, doi:10.1093/nar/gkm957.
8. Wishart, D.S.; Feunang, Y.D.; Marcu, A.; Guo, A.C.; Liang, K.; Vázquez-Fresno, R.; Sajed, T.; Johnson, D.; Li, C.; Karu, N.; et al. HMDB 4.0: The Human Metabolome Database for 2018. *Nucleic Acids Research* **2018**, *46*, D608–D617, doi:10.1093/nar/gkx1089.
9. Tomasi, G.; van den Berg, F.; Andersson, C. Correlation Optimized Warping and Dynamic Time Warping as Preprocessing Methods for Chromatographic Data. *Journal of Chemometrics* **2004**, *18*, 231–241, doi:10.1002/cem.859.
10. Savorani, F.; Tomasi, G.; Engelsen, S.B. Icoshift: A Versatile Tool for the Rapid Alignment of 1D NMR Spectra. *Journal of Magnetic Resonance* **2010**, *202*, 190–202, doi:10.1016/j.jmr.2009.11.012.
11. Al Tameemi, W.; Dale, T.P.; Al-Jumaily, R.M.K.; Forsyth, N.R. Hypoxia-Modified Cancer Cell Metabolism. *Frontiers in Cell and Developmental Biology* **2019**, *7*.
12. Infantino, V.; Santarsiero, A.; Convertini, P.; Todisco, S.; Iacobazzi, V. Cancer Cell Metabolism in Hypoxia: Role of HIF-1 as Key Regulator and Therapeutic Target. *International Journal of Molecular Sciences* **2021**, *22*, 5703, doi:10.3390/ijms22115703.
13. Fu, Y.M.; Yu, Z.X.; Ferrans, V.J.; Meadows, G.G. Tyrosine and Phenylalanine Restriction Induces G0/G1 Cell Cycle Arrest in Murine Melanoma in Vitro and in Vivo. *Nutr Cancer* **1997**, *29*, 104–113, doi:10.1080/01635589709514610.
14. Kaufman, S. A Model of Human Phenylalanine Metabolism in Normal Subjects and in Phenylketonuric Patients. *Proceedings of the National Academy of Sciences* **1999**, *96*, 3160–3164, doi:10.1073/pnas.96.6.3160.
15. Lai, H.-S.; Lee, J.-C.; Lee, P.-H.; Wang, S.-T.; Chen, W.-J. Plasma Free Amino Acid Profile in Cancer Patients. *Semin Cancer Biol* **2005**, *15*, 267–276, doi:10.1016/j.semcancer.2005.04.003.
16. Neurauter, G.; Grahmann, A.V.; Klieber, M.; Zeimet, A.; Ledochowski, M.; Sperner-Unterweger, B.; Fuchs, D. Serum Phenylalanine Concentrations in Patients with Ovarian Carcinoma Correlate with Concentrations of Immune Activation Markers and of Isoprostane-8. *Cancer Lett* **2008**, *272*, 141–147, doi:10.1016/j.canlet.2008.07.002.

17. Ploder, M.; Neurauter, G.; Spittler, A.; Schroecksnadel, K.; Roth, E.; Fuchs, D. Serum Phenylalanine in Patients Post Trauma and with Sepsis Correlate to Neopterin Concentrations. *Amino Acids* **2008**, *35*, 303–307, doi:10.1007/s00726-007-0625-x.
18. Engbring, J.A.; Kleinman, H.K. The Basement Membrane Matrix in Malignancy. *J Pathol* **2003**, *200*, 465–470, doi:10.1002/path.1396.
19. Seftor, R.E.; Seftor, E.A.; Koshikawa, N.; Meltzer, P.S.; Gardner, L.M.; Bilban, M.; Stetler-Stevenson, W.G.; Quaranta, V.; Hendrix, M.J. Cooperative Interactions of Laminin 5 Gamma2 Chain, Matrix Metalloproteinase-2, and Membrane Type-1-Matrix/Metalloproteinase Are Required for Mimicry of Embryonic Vasculogenesis by Aggressive Melanoma. *Cancer Res* **2001**, *61*, 6322–6327.
20. Deng, K.; Lin, S.; Zhou, L.; Geng, Q.; Li, Y.; Xu, M.; Na, R. Three Aromatic Amino Acids in Gastric Juice as Potential Biomarkers for Gastric Malignancies. *Anal Chim Acta* **2011**, *694*, 100–107, doi:10.1016/j.aca.2011.03.053.
21. Wiggins, T.; Kumar, S.; Markar, S.R.; Antonowicz, S.; Hanna, G.B. Tyrosine, Phenylalanine, and Tryptophan in Gastroesophageal Malignancy: A Systematic Review. *Cancer Epidemiology, Biomarkers & Prevention* **2015**, *24*, 32–38, doi:10.1158/1055-9965.EPI-14-0980.
22. van Spronsen, F.J.; van Rijn, M.; Bekhof, J.; Koch, R.; Smit, P.G. Phenylketonuria: Tyrosine Supplementation in Phenylalanine-Restricted Diets. *The American Journal of Clinical Nutrition* **2001**, *73*, 153–157, doi:10.1093/ajcn/73.2.153.
23. Lieu, E.L.; Nguyen, T.; Rhyne, S.; Kim, J. Amino Acids in Cancer. *Exp Mol Med* **2020**, *52*, 15–30, doi:10.1038/s12276-020-0375-3.
24. Choi, B.-H.; Coloff, J.L. The Diverse Functions of Non-Essential Amino Acids in Cancer. *Cancers* **2019**, *11*, 675, doi:10.3390/cancers11050675.
25. Zhang, B.; Chen, Y.; Shi, X.; Zhou, M.; Bao, L.; Hatanpaa, K.J.; Patel, T.; DeBerardinis, R.J.; Wang, Y.; Luo, W. Regulation of Branched-Chain Amino Acid Metabolism by Hypoxia-Inducible Factor in Glioblastoma. *Cell. Mol. Life Sci.* **2021**, *78*, 195–206, doi:10.1007/s00018-020-03483-1.
26. Martin, S.B.; Reiche, W.S.; Fifelski, N.A.; Schultz, A.J.; Stanford, S.J.; Martin, A.A.; Nack, D.L.; Radlwimmer, B.; Boyer, M.P.; Ananieva, E.A. Leucine and Branched-Chain Amino Acid Metabolism Contribute to the Growth of Bone Sarcomas by Regulating AMPK and MTORC1 Signaling. *Biochem J* **2020**, *477*, 1579–1599, doi:10.1042/BCJ20190754.
27. Ericksen, R.E.; Lim, S.L.; McDonnell, E.; Shuen, W.H.; Vadiveloo, M.; White, P.J.; Ding, Z.; Kwok, R.; Lee, P.; Radda, G.K.; et al. Loss of BCAA Catabolism during Carcinogenesis Enhances MTORC1 Activity and Promotes Tumor Development and Progression. *Cell Metab* **2019**, *29*, 1151-1165.e6, doi:10.1016/j.cmet.2018.12.020.
28. Zhang, L.; Han, J. Branched-Chain Amino Acid Transaminase 1 (BCAT1) Promotes the Growth of Breast Cancer Cells through Improving MTOR-Mediated Mitochondrial Biogenesis and Function. *Biochem Biophys Res Commun* **2017**, *486*, 224–231, doi:10.1016/j.bbrc.2017.02.101.
29. Gu, Z.; Liu, Y.; Cai, F.; Patrick, M.; Zmajkovic, J.; Cao, H.; Zhang, Y.; Tasdogan, A.; Chen, M.; Qi, L.; et al. Loss of EZH2 Reprograms BCAA Metabolism to Drive Leukemic Transformation. *Cancer Discov* **2019**, *9*, 1228–1247, doi:10.1158/2159-8290.CD-19-0152.
30. Mayers, J.R.; Wu, C.; Clish, C.B.; Kraft, P.; Torrence, M.E.; Fiske, B.P.; Yuan, C.; Bao, Y.; Townsend, M.K.; Tworoger, S.S.; et al. Elevation of Circulating Branched-Chain Amino Acids Is an Early Event in Human Pancreatic Adenocarcinoma Development. *Nat Med* **2014**, *20*, 1193–1198, doi:10.1038/nm.3686.
31. Qu, Y.-Y.; Zhao, R.; Zhang, H.-L.; Zhou, Q.; Xu, F.-J.; Zhang, X.; Xu, W.-H.; Shao, N.; Zhou, S.-X.; Dai, B.; et al. Inactivation of the AMPK-GATA3-ECHS1 Pathway Induces Fatty Acid

Synthesis That Promotes Clear Cell Renal Cell Carcinoma Growth. *Cancer Res* **2020**, *80*, 319–333, doi:10.1158/0008-5472.CAN-19-1023.
32. Hattori, A.; Tsunoda, M.; Konuma, T.; Kobayashi, M.; Nagy, T.; Glushka, J.; Tayyari, F.; McSkimming, D.; Kannan, N.; Tojo, A.; et al. Cancer Progression by Reprogrammed BCAA Metabolism in Myeloid Leukaemia. *Nature* **2017**, *545*, 500–504, doi:10.1038/nature22314.
33. Wolfson, R.L.; Chantranupong, L.; Saxton, R.A.; Shen, K.; Scaria, S.M.; Cantor, J.R.; Sabatini, D.M. Sestrin2 Is a Leucine Sensor for the MTORC1 Pathway. *Science (New York, N.Y.)* **2016**, *351*, 43, doi:10.1126/science.aab2674.
34. Mossmann, D.; Park, S.; Hall, M.N. MTOR Signalling and Cellular Metabolism Are Mutual Determinants in Cancer. *Nat Rev Cancer* **2018**, *18*, 744–757, doi:10.1038/s41568-018-0074-8.
35. Warburg, O.; Negelein, E.; Posener, K. Versuche an Überlebendem Carcinomgewebe. *Klin Wochenschr* **1924**, *3*, 1062–1064, doi:10.1007/BF01736087.
36. Pavlova, N.N.; Thompson, C.B. The Emerging Hallmarks of Cancer Metabolism. *Cell Metab* **2016**, *23*, 27–47, doi:10.1016/j.cmet.2015.12.006.
37. DeBerardinis, R.J.; Cheng, T. Q's next: The Diverse Functions of Glutamine in Metabolism, Cell Biology and Cancer. *Oncogene* **2010**, *29*, 313–324, doi:10.1038/onc.2009.358.
38. Hensley, C.T.; Wasti, A.T.; DeBerardinis, R.J. Glutamine and Cancer: Cell Biology, Physiology, and Clinical Opportunities. *J Clin Invest* **2013**, *123*, 3678–3684, doi:10.1172/JCI69600.
39. Still, E.R.; Yuneva, M.O. Hopefully Devoted to Q: Targeting Glutamine Addiction in Cancer. *Br J Cancer* **2017**, *116*, 1375–1381, doi:10.1038/bjc.2017.113.
40. Pantel, A.R.; Ackerman, D.; Lee, S.-C.; Mankoff, D.A.; Gade, T.P. Imaging Cancer Metabolism: Underlying Biology and Emerging Strategies. *Journal of Nuclear Medicine* **2018**, *59*, 1340–1349, doi:10.2967/jnumed.117.199869.
41. Zhang, J.; Pavlova, N.N.; Thompson, C.B. Cancer Cell Metabolism: The Essential Role of the Nonessential Amino Acid, Glutamine. *The EMBO Journal* **2017**, *36*, 1302–1315, doi:10.15252/embj.201696151.
42. Lacey, J.M.; Wilmore, D.W. Is Glutamine a Conditionally Essential Amino Acid? *Nutrition Reviews* **1990**, *48*, 297–309, doi:10.1111/j.1753-4887.1990.tb02967.x.
43. DeBerardinis, R.J.; Mancuso, A.; Daikhin, E.; Nissim, I.; Yudkoff, M.; Wehrli, S.; Thompson, C.B. Beyond Aerobic Glycolysis: Transformed Cells Can Engage in Glutamine Metabolism That Exceeds the Requirement for Protein and Nucleotide Synthesis. *Proceedings of the National Academy of Sciences* **2007**, *104*, 19345–19350, doi:10.1073/pnas.0709747104.
44. Metallo, C.M.; Gameiro, P.A.; Bell, E.L.; Mattaini, K.R.; Yang, J.; Hiller, K.; Jewell, C.M.; Johnson, Z.R.; Irvine, D.J.; Guarente, L.; et al. Reductive Glutamine Metabolism by IDH1 Mediates Lipogenesis under Hypoxia. *Nature* **2012**, *481*, 380–384, doi:10.1038/nature10602.
45. Rosiers, C.D.; Donato, L.D.; Comte, B.; Laplante, A.; Marcoux, C.; David, F.; Fernandez, C.A.; Brunengraber, H. Isotopomer Analysis of Citric Acid Cycle and Gluconeogenesis in Rat Liver: REVERSIBILITY OF ISOCITRATE DEHYDROGENASE AND INVOLVEMENT OF ATP-CITRATE LYASE IN GLUCONEOGENESIS *. *Journal of Biological Chemistry* **1995**, *270*, 10027–10036, doi:10.1074/jbc.270.17.10027.
46. Yoo, H.; Antoniewicz, M.R.; Stephanopoulos, G.; Kelleher, J.K. Quantifying Reductive Carboxylation Flux of Glutamine to Lipid in a Brown Adipocyte Cell Line *. *Journal of Biological Chemistry* **2008**, *283*, 20621–20627, doi:10.1074/jbc.M706494200.
47. Ward, P.S.; Patel, J.; Wise, D.R.; Abdel-Wahab, O.; Bennett, B.D.; Coller, H.A.; Cross, J.R.; Fantin, V.R.; Hedvat, C.V.; Perl, A.E.; et al. The Common Feature of Leukemia-Associated IDH1 and IDH2 Mutations Is a Neomorphic Enzyme Activity Converting α-Ketoglutarate to 2-Hydroxyglutarate. *Cancer Cell* **2010**, *17*, 225–234, doi:10.1016/j.ccr.2010.01.020.

48. Lemons, J.M.S.; Feng, X.-J.; Bennett, B.D.; Legesse-Miller, A.; Johnson, E.L.; Raitman, I.; Pollina, E.A.; Rabitz, H.A.; Rabinowitz, J.D.; Coller, H.A. Quiescent Fibroblasts Exhibit High Metabolic Activity. *PLOS Biology* **2010**, *8*, e1000514, doi:10.1371/journal.pbio.1000514.
49. Metallo, C.M.; Walther, J.L.; Stephanopoulos, G. Evaluation of 13C Isotopic Tracers for Metabolic Flux Analysis in Mammalian Cells. *Journal of Biotechnology* **2009**, *144*, 167–174, doi:10.1016/j.jbiotec.2009.07.010.
50. Yoo, H.C.; Yu, Y.C.; Sung, Y.; Han, J.M. Glutamine Reliance in Cell Metabolism. *Exp Mol Med* **2020**, *52*, 1496–1516, doi:10.1038/s12276-020-00504-8.
51. Yaku, K.; Okabe, K.; Nakagawa, T. NAD Metabolism: Implications in Aging and Longevity. *Ageing Res Rev* **2018**, *47*, 1–17, doi:10.1016/j.arr.2018.05.006.
52. Jayaram, H.N.; Kusumanchi, P.; Yalowitz, J.A. NMNAT Expression and Its Relation to NAD Metabolism. *Curr Med Chem* **2011**, *18*, 1962–1972, doi:10.2174/092986711795590138.
53. Tan, B.; Young, D.A.; Lu, Z.-H.; Wang, T.; Meier, T.I.; Shepard, R.L.; Roth, K.; Zhai, Y.; Huss, K.; Kuo, M.-S.; et al. Pharmacological Inhibition of Nicotinamide Phosphoribosyltransferase (NAMPT), an Enzyme Essential for NAD+ Biosynthesis, in Human Cancer Cells. *J Biol Chem* **2013**, *288*, 3500–3511, doi:10.1074/jbc.M112.394510.
54. Hara, N.; Yamada, K.; Shibata, T.; Osago, H.; Hashimoto, T.; Tsuchiya, M. Elevation of Cellular NAD Levels by Nicotinic Acid and Involvement of Nicotinic Acid Phosphoribosyltransferase in Human Cells. *J Biol Chem* **2007**, *282*, 24574–24582, doi:10.1074/jbc.M610357200.
55. Ceni, C.; Pochon, N.; Brun, V.; Muller-Steffner, H.; Andrieux, A.; Grunwald, D.; Schuber, F.; De Waard, M.; Lund, F.; Villaz, M.; et al. CD38-Dependent ADP-Ribosyl Cyclase Activity in Developing and Adult Mouse Brain. *Biochem J* **2003**, *370*, 175–183, doi:10.1042/BJ20020604.
56. Wilk, A.; Hayat, F.; Cunningham, R.; Li, J.; Garavaglia, S.; Zamani, L.; Ferraris, D.M.; Sykora, P.; Andrews, J.; Clark, J.; et al. Extracellular NAD+ Enhances PARP-Dependent DNA Repair Capacity Independently of CD73 Activity. *Sci Rep* **2020**, *10*, 651, doi:10.1038/s41598-020-57506-9.
57. Gulshan, M.; Yaku, K.; Okabe, K.; Mahmood, A.; Sasaki, T.; Yamamoto, M.; Hikosaka, K.; Usui, I.; Kitamura, T.; Tobe, K.; et al. Overexpression of Nmnat3 Efficiently Increases NAD and NGD Levels and Ameliorates Age-Associated Insulin Resistance. *Aging Cell* **2018**, *17*, e12798, doi:10.1111/acel.12798.
58. Berger, F.; Lau, C.; Dahlmann, M.; Ziegler, M. Subcellular Compartmentation and Differential Catalytic Properties of the Three Human Nicotinamide Mononucleotide Adenylyltransferase Isoforms. *J Biol Chem* **2005**, *280*, 36334–36341, doi:10.1074/jbc.M508660200.
59. Groen, A.K.; Sips, H.J.; Vervoorn, R.C.; Tager, J.M. Intracellular Compartmentation and Control of Alanine Metabolism in Rat Liver Parenchymal Cells. *Eur J Biochem* **1982**, *122*, 87–93, doi:10.1111/j.1432-1033.1982.tb05851.x.
60. Vettore, L.; Westbrook, R.L.; Tennant, D.A. New Aspects of Amino Acid Metabolism in Cancer. *Br J Cancer* **2020**, *122*, 150–156, doi:10.1038/s41416-019-0620-5.
61. Elia, I.; Rossi, M.; Stegen, S.; Broekaert, D.; Doglioni, G.; van Gorsel, M.; Boon, R.; Escalona-Noguero, C.; Torrekens, S.; Verfaillie, C.; et al. Breast Cancer Cells Rely on Environmental Pyruvate to Shape the Metastatic Niche. *Nature* **2019**, *568*, 117–121, doi:10.1038/s41586-019-0977-x.
62. Sousa, C.M.; Biancur, D.E.; Wang, X.; Halbrook, C.J.; Sherman, M.H.; Zhang, L.; Kremer, D.; Hwang, R.F.; Witkiewicz, A.K.; Ying, H.; et al. Pancreatic Stellate Cells Support Tumour Metabolism through Autophagic Alanine Secretion. *Nature* **2016**, *536*, 479–483, doi:10.1038/nature19084.

63. Vaughan, R.A.; Gannon, N.P.; Garcia-Smith, R.; Licon-Munoz, Y.; Barberena, M.A.; Bisoffi, M.; Trujillo, K.A. β-Alanine Suppresses Malignant Breast Epithelial Cell Aggressiveness through Alterations in Metabolism and Cellular Acidity in Vitro. *Mol Cancer* **2014**, *13*, 14, doi:10.1186/1476-4598-13-14.
64. Jordan, T.; Lukaszuk, J.; Misic, M.; Umoren, J. Effect of Beta-Alanine Supplementation on the Onset of Blood Lactate Accumulation (OBLA) during Treadmill Running: Pre/Post 2 Treatment Experimental Design. *J Int Soc Sports Nutr* **2010**, *7*, 20, doi:10.1186/1550-2783-7-20.
65. Asperger, A.; Renner, C.; Menzel, M.; Gebhardt, R.; Meixensberger, J.; Gaunitz, F. Identification of Factors Involved in the Anti-Tumor Activity of Carnosine on Glioblastomas Using a Proteomics Approach. *Cancer Investigation* **2011**, *29*, 272–281, doi:10.3109/07357907.2010.550666.
66. Gaunitz, F.; Hipkiss, A.R. Carnosine and Cancer: A Perspective. *Amino Acids* **2012**, *43*, 135–142, doi:10.1007/s00726-012-1271-5.
67. Pandurangan, M.; Enkhtaivan, G.; Kim, D.H. Cytotoxic Effects of Aspartame on Human Cervical Carcinoma Cells. *Toxicol. Res.* **2015**, *5*, 45–52, doi:10.1039/C5TX00269A.
68. Holliday, R.; McFarland, G.A. Inhibition of the Growth of Transformed and Neoplastic Cells by the Dipeptide Carnosine. *Br J Cancer* **1996**, *73*, 966–971, doi:10.1038/bjc.1996.189.
69. Chen, P.-C.; Pan, C.; Gharibani, P.M.; Prentice, H.; Wu, J.-Y. Taurine Exerts Robust Protection Against Hypoxia and Oxygen/Glucose Deprivation in Human Neuroblastoma Cell Culture. In Proceedings of the Taurine 8; El Idrissi, A., L'Amoreaux, W.J., Eds.; Springer: New York, NY, 2013; pp. 167–175.
70. Zhang, X.; Tu, S.; Wang, Y.; Xu, B.; Wan, F. Mechanism of Taurine-Induced Apoptosis in Human Colon Cancer Cells. *Acta Biochimica et Biophysica Sinica* **2014**, *46*, 261–272, doi:10.1093/abbs/gmu004.
71. Griffiths, J.R.; Cady, E.; Edwards, R.H.; McCready, V.R.; Wilkie, D.R.; Wiltshaw, E. 31P-NMR Studies of a Human Tumour in Situ. *Lancet* **1983**, *1*, 1435–1436, doi:10.1016/s0140-6736(83)92375-9.
72. Griffiths, J.R.; Stevens, A.N.; Iles, R.A.; Gordon, R.E.; Shaw, D. 31P-NMR Investigation of Solid Tumours in the Living Rat. *Biosci Rep* **1981**, *1*, 319–325, doi:10.1007/BF01114871.
73. Daly, P.F.; Lyon, R.C.; Faustino, P.J.; Cohen, J.S. Phospholipid Metabolism in Cancer Cells Monitored by 31P NMR Spectroscopy. *J Biol Chem* **1987**, *262*, 14875–14878.
74. Aboagye, E.O.; Bhujwalla, Z.M. Malignant Transformation Alters Membrane Choline Phospholipid Metabolism of Human Mammary Epithelial Cells. *Cancer Res* **1999**, *59*, 80–84.
75. Gillies, R.J.; Raghunand, N.; Karczmar, G.S.; Bhujwalla, Z.M. MRI of the Tumor Microenvironment. *J Magn Reson Imaging* **2002**, *16*, 430–450, doi:10.1002/jmri.10181.
76. Galons, J.P.; Job, C.; Gillies, R.J. Increase of GPC Levels in Cultured Mammalian Cells during Acidosis. A 31P MR Spectroscopy Study Using a Continuous Bioreactor System. *Magn Reson Med* **1995**, *33*, 422–426, doi:10.1002/mrm.1910330317.
77. Glunde, K.; Shah, T.; Winnard, P.T.; Raman, V.; Takagi, T.; Vesuna, F.; Artemov, D.; Bhujwalla, Z.M. Hypoxia Regulates Choline Kinase Expression through Hypoxia-Inducible Factor-1 Alpha Signaling in a Human Prostate Cancer Model. *Cancer Res* **2008**, *68*, 172–180, doi:10.1158/0008-5472.CAN-07-2678.
78. Mori, N.; Natarajan, K.; Chacko, V.P.; Artemov, D.; Bhujwalla, Z.M. Choline Phospholipid Metabolites of Human Vascular Endothelial Cells Altered by Cyclooxygenase Inhibition, Growth Factor Depletion, and Paracrine Factors Secreted by Cancer Cells. *Mol Imaging* **2003**, *2*, 124–130, doi:10.1162/15353500200303127.

79. Hirai, K.; Watanabe, S.; Nishijima, N.; Shibata, K.; Hase, A.; Yamanaka, T.; Inazu, M. Molecular and Functional Analysis of Choline Transporters and Antitumor Effects of Choline Transporter-Like Protein 1 Inhibitors in Human Pancreatic Cancer Cells. *International Journal of Molecular Sciences* **2020**, *21*, 5190, doi:10.3390/ijms21155190.
80. Glunde, K.; Penet, M.-F.; Jiang, L.; Jacobs, M.A.; Bhujwalla, Z.M. Choline Metabolism-Based Molecular Diagnosis of Cancer: An Update. *Expert Rev Mol Diagn* **2015**, *15*, 735–747, doi:10.1586/14737159.2015.1039515.
81. Nagashima, F.; Nishiyama, R.; Iwao, B.; Kawai, Y.; Ishii, C.; Yamanaka, T.; Uchino, H.; Inazu, M. Molecular and Functional Characterization of Choline Transporter-Like Proteins in Esophageal Cancer Cells and Potential Therapeutic Targets. *Biomol Ther (Seoul)* **2018**, *26*, 399–408, doi:10.4062/biomolther.2017.113.
82. Bansal, A.; Harris, R.A.; DeGrado, T.R. Choline Phosphorylation and Regulation of Transcription of Choline Kinase α in Hypoxia [S]. *Journal of Lipid Research* **2012**, *53*, 149–157, doi:10.1194/jlr.M021030.
83. García-Molina, P.; Sola-Leyva, A.; Luque-Navarro, P.M.; Laso, A.; Ríos-Marco, P.; Ríos, A.; Lanari, D.; Torretta, A.; Parisini, E.; López-Cara, L.C.; et al. Anticancer Activity of the Choline Kinase Inhibitor PL48 Is Due to Selective Disruption of Choline Metabolism and Transport Systems in Cancer Cell Lines. *Pharmaceutics* **2022**, *14*, 426, doi:10.3390/pharmaceutics14020426.
84. Lagarde, D.; Kazak, L. Creatine Promotes Metastatic Dissemination. *Cell Metab* **2021**, *33*, 1065–1067, doi:10.1016/j.cmet.2021.05.012.
85. Murphy, R.; McConell, G.; Cameron-Smith, D.; Watt, K.; Ackland, L.; Walzel, B.; Wallimann, T.; Snow, R. Creatine Transporter Protein Content, Localization, and Gene Expression in Rat Skeletal Muscle. *Am J Physiol Cell Physiol* **2001**, *280*, C415-422, doi:10.1152/ajpcell.2001.280.3.C415.
86. Wyss, M.; Kaddurah-Daouk, R. Creatine and Creatinine Metabolism. *Physiol Rev* **2000**, *80*, 1107–1213, doi:10.1152/physrev.2000.80.3.1107.
87. Zhang, L.; Bu, P. The Two Sides of Creatine in Cancer. *Trends in Cell Biology* **2022**, *32*, 380–390, doi:10.1016/j.tcb.2021.11.004.
88. Jm, L.; A, S.; A, N.; Fy, M.; E, W.; Z, Z.; L, S.; Pb, P.; Sf, T. Extracellular Metabolic Energetics Can Promote Cancer Progression. *Cell* **2015**, *160*, doi:10.1016/j.cell.2014.12.018.
89. Li, Q.; Liu, M.; Sun, Y.; Jin, T.; Zhu, P.; Wan, X.; Hou, Y.; Tu, G. SLC6A8-Mediated Intracellular Creatine Accumulation Enhances Hypoxic Breast Cancer Cell Survival via Ameliorating Oxidative Stress. *J Exp Clin Cancer Res* **2021**, *40*, 168, doi:10.1186/s13046-021-01933-7.
90. Schwameis, R.; Postl, M.; Bekos, C.; Hefler, L.; Reinthaller, A.; Seebacher, V.; Grimm, C.; Polterauer, S.; Helmy-Bader, S. Prognostic Value of Serum Creatine Level in Patients with Vulvar Cancer. *Sci Rep* **2019**, *9*, 11129, doi:10.1038/s41598-019-47560-3.
91. Kim, J.U.; Shariff, M.I.F.; Crossey, M.M.E.; Gomez-Romero, M.; Holmes, E.; Cox, I.J.; Fye, H.K.S.; Njie, R.; Taylor-Robinson, S.D. Hepatocellular Carcinoma: Review of Disease and Tumor Biomarkers. *World J Hepatol* **2016**, *8*, 471–484, doi:10.4254/wjh.v8.i10.471.
92. Ladep, N.G.; Dona, A.C.; Lewis, M.R.; Crossey, M.M.E.; Lemoine, M.; Okeke, E.; Shimakawa, Y.; Duguru, M.; Njai, H.F.; Fye, H.K.S.; et al. Discovery and Validation of Urinary Metabotypes for the Diagnosis of Hepatocellular Carcinoma in West Africans. *Hepatology* **2014**, *60*, 1291–1301, doi:10.1002/hep.27264.
93. Lécuyer, L.; Victor Bala, A.; Deschasaux, M.; Bouchemal, N.; Nawfal Triba, M.; Vasson, M.-P.; Rossary, A.; Demidem, A.; Galan, P.; Hercberg, S.; et al. NMR Metabolomic Signatures Reveal Predictive Plasma Metabolites Associated with Long-Term Risk of Developing

Breast Cancer. *International Journal of Epidemiology* **2018**, *47*, 484–494, doi:10.1093/ije/dyx271.
94. Pirzkall, A.; McGue, C.; Saraswathy, S.; Cha, S.; Liu, R.; Vandenberg, S.; Lamborn, K.R.; Berger, M.S.; Chang, S.M.; Nelson, S.J. Tumor Regrowth between Surgery and Initiation of Adjuvant Therapy in Patients with Newly Diagnosed Glioblastoma. *Neuro-Oncology* **2009**, *11*, 842–852, doi:10.1215/15228517-2009-005.
95. Kamphorst, J.J.; Nofal, M.; Commisso, C.; Hackett, S.R.; Lu, W.; Grabocka, E.; Vander Heiden, M.G.; Miller, G.; Drebin, J.A.; Bar-Sagi, D.; et al. Human Pancreatic Cancer Tumors Are Nutrient Poor and Tumor Cells Actively Scavenge Extracellular Protein. *Cancer Research* **2015**, *75*, 544–553, doi:10.1158/0008-5472.CAN-14-2211.
96. Patra, S.; Ghosh, A.; Roy, S.S.; Bera, S.; Das, M.; Talukdar, D.; Ray, S.; Wallimann, T.; Ray, M. A Short Review on Creatine–Creatine Kinase System in Relation to Cancer and Some Experimental Results on Creatine as Adjuvant in Cancer Therapy. *Amino Acids* **2012**, *42*, 2319–2330, doi:10.1007/s00726-011-0974-3.
97. Patel, R.; Ford, C.A.; Rodgers, L.; Rushworth, L.K.; Fleming, J.; Mui, E.; Zhang, T.; Watson, D.; Lynch, V.; Mackay, G.; et al. Cyclocreatine Suppresses Creatine Metabolism and Impairs Prostate Cancer Progression. *Cancer Res* **2022**, *82*, 2565–2575, doi:10.1158/0008-5472.CAN-21-1301.
98. Jiang, Y.; Su, Z.; Lin, Y.; Xiong, Y.; Li, C.; Li, J.; Wang, R.; Zhong, R.; Cheng, B.; He, J.; et al. Prognostic and Predictive Impact of Creatine Kinase Level in Non-Small Cell Lung Cancer Treated with Tyrosine Kinase Inhibitors. *Transl Lung Cancer Res* **2021**, *10*, 3771–3781, doi:10.21037/tlcr-21-600.
99. Geeraerts, S.L.; Heylen, E.; De Keersmaecker, K.; Kampen, K.R. The Ins and Outs of Serine and Glycine Metabolism in Cancer. *Nat Metab* **2021**, *3*, 131–141, doi:10.1038/s42255-020-00329-9.
100. de Koning, T.J.; Snell, K.; Duran, M.; Berger, R.; Poll-The, B.-T.; Surtees, R. L-Serine in Disease and Development. *Biochem J* **2003**, *371*, 653–661, doi:10.1042/BJ20021785.
101. Achouri, Y.; Rider, M.H.; Schaftingen, E.V.; Robbi, M. Cloning, Sequencing and Expression of Rat Liver 3-Phosphoglycerate Dehydrogenase. *Biochem J* **1997**, *323 (Pt 2)*, 365–370, doi:10.1042/bj3230365.
102. Singh, M.; Warita, K.; Warita, T.; Faeder, J.R.; Lee, R.E.C.; Sant, S.; Oltvai, Z.N. Shift from Stochastic to Spatially-Ordered Expression of Serine-Glycine Synthesis Enzymes in 3D Microtumors. *Sci Rep* **2018**, *8*, 9388, doi:10.1038/s41598-018-27266-8.
103. Zhang, W.C.; Shyh-Chang, N.; Yang, H.; Rai, A.; Umashankar, S.; Ma, S.; Soh, B.S.; Sun, L.L.; Tai, B.C.; Nga, M.E.; et al. Glycine Decarboxylase Activity Drives Non-Small Cell Lung Cancer Tumor-Initiating Cells and Tumorigenesis. *Cell* **2012**, *148*, 259–272, doi:10.1016/j.cell.2011.11.050.
104. Kim, D.; Fiske, B.P.; Birsoy, K.; Freinkman, E.; Kami, K.; Possemato, R.L.; Chudnovsky, Y.; Pacold, M.E.; Chen, W.W.; Cantor, J.R.; et al. SHMT2 Drives Glioma Cell Survival in Ischaemia but Imposes a Dependence on Glycine Clearance. *Nature* **2015**, *520*, 363–367, doi:10.1038/nature14363.
105. Kikuchi, G.; Motokawa, Y.; Yoshida, T.; Hiraga, K. Glycine Cleavage System: Reaction Mechanism, Physiological Significance, and Hyperglycinemia. *Proc Jpn Acad Ser B Phys Biol Sci* **2008**, *84*, 246–263, doi:10.2183/pjab/84.246.
106. Rose, M.L.; Madren, J.; Bunzendahl, H.; Thurman, R.G. Dietary Glycine Inhibits the Growth of B16 Melanoma Tumors in Mice. *Carcinogenesis* **1999**, *20*, 793–798, doi:10.1093/carcin/20.5.793.

107. Rose, M.L.; Cattley, R.C.; Dunn, C.; Wong, V.; Li, X.; Thurman, R.G. Dietary Glycine Prevents the Development of Liver Tumors Caused by the Peroxisome Proliferator WY-14,643. *Carcinogenesis* **1999**, *20*, 2075–2081, doi:10.1093/carcin/20.11.2075.
108. Labuschagne, C.F.; van den Broek, N.J.F.; Mackay, G.M.; Vousden, K.H.; Maddocks, O.D.K. Serine, but Not Glycine, Supports One-Carbon Metabolism and Proliferation of Cancer Cells. *Cell Rep* **2014**, *7*, 1248–1258, doi:10.1016/j.celrep.2014.04.045.
109. Ducker, G.S.; Chen, L.; Morscher, R.J.; Ghergurovich, J.M.; Esposito, M.; Teng, X.; Kang, Y.; Rabinowitz, J.D. Reversal of Cytosolic One-Carbon Flux Compensates for Loss of the Mitochondrial Folate Pathway. *Cell Metab* **2016**, *23*, 1140–1153, doi:10.1016/j.cmet.2016.04.016.
110. Pedley, A.M.; Benkovic, S.J. A New View into the Regulation of Purine Metabolism: The Purinosome. *Trends in Biochemical Sciences* **2017**, *42*, 141–154, doi:10.1016/j.tibs.2016.09.009.
111. Yin, J.; Ren, W.; Huang, X.; Deng, J.; Li, T.; Yin, Y. Potential Mechanisms Connecting Purine Metabolism and Cancer Therapy. *Frontiers in Immunology* **2018**, *9*.
112. Tong, X.; Zhao, F.; Thompson, C.B. The Molecular Determinants of de Novo Nucleotide Biosynthesis in Cancer Cells. *Curr Opin Genet Dev* **2009**, *19*, 32–37, doi:10.1016/j.gde.2009.01.002.
113. Doigneaux, C.; Pedley, A.M.; Mistry, I.N.; Papayova, M.; Benkovic, S.J.; Tavassoli, A. Hypoxia Drives the Assembly of the Multienzyme Purinosome Complex. *J Biol Chem* **2020**, *295*, 9551–9566, doi:10.1074/jbc.RA119.012175.
114. Minchenko, A.; Leshchinsky, I.; Opentanova, I.; Sang, N.; Srinivas, V.; Armstead, V.; Caro, J. Hypoxia-Inducible Factor-1-Mediated Expression of the 6-Phosphofructo-2-Kinase/Fructose-2,6-Bisphosphatase-3 (PFKFB3) Gene. Its Possible Role in the Warburg Effect. *J Biol Chem* **2002**, *277*, 6183–6187, doi:10.1074/jbc.M110978200.
115. Obach, M.; Navarro-Sabaté, A.; Caro, J.; Kong, X.; Duran, J.; Gómez, M.; Perales, J.C.; Ventura, F.; Rosa, J.L.; Bartrons, R. 6-Phosphofructo-2-Kinase (Pfkfb3) Gene Promoter Contains Hypoxia-Inducible Factor-1 Binding Sites Necessary for Transactivation in Response to Hypoxia. *J Biol Chem* **2004**, *279*, 53562–53570, doi:10.1074/jbc.M406096200.
116. Chesney, J.; Mitchell, R.; Benigni, F.; Bacher, M.; Spiegel, L.; Al-Abed, Y.; Han, J.H.; Metz, C.; Bucala, R. An Inducible Gene Product for 6-Phosphofructo-2-Kinase with an AU-Rich Instability Element: Role in Tumor Cell Glycolysis and the Warburg Effect. *Proc Natl Acad Sci U S A* **1999**, *96*, 3047–3052, doi:10.1073/pnas.96.6.3047.
117. Davydova, E.; Shimazu, T.; Schuhmacher, M.K.; Jakobsson, M.E.; Willemen, H.L.D.M.; Liu, T.; Moen, A.; Ho, A.Y.Y.; Małecki, J.; Schroer, L.; et al. The Methyltransferase METTL9 Mediates Pervasive 1-Methylhistidine Modification in Mammalian Proteomes. *Nat Commun* **2021**, *12*, 891, doi:10.1038/s41467-020-20670-7.
118. QuanJun, Y.; GenJin, Y.; LiLi, W.; Yan, H.; YongLong, H.; Jin, L.; Jie, L.; JinLu, H.; Cheng, G. Integrated Analysis of Serum and Intact Muscle Metabonomics Identify Metabolic Profiles of Cancer Cachexia in a Dynamic Mouse Model. *RSC Adv.* **2015**, *5*, 92438–92448, doi:10.1039/C5RA19004E.
119. Cui, P.; Huang, C.; Guo, J.; Wang, Q.; Liu, Z.; Zhuo, H.; Lin, D. Metabolic Profiling of Tumors, Sera, and Skeletal Muscles from an Orthotopic Murine Model of Gastric Cancer Associated-Cachexia. *J. Proteome Res.* **2019**, *18*, 1880–1892, doi:10.1021/acs.jproteome.9b00088.
120. Ruiz-Rodado, V.; Luque-Baena, R.M.; Vruchte, D. te; Probert, F.; Lachmann, R.H.; Hendriksz, C.J.; Wraith, J.E.; Imrie, J.; Elizondo, D.; Sillence, D.; et al. 1H NMR-Linked Urinary Metabolic Profiling of Niemann-Pick Class C1 (NPC1) Disease: Identification of Potential New Biomarkers Using Correlated Component Regression (CCR) and Genetic Algorithm (GA) Analysis Strategies. *Current Metabolomics 2*, 88–121.

121. Aranibar, N.; Vassallo, J.D.; Rathmacher, J.; Stryker, S.; Zhang, Y.; Dai, J.; Janovitz, E.B.; Robertson, D.; Reily, M.; Lowe-Krentz, L.; et al. Identification of 1- and 3-Methylhistidine as Biomarkers of Skeletal Muscle Toxicity by Nuclear Magnetic Resonance-Based Metabolic Profiling. *Anal Biochem* **2011**, *410*, 84–91, doi:10.1016/j.ab.2010.11.023.
122. Wang, H.; Hu, P.; Jiang, J. Measurement of 1- and 3-Methylhistidine in Human Urine by Ultra Performance Liquid Chromatography-Tandem Mass Spectrometry. *Clin Chim Acta* **2012**, *413*, 131–138, doi:10.1016/j.cca.2011.09.007.
123. Vesali, R.F.; Klaude, M.; Thunblad, L.; Rooyackers, O.E.; Wernerman, J. Contractile Protein Breakdown in Human Leg Skeletal Muscle as Estimated by [2H3]-3-Methylhistidine: A New Method. *Metabolism - Clinical and Experimental* **2004**, *53*, 1076–1080, doi:10.1016/j.metabol.2004.02.017.
124. Munro, H.N. Adaptation of Body Protein Metabolism in Adult and Aging Man. *Clinical Nutrition* **1982**, *1*, 95–108, doi:10.1016/0261-5614(82)90031-0.
125. Isaacs, J.S.; Jung, Y.J.; Mole, D.R.; Lee, S.; Torres-Cabala, C.; Chung, Y.-L.; Merino, M.; Trepel, J.; Zbar, B.; Toro, J.; et al. HIF Overexpression Correlates with Biallelic Loss of Fumarate Hydratase in Renal Cancer: Novel Role of Fumarate in Regulation of HIF Stability. *Cancer Cell* **2005**, *8*, 143–153, doi:10.1016/j.ccr.2005.06.017.
126. Pollard, P.J.; Brière, J.J.; Alam, N.A.; Barwell, J.; Barclay, E.; Wortham, N.C.; Hunt, T.; Mitchell, M.; Olpin, S.; Moat, S.J.; et al. Accumulation of Krebs Cycle Intermediates and Over-Expression of HIF1alpha in Tumours Which Result from Germline FH and SDH Mutations. *Hum Mol Genet* **2005**, *14*, 2231–2239, doi:10.1093/hmg/ddi227.
127. Ratcliffe, P.J. Fumarate Hydratase Deficiency and Cancer: Activation of Hypoxia Signaling? *Cancer Cell* **2007**, *11*, 303–305, doi:10.1016/j.ccr.2007.03.015.
128. Adam, J.; Hatipoglu, E.; O'Flaherty, L.; Ternette, N.; Sahgal, N.; Lockstone, H.; Baban, D.; Nye, E.; Stamp, G.W.; Wolhuter, K.; et al. Renal Cyst Formation in Fh1-Deficient Mice Is Independent of the Hif/Phd Pathway: Roles for Fumarate in KEAP1 Succination and Nrf2 Signaling. *Cancer Cell* **2011**, *20*, 524–537, doi:10.1016/j.ccr.2011.09.006.
129. Ooi, A.; Wong, J.-C.; Petillo, D.; Roossien, D.; Perrier-Trudova, V.; Whitten, D.; Min, B.W.H.; Tan, M.-H.; Zhang, Z.; Yang, X.J.; et al. An Antioxidant Response Phenotype Shared between Hereditary and Sporadic Type 2 Papillary Renal Cell Carcinoma. *Cancer Cell* **2011**, *20*, 511–523, doi:10.1016/j.ccr.2011.08.024.
130. Tomlinson, I.P.M.; Alam, N.A.; Rowan, A.J.; Barclay, E.; Jaeger, E.E.M.; Kelsell, D.; Leigh, I.; Gorman, P.; Lamlum, H.; Rahman, S.; et al. Germline Mutations in FH Predispose to Dominantly Inherited Uterine Fibroids, Skin Leiomyomata and Papillary Renal Cell Cancer. *Nat Genet* **2002**, *30*, 406–410, doi:10.1038/ng849.
131. Astuti, D.; Douglas, F.; Lennard, T.W.; Aligianis, I.A.; Woodward, E.R.; Evans, D.G.R.; Eng, C.; Latif, F.; Maher, E.R. Germline SDHD Mutation in Familial Phaeochromocytoma. *The Lancet* **2001**, *357*, 1181–1182, doi:10.1016/S0140-6736(00)04378-6.
132. Wentzel, J.F.; Lewies, A.; Bronkhorst, A.J.; van Dyk, E.; du Plessis, L.H.; Pretorius, P.J. Exposure to High Levels of Fumarate and Succinate Leads to Apoptotic Cytotoxicity and Altered Global DNA Methylation Profiles in Vitro. *Biochimie* **2017**, *135*, 28–34, doi:10.1016/j.biochi.2017.01.004.
133. Brody, L.P.; Sahuri-Arisoylu, M.; Parkinson, J.R.; Parkes, H.G.; So, P.W.; Hajji, N.; Thomas, E.L.; Frost, G.S.; Miller, A.D.; Bell, J.D. Cationic Lipid-Based Nanoparticles Mediate Functional Delivery of Acetate to Tumor Cells in Vivo Leading to Significant Anticancer Effects. *IJN* **2017**, *12*, 6677–6685, doi:10.2147/IJN.S135968.
134. Sahuri-Arisoylu, M.; Mould, R.R.; Shinjyo, N.; Bligh, S.W.A.; Nunn, A.V.W.; Guy, G.W.; Thomas, E.L.; Bell, J.D. Acetate Induces Growth Arrest in Colon Cancer Cells Through

Modulation of Mitochondrial Function. *Front Nutr* **2021**, *8*, 588466, doi:10.3389/fnut.2021.588466.
135. Kamphorst, J.J.; Cross, J.R.; Fan, J.; de Stanchina, E.; Mathew, R.; White, E.P.; Thompson, C.B.; Rabinowitz, J.D. Hypoxic and Ras-Transformed Cells Support Growth by Scavenging Unsaturated Fatty Acids from Lysophospholipids. *Proc Natl Acad Sci U S A* **2013**, *110*, 8882–8887, doi:10.1073/pnas.1307237110.
136. Knowles, S.E.; Jarrett, I.G.; Filsell, O.H.; Ballard, F.J. Production and Utilization of Acetate in Mammals. *Biochem J* **1974**, *142*, 401–411, doi:10.1042/bj1420401.
137. Tibbetts, A.S.; Appling, D.R. Compartmentalization of Mammalian Folate-Mediated One-Carbon Metabolism. *Annu Rev Nutr* **2010**, *30*, 57–81, doi:10.1146/annurev.nutr.012809.104810.
138. Garcia-Martinez, L.F.; Appling, D.R. Characterization of the Folate-Dependent Mitochondrial Oxidation of Carbon 3 of Serine. *Biochemistry* **1993**, *32*, 4671–4676, doi:10.1021/bi00068a027.
139. Meiser, J.; Tumanov, S.; Maddocks, O.; Labuschagne, C.F.; Athineos, D.; Van Den Broek, N.; Mackay, G.M.; Gottlieb, E.; Blyth, K.; Vousden, K.; et al. Serine One-Carbon Catabolism with Formate Overflow. *Sci Adv* **2016**, *2*, e1601273, doi:10.1126/sciadv.1601273.
140. Meiser, J.; Schuster, A.; Pietzke, M.; Vande Voorde, J.; Athineos, D.; Oizel, K.; Burgos-Barragan, G.; Wit, N.; Dhayade, S.; Morton, J.P.; et al. Increased Formate Overflow Is a Hallmark of Oxidative Cancer. *Nat Commun* **2018**, *9*, 1368, doi:10.1038/s41467-018-03777-w.
141. Taware, R.; Taunk, K.; Kumar, T.V.S.; Pereira, J.A.M.; Câmara, J.S.; Nagarajaram, H.A.; Kundu, G.C.; Rapole, S. Extracellular Volatilomic Alterations Induced by Hypoxia in Breast Cancer Cells. *Metabolomics* **2020**, *16*, 21, doi:10.1007/s11306-020-1635-x.
142. Ratnikov, B.; Aza-Blanc, P.; Ronai, Z.A.; Smith, J.W.; Osterman, A.L.; Scott, D.A. Glutamate and Asparagine Cataplerosis Underlie Glutamine Addiction in Melanoma. *Oncotarget* **2015**, *6*, 7379–7389, doi:10.18632/oncotarget.3132.
143. Zhang, J.; Fan, J.; Venneti, S.; Cross, J.R.; Takagi, T.; Bhinder, B.; Djaballah, H.; Kanai, M.; Cheng, E.H.; Judkins, A.R.; et al. Asparagine Plays a Critical Role in Regulating Cellular Adaptation to Glutamine Depletion. *Mol Cell* **2014**, *56*, 205–218, doi:10.1016/j.molcel.2014.08.018.
144. Krall, A.S.; Xu, S.; Graeber, T.G.; Braas, D.; Christofk, H.R. Asparagine Promotes Cancer Cell Proliferation through Use as an Amino Acid Exchange Factor. *Nat Commun* **2016**, *7*, 11457, doi:10.1038/ncomms11457.
145. Pavlova, N.N.; Hui, S.; Ghergurovich, J.M.; Fan, J.; Intlekofer, A.M.; White, R.M.; Rabinowitz, J.D.; Thompson, C.B.; Zhang, J. As Extracellular Glutamine Levels Decline, Asparagine Becomes an Essential Amino Acid. *Cell Metab* **2018**, *27*, 428-438.e5, doi:10.1016/j.cmet.2017.12.006.
146. Dyachok, J.; Earnest, S.; Iturraran, E.N.; Cobb, M.H.; Ross, E.M. Amino Acids Regulate MTORC1 by an Obligate Two-Step Mechanism. *J Biol Chem* **2016**, *291*, 22414–22426, doi:10.1074/jbc.M116.732511.
147. Gwinn, D.M.; Lee, A.G.; Briones-Martin-del-Campo, M.; Conn, C.S.; Simpson, D.R.; Scott, A.I.; Le, A.; Cowan, T.M.; Ruggero, D.; Sweet-Cordero, E.A. Oncogenic KRAS Regulates Amino Acid Homeostasis and Asparagine Biosynthesis via ATF4 and Alters Sensitivity to L-Asparaginase. *Cancer Cell* **2018**, *33*, 91-107.e6, doi:10.1016/j.ccell.2017.12.003.
148. Scalise, M.; Pochini, L.; Galluccio, M.; Console, L.; Indiveri, C. Glutamine Transport and Mitochondrial Metabolism in Cancer Cell Growth. *Frontiers in Oncology* **2017**, *7*.
149. Sivashanmugam, M.; J, J.; V, U.; K N, S. Ornithine and Its Role in Metabolic Diseases: An Appraisal. *Biomed Pharmacother* **2017**, *86*, 185–194, doi:10.1016/j.biopha.2016.12.024.

150. Hata, A.; Tsuzuki, T.; Shimada, K.; Takiguchi, M.; Mori, M.; Matsuda, I. Isolation and Characterization of the Human Ornithine Transcarbamylase Gene: Structure of the 5′-End Region. *J Biochem* **1986**, *100*, 717–725, doi:10.1093/oxfordjournals.jbchem.a121764.
151. Zhang, J.; Tao, B.; Chong, Y.; Ma, S.; Wu, G.; Zhu, H.; Zhao, Y.; Zhao, S.; Niu, M.; Zhang, S.; et al. Ornithine and Breast Cancer: A Matched Case-Control Study. *Sci Rep* **2020**, *10*, 15502, doi:10.1038/s41598-020-72699-9.
152. Kucharzewska, P.; Welch, J.E.; Svensson, K.J.; Belting, M. The Polyamines Regulate Endothelial Cell Survival during Hypoxic Stress through PI3K/AKT and MCL-1. *Biochem Biophys Res Commun* **2009**, *380*, 413–418, doi:10.1016/j.bbrc.2009.01.097.
153. Wang, C.; Ruan, P.; Zhao, Y.; Li, X.; Wang, J.; Wu, X.; Liu, T.; Wang, S.; Hou, J.; Li, W.; et al. Spermidine/Spermine N1-Acetyltransferase Regulates Cell Growth and Metastasis via AKT/β-Catenin Signaling Pathways in Hepatocellular and Colorectal Carcinoma Cells. *Oncotarget* **2017**, *8*, 1092–1109, doi:10.18632/oncotarget.13582.
154. Gomes, A.P.; Ilter, D.; Low, V.; Endress, J.E.; Fernández-García, J.; Rosenzweig, A.; Schild, T.; Broekaert, D.; Ahmed, A.; Planque, M.; et al. Age-Induced Accumulation of Methylmalonic Acid Promotes Tumour Progression. *Nature* **2020**, *585*, 283–287, doi:10.1038/s41586-020-2630-0.
155. Gomes, A.P.; Ilter, D.; Low, V.; Drapela, S.; Schild, T.; Mullarky, E.; Han, J.; Elia, I.; Broekaert, D.; Rosenzweig, A.; et al. Altered Propionate Metabolism Contributes to Tumour Progression and Aggressiveness. *Nat Metab* **2022**, *4*, 435–443, doi:10.1038/s42255-022-00553-5.
156. Chisari, A.; Golán, I.; Campisano, S.; Gélabert, C.; Moustakas, A.; Sancho, P.; Caja, L. Glucose and Amino Acid Metabolic Dependencies Linked to Stemness and Metastasis in Different Aggressive Cancer Types. *Frontiers in Pharmacology* **2021**, *12*.
157. Folkman, J. Tumor Angiogenesis: Therapeutic Implications. *N Engl J Med* **1971**, *285*, 1182–1186, doi:10.1056/NEJM197111182852108.
158. Muthukkaruppan, V.R.; Kubai, L.; Auerbach, R. Tumor-Induced Neovascularization in the Mouse Eye. *J Natl Cancer Inst* **1982**, *69*, 699–708.
159. Holmgren, L.; O'Reilly, M.S.; Folkman, J. Dormancy of Micrometastases: Balanced Proliferation and Apoptosis in the Presence of Angiogenesis Suppression. *Nature medicine* **1995**, doi:10.1038/nm0295-149.
160. Parangi, S.; O'Reilly, M.; Christofori, G.; Holmgren, L.; Grosfeld, J.; Folkman, J.; Hanahan, D. Antiangiogenic Therapy of Transgenic Mice Impairs de Novo Tumor Growth. *Proceedings of the National Academy of Sciences* **1996**, *93*, 2002–2007, doi:10.1073/pnas.93.5.2002.
161. Semenza, G.L. Oxygen Sensing, Hypoxia-Inducible Factors, and Disease Pathophysiology. *Annual Review of Pathology: Mechanisms of Disease* **2014**, *9*, 47–71, doi:10.1146/annurev-pathol-012513-104720.
162. Zhong, H.; De Marzo, A.M.; Laughner, E.; Lim, M.; Hilton, D.A.; Zagzag, D.; Buechler, P.; Isaacs, W.B.; Semenza, G.L.; Simons, J.W. Overexpression of Hypoxia-Inducible Factor 1alpha in Common Human Cancers and Their Metastases. *Cancer Res* **1999**, *59*, 5830–5835.
163. Semenza, G.L. Defining the Role of Hypoxia-Inducible Factor 1 in Cancer Biology and Therapeutics. *Oncogene* **2010**, *29*, 625–634, doi:10.1038/onc.2009.441.
164. Wellen, K.E.; Thompson, C.B. Cellular Metabolic Stress: Considering How Cells Respond to Nutrient Excess. *Mol Cell* **2010**, *40*, 323–332, doi:10.1016/j.molcel.2010.10.004.
165. Ying, H.; Kimmelman, A.C.; Lyssiotis, C.A.; Hua, S.; Chu, G.C.; Fletcher-Sananikone, E.; Locasale, J.W.; Son, J.; Zhang, H.; Coloff, J.L.; et al. Oncogenic Kras Maintains Pancreatic Tumors through Regulation of Anabolic Glucose Metabolism. *Cell* **2012**, *149*, 656–670, doi:10.1016/j.cell.2012.01.058.

166. Moloughney, J.G.; Vega-Cotto, N.M.; Liu, S.; Patel, C.; Kim, P.K.; Wu, C.-C.; Albaciete, D.; Magaway, C.; Chang, A.; Rajput, S.; et al. MTORC2 Modulates the Amplitude and Duration of GFAT1 Ser-243 Phosphorylation to Maintain Flux through the Hexosamine Pathway during Starvation. *J Biol Chem* **2018**, *293*, 16464–16478, doi:10.1074/jbc.RA118.003991.
167. Moloughney, J.G.; Kim, P.K.; Vega-Cotto, N.M.; Wu, C.-C.; Zhang, S.; Adlam, M.; Lynch, T.; Chou, P.-C.; Rabinowitz, J.D.; Werlen, G.; et al. MTORC2 Responds to Glutamine Catabolite Levels to Modulate the Hexosamine Biosynthesis Enzyme GFAT1. *Mol Cell* **2016**, *63*, 811–826, doi:10.1016/j.molcel.2016.07.015.
168. Bond, M.R.; Hanover, J.A. A Little Sugar Goes a Long Way: The Cell Biology of O-GlcNAc. *J Cell Biol* **2015**, *208*, 869–880, doi:10.1083/jcb.201501101.
169. Love, D.C.; Hanover, J.A. The Hexosamine Signaling Pathway: Deciphering the "O-GlcNAc Code." *Sci STKE* **2005**, *2005*, re13, doi:10.1126/stke.3122005re13.
170. Abdel Rahman, A.M.; Ryczko, M.; Pawling, J.; Dennis, J.W. Probing the Hexosamine Biosynthetic Pathway in Human Tumor Cells by Multitargeted Tandem Mass Spectrometry. *ACS Chem Biol* **2013**, *8*, 2053–2062, doi:10.1021/cb4004173.
171. Vasconcelos-Dos-Santos, A.; Loponte, H.F.B.R.; Mantuano, N.R.; Oliveira, I.A.; de Paula, I.F.; Teixeira, L.K.; de-Freitas-Junior, J.C.M.; Gondim, K.C.; Heise, N.; Mohana-Borges, R.; et al. Hyperglycemia Exacerbates Colon Cancer Malignancy through Hexosamine Biosynthetic Pathway. *Oncogenesis* **2017**, *6*, e306, doi:10.1038/oncsis.2017.2.
172. Nakajima, K.; Kitazume, S.; Angata, T.; Fujinawa, R.; Ohtsubo, K.; Miyoshi, E.; Taniguchi, N. Simultaneous Determination of Nucleotide Sugars with Ion-Pair Reversed-Phase HPLC. *Glycobiology* **2010**, *20*, 865–871, doi:10.1093/glycob/cwq044.
173. Pham, L.V.; Bryant, J.L.; Mendez, R.; Chen, J.; Tamayo, A.T.; Xu-Monette, Z.Y.; Young, K.H.; Manyam, G.C.; Yang, D.; Medeiros, L.J.; et al. Targeting the Hexosamine Biosynthetic Pathway and O-Linked N-Acetylglucosamine Cycling for Therapeutic and Imaging Capabilities in Diffuse Large B-Cell Lymphoma. *Oncotarget* **2016**, *7*, 80599–80611, doi:10.18632/oncotarget.12413.
174. Akella, N.M.; Ciraku, L.; Reginato, M.J. Fueling the Fire: Emerging Role of the Hexosamine Biosynthetic Pathway in Cancer. *BMC Biology* **2019**, *17*, 52, doi:10.1186/s12915-019-0671-3.
175. Balasubramanian, M.N.; Butterworth, E.A.; Kilberg, M.S. Asparagine Synthetase: Regulation by Cell Stress and Involvement in Tumor Biology. *Am J Physiol Endocrinol Metab* **2013**, *304*, E789-799, doi:10.1152/ajpendo.00015.2013.
176. Jousse, C.; Averous, J.; Bruhat, A.; Carraro, V.; Mordier, S.; Fafournoux, P. Amino Acids as Regulators of Gene Expression: Molecular Mechanisms. *Biochem Biophys Res Commun* **2004**, *313*, 447–452, doi:10.1016/j.bbrc.2003.07.020.
177. Scioscia, K.A.; Snyderman, C.H.; Wagner, R. Altered Serum Amino Acid Profiles in Head and Neck Cancer. *Nutr Cancer* **1998**, *30*, 144–147, doi:10.1080/01635589809514654.
178. Aslanian, A.M.; Fletcher, B.S.; Kilberg, M.S. Asparagine Synthetase Expression Alone Is Sufficient to Induce L-Asparaginase Resistance in MOLT-4 Human Leukaemia Cells. *Biochem J* **2001**, *357*, 321–328, doi:10.1042/0264-6021:3570321.
179. Dutta, A.D.; Kumar, A.; Lokhande, K.; Mitruka, M.; Pal, J.K.; Sarode, S.C.; Sharma, N.K. Detection of Oncometabolites 1-Methylnicotinamide, Nicotine Imine and N-Methylnicotinium in Nails of Oral Cancer Patients and Prediction of Them as Modulators of DNMT1 2020, 2020.09.20.20198101.
180. Spivak-Kroizman, T.R.; Hostetter, G.; Posner, R.; Aziz, M.; Hu, C.; Demeure, M.J.; Von Hoff, D.; Hingorani, S.R.; Palculict, T.B.; Izzo, J.; et al. Hypoxia Triggers Hedgehog-

Mediated Tumor-Stromal Interactions in Pancreatic Cancer. *Cancer Res* **2013**, *73*, 3235–3247, doi:10.1158/0008-5472.CAN-11-1433.
181. Guillaumond, F.; Iovanna, J.L.; Vasseur, S. Pancreatic Tumor Cell Metabolism: Focus on Glycolysis and Its Connected Metabolic Pathways. *Arch Biochem Biophys* **2014**, *545*, 69–73, doi:10.1016/j.abb.2013.12.019.
182. Xu, Y.; Liu, P.; Zheng, D.-H.; Wu, N.; Zhu, L.; Xing, C.; Zhu, J. Expression Profile and Prognostic Value of NNMT in Patients with Pancreatic Cancer. *Oncotarget* **2016**, *7*, 19975–19981, doi:10.18632/oncotarget.7891.
183. Allison, S.J.; Knight, J.R.P.; Granchi, C.; Rani, R.; Minutolo, F.; Milner, J.; Phillips, R.M. Identification of LDH-A as a Therapeutic Target for Cancer Cell Killing via (i) P53/NAD(H)-Dependent and (Ii) P53-Independent Pathways. *Oncogenesis* **2014**, *3*, e102–e102, doi:10.1038/oncsis.2014.16.
184. Warburg, O. On the Origin of Cancer Cells. *Science* **1956**, *123*, 309–314, doi:10.1126/science.123.3191.309.
185. HALESTRAP, A.P.; PRICE, N.T. The Proton-Linked Monocarboxylate Transporter (MCT) Family: Structure, Function and Regulation. *Biochemical Journal* **1999**, *343*, 281–299, doi:10.1042/bj3430281.
186. Psychogios, N.; Hau, D.D.; Peng, J.; Guo, A.C.; Mandal, R.; Bouatra, S.; Sinelnikov, I.; Krishnamurthy, R.; Eisner, R.; Gautam, B.; et al. The Human Serum Metabolome. *PLOS ONE* **2011**, *6*, e16957, doi:10.1371/journal.pone.0016957.
187. Rabinowitz, J.D.; Enerbäck, S. Lactate: The Ugly Duckling of Energy Metabolism. *Nat Metab* **2020**, *2*, 566–571, doi:10.1038/s42255-020-0243-4.
188. Halestrap, A.P.; Wilson, M.C. The Monocarboxylate Transporter Family--Role and Regulation. *IUBMB Life* **2012**, *64*, 109–119, doi:10.1002/iub.572.
189. Zhang, D.; Tang, Z.; Huang, H.; Zhou, G.; Cui, C.; Weng, Y.; Liu, W.; Kim, S.; Lee, S.; Perez-Neut, M.; et al. Metabolic Regulation of Gene Expression by Histone Lactylation. *Nature* **2019**, *574*, 575–580, doi:10.1038/s41586-019-1678-1.
190. Rani, R.; Kumar, V. Recent Update on Human Lactate Dehydrogenase Enzyme 5 (HLDH5) Inhibitors: A Promising Approach for Cancer Chemotherapy. *J Med Chem* **2016**, *59*, 487–496, doi:10.1021/acs.jmedchem.5b00168.
191. Brisson, L.; Bański, P.; Sboarina, M.; Dethier, C.; Danhier, P.; Fontenille, M.-J.; Van Hée, V.F.; Vazeille, T.; Tardy, M.; Falces, J.; et al. Lactate Dehydrogenase B Controls Lysosome Activity and Autophagy in Cancer. *Cancer Cell* **2016**, *30*, 418–431, doi:10.1016/j.ccell.2016.08.005.
192. Wei, Z.; Liu, X.; Cheng, C.; Yu, W.; Yi, P. Metabolism of Amino Acids in Cancer. *Frontiers in Cell and Developmental Biology* **2021**, *8*.
193. Bröer, S.; Bröer, A. Amino Acid Homeostasis and Signalling in Mammalian Cells and Organisms. *Biochem J* **2017**, *474*, 1935–1963, doi:10.1042/BCJ20160822.
194. Christensen, H.N. Role of Amino Acid Transport and Countertransport in Nutrition and Metabolism. *Physiological Reviews* **1990**, *70*, 43–77, doi:10.1152/physrev.1990.70.1.43.
195. Bröer, A.; Rahimi, F.; Bröer, S. Deletion of Amino Acid Transporter ASCT2 (SLC1A5) Reveals an Essential Role for Transporters SNAT1 (SLC38A1) and SNAT2 (SLC38A2) to Sustain Glutaminolysis in Cancer Cells *. *Journal of Biological Chemistry* **2016**, *291*, 13194–13205, doi:10.1074/jbc.M115.700534.
196. Bhutia, Y.D.; Ganapathy, V. Glutamine Transporters in Mammalian Cells and Their Functions in Physiology and Cancer. *Biochimica et Biophysica Acta (BBA) - Molecular Cell Research* **2016**, *1863*, 2531–2539, doi:10.1016/j.bbamcr.2015.12.017.
197. Bröer, A.; Gauthier-Coles, G.; Rahimi, F.; van Geldermalsen, M.; Dorsch, D.; Wegener, A.; Holst, J.; Bröer, S. Ablation of the ASCT2 (SLC1A5) Gene Encoding a Neutral Amino Acid

Transporter Reveals Transporter Plasticity and Redundancy in Cancer Cells. *J Biol Chem* **2019**, *294*, 4012–4026, doi:10.1074/jbc.RA118.006378.
198. Weinberg, F.; Hamanaka, R.; Wheaton, W.W.; Weinberg, S.; Joseph, J.; Lopez, M.; Kalyanaraman, B.; Mutlu, G.M.; Budinger, G.R.S.; Chandel, N.S. Mitochondrial Metabolism and ROS Generation Are Essential for Kras-Mediated Tumorigenicity. *Proc Natl Acad Sci U S A* **2010**, *107*, 8788–8793, doi:10.1073/pnas.1003428107.
199. Fan, J.; Kamphorst, J.J.; Mathew, R.; Chung, M.K.; White, E.; Shlomi, T.; Rabinowitz, J.D. Glutamine-Driven Oxidative Phosphorylation Is a Major ATP Source in Transformed Mammalian Cells in Both Normoxia and Hypoxia. *Mol Syst Biol* **2013**, *9*, 712, doi:10.1038/msb.2013.65.
200. Early Breast Cancer Trialists' Collaborative Group (EBCTCG) Long-Term Outcomes for Neoadjuvant versus Adjuvant Chemotherapy in Early Breast Cancer: Meta-Analysis of Individual Patient Data from Ten Randomised Trials. *Lancet Oncol* **2018**, *19*, 27–39, doi:10.1016/S1470-2045(17)30777-5.
201. Salisbury, T.B.; Arthur, S. The Regulation and Function of the L-Type Amino Acid Transporter 1 (LAT1) in Cancer. *Int J Mol Sci* **2018**, *19*, 2373, doi:10.3390/ijms19082373.
202. Sato, M.; Harada-Shoji, N.; Toyohara, T.; Soga, T.; Itoh, M.; Miyashita, M.; Tada, H.; Amari, M.; Anzai, N.; Furumoto, S.; et al. L-Type Amino Acid Transporter 1 Is Associated with Chemoresistance in Breast Cancer via the Promotion of Amino Acid Metabolism. *Sci Rep* **2021**, *11*, 589, doi:10.1038/s41598-020-80668-5.
203. Lopes, C.; Pereira, C.; Medeiros, R. ASCT2 and LAT1 Contribution to the Hallmarks of Cancer: From a Molecular Perspective to Clinical Translation. *Cancers (Basel)* **2021**, *13*, 203, doi:10.3390/cancers13020203.
204. Closs, E.I.; Boissel, J.-P.; Habermeier, A.; Rotmann, A. Structure and Function of Cationic Amino Acid Transporters (CATs). *J Membrane Biol* **2006**, *213*, 67–77, doi:10.1007/s00232-006-0875-7.
205. Werner, A.; Pieh, D.; Echchannaoui, H.; Rupp, J.; Rajalingam, K.; Theobald, M.; Closs, E.I.; Munder, M. Cationic Amino Acid Transporter-1-Mediated Arginine Uptake Is Essential for Chronic Lymphocytic Leukemia Cell Proliferation and Viability. *Frontiers in Oncology* **2019**, *9*, doi:10.3389/fonc.2019.01268.
206. Scalise, M.; Console, L.; Rovella, F.; Galluccio, M.; Pochini, L.; Indiveri, C. Membrane Transporters for Amino Acids as Players of Cancer Metabolic Rewiring. *Cells* **2020**, *9*, 2028, doi:10.3390/cells9092028.
207. Chen, C.-L.; Hsu, S.-C.; Ann, D.K.; Yen, Y.; Kung, H.-J. Arginine Signaling and Cancer Metabolism. *Cancers (Basel)* **2021**, *13*, 3541, doi:10.3390/cancers13143541.
208. Boroughs, L.K.; DeBerardinis, R.J. Metabolic Pathways Promoting Cancer Cell Survival and Growth. *Nat Cell Biol* **2015**, *17*, 351–359, doi:10.1038/ncb3124.
209. Liu, H.; Heaney, A.P. Refined Fructose and Cancer. *Expert Opin Ther Targets* **2011**, *15*, 1049–1059, doi:10.1517/14728222.2011.588208.
210. Weng, Y.; Fan, X.; Bai, Y.; Wang, S.; Huang, H.; Yang, H.; Zhu, J.; Zhang, F. SLC2A5 Promotes Lung Adenocarcinoma Cell Growth and Metastasis by Enhancing Fructose Utilization. *Cell Death Discovery* **2018**, *4*, 1–12, doi:10.1038/s41420-018-0038-5.
211. Chen, W.-L.; Wang, Y.-Y.; Zhao, A.; Xia, L.; Xie, G.; Su, M.; Zhao, L.; Liu, J.; Qu, C.; Wei, R.; et al. Enhanced Fructose Utilization Mediated by SLC2A5 Is a Unique Metabolic Feature of Acute Myeloid Leukemia with Therapeutic Potential. *Cancer Cell* **2016**, *30*, 779–791, doi:10.1016/j.ccell.2016.09.006.
212. Zamora-León, S.P.; Golde, D.W.; Concha, I.I.; Rivas, C.I.; Delgado-López, F.; Baselga, J.; Nualart, F.; Vera, J.C. Expression of the Fructose Transporter GLUT5 in Human Breast Cancer. *Proc Natl Acad Sci U S A* **1996**, *93*, 1847–1852, doi:10.1073/pnas.93.5.1847.

213. Godoy, A.; Ulloa, V.; Rodríguez, F.; Reinicke, K.; Yañez, A.J.; García, M. de los A.; Medina, R.A.; Carrasco, M.; Barberis, S.; Castro, T.; et al. Differential Subcellular Distribution of Glucose Transporters GLUT1-6 and GLUT9 in Human Cancer: Ultrastructural Localization of GLUT1 and GLUT5 in Breast Tumor Tissues. *J Cell Physiol* **2006**, *207*, 614–627, doi:10.1002/jcp.20606.
214. Vultaggio-Poma, V.; Sarti, A.C.; Virgilio, F.D. Extracellular ATP: A Feasible Target for Cancer Therapy. *Cells* **2020**, *9*, doi:10.3390/cells9112496.
215. Allard, B.; Longhi, M.S.; Robson, S.C.; Stagg, J. The Ectonucleotidases CD39 and CD73: Novel Checkpoint Inhibitor Targets. *Immunol Rev* **2017**, *276*, 121–144, doi:10.1111/imr.12528.
216. Qian, Y.; Wang, X.; Li, Y.; Cao, Y.; Chen, X. Extracellular ATP a New Player in Cancer Metabolism: NSCLC Cells Internalize ATP In Vitro and In Vivo Using Multiple Endocytic Mechanisms. *Molecular Cancer Research* **2016**, *14*, 1087–1096, doi:10.1158/1541-7786.MCR-16-0118.

List of publications

A. Thesis publications

1. **Qasem, B**.; P. Młynarz, The metabolic change during hypoxic, normoxic and hyperoxic conditions within time intervals for the HT1080 cell line. In preparation will be send to the journal
2. **Qasem, B**.; P. Młynarz, The hypoxia reoxygenation and normoxia deoxygenation approach as novel *in vitro* model of understanding the HT1080 cell line metabolome by ^{1}H NMR. In preparation will be send to the journal.

B. Other publications

1. Dawiskiba, T., Wojtowicz, W., **Qasem, B**. *et al.* Brain-dead, and coma patients exhibit different serum metabolic profiles: preliminary investigation of a novel diagnostic approach in neurocritical care. *Sci Rep* **11,** 15519 (2021). https://doi.org/10.1038/s41598-021-94625-3
2. Bogunia-Kubik K, Wojtowicz W, Swierkot J, Mielko KA, **Qasem B**, Wielińska J, Sokolik R, Pruss Ł, Młynarz P. Disease Differentiation and Monitoring of Anti-TNF Treatment in Rheumatoid Arthritis and Spondyloarthropathies. *International Journal of Molecular Sciences*. 2021; 22(14):7389. https://doi.org/10.3390/ijms22147389
3. Warowicka A, **Qasem B**, Dera-Szymanowska A, Wołuń-Cholewa M, Florczak P, Horst N, Napierała M, Szymanowski K, Popenda Ł, Bartkowiak G, Florek E, Goździcka-Józefiak A, Młynarz P. Effect of Protoberberine-Rich Fraction of *Chelidonium majus* L. on Endometriosis Regression. *Pharmaceutics*. 2021; 13(7):931. https://doi.org/10.3390/pharmaceutics13070931
4. Szymanski H, Mlynarz P, **Qasem B**, Agnieszka Korzeniowska-Kowal A, Szponar B, Kałwak-Baran M, Szajewska H. Post hoc analysis of fecal samples from responders and non- responders to Lactobacillus reuteri DSM 17938 intervention. *Acta biochimica Polonica.* 2020. 67(3):393-399. https://doi.org/10.18388/abp.2020_5344
5. Gawron K, Wojtowicz W, Łazarz-Bartyzel K, Łamasz A, **Qasem B**, Mydel P, Mlynarz P. Metabolomic Status of The Oral Cavity in Chronic Periodontitis. In Vivo. 2019; , 33(4), 1165–1174. https://doi.org/10.21873/invivo.11587
6. Padjasek, M.; **Qasem, B**.; Cisło-Pakuluk, A.; Marycz, K. Cyclosporine A Delivery Platform for Veterinary Ophthalmology—A New Concept for Advanced Ophthalmology. *Biomolecules* **2022**, *12*, 1525. https://doi.org/10.3390/biom12101525
7. Stachowska, E.; Maciejewska-Markiewicz, D.; Palma, J.; Mielko, K.A.; **Qasem, B**.; Kozłowska-Petriczko, K.; Ufnal, M.; Sokolowska, K.E.; Hawryłkowicz, V.; Załęska, P.; Jakubczyk, K.; Wunsch, E.; Ryterska, K.; Skonieczna-Żydecka, K.; Młynarz, P. Precision Nutrition in NAFLD: Effects of a High-Fiber Intervention on the Serum Metabolome of NAFD Patients—A Pilot Study. *Nutrients* **2022**, *14*, 5355. https://doi.org/10.3390/nu14245355
8. Padjasek M, Cisło-Sankowska A, Lis-Bartos A, **Qasem B**, Marycz K. PLDLA/TPU Matrix Enriched with Cyclosporine A as a Therapeutic Platform for Immune-Mediated Keratitis (IMMK) in Horses. *International Journal of Molecular Sciences*. **2023**; 24(6):5735. https://doi.org/10.3390/ijms24065735

9. **Badr Qasem**, Lynda Bourebaba, Agnieszka Dąbrowska, Jarosław Króliczewski, Krzysztof Marycz. Trodusquemine (MSI-1436) restores metabolic flexibility and mitochondrial dynamics in insulin-resistant equine hepatic progenitor cells (HPCs). *Stem cells reviews and reports* **2023**. Under review.
10. Krzysztof Marycz, Lynda Bourebaba, Sylwia Groborz, **Badr Qasem**, Anna Cisło-Pakuluk, Ron Ofri. Extracellular vesicles isolated from equine adipose-derived stromal stem cells (ASCs) mitigate tunicamycin-induced ER stress in equine corneal stromal stem cells (CSSCs) – a novel perspective for corneal regeneration. *Journal of Extracellular Biology* **2023**. JEXB-2023-03-0018. Under review.
11. Nabila Bourebaba; Mateusz Sikora; **Badr Qasem**; Lynda Bourebaba; Krzysztof Marycz. Sex hormone-binding globulin (SHBG) mitigates ER stress and improves viability and insulin sensitivity in adipose-derived mesenchymal stem cells (ASCs) of equine metabolic syndrome (EMS)-affected horses. *Endocrinology* **2023**. en.2023-00192. Under review.
12. **Qasem, B**.; M, Krzysztof, The chemistry of adipose tissue. In preparation will be send to the journal.
13. Lynda Bourebaba, **Qasem, B**.; M, Krzysztof. SHBG regulates lipolysis and insulin signaling in EMS SAT. In preparation will be send to the journal.

List of conferences and webinars

1. **Participant**: Artificial Intelligence and Data Analytics (CAIDA 2021), *1st International Conference* online, Prince Sultan University, Riyadh, Saudi Arabia, 6 - 7 April 2021.
2. **Participant**: "Robust metabolic profiling for routine quantitation and confident unknown identification", for Metabolomics researchers embarking on large-scale studies in need of suitable LC-MS instrumentation webinar via *SelectScience*, by Thermo Fisher Scientific, March 2021.
3. **Participant**: "2020–A Year of Clinical Research Change, Challenge, and Champions" for Clinical project manager, development managers, operations managers & directors webinar via *SelectScience*, by National Health Service (NHS), Mar. 2021.
4. **Participant**: Advancing oncology therapeutics development with 2D & 3D cell screening for Scientists and researchers webinar via *SelectScience*, by Horizon Discovery, March 2021
5. **Participant**: Lean manufacturing practices with Raman spectroscopy for biopharmaceutical production for Analytical science and technology transfer leaders, Analytical scientists in biopharmaceutical manufacturing and QC managers webinar via *SelectScience*, by **Thermo Fisher Scientific**, 2021.
6. **Author poster**: Badr Qasem*, Dariusz Rakus, Agnieszka Gizak, Piotr Młynarz. The ^{1}H NMR studies for rare changes in metabolic adaptations depend on the availability of oxygen and time for the fibrosarcoma cell line. *16th Annual Conference of the Metabolomics Society (Metabolomics2020 Online)* 27-29.11.2020.
7. **Author poster**: Badr Qasem*, Dariusz Rakus, Agnieszka Gizak, Piotr Młynarz. The ^{1}H NMR studies for monitoring of unique changes in metabolic response of fibrosarcoma cell line on oxygen availability and cultivation time at *VII Konferencja Polskiego Towarzytwa Metabolomicznego (Metabolomics Circle)* 04-06.11.2020.

8. **Author poster:** Conference Instytut Rozrodu Zwierząt i Badań Żywności PAN Polskiej Akademii Nauk w Olsztynie, 14-16 Listopad 2019.
9. **Author oral presentation** at *5th Metabolomics Circle Scientific International Conference 2018*, NICOLAUS COPERNICUS UNIVERSITY IN TORUN. October 26-28, 2018.
10. **Author poster**: Badr Qasem*, Magdalena Michalkiewicz, Wojciech Wojtowicz, Piotr Mlynarz. NMR - based population studies, *Euromar2018 conference*, Nantes, France. July. 2018.
11. **Author poster**: Badr Qasem*, Magdalena Michalkiewicz, Wojciech Wojtowicz, Piotr Mlynarz. NMR - based population studies, *Multi-omika - biologia systemów w badaniach medycznych*. Katedra i Zakład Biochemii Lekarskiej, Uniwersytetu Medycznego we Wrocławiu. June. 2018
12. **Co-organizer** *OMICS national conference* at Wroclaw university of Science and Technology, Poland, 10/2017
13. **Participation** at *Nanotox national conference* at Wroclaw Research Centre EIT+ for Safety of using Nanomaterials, 2017.